Physical Layer Techniques for High Frequency Wireline Broadband Systems

Lins de Medeiros, Eduardo

2018

Document Version:
Publisher's PDF, also known as Version of record

Physical Layer Techniques for High Frequency Wireline Broadband Systems

Eduardo Lins de Medeiros

LUND UNIVERSITY

Doctorate Dissertation
Electrical Engineering
Lund, March 2018

Eduardo Lins de Medeiros
Department of Electrical and Information Technology
Lund University
P.O. Box 118, 221 00 Lund, Sweden

Series of licentiate and doctoral dissertations
ISSN 1654-790X; No. 111
ISBN 978-91-7753-549-2 (print)
ISBN 978-91-7753-550-8 (pdf)

Typeset in Palatino and Helvetica using LaTeX 2_ε.
Printed in Sweden by Tryckeriet i E-huset, Lund University, Lund.

To Alina

Abstract

This thesis collects contributions to wireline and wireless communication systems with an emphasis on multiuser and multicarrier physical layer technology.

To deliver increased capacity, modern wireline access systems such as G.fast extend the signal bandwidth up from tens to hundreds of MHz. This ambitious development revealed a number of unforeseen hurdles such as the impact of impedance changes in various forms. Impedance changes have a strong effect on the performance of multi-user crosstalk mitigation techniques such as vectoring. The first part of the thesis presents papers covering the identification of one of these problems, a model describing why it occurs and a method to mitigate its effects, improving line stability for G.fast systems.

A second part of the thesis deals with the effects of temperature changes on wireline channels. When a vectored (MIMO) wireline system is initialized, channel estimates need to be obtained. This thesis presents contributions on the feasibility of re-using channel coefficients to speed up the vectoring startup procedures, even after the correct coefficients have changed, e.g., due to temperature changes. We also present extensive measurement results showing the effects of temperature changes on copper channels using a temperature chamber and British cables.

The last part of the thesis presents three papers on the convergence of physical layer technologies, more specifically the deployment of OFDM-based radio systems using twisted pairs in different ways. In one proposed scenario, the idea of using the access copper lines to deploy small cells inside users' homes is explored. The feasibility of the concept, the design of radio-heads and a practical scheme for crosstalk mitigation are presented in three contributions.

Preface

This dissertation consists of an introduction, followed by a compilation of three published journal papers, two unpublished papers and five published conference papers. One filed patent application is also included. The thesis is organized into three parts. The first parts deals with the side effects of impedance changes to vectored wireline systems. The second part deals with the effects of temperature changes on wireline channels and the third part with combinations of radio and fixed communication systems.

1. Part I: Side effects of impedance changes to vectored wireline systems

   - Eduardo Medeiros, Thomas Magesacher, Per-Erik Eriksson, Chenguang Lu and Per Ödling, »How Vectoring in G.fast May Cause Neighborhood Wars«, *IEEE International Conference on Communications (ICC)*, Jun 2014.
   - Eduardo Medeiros, Thomas Magesacher, Per Ödling, Dong Wei, Xiang Wang, Qiaojie Li, Per-Erik Eriksson, Chenguang Lu, Jeroen Boschma and Bas van den Heuvel, »Modeling Alien-Line Impedance Mismatch in Wideband Vectored Wireline Systems«, *IEEE Communications Letters*, Sep 2014, vol. 18, number 9.
   - Yezi Huang, Thomas Magesacher, Eduardo Medeiros, Per-Erik Eriksson, Chenguang Lu and Per Ödling, »Mitigating Disorderly Leaving Events in G.fast«, *IEEE International Conference on Communications (ICC)*, Jun 2015.
   - Diego Gomes, Eduardo Medeiros, Aldebaro Klautau and Evaldo Pelaes, »Mitigation of Alien Crosstalk for Downstream DSL Impaired by Multiple Interferers«, *IEEE Communications Letters*, August 2017, vol. 21, number 11.

2. Part II: Effects of temperature changes on wireline channels

    - Driton Statovci, Thomas Magesacher, Martin Wolkerstorfer and Eduardo Medeiros, »Analysis of Fast Initialization for Vectored Wireline Systems«, *IEEE Global Telecommunications Conference (GLOBECOM)*, Dec 2013.
    - Eduardo Medeiros, Per Ödling, Ian Cooper, Trevor Morsman, Stefan Höst and Per Ola Börjesson, »The Cold Cables Case«, *unpublished*, March 2018.
    - Eduardo Medeiros, Per Ödling, Ian Cooper, Trevor Morsman, Stefan Höst and Per Ola Börjesson, »Temperature-dependent Shift of Notches in the Frequency Response of Twisted-Pairs«, *unpublished*, March 2018.

3. Part III: Combinations of radio and fixed communication systems

    - Yezi Huang, Eduardo Medeiros, Stefan Höst, Thomas Magesacher, Per-Erik Eriksson, Chenguang Lu, Per Ödling and Per Ola Börjesson, »Enabling DSL and Radio on the Same Copper Pair«, *IEEE International Conference on Communications (ICC)*, Jun 2015.
    - Yezi Huang, Eduardo Medeiros, Stefan Höst, Thomas Magesacher, Per-Erik Eriksson, Chenguang Lu, Per Ödling and Per Ola Börjesson, »LTE Over Copper - Potential and Limitations«, *IEEE International Symposium on Personal, Indoor and Mobile Radio Communications - (PIMRC)*, Sep 2015.
    - Eduardo Medeiros, Yezi Huang, Thomas Magesacher, Stefan Höst, Per-Erik Eriksson, Chenguang Lu, Per Ödling and Per Ola Börjesson, »Crosstalk Mitigation for LTE-over-Copper in Downlink Direction«, *IEEE Communications Letters*, July 2016, vol. 20, number 7.
    - Eduardo Medeiros, Yezi Huang, Per-Erik Eriksson and Chenguang Lu, »Methods and Nodes of a Wireless Communication Network for Mitigating Crosstalk in a Base Station System«, *filed patent application*, 2015.

Acknowledgments

When a thesis is written and published it usually looks great. A lot of effort is spent typesetting it and “ironing out" every detail. At the same time, its immaculate form hides most of the struggle that led to the final product. The failures, the ups-and-downs, the self-questioning and the anxiety. As a window into the human aspects of the process, I was always attracted to reading acknowledgment sections. As such, here comes my attempt at giving thanks to those that helped and were part of this effort, listed in no particular order.

The first question every PhD student is asked (first by her/himself and later by most people) is “Why do it?”. Prior to accepting a position I surveyed many of the PhD holders I knew. The best answer I’ve got, and the one that ultimately convinced me, was given by Per Ola Börjesson. If you’ve met him, you can imagine Per Ola wearing his suit, maybe even holding a cigar saying: “The end product of a doctorate is not the thesis, it is yourself, the researcher”. That was the first insight I got from him. Many would follow. His expertise is only matched by his generosity. Thank you Per Ola!

After answering the first few questions, a student proceeds to work on another fundamental skill, *asking questions*. In this pursuit I was guided by one of the best, my supervisor Per Ödling. Of his many special talents, the one that impresses me the most, is his ability to ask questions that are deep, clearly stated and that usually lead to deep understanding. As an aside, it must be mentioned that he makes excellent apple jack and apparently is a competent gamer claiming to hold a Platinum V ranking in LoL.

In pursuing any career it is very important to have role models. In this regard, my time with the broadband research group in Lund was very fruitful, for I could observe, cooperate and learn from people such as Thomas Magesacher and Stefan Höst. I am especially indebted to Thomas for his help on

many papers. He is prolific in ideas, a brilliant engineer and, as with most great athletes or performers, watching Thomas solve problems is exciting because he makes them seem easy, no matter what. During this PhD I had the great pleasure of working with Stefan Höst. His office in Lund was always open and his whiteboards prepared for any discussion. He helped me with so many papers. During a couple of years, I've helped Stefan with the Information Theory course in Lund and that was a transformative experience. Every time I speak in public I remember Stefan now.

Yezi Huang deserves special mention, as my fellow PhD student. We worked together, ate together, met in classrooms, laboratories, conference sessions and on all kinds of transportation between Stockholm and Lund, always at the most inconvenient hours. Yezi is full of potential and I am excited to watch what will she do next.

To my friend Pernilla Schuber who helped at all stages of this thesis (and even before) I say thank you! Pernilla is warm, a natural leader and plain fun to be around. At LTH, I would also like to thank my colleagues Antoni, Jens, Kaan and Adriana.

At Ericsson, I especially would like to thank Henrik Almeida and his Fronthaul Technologies team, namely my colleagues and co-authors Pelle, Chenguang, Boris, Miguel, Daniel, Elmar, André and Igor. Also at Ericsson I would like to thank Kim Laraqui, Neiva Linder, João M. Soares, Kåre Gustafsson, the Network, Architecture and Protocols team, and Sándor Albrecht.

During this time, I've worked in many international projects and met a lot of wonderful people. Thanks to Martin, Torsten, Jochen, Anas, Trevor, Les, Marcos, Hubert, Orem, Marta, José, Enrique, and Rob. A special thanks to Ian and Julia for hosting me at their house while I worked on measurements in Ipswich.

I was fortunate to collaborate with very talented individuals like Driton, Martin and Sanda, from TU Wien, Bas van den Heuvel and Jeroen Boschma from TNO, Dong Wei, Xiang Wang and Qiaojie Li from Huawei, Diego Gomes, Evaldo Pelaes and Nilma Fonseca from UFPA. It is an honor to have them as co-authors on some of the papers included in this thesis.

I come from a family of teachers, amongst them my mother, from whom I've learned to read and write. My parents always invested in my education and for that I am extremely grateful.

At last, but most importantly, I acknowledge my partner for life Alina. She's was with me at each high and each low of this pursuit and gave me strength all the way. Without her nothing would have been accomplished nor would it have any meaning.

Eduardo
Stockholm, March 2018

List of Acronyms and Abbreviations

3GPP	Third Generation Partnership Project
ACLR	Adjacent Channel Leakage power Ratio
ACS	Adjacent Channel Selectivity
AFE	Analog Front-end
AL	Alien Lines
AMMIS	Alien crosstalk Mitigation for Multiple Interference Sources
AXT	Alien Crosstalk
BBU	Baseband Unit
CCDF	Complementary Cumulative Distribution Function
CO	Central Office
CP	Cyclic Prefix
CPE	Customer Premises Equipment
CPRI	Common Public Radio Interface
CRS	Cell-specific Reference Signals
CST	Computer Simulation Technology
DC	Direct Current

DELT	Dual-ended Line Testing
DFC	Decision Feedback Canceller
DFT	Discrete Fourier Transform
DL	Downlink
DLE	Disorderly Leaving Event
DMT	Discrete Multi-tone
DP	Distribution Point
DPU	Distribution Point Unit
DSL	Digital Subscriber Line
DSLAM	Digital Subscriber Line Access Multiplexer
DSM	Dynamic Spectrum Management
DSP	Digital Signal Processor
ECTFE	Ethylene ChloroTriFluoroEthylene
EEPROM	Electrical Erasable Programmable ROM
EVM	Error Vector Magnitude
FDD	Frequency Division Duplexing
FDM	Frequency Domain Multiplexing
FEP	Fluorinated Ethylene Propylene
FEQ	Frequency Domain Equalizer
FEXT	Far-end Crosstalk
FFT	Fast Fourier Transform
FRN	FEXT-reflected-NEXT
ICI	Inter-carrier Interference
IDFT	Inverse Discrete Fourier Transform
IF	Intermediate Frequency

IFFT	Inverse Fast Fourier Transform
IQ	In-phase and Quadrature
IRU	Intermediate Radio Unit
ISI	Inter-symbol Interference
ITU	International Telecommunication Union
ITU-T	ITU - Telecommunication Standardization Sector
LAN	Local Area Network
LMS	Least Mean Squares
LP	Low-pass
LS	Least Squares
LTE	Long Term Evolution
LTI	Linear Time-invariant
MIMO	Multiple-input Multiple-output
MMSE	Minimum Mean Square Error
NEXT	Near-end Crosstalk
OFDM	Orthogonal Frequency Division Multiplexing
PDSCH	Physical Downlink Shared Channel
PLD	Programmable Logic Device
POTS	Plain Old Telephony Service
PSD	Power Spectral Density
PSTN	Public Switched Telephone Network
PVC	Polyvinyl Chloride
QAM	Quadrature Amplitude Modulation
QPSK	Quadrature Phase-shift Keying
RAM	Random-access Memory

RC	Reference Channel
RDS	Radio Dot System
RF	Radio Frequency
RFI	Radio Frequency Interference
RH	Radio Head
ROM	Read-only Memory
RRH	Remote Radio Head
RRU	Remote Radio Unit
RU	Radio Unit
SELT	Single-ended Line Testing
SEM	Spectrum Emission Mask
SINR	Signal-to-interference-plus-noise Ratio
SNR	Signal-to-noise Ratio
TC	Transmission Channel
TDD	Time Division Duplexing
THP	Tomlinson-Harashima Precoder
UE	User Equipment
UL	Uplink
VDSL2	Very High Speed Digital Subscriber Line 2
VG	Vectored Group
ZF	Zero-forcing
los	Loss of signal

Contents

1

Introduction

As you hold this thesis in your hands, stop for a moment and consider your environment. Very likely, a number of Internet connected devices will surround you. Looking around you may see computers, phones, televisions, loudspeakers, cameras and other gadgets capable of pulling data out of the Ether, to serve you in one way or the other.

While all this connectivity seems effortless and ubiquitous, even natural, it is the result of decades of relentless work by telecommunication engineers and researchers. The widespread deployment of fixed and mobile broadband systems has altered the way we communicate, work and socialize. In a twenty-five year span, we have gone from a handful of webpages that were hand-indexed to billions of websites, services, applications and business that rely on connectivity for their existence.

The growth of online content and number of connected devices is paralleled by the increase in connection speeds. Typically, the latter have observed a thousandfold increase over the last two decades. More than that, they have increased similarly for both wireline and wireless services.

To enable our exuberant online ecosystem, the telecommunications industry and research institutes have invested massively into producing standards that guarantee interoperability to enable economy of scale, and offer high spectral and power efficiency. Examples of these standards include the many variants of Digital Subscriber Line (DSL) [1–5], Long Term Evolution (LTE) [6] and wireless local area networks (WiFi) [7]. Summed up, these technologies are responsible for a significant percentage of all Internet connections. Although each of them targets very different use cases, such as home connection, outdoor mobility and indoor mobility, there is a great degree of similarity at the most basic level, the physical layer. During the past decades, many different avenues of technology and research have been pursued, but lately a few

ideas have emerged dominant in the common communication systems. The dominating principle for accessing the physical layer is nowadays *multicarrier modulation* (for a historical perspective of the contributions that led to its development see [8]). Multicarrier modulation is a central method for this thesis and we will go into further details in the next section.

Another example of principles that have come to dominate concerns how to allow the signals of many users to access shared or connected media simultaneously. The subsequent chapter, 1.2, discusses a mathematical family of techniques that, in wireline systems, are called vectoring. In the wireless area this mathematical family is known as MU-MIMO, or multiuser multiple-input, multiple-output techniques. Vectoring is another central theme of this thesis. For vectoring to work well, very precise knowledge about the transmission channel is needed. This is reflected in both Part I of the thesis that deals with the effects of impedance changes, Part II that investigates the effects from temperature changes and in Part III that combines radio and wireline systems.

1.1 MULTICARRIER MODULATION

Digital communication systems are used to transfer messages reliably between a source and a recipient. In achieving this task a system's physical layer is responsible for delivering the messages (sequences of binary digits) between two or more communicating hosts over a transmission medium (channel).

For the physical layer, the contents or meaning of the binary digits to be transmitted are irrelevant. On the other hand, it is responsible to adapt the message to the properties of the channel to facilitate transmission. Usually, this requires converting the digital information to a continuous-time waveform, whose characteristics are manipulated to relay different messages. At the receiver, after passing through the channel, waveforms are ideally translated back to the binary digits.

Before introducing multicarrier modulation it is worthwhile to describe conventional single carrier techniques, and gradually add the concepts that make it such a dominant digital communications technique.

1.1.1 A SINGLE CARRIER MODULATION EXAMPLE

As an example, let us consider the case of a transmitter using Quadrature Amplitude modulation (QAM) [9][10] to send the binary string[1] $1010-1100-0001$ to its counterpart. The translation between data and continuous waveform is represented in Fig. 1.1.

At first, the binary string to be transmitted is cut in smaller chunks of

[1] Hyphens inserted for legibility.

$\log_2(K)$ bits where K is the modulation order (the number of distinct symbols the modulator can represent in a given transmission interval). With $K = 16$, as in our example, a twelve-bit message is broken into three four-bit words.

Each word is translated to a QAM symbol using the *constellation diagram* presented in the left plot of Fig 1.1. A QAM symbol is a complex number of the form

$$x_l = x_l^{(i)} + x_l^{(q)} j, \tag{1.1}$$

where the real and imaginary coefficients are the coordinates of the respective word in the constellation plot. The subscript l represents the symbol number (the order in which the symbol was transmitted).

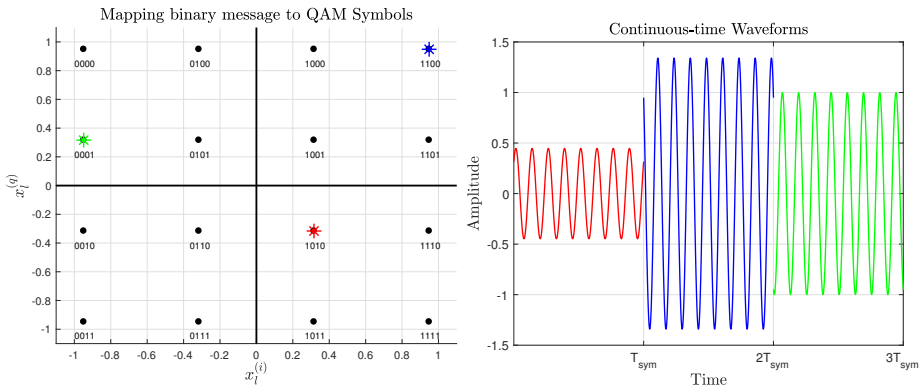

Figure 1.1: 16-QAM Constellation diagram and waveforms for the binary string $1010 - 1100 - 0001$. In the left plot we illustrate the translation between each binary four-bit word and a corresponding complex symbol. On the right side we present the result of modulating a sinusoid with said complex symbol.

In our example the binary words result in the symbols

- 1010 (represented in red) $\rightarrow x_1 = 0.3162 - 0.3162j$
- 1100 (represented in blue) $\rightarrow x_2 = 0.9487 + 0.9487j$
- 0001 (represented in green) $\rightarrow x_3 = -0.9487 + 0.3162j$

After the symbols are mapped, they are translated to a continuous waveform as

$$s(t) = \text{Re}\left\{ p(t - kT_{\text{sym}}) \left(x_k e^{j2\pi F_c t} \right) \right\}, \tag{1.2}$$

where p represents a square pulse of duration T_{sym}, and F_c is the carrier frequency. Our three symbols result in the waveform shown in the right plot

of Fig. 1.1. For each symbol a sinusoid waveform of corresponding amplitude and phase is generated.

Given a finite transmit power and a band-limited channel with additive noise, let's consider the obvious ways to improve the capacity of the system described in this example.

- The modulation order K could be increased, so each QAM symbol would represent more bits for the same waveform duration.

There are no direct drawbacks to this, but it is worth mentioning that the improvement will be limited by noise. If the signal-to-noise ratio (SNR) is low, higher modulation orders will lead to more transmission errors.

- T_{sym} could be shortened, making the transitions between symbols more frequent.

When the symbol duration is reduced the bandwidth necessary to transmit the signal increases. The available bandwidth of the channel will eventually limit how short the symbols can be. A second drawback to this approach is dispersion, which will be described in the next section.

- We could increase the number of QAM modulators by transmitting waveforms at different carrier frequencies, an approach known as Frequency Domain Multiplexing (FDM).

If the carrier frequencies in an FDM scheme are not sufficiently apart from each other, inter-carrier interference (ICI) will significantly harm the performance.

1.1.2 DISPERSION

The transmission media, such as the air, metallic wires or optical fibres, present constraints to the propagation of signals. Signals traversing a channel will suffer attenuation, delays and other kinds of impairments. As an example, twisted pairs are frequency selective, attenuating high-frequency signals much more than low-frequency ones.

Continuing our QAM modulation example, let's consider what happens to the transmitted signal when it traverses a linear time-invariant (LTI) channel. Let $s(t)$ represent the the channel's impulse response. The channel's output $r(t)$ is given by the linear convolution

$$r(t) = h(t) * s(t). \tag{1.3}$$

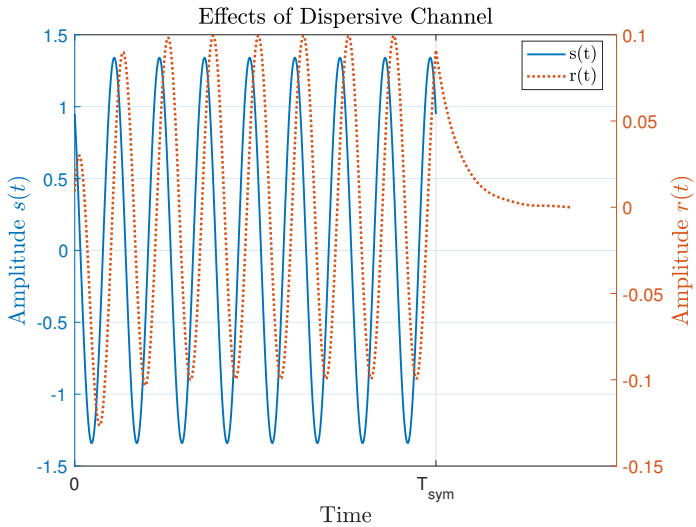

Figure 1.2: Effects of a time-dispersive LTI channel over the transmit waveform for x_2. The output $r(t)$ has the same carrier frequency, but amplitude and phase are modified. The channel output is longer than the transmit symbol due to non-negligible impulse response duration.

For frequency selective channels, the impulse response length (interval with significant energy) may not be negligible when compared to the symbol duration. This is illustrated in Fig. 1.2 below.

The transmit waveform $s(t)$ has duration T_{sym}, but the output of the channel is longer. If more than one symbol were transmitted, the tail of the red curve would interfere with the next symbol waveform, causing inter-symbol interference (ISI).

At the receiver, the output of the channel is processed to map received waveforms to symbols and finally binary words. The distortion caused by the channel is mitigated by e.g., an equalizer. In the presence of ISI, the complexity of equalization can be greatly increased, since the output of the channel will depend not only on the current symbol, but also on the preceding ones.

An alternative for avoiding the impact of ISI would be to insert guard intervals (silent periods) between symbols that are longer than the channel impulse response length. This has the drawback of lowering the overall efficiency of the modulation scheme used.

Multicarrier modulation techniques such as Discrete Multitone (DMT) and Orthogonal Frequency Division Multiplexing (OFDM) manage to avoid both

ISI and ICI, while providing high spectral efficiency, convenient hardware implementations and simple receiver processing. A brief description of both techniques is given in the following section. For more details see [9] [11–13].

1.1.3 DMT & OFDM

Let's assume that the LTI channel considered previously is band-limited, that its output is sampled obeying the Nyquist criterion and that its sampled impulse response, denoted $h(n)$, is finite with length $M+1$. If the sampled transmit signal has length N and is denoted by $s(n)$, a discrete-time version of (1.3) can be written as

$$r(n) = \sum_k h(n-k)s(k). \tag{1.4}$$

The sampled channel output $r(n)$ has length $N+M$. As a consequence, if multiple symbols are transmitted sequentially, the first M received samples of a symbol will be corrupted by the channel output of its predecessor.

To avoid the impact of dispersion, one could introduce a guard period of $L \geq M$ samples at the beginning of each symbol, subsequently discarding these ISI-distorted samples at the receiver.

In OFDM and DMT, this guard period is named *cyclic prefix* and it has a specific formulation. A copy of the last L samples of each symbol is inserted at the beginning of the transmit signal, as described by the matrix multiplication below, where $\mathbf{0}$, $\boldsymbol{I}$ represent, respectively, the zero and identity matrices of appropriate size and the samples $s(n)$, $n = 0, \ldots, N-1$ are collected in the vector $\boldsymbol{s}$.

$$\bar{\boldsymbol{s}} = \boldsymbol{A}\boldsymbol{s}$$

$$\begin{bmatrix} s(N-1-L) \\ \vdots \\ s(N-1) \\ s(0) \\ \vdots \\ s(N-1) \end{bmatrix} = \begin{bmatrix} \mathbf{0} & \boldsymbol{I} \\ \boldsymbol{I} & \end{bmatrix} \begin{bmatrix} s(0) \\ \vdots \\ s(N-1) \end{bmatrix}.$$

Assuming that $L = M$, the linear convolution between the cyclic prefix appended samples $\bar{s}(n)$, $n = N-1-L, \ldots, N-1$ and the channel in (1.4) can

be expressed in matrix notation as

$$\boldsymbol{r} = \boldsymbol{R}\boldsymbol{H}\bar{\boldsymbol{s}},$$

$$\begin{bmatrix} r(0) \\ \vdots \\ r(N-1) \end{bmatrix} = \begin{bmatrix} \boldsymbol{0} \\ \boldsymbol{I} \end{bmatrix} \begin{bmatrix} h(0) & 0 & \dots & \dots & \dots & 0 \\ \vdots & h(0) & \ddots & & & \vdots \\ h(L) & \vdots & \ddots & \ddots & & \vdots \\ 0 & h(L) & \vdots & \ddots & \ddots & \vdots \\ \vdots & \ddots & \ddots & \vdots & \ddots & 0 \\ 0 & \dots & 0 & h(L) & \dots & h(0) \end{bmatrix} \begin{bmatrix} s(N-1-L) \\ \vdots \\ s(N-1) \\ s(0) \\ \vdots \\ s(N-1) \end{bmatrix}.$$

Here, $\boldsymbol{R}$ represents the removal of the first L received samples at the receiver. If we denote the mapping between between $\boldsymbol{s}$ and $\boldsymbol{r}$ as $\boldsymbol{r} = \tilde{\boldsymbol{H}}\boldsymbol{s}$, the equivalent channel $\tilde{\boldsymbol{H}}$ is given by

$$\tilde{\boldsymbol{H}} = \boldsymbol{R}\boldsymbol{H}\boldsymbol{A} = \begin{bmatrix} h(0) & 0 & \dots & h(L) & \dots & h(1) \\ \vdots & h(0) & \ddots & & \ddots & \vdots \\ h(L) & \vdots & \ddots & \ddots & & h(L) \\ 0 & h(L) & \vdots & \ddots & \ddots & \vdots \\ \vdots & \ddots & \ddots & \vdots & \ddots & 0 \\ 0 & \dots & 0 & h(L) & \dots & h(0) \end{bmatrix}.$$

The matrix $\tilde{\boldsymbol{H}}$ is circulant and as such can be diagonalized [12] by the N-point Discrete Fourier Transform pair as

$$\boldsymbol{\Lambda} = \boldsymbol{Q}\tilde{\boldsymbol{H}}\boldsymbol{Q}^{\mathrm{H}} = \begin{bmatrix} \lambda_0 & & \\ & \ddots & \\ & & \lambda_{N-1} \end{bmatrix}$$

where

$$\boldsymbol{Q} = \frac{1}{\sqrt{N}} \begin{bmatrix} 1 & 1 & 1 & \dots & 1 \\ 1 & w & w^2 & \dots & w^{N-1} \\ 1 & w^2 & w^4 & \dots & w^{2(N-1)} \\ \vdots & \vdots & \vdots & & \vdots \\ 1 & w^{N-1} & w^{2(N-1)} & \dots & w^{(N-1)^2} \end{bmatrix}.$$

and $\boldsymbol{Q}^{\mathrm{H}}$ is its conjugate transpose.

The fact that $\tilde{\boldsymbol{H}}$ is diagonalized by the DFT leads to the structures for transmitter and receiver as follows. Let $\boldsymbol{x} = \begin{bmatrix} x_0, & \dots, & x_{N-1} \end{bmatrix}^{\mathrm{T}}$ be a vector collecting multiple complex symbols, such as defined in (1.1). Choose $\boldsymbol{s} = \boldsymbol{Q}^{\mathrm{H}}\boldsymbol{x}$ and

$\boldsymbol{y} = \boldsymbol{Qr}$ to obtain

$$\boldsymbol{y} = \boldsymbol{Qr} = \boldsymbol{QRHAs} = \underbrace{\boldsymbol{QR}}_{\text{receiver}}\ \boldsymbol{H}\ \underbrace{\boldsymbol{AQ}^{\mathrm{H}}}_{\text{transmitter}}\ \boldsymbol{x} = \boldsymbol{\Lambda x} = \begin{bmatrix} \lambda_0 x_0 \\ \vdots \\ \lambda_{N-1} x_{N-1} \end{bmatrix}. \tag{1.5}$$

Instead of transmitting the complex QAM symbols serially at a high rate, a multicarrier system groups a number of symbols and transmits then in parallel. The addition of a cyclic prefix and the IDFT operation at the transmitter, coupled with the cyclic prefix removal and DFT at the receiver diagonalize the channel. For a long enough cyclic prefix, this scheme removes ISI and ICI simultaneously.

The channel diagonalization described in (1.5) establishes at most N independent complex channels between transmitter and receiver. Their transfer functions are given by

$$\begin{bmatrix} \lambda_0 \\ \lambda_1 \\ \vdots \\ \lambda_{N-1} \end{bmatrix} = \sqrt{N}\boldsymbol{Q} \begin{bmatrix} h(0) \\ h(1) \\ \vdots \\ h(L-1) \\ 0 \\ \vdots \\ 0 \end{bmatrix}, \tag{1.6}$$

which is a discrete Fourier transform of the channel impulse response. The parallel complex channels are referred in literature and in the remainder of this thesis as "subcarriers", "subchannels" or "tones" interchangeably.

Frequency selective channels such as twisted pairs or a radio channel have a non-flat transfer function over the system's bandwidth. The channel partitioning performed by OFDM/DMT causes this broadband channel to be evaluated at regularly-spaced discrete frequencies. This is exemplified in Fig. 1.3. The blue solid curve represents the magnitude of the transfer function of a real twisted pair channel from around DC to 6.5 MHz. A hypothetical multicarrier system with $N = 8$ would experience parallel channels defined by the red dots. The phase response is not shown in the plot.

The plot in Fig. 1.3 also illustrates another important aspect of multicarrier modulation. Since the subchannels are independent, each one can be optimized according to its own signal-to-noise ratio. In other words, subchannels with low attenuation and low noise can use very high modulation orders. Some DSL technologies, for example, employ constellations of up to 15 bits [2–4]. The opposite condition is also true. When a given subcarrier has poor signal-to-noise ratio it will carry low-order constellations or be deactivated entirely.

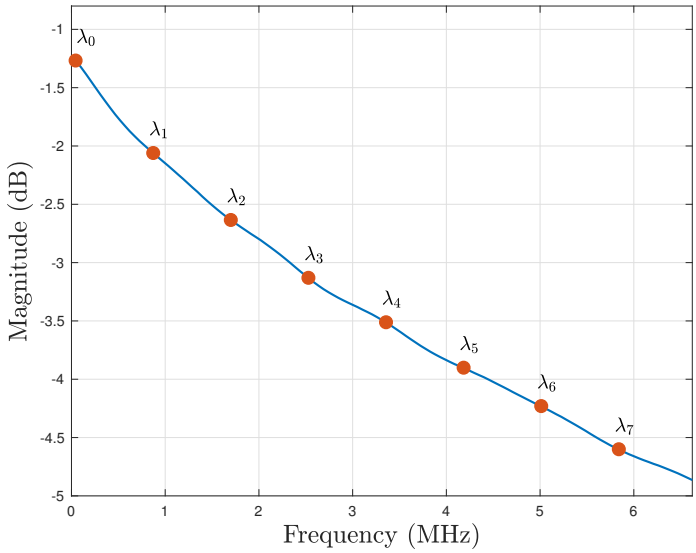

Figure 1.3: An example of measured frequency selective channel, with superimposed discrete subchannels, for a system with $N = 8$. The blue solid line represents a twisted pair's transfer function magnitude. The magnitude of the flat subchannels is represented by the red circles.

HARDWARE IMPLEMENTATION

The implementation of multicarrier OFDM/DMT transceivers requires an IDFT operation at the transmitter and a DFT at the receiver. These are both performed via the Fast Fourier Transform (FFT) algorithm [14] and benefit from its low-complexity properties.

Another consequence of (1.5) is a significant reduction of receiver hardware complexity, because the equalization process (the removal of channel influence) can be performed per subcarrier as

$$\hat{x}_k = \frac{1}{\hat{\lambda}_k} y_k, \tag{1.7}$$

where k is the subcarrier index, $\hat{x}_k$ represents an estimate of the transmitted symbol and $\hat{\lambda}$ an estimate of the channel transfer function.

DIFFERENCES BETWEEN OFDM AND DMT

Up to now multicarrier modulation has been presented without addressing the differences between OFDM, used for instance in radio systems and DMT,

used in wireline systems. From a baseband implementation perspective, both techniques are very similar. Both exploit the DFT pair and cyclic prefixes as shown in (1.5).

The main differences come from the characteristics of the channels addressed by these techniques. DMT is commonly used in wireline channels, where the signalling is done in baseband. In other words, the transmit DMT transmit multiplex signal $s(t)$ is not modulated (shifted) by a carrier frequency.

As a consequence of the baseband signalling, the output of a DMT transmitter must be real valued. To assure this, DMT imposes the condition that the transmit symbol vector $\boldsymbol{x}$ has hermitian symmetry. When a DMT transmitter is implemented with an N-point FFT the number of available subcarriers is reduced[2] to $\approx \frac{N}{2}$.

Radio channels on the other hand are passband. The implementer typically has access to a band-limited channel around a carrier frequency. WiFi transmitters, for example, often use carrier frequencies of 2.4 or 5 GHz. The baseband OFDM signal is used to modulate the amplitude and phase of a sinusoid at the desired carrier frequency. Since both amplitude and phase can be manipulated, the OFDM transmit multiplex is complex valued. Due to the absence of the hermitian symmetry requirement for OFDM, the number of useful subcarriers is the same as the number of bins in the FFT. On the other hand, due to the modulation to the carrier frequency, an OFDM system occupies twice the bandwidth required by a DMT transmitter using the same FFT size.

A major difference between the two systems is the availability of channel information at the transmitter. Wireline channels have much longer coherence times than radio channels. As a result, in DMT systems it is usual that the transmitter have fairly good channel estimates. These channel estimates are used by the DMT modems to optimize how much power is allocated to each subchannel and what modulation order to use (a process called bit-loading).

In OFDM systems, due to the channel being time-variant, the amount of channel information available at the transmitter is limited. As a consequence, OFDM transmitters use the same modulation order over blocks of subcarriers, coupled with strong error correcting coding schemes.

In parts I and II of this thesis, the contributions address DMT systems. In part III an OFDM system is coupled to a copper channel to enable the deployment of indoor cellular systems.

[2]Two of the available subchannels are real valued and typically not used.

1.2 TWISTED-PAIR CHANNELS

The introduction of twisted-pairs and differential signalling led to widespread development in fixed telephony. Twisted-pairs have been employed ever since, in later years finding use in DSL systems and other indoor systems such as the twisted pair profiles of Ethernet. In this section, a short description of the important parameters will be presented, while a more complete treatment is given in [13] [15] [16].

The use of twisted pairs and differential signalling improve the resiliency of transmission when compared to a common-mode approach. In differential signalling system, the signal is transmitted with opposite polarity in each of the conductors. The receiver takes the difference between both signals, reducing the effect of common mode interference.

An ideal twisted pair can be modelled as an uniform transmission line. The pair is described as a concatenation of infinitely short line segments as the one presented in Fig. 1.4.

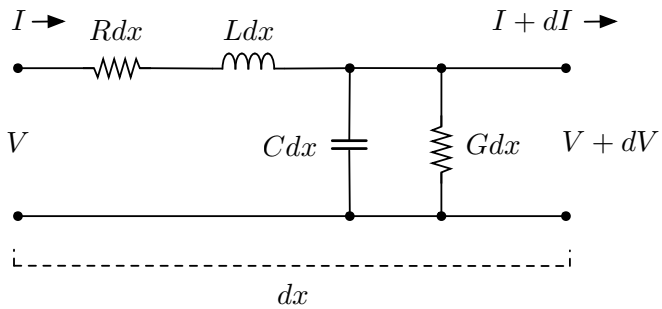

Figure 1.4: A uniform transmission line segment of length dx. The voltage and current at the input of the line segment are represented by V, I, respectively. The line segment can be thought of as a dissipative low-pass filter.

The so-called primary parameters R, L, C, G represent, respectively, the distributed resistance, inductance, capacitance and conductance. In turn, these can be used to derive the secondary parameters, namely, the characteristic impedance Z_0 and the propagation constant γ as

$$\begin{aligned} \gamma(\omega) &= \sqrt{(R + jL\omega)\,(G + jC\omega)} \\ Z_0(\omega) &= \sqrt{\frac{R + jL\omega}{G + jC\omega}} \end{aligned} \tag{1.8}$$

where ω represents the angular frequency. If the transmission line is terminated by an impedance Z_L, we can obtain the reflection coefficient as

$$\rho = \frac{Z_L - Z_0}{Z_L + Z_0}. \tag{1.9}$$

The reflection coefficient expresses the ratio between incident and reflected waves for a uniform transmission line. An important consequence of this definition is that, if the load of the line equals its characteristic impedance, the reflected wave vanishes. The matching between load and line impedance is very significant for vectored DSL systems (see Sec. 1.3). Transitions in the matching condition lead to changes in the channel properties that may negatively impact multiuser signal processing algorithms. The implications of this are explored in chapters 2 to 4.

In practice, real cables deviate from the uniform transmission line assumptions, especially as the length of the cable increases beyond tens of meters. Due to manufacturing tolerances the dimensions of conductors, insulation and the twist-rate vary [17–22]. Besides that, external factors such as handling, installation and age may further influence the properties of a twisted pair.

There is extensive literature modelling the characteristics of twisted-pairs, some examples including [23–29]. The main use of such models is to predict the capacity of DSL systems deployed over different topologies. Cable models are also used in loop[3] diagnostic and loop make-up identification methods. The basic idea is to probe the lines and analyze reflected signals to determine the location of faults or the parameters associated with sections of a loop [30] [31]. A good comparison between cable models is presented in [28].

While cable models vary in many ways, most are based on the equivalence between a twisted-pair and uniform transmission lines. This leads to a good match between model and the *average* behavior of cables, but fail to capture effects of non-uniformities [18] [22] [27].

Chapters 6 and 8 present contributions related to how the twisted pairs are influenced by environmental factors and consequences to the functioning of vectored systems.

1.2.1 CROSSTALK

Due to the proximity between pairs in a cable, signals transmitted in one pair leak to the ones nearby. The term *crosstalk* is commonly used to denote both the power leaked from one line to the next as the coupling path itself. The magnitude of crosstalk paths is influenced by the proximity between pairs (an

[3] A concatenation of cable sections connecting transmitter and receiver.

adjacent pairs is usually the stronger source of interference) and by the length of the shared cable section.

Suppose a cable with two pairs is under consideration. At one end of the cable, each pair is connected to equipment transmitting signals to a receiver on the opposite end. This situation is presented in schematic form in Fig. 1.5. The coupling between the first transmitter and equipment connected to the same cable extremity is referred to as near-end crosstalk (NEXT). The coupling between the first transmitter (TX1) and the opposite receiver (RX_2 in the figure) is termed far-end crosstalk (FEXT).

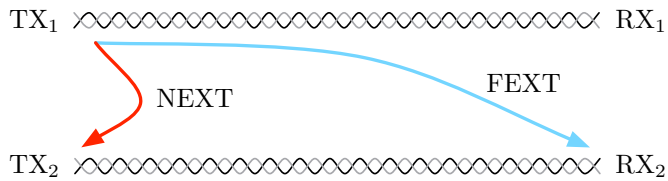

Figure 1.5: A schematic description of NEXT and FEXT between two pairs. For near-end crosstalk the source of interference and victim are connected at the same cable end. For far-end crosstalk the opposite is true.

The negative influence of near-end crosstalk can be mitigated if the transmitters are synchronized. If that is not the case an alternative is to use different bands for communicating in uplink and downlink directions. Similarly, FEXT can be suppressed efficiently if synchronous transmission and some multi-user processing is used (see Sec. 1.3). In case the coordination between transceivers is not possible, the effective reach or capacity will be limited by crosstalk.

Models for crosstalk are discussed in e.g. [22] [32–35].

1.3 VECTORED DMT SYSTEMS

Historically, the copper line connections between telephone exchanges and end-user homes were built in tree structures. Immense cable bundles would leave an operators' central office (CO) and gradually branch out geographically down to one of a few twisted-pairs connecting individual homes.

When DMT transceivers became available in the early nineties, this copper line tree structure was used to deploy DSL equipment to provide Internet access at much higher speeds than voiceband modems could achieve. Successive generations of standards have increased the bandwidth, resiliency and flexibility of the technology, while also introducing new terminology. A brief

summary is given here

- The modem in a user's home is usually referred to as *customer premises equipment* (CPE).
- The equipment connecting many CPEs to the operator's network is a *Digital Subscriber Line Access Multiplexer* (DSLAM) or a *Distribution Point Unit* (DPU).
- Communication from the DPU to a CPE is said to be in *downstream* direction.
- Communication from a CPE to the DPU is said to be in *upstream* direction.

While each CPE contains a single DMT transceiver, a DPU contains many. If we consider an isolated system where a single DPU is connected to a plurality of CPEs, all transmitters in downstream direction and all receivers in upstream direction are colocated. An example with three CPEs is shown in Fig. 1.6.

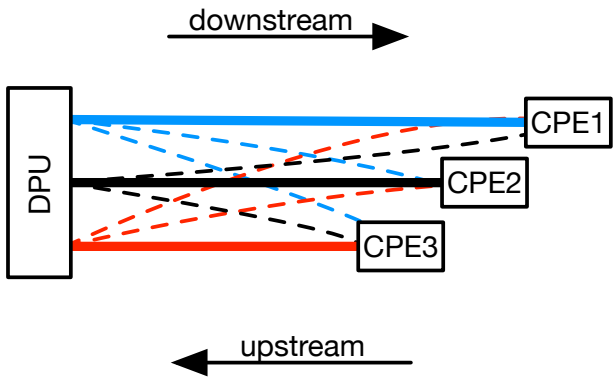

Figure 1.6: A diagram illustrating a wireline access deployment with tree subscribers. The DPU contains multiple DMT transceivers, making each transmitter for the downstream and each receiver to the upstream directions collocated. The direct paths between transmitter and receiver are represented as solid lines, while far-end crosstalk is shown in dashed lines.

Due to the proximity between twisted-pairs in a cable bundle, the signal transmitted between the DPU and any of the CPEs will induce currents in neighboring pairs. As a result, not only is the signal transferred to the intended recipient, but also to other modems in the system. In Fig. 1.6 this is represented by dashed lines.

The input-output relationship between all pairs connected to a DPU can be thought of as a multiple-input multiple-output (MIMO) channel. If the DMT transceivers connected to each twisted pair are synchronized, this MIMO channel can be modelled per subcarrier as

$$\underline{\boldsymbol{y}} = \underline{\boldsymbol{H}}\underline{\boldsymbol{x}} + \underline{\boldsymbol{z}}, \tag{1.10}$$

where the vectors $\underline{\boldsymbol{x}} = \left[\underline{x}_1, \ \ldots, \ \underline{x}_U\right]^{\mathrm{T}}$, $\underline{\boldsymbol{y}} = \left[\underline{y}_1, \ \ldots, \ \underline{y}_U\right]^{\mathrm{T}}$ and $\underline{\boldsymbol{z}} = \left[\underline{z}_1, \ \ldots, \ \underline{z}_U\right]^{\mathrm{T}}$ collect, respectively, the transmit symbols, the received symbols and additive noise in each of the U pairs connected to a DPU. The complex channel gains between transmitter j and receiver i are represented as the elements $\underline{\boldsymbol{H}}_{i,j}$ of the square matrix $\underline{\boldsymbol{H}}$.

The received symbol at receiver i is

$$\underline{y}_i = \underline{H}_{i,i}\underline{x}_i + \underbrace{\sum_{i \neq j} \underline{H}_{i,j}\underline{x}_j}_{\text{crosstalk}} + \underline{z}_i. \tag{1.11}$$

The crosstalk term, highlighted in the previous equation is significant, being a major impairment to high data rate transmission in DSL systems.

If transmitters are not synchronized, but some channel information is available, the power allocation per user can be optimized, for example, to maximize rate or minimize power while offering a desired quality of service. Some examples are given in [36–39].

With the intention of mitigating the negative effect of crosstalk and taking advantage of collocated, synchronized transceivers at the DPU, a technique termed *vectoring* was introduced [40] [41]. The main idea in downstream is to use channel information (estimates) at the transmitter to precode (pre-distort) the transmit symbols so that the crosstalk contribution is cancelled out at the output of the channel. Similar crosstalk mitigation can be achieved in upstream by jointly equalizing the received symbols from multiple users at the DPU.

For frequencies up to around 30 MHz, a zero-forcing-based precoder and equalizers were shown to be near optimal in [42] [43]. For downstream, the precoder has the form

$$\boldsymbol{P} = (1/\eta)\, \underline{\boldsymbol{H}}^{-1} \mathrm{diag}\{\underline{H}_{1,1}, \ldots, \underline{H}_{U,U}\}, \tag{1.12}$$

where η is a normalization factor and $\text{diag}\{\underline{H}_{1,1}, \ldots, \underline{H}_{U,U}\}$ represents a diagonal matrix with elements $\underline{H}_{1,1}, \ldots, \underline{H}_{U,U}$ along its main diagonal. The precoding operation with (1.12) leads to the channel output

$$\begin{aligned} \underline{\boldsymbol{y}} &= \underline{\boldsymbol{H}}\boldsymbol{P}\underline{\boldsymbol{x}} + \underline{\boldsymbol{z}} \\ &= (1/\eta)\,\text{diag}\{\underline{H}_{1,1}, \ldots, \underline{H}_{U,U}\}\underline{\boldsymbol{x}} + \underline{\boldsymbol{z}} \end{aligned} \tag{1.13}$$

where the crosstalk terms have been removed and the equivalent channel for each CPE is a scaled version of its original direct path gain.

To ensure that DSL systems do not interfere with other services, the standard compliant modems are subject to limitations on the total transmit power as well as maximum transmit power per subcarrier. The per subcarrier limit is usually referred to as a *power spectrum density* (PSD) *mask* (for an example see [44]).

If a transceiver is already using close to the per-subcarrier PSD mask, the precoding operation can lead to violations of the power constraint. One way to avoid this is to introduce the normalization step, choosing η as

$$\eta = \max_i \left\| \left[\underline{\boldsymbol{H}}^{-1} \text{diag}\{\underline{H}_{1,1}, \ldots, \underline{H}_{U,U}\} \right]_{\text{row } i} \right\| \tag{1.14}$$

This scheme is near optimal for diagonally dominant channels and it has a low complexity when compared with alternatives such as the Tomlinson-Harashima precoder (THP) [40] [45] [46].

At low enough frequencies ($\leq$ 30 MHz), most copper channel matrices exhibit a high degree of diagonal dominance, indicating that the direct paths between DPU and CPE attenuate the signals much less than the crosstalk paths. This is illustrated using measured channels in Fig. 1.7.

With the development of the G.fast standard, the wireline access industry decided to target shorter copper lines, taking advantage of the rollout of fiber to distribution points close to the end user. With shorter copper pairs, bandwidths of hundreds of MHz became available. As seen in Fig. 1.7, for these high frequencies, the direct channel gains get closer to the magnitude of the crosstalk paths. To cope with the smaller degree of diagonal dominance, while using a linear zero-forcing precoder, some alternatives were proposed in [47] [48]. Joint optimization of precoder, power allocation and equalizers is discussed in [49].

The introduction of G.fast also brought power-saving features, allowing transceivers to be inactivated while there is no data to be transmitted [5] [50]. The presence of unused lines led to the idea of designing precoders such that the crosstalk channels could be exploited to *boost* the signal to groups of users [51].

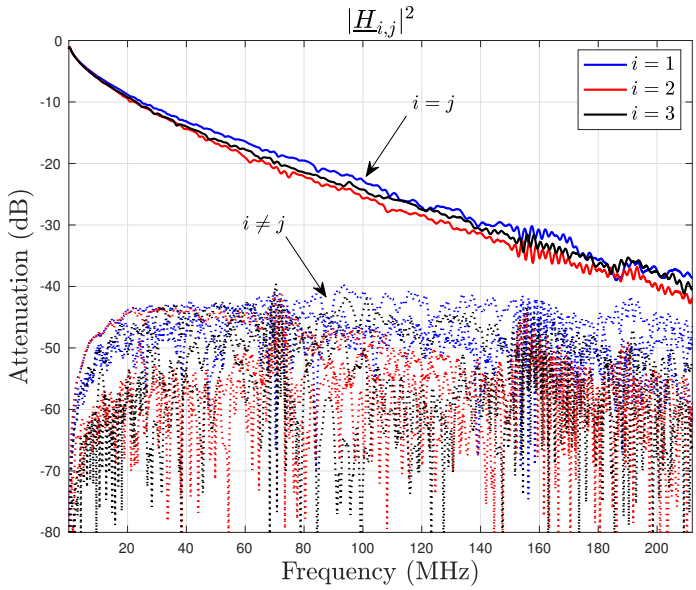

Figure 1.7: Plot of the transfer function magnitudes for three twisted-pairs. Both direct (solid lines) and crosstalk paths (points) are displayed, color-coded by the receiver number i. At low frequencies, the direct paths clearly dominate over crosstalk. The degree of diagonal dominance decreases as frequency increases.

What most precoder (and equalizer) designs have in common is the need for accurate channel estimates. When there is a mismatch between the true channel and the channel estimates, the performance will be affected by *residual crosstalk* [52].

1.4 RESEARCH CONTRIBUTIONS

This section present a summary of the research contributions aggregated in this dissertation. It is divided in three parts. The contributions of part I deal with the impact of impedance changes at the termination of twisted pairs, some of which are connected to a vectored system, leading to channel variations and therefore mismatched precoders.

A second part of the thesis covers the impact of environmental effects on copper channels, such as temperature variations. It also investigates the reuse of channel estimates to shorten the time a vectored system takes to initialize by shortening the channel estimate acquisition process.

Lastly in part III, the subject of crosstalk mitigation in an analog radio-over-copper system is presented. One of the contributions is the development of a channel estimation method using the pilot symbols already embedded in the radio signal.

1.4.1 PART I - SIDE EFFECTS OF IMPEDANCE CHANGES TO VECTORED WIRELINE SYSTEMS

The capacity of wireline multicarrier transceivers has improved over time, by among other means, transmitting over higher and higher bandwidths. Another factor driving the increased speeds is the use of joint multi-user processing (vectoring).

During the development of the latest ITU standard for wireline access, named G.fast [5], both increased bandwidths and improved vectoring algorithms were explored. This has enabled the maximum aggregated capacity to improve from around 100 Mbps in VDSL2 to more than 1 Gbps. It also brought up a new set of unforeseen challenges.

In a well functioning vectored system, the transmitter or receiver uses channel estimates to either precode or post-cancel (equalize) the crosstalk from neighboring lines. Usually, the channel is estimated between each pair of transmitter and receiver in the system. The resulting MIMO channel estimate is used to design signal processing algorithms that, for example, diagonalize the channel.

Sudden changes in the channel characteristics cause a mismatch between the crosstalk mitigation algorithms and the channel, leading to performance degradation in the form of residual crosstalk. Compared with wireless channels, the twisted pair changes slowly, often due to environmental effects.

While the transmission line properties might be unchanged, the impedances of the devices connected to it might. A simple example of this is the different impedances of a telephone set when it is taken on or off-hook.

During the VDSL2 era, the changes in impedance were identified as a source of problems and methods were suggested to address situations that occur when a modem that is part of a vectored group change impedance [53].

In G.fast the same problems were observed but with more gravity. If an impedance change occurs even in a line that is not part of a vectored group, all lines in the vectored set would have its channel coefficients changed. This problem is identified, modelled and solved in papers I to III of this thesis.

PAPER I: HOW VECTORING IN G.FAST MAY CAUSE NEIGHBORHOOD WARS

When modems are turned on/off or unplugged from the twisted-pair, the impedance terminating that particular circuit changes. If the modem in question is part of a vectored system, the channel estimates used to design precoders will be outdated. To avoid residual crosstalk, some solutions were proposed to guarantee that before a modem leaves a vectored group, others can prepare by, for example, experiencing the impedance change during training symbols [54].

However, when vectored wireline systems are deployed, there is no guarantee that all copper pairs in a bundle will be part of a vectored group (not all lines may be managed, or even be connected to DSL service).

This paper presents measurements evidencing the severe impact of changes to loads terminating twisted pairs that are **outside** vectored groups. A practical situation where this might occur is a neighborhood where a high-frequency vectored system is deployed, but some houses connected to the distribution point do not sign up. If one of the non-subscriber neighbors pick up his phone, the change in impedance could seriously affect the quality of service for the vectored lines. Besides measurements, the paper discusses the feasibility of recovering from such an impedance change event using a decision-directed channel estimation method in upstream.

I am the main author of the paper, having conducted measurements, simulations and writing. The paper was published in *Proc. IEEE International Conference on Communications (ICC 2014)*, Sydney, NSW, 10-14 Jun. 2014.

This paper received the following accolades

- IEEE ICC 2014 Best Paper Award,
- Best Paper Award in Transmission, Access Networks and Systems, by the IEEE TAOS Committee - 2014.

The contents of this paper were also presented as a contribution to the ITU SG15 workgroup standardizing G.fast.

PAPER II: MODELING ALIEN-LINE IMPEDANCE-MISMATCH IN WIDEBAND VECTORED WIRELINE SYSTEMS

This letter presents a model that explains why the changes in termination impedances cause negative effects to neighboring vectored lines (reported in paper I). In brief, if the impedance changes from a matched state to unmatched, the end of the line starts to reflect incoming signals and the reflected

signal couples to the neighboring lines via near-end crosstalk paths. The proposed model is verified with channel measurements and the model's error sources are also discussed.

I am the main author of this paper, having conducted measurements, simulations and writing. The letter was published in *IEEE Communications Letters*, vol. 18, no. 9, September 2014.

PAPER III: MITIGATING DISORDERLY LEAVING EVENTS IN G.FAST

When a line in a vectored group is powered off it can conduct an "orderly leave" procedure [54], essentially allowing the other modems to estimate the channel in the state it will be once it is powered off and its analog front-end has its impedance changed.

This paper treats cases where a *disorderly leave* event occurs. In this situation, the resulting channel matrix can be modelled by the contribution presented in paper II. Here in paper III we observe that, if a modem changes impedance abruptly and the change is detected, an efficient precoder update procedure can be performed that restores stability. The precoder update is proposed, simulated and verified in accordance with the G.fast standardized pilot symbols and timing. The proposed method shortens the time to update the precoder and reduces the complexity of the estimation procedure from quadratic to linear in the number of vectored lines.

I have conducted measurements and contributed to the development of the results and to the writing. The paper was published in *Proc. IEEE International Conference on Communications (ICC 2015)*, London, United Kingdom, 08-12 Jun. 2015.

This paper received the following accolades

- IEEE ICC 2015 Best Paper Award,
- Best Paper Award in Transmission, Access Networks and Systems, by the IEEE TAOS Committee - 2015.

PAPER IV - MITIGATION OF ALIEN CROSSTALK FOR DOWNSTREAM DSL IMPAIRED BY MULTIPLE INTERFERERS

When not all copper pairs in a cable are connected to a vectored system, the crosstalk signals from these unmanaged lines will not be cancelled by the precoder/equalizer. The crosstalk from unmanaged sources is referred to as *alien crosstalk*.

This letter proposes a method to mitigate the negative influence of alien crosstalk. In particular it is applicable to situations where there are multiple sources of alien crosstalk and more than one pair at the victim line.

I took part in discussions developing the results and contributed to the writing. The letter was published in *IEEE Communications Letters*, vol. 21, no. 11, November 2017.

1.4.2 PART II - EFFECTS OF TEMPERATURE CHANGES ON WIRELINE CHANNELS

This part addresses the effect that temperature changes have on the wireline channel. Temperature changes have always been around but their effect has gotten renewed attention as the frequency range that is used by wireline broadband systems has increased. Traditionally, single user systems will acquire channel information between transmitter and receiver once powered-on. This channel estimation is used to decide what modulation to use and also serves to train or adapt equalizers that eliminate the influence of the channel on transmitted symbols. In a vectored system, this is more complicated because not only the direct paths, but also the interference paths must be estimated. All of these change if the temperatures of the lines change.

In this part we present three contributions with special attention given to temperature. A first contribution, Paper V, is related to the design of initialization methods in wireline systems and channel tracking. In particular, we will focus on the shortening of VDSL2 initialization through reuse of channel estimates and spectral protection and the effects of temperature changes to the performance of twisted pairs. This paper spawned our interest in the importance of temperature changes and led to the in-depth studies of Paper VI and VII.

A reader somewhat familiar with G.fast may think that the new paradigm of reverse power feeding, a standardized option for G.fast where the DPU draws power over the copper lines from the CPEs in the homes, has contributed to the new interest in temperature changes of the lines. However, although the dissipated power does warm the lines, it is insignificant compared to temperature changes due to for instance weather. The power dissipated due to the reverse power feeding is only in the order of 1 W over 100 meters of copper line.

PAPER V - ANALYSIS OF FAST INITIALIZATION FOR VECTORED WIRELINE SYSTEMS

This paper proposes a fast initialization scheme for VDSL2 based on spectral protection. Two scenarios are considered, where in the first one no prior channel information is available. The second one is based on erroneous prior knowledge of channel coefficients being available, for instance acquired when the transmission lines had a different temperature. Measurements on a com-

mercial VDSL2 vectoring platform and throughput simulations are used to evaluate the feasibility of the proposed scheme.

I have conducted measurements, participated in the discussions that developed the ideas and contributed to the writing. The paper was published in *Proc. IEEE Global Communications Conference (GLOBECOM 2013)*, Atlanta, USA, 9-13 Dec. 2013.

PAPER VI - THE COLD CABLES CASE

This paper responds to the question: by how much do copper cables change when temperature changes? The paper presents measurements over a broad temperature range quantifying the effect on cable attenuation over frequency for two cables commonly deployed in the United Kingdom. The paper also attempts to give practical advice for how to adapt commonly used channel models so that they can reflect temperature changes, as well as how to adjust any available channel measurement taken at one temperature so that it reflects the same channel at a different temperature.

I am the main author, having presented the main ideas and conducted measurements, simulations and writing. This paper has not been published.

PAPER VII - TEMPERATURE-DEPENDENT SHIFT OF NOTCHES IN THE FREQUENCY RESPONSE OF TWISTED-PAIRS

A second result extracted from the same set of measurements explain how dips in the frequency response shift in frequency as temperature changes. The result is interesting as it may seem counterintuitive. A line that warms up becomes longer as the conducting metal expands, thus it would be natural to assume that it would take longer for a signal to traverse the line. However, this does not seem to be the case. Furthermore, when the conducting metal expands, the distance between the reflection points that cause dips in the frequency response also increase, corresponding to a larger wavelength, which should move the dips in the frequency response down in frequency. However, the notches in the transfer function move up in frequency, by as much as 1 MHz over a 85 degrees Celsius temperature increase. The paper suggests that the propagation velocity of the signal increases so much due to the temperature shift that it overwhelms the effects of the expanding metal. The propagation velocity depends largely on the dielectric, the plastic that insulates the cables. A similar result can be found for coaxial cables in [55] [56].

I am the main author, having presented the main ideas and conducted measurements, simulations and writing. This paper has not been published.

1.4.3 PART III - COMBINATIONS OF RADIO AND FIXED COMMUNICATION SYSTEMS

The last part of this thesis investigates the use of twisted-pairs to deliver indoors wireless service. Since the copper network has considerable penetration in many markets it is a viable infrastructure for connecting small cells and increase the capacity of 3GPP compliant networks.

As discussed in previous sections, OFDM and DMT share many properties, differing in the channel types each one targets. The main idea explored by the papers in this part is to deliver OFDM-based radio access by deploying a radio-head (a component with antennas and some RF processing capabilities) at a user's home. The radio signal, converted to appropriate frequencies, is transmitted using twisted-pairs to a nearby cabinet and from there connected to the core network where baseband processing and other functions are done.

The contributions cover the development of a radio-over-copper solution over twisted-pairs, the development and analysis of a 3GPP compliant radio-head and the development of a method estimate the MIMO copper channel and mitigate the crosstalk between multiple cells, using the standardized pilot symbols already present in the radio signal.

PAPER VIII - ENABLING DSL AND RADIO ON THE SAME COPPER PAIR

This paper proposes to use twisted-pairs to deploy an analog radio-over-copper solution. The system is cabinet-based, collocated with VDSL2 and uses small pieces of spectrum next to VDSL2. Instead of modulating the radio signal to the desired carrier frequency, the signal is shifted to a carrier frequency adequate for copper transmission. At the end-user premises, the radio head performs RF conversion to the proper LTE bands. The paper investigates the feasibility of the concept and analyses the reach of such a solution.

I contributed to the development of ideas, simulations and writing. The paper was published in *Proc. IEEE International Conference on Communications (ICC 2015)*, London, United Kingdom, 08-12 Jun. 2015.

PAPER IX - LTE OVER COPPER - POTENTIAL AND LIMITATIONS

This paper discusses the design of radio-heads for radio-over-copper systems such as the one proposed in paper VII. The investigation considers 3GPP requirements and assumes that the radio-head is connected to a single twisted-pair through an imperfect hybrid circuit. The adjacent channel leakage ratio and error vector magnitude requirements lead to results in what filter designs the radio-head should be equipped with.

I contributed to the development of ideas, simulations and writing. The

paper was published in *Proc. IEEE Symposium on Personal, Indoor and Mobile Radio Communications - (PIMRC)*, Hong Kong, China, 30 Aug. - 03 Sep. 2015.

PAPER X - CROSSTALK MITIGATION FOR LTE-OVER-COPPER IN DOWNLINK DIRECTION

In this last paper, we address the issue of crosstalk mitigation in LTE-over-copper systems. By taking advantage of reference symbols present in the downlink LTE signals we propose two methods for estimating the copper channel. System performance is evaluated using channel measurements and error vector magnitude calculations with promising results.

I am the main author, having proposed the main idea, conducted measurements, simulations and writing. Published in *IEEE Communications Letters*, vol. 20, no. 7, July 2016.

PATENT APPLICATION - METHODS AND NODES OF A WIRELESS COMMUNICATION NETWORK FOR MITIGATING CROSSTALK IN A BASE STATION SYSTEM

The work developed in paper IX was the subject of a patent application named "Methods and Nodes of a Wireless Communication Network for Mitigating Crosstalk in a Base Station System", also included in the thesis.

I am the main author, having proposed the main idea, conducted measurements, simulations and writing. The application has been disclosed and is under evaluation by the European Patent Office.

References

[1] *Asymmetric digital subscriber line (ADSL) transceivers*, ITU Recommendation G.992.1, Jun. 1999. [Online]. Available: http://www.itu.int/rec/T-REC-G.992.1

[2] *Asymmetric digital subscriber line transceivers 2 (ADSL2)*, ITU Recommendation G.992.3, Apr. 2009. [Online]. Available: http://www.itu.int/rec/T-REC-G.992.3

[3] *Asymmetric digital subscriber line transceivers 2 (ADSL2) - Extended bandwidth (ADSL2plus)*, ITU Recommendation G.992.5, Jan. 2009. [Online]. Available: http://www.itu.int/rec/T-REC-G.992.5

[4] *Very high speed digital subscriber line transceivers 2 (VDSL2)*, ITU Recommendation ITU-T G.993.2, Jan. 2015. [Online]. Available: http://www.itu.int/rec/T-REC-G.993.2

[5] *Fast access to subscriber terminals (G.fast) - Physical layer specification*, ITU Recommendation ITU-T G.9701, Dec. 2014. [Online]. Available: http://www.itu.int/rec/T-REC-G.9701

[6] *LTE; Evolved Universal Terrestrial Radio Access (E-UTRA); LTE physical layer; General description*, 3rd Generation Partnership Project (3GPP) TS 36.201 V14.1.0, Apr. 2017. [Online]. Available: http://goo.gl/7swwPm

[7] "IEEE Standard for Information technology - Telecommunications and information exchange between systems Local and metropolitan area networks - Specific requirements - Part 11: Wireless LAN Medium Access Control (MAC) and Physical Layer (PHY) Specifications," *IEEE Std 802.11-2016 (Revision of IEEE Std 802.11-2012)*, Dec. 2016. [Online]. Available: http://ieeexplore.ieee.org/document/7786995/

[8] S. B. Weinstein, "The history of orthogonal frequency-division multiplexing [history of communications]," *IEEE Communications Magazine*, vol. 47, no. 11, pp. 26–35, Nov. 2009. [Online]. Available: http://dx.doi.org/10.1109/MCOM.2009.5307460

[9] L. Hanzo, W. Webb, and T. Keller, *Single-and multi-carrier quadrature amplitude modulation: principles and applications for personal communications, WLANs and broadcasting*. John Wiley & Sons, 2000.

[10] J. G. Proakis, *Digital Communications*, 4th ed. McGraw-Hill, 2001.

[11] T. Magesacher, Ed., *OFDM for Broadband Communication - Course Reader (EIT 140)*. Lund University, 2013. [Online]. Available: http://goo.gl/aUEjoR

[12] J. M. Cioffi, *Advanced Digital Communication*. Stanford University. [Online]. Available: http://web.stanford.edu/group/cioffi/doc/book/

[13] P. Golden, H. Dedieu, and K. S. Jacobsen, Eds., *Fundamentals of DSL Technology*. Auerbach Publications, 2006.

[14] J. W. Cooley and J. W. Tukey, "An algorithm for the machine calculation of complex fourier series," *Mathematics of Computation*, vol. 19, no. 90, pp. 297–301, Apr. 1965. [Online]. Available: http://www.jstor.org/stable/2003354

[15] C. R. Paul, *Analysis of Multiconductor Transmission Lines*, 1st ed. John Wiley & Sons, 1994.

[16] W. Y. Chen, *DSL: Simulation Techniques and Standards Development for Digital Subscriber Lines*, 1st ed. Macmillan Technical Publishing, 1998.

[17] G. S. Borges, R. M. Rodrigues, J. C. W. A. Costa, A. Santos, and A. Fertner, "Effect of periodic cable nonuniformities on transmission measurements," in *2015 IEEE International Instrumentation and Measurement Technology Conference (I2MTC) Proceedings*, May 2015, pp. 315–319. [Online]. Available: http://www.dx.doi.org/10.1109/I2MTC.2015.7151286

[18] G. S. Borges, "Modelagem de par-trançado para comunicações em banda larga," Ph.D. dissertation, Universidade Federal do Pará, Belém, Brazil, Aug. 2016. [Online]. Available: http://goo.gl/pfk7vx

[19] A. Lago, C. M. Peñalver, J. Marcos, J. Doval-Gandoy, A. Meléndez, Ó. López, F. Santiago, F. D. Freijedo, J. M. Vilas, and J. C. Lorenzo, "Geometric analysis and manufacturing considerations for optimizing the characteristics of a twisted pair," *IEEE Transactions on Electronics Packaging Manufacturing*, vol. 32, no. 1, pp. 22–31, Jan. 2009. [Online]. Available: http://www.dx.doi.org/10.1109/TEPM.2008.2005779

[20] A. Lago, C. M. Peñalver, J. Marcos, J. Doval-Gandoy, A. A. N. Meléndez, O. Lopez, F. D. Freijedo, J. M. Vilas, and J. C. L. López, "Electrical design automation of a twisted pair to optimize the manufacturing process," *IEEE Transactions on Components, Packaging and Manufacturing Technology*, vol. 1, no. 8, pp. 1269–1281, Aug. 2011. [Online]. Available: http://www.dx.doi.org/10.1109/TCPMT.2011.2144989

[21] J. Poltz, J. Beckett, and M. Josefsson, "Near end crosstalk in twisted pair cables - a comparison of simulation versus measurement," in *2005 International Symposium on Electromagnetic Compatibility*, vol. 2, Aug. 2005, pp. 572–577. [Online]. Available: http://www.dx.doi.org/10.1109/ISEMC.2005.1513580

[22] R. Strobel, R. Stolle, and W. Utschick, "Wideband modeling of twisted-pair cables for MIMO applications," in *2013 IEEE Global Communications Conference (GLOBECOM)*, Dec. 2013, pp. 2828–2833. [Online]. Available: http://dx.doi.org/10.1109/GLOCOM.2013.6831503

[23] R. F. M. van den Brink, "Measurements and models on Dutch cables," ETSI contribution TD15, Mar. 1997.

[24] J. W. Cook, "Parametric modelling of twisted pair cables for VDSL," ETSI contribution TD22, Mar. 1996.

[25] TNO, "G.fast: Parametric cable models for specifying reference loops," ITU-T SG15 Contribution, Sep. 2011.

[26] F. Lindqvist, P. O. Börjesson, P. Ödling, S. Höst, K. Eriksson, and T. Magesacher, "Low-order and causal twisted-pair cable modeling by means of the hilbert transform," in *20TH Nordic Conference on Radio Science and Communications*, Jun. 2008, pp. 301–310. [Online]. Available: http://dx.doi.org/10.1063/1.3117107

[27] R. F. M. van den Brink, "Cable reference models for simulating metallic access networks," ETSI, TS, Jul. 1998.

[28] D. Acatauassu, S. Höst, C. Lu, M. Berg, A. Klautau, and P. O. Börjesson, "Simple and causal copper cable model suitable for G.fast frequencies," *IEEE Transactions on Communications*, vol. 62, no. 11, pp. 4040–4051, Nov. 2014. [Online]. Available: http://www.dx.doi.org/10.1109/TCOMM.2014.2364585

[29] ——, "Simple and causal twisted-pair channel models for G.fast systems," in *2013 IEEE Global Communications Conference (GLOBECOM)*, Dec. 2013, pp. 2834–2839. [Online]. Available: http://www.dx.doi.org/10.1109/GLOCOM.2013.6831504

[30] S. Galli and D. L. Waring, "Loop makeup identification via single ended testing: beyond mere loop qualification," *IEEE Journal on Selected Areas in Communications*, vol. 20, no. 5, pp. 923–935, Jun. 2002. [Online]. Available: http://dx.doi.org/10.1109/JSAC.2002.1007375

[31] F. Lindqvist, "Estimation and detection of transmission line characteristics in the copper access network," Ph.D. dissertation, Lund University, 2011. [Online]. Available: http://goo.gl/uWaUnS

[32] J. Maes, M. Guenach, and M. Peeters, "Statistical MIMO channel model for gain quantification of DSL crosstalk mitigation techniques," in *2009 IEEE International Conference on Communications (ICC)*, Jun. 2009, pp. 1–5. [Online]. Available: http://www.dx.doi.org/10.1109/ICC.2009.5199490

[33] M. Sorbara, P. Duvaut, F. Shmulyian, S. Singh, and A. Mahadevan, "Construction of a DSL-MIMO channel model for evaluation of FEXT cancellation systems in VDSL2," in *2007 IEEE Sarnoff Symposium*, Apr. 2007, pp. 1–6. [Online]. Available: http://www.dx.doi.org/10.1109/SARNOF.2007.4567335

[34] B. Lee, J. M. Cioffi, S. Jagannathan, K. Seong, Y. Kim, M. Mohseni, and M. H. Brady, "Binder MIMO channels," *IEEE Transactions on Communications*, vol. 55, no. 8, pp. 1617–1628, Aug. 2007. [Online]. Available: http://www.dx.doi.org/10.1109/TCOMM.2007.902597

[35] R. F. M. van den Brink, "Modeling the dual-slope behavior of in-quad EL-FEXT in twisted pair quad cables," *IEEE Transactions on Communications*, vol. 65, no. 5, pp. 2153–2163, May 2017. [Online]. Available: http://www.dx.doi.org/10.1109/TCOMM.2017.2669032

[36] W. Yu, G. Ginis, and J. M. Cioffi, "Distributed multiuser power control for digital subscriber lines," *IEEE Journal on Selected Areas in Communications*, vol. 20, no. 5, pp. 1105–1115, Jun. 2002. [Online]. Available: http://www.dx.doi.org/10.1109/JSAC.2002.1007390

[37] R. Cendrillon, M. Moonen, J. Verlinden, T. Bostoen, and W. Yu, "Optimal multiuser spectrum management for digital subscriber lines," in *2004 IEEE International Conference on Communications (ICC)*, vol. 1, 2004, pp. 1–5. [Online]. Available: http://www.dx.doi.org/10.1109/ICC.2004.1312441

[38] R. Cendrillon and M. Moonen, "Iterative spectrum balancing for digital subscriber lines," in *2005 IEEE International Conference on Communications (ICC)*, vol. 3, May 2005, pp. 1937–1941. [Online]. Available: http://www.dx.doi.org/10.1109/ICC.2005.1494677

[39] R. Cendrillon, J. Huang, M. Chiang, and M. Moonen, "Autonomous spectrum balancing for digital subscriber lines," *IEEE Transactions on Signal Processing*, vol. 55, no. 8, pp. 4241–4257, Aug. 2007. [Online]. Available: http://www.dx.doi.org/10.1109/TSP.2007.895989

[40] G. Ginis and J. M. Cioffi, "Vectored transmission for digital subscriber line systems," *IEEE Journal on Selected Areas in Communications*, vol. 20, no. 5, pp. 1085–1104, Jun. 2002. [Online]. Available: http://www.dx.doi.org/10.1109/JSAC.2002.1007389

[41] *Self-FEXT cancellation (vectoring) for use with VDSL2 transceivers*, ITU Recommendation ITU-T G.993.5, Jan. 2015. [Online]. Available: http://www.itu.int/rec/T-REC-G.993.5

[42] R. Cendrillon, G. Ginis, E. V. D. Bogaert, and M. Moonen, "A near-optimal linear crosstalk canceler for upstream vdsl," *IEEE Transactions on Signal Processing*, vol. 54, no. 8, pp. 3136–3146, Aug. 2006. [Online]. Available: http://www.dx.doi.org/10.1109/TSP.2006.874822

[43] R. Cendrillon, G. Ginis, E. V. den Bogaert, and M. Moonen, "A near-optimal linear crosstalk precoder for downstream vdsl," *IEEE Transactions on Communications*, vol. 55, no. 5, pp. 860–863, May 2007. [Online]. Available: http://www.dx.doi.org/10.1109/TCOMM.2007.896121

[44] *Fast access to subscriber terminals (G.fast) - Power spectral density specification*, ITU Recommendation ITU-T G.9700, Apr. 2014. [Online]. Available: http://www.itu.int/rec/T-REC-G.9700/

[45] M. Tomlinson, "New automatic equaliser employing modulo arithmetic," *Electronics Letters*, vol. 7, no. 5, pp. 138–139, Mar. 1971. [Online]. Available: http://www.dx.doi.org/10.1049/el:19710089

[46] H. Harashima and H. Miyakawa, "Matched-transmission technique for channels with intersymbol interference," *IEEE Transactions on Communications*, vol. 20, no. 4, pp. 774–780, Aug. 1972. [Online]. Available: http://www.dx.doi.org/10.1109/TCOM.1972.1091221

[47] M. Guenach, C. Nuzman, P. Tsiaflakis, and J. Maes, "Power optimization in vectored and non-vectored G.fast transmission," in *2014 IEEE Global Communications Conference (GLOBECOM)*, Dec. 2014, pp. 2229–2233. [Online]. Available: http://www.dx.doi.org/10.1109/GLOCOM.2014.7037139

[48] F. C. B. F. Müller, C. Lu, P. E. Eriksson, S. Höst, and A. Klautau, "Optimizing power normalization for G.fast linear precoder by linear programming," in *2014 IEEE International Conference on Communications (ICC)*, Jun. 2014, pp. 4160–4165. [Online]. Available: http://www.dx.doi.org/10.1109/ICC.2014.6883973

[49] W. Lanneer, P. Tsiaflakis, J. Maes, and M. Moonen, "Linear and nonlinear precoding based dynamic spectrum management for downstream vectored G.fast transmission," *IEEE Transactions on Communications*, vol. 65, no. 3, pp. 1247–1259, Mar. 2017. [Online]. Available: http://www.dx.doi.org/10.1109/TCOMM.2016.2641952

[50] R. Strobel and W. Utschick, "Discontinuous operation for precoded G.fast," in *2016 IEEE International Conference on Acoustics, Speech and Signal Processing (ICASSP)*, Mar. 2016, pp. 3551–3555. [Online]. Available: http://www.dx.doi.org/10.1109/ICASSP.2016.7472338

[51] Y. Huang, T. Magesacher, E. Medeiros, C. Lu, P. E. Eriksson, and P. Ödling, "Rate-boosting using strong crosstalk in next generation wireline systems," in *2015 IEEE Global Communications Conference (GLOBECOM)*, Dec. 2015, pp. 1–6. [Online]. Available: http://www.dx.doi.org/10.1109/GLOCOM.2015.7417753

[52] J. Maes, C. Nuzman, and P. Tsiaflakis, "Sensitivity of nonlinear precoding to imperfect channel state information in G.fast," in *2016 24th European Signal Processing Conference (EUSIPCO)*, Aug. 2016, pp. 290–294. [Online]. Available: http://www.dx.doi.org/10.1109/EUSIPCO.2016.7760256

[53] C. Lu and P. E. Eriksson, "A fast channel estimation method for disorderly leaving events in vectored DSL systems," in *2011 IEEE International Conference on Communications (ICC)*, Jun. 2011, pp. 1–6. [Online]. Available: http://www.dx.doi.org/10.1109/icc.2011.5962433

[54] Alcatel-Lucent, "Influence of an Impedance Change on a Leaving Line onto the Direct and Crosstalk Channels of the Active Lines," ITU-T SG15 Contribution 2013-10-Q4-058, Oct. 2013.

[55] K. Czuba and D. Sikora, "Temperature Stability of Coaxial Cables," *Acta Phys. Pol. A*, vol. 119, no. EuCARD-PUB-2011-001, 2011. [Online]. Available: https://cds.cern.ch/record/1349292

[56] ——, "Phase drift versus temperature measurements of coaxial cables," in *18-th International Conference On Microwaves, Radar And Wireless Communications*, Jun. 2010, pp. 1–3.

2

How Vectoring in G.fast May Cause Neighborhood Wars

Eduardo Medeiros, Thomas Magesacher, Per-Erik Eriksson, Chenguang Lu and Per Ödling

Abstract

Emerging wireline transmission systems such as G.fast use bands up to around 200 MHz on short cables. A key enabler for achieving the aspired throughput of several hundred Mbit/s is joint processing of transmit signals in downstream direction as well as joint processing of receive signals in upstream direction through techniques referred to as vectoring. A new challenge in such systems are sudden and severe changes in the channel matrix caused by changing terminations on lines *outside* the vectoring group. Such events can be caused by users disconnecting their modems, turning them on or off, or on-/off-hook events on lines that still support the plain old telephony service.

This work presents channel measurements capturing the impact of termination changes caused by modems or handsets. An analysis of the impact of these sudden changes on the signal-to-noise-power-ratio in vectoring systems reveals that throughput and stability can be seriously degraded. The potential of decision-directed channel tracking based on least squares estimation is investigated.[1]

[1]Published in *Proc. IEEE International Conference on Communications (ICC 2014)*, Sydney, NSW, 10-14 Jun. 2014.

2.1 INTRODUCTION

The implementation of precoding and crosstalk cancellation schemes has enabled multi-carrier copper-based systems to reach bit rates around 100 Mbit/s [1] [2]. These advances have prolonged the life expectancy of copper cables in the field, while allowing operators to extend their fiber-based access network to distribution points, avoiding the massive investment step of deploying fiber to the customer premises.

As deployments of vectored VDSL2 hit the market, vendors and academia [3] have been involved in drafting a new standard (G.fast), with features that support even higher bit-rates, improved energy efficiency through discontinuous operation and enable new business models through reverse powering.

One of the practical challenges of deploying vectored VDSL2 schemes is referred to in the literature as disorderly leaving events (DLEs). A DLE happens when one of the lines in the vectoring group is disconnected or powered off. This causes the termination impedance to change and consequently a change in the crosstalk coupling gains. When dealing with DLEs, the ITU-G.vector standard [1] advises implementors to mute (turn off) transmitters as soon as possible. DLEs have been addressed in [4] by means of a fast tracking algorithm. That work has influenced a corrigendum to the standard [5], where a procedure for fast precoder coefficient update is described.

Differently from its predecessors, G.fast will be a time-division duplex (TDD) system. One of the envisioned features, the so-called discontinuous operation, allows transceivers to switch to an energy-saving mode during portions of a TDD frame where there is no useful data to send. This has serious implications for the vectoring engine design [6]. In a precoding scheme, for example, turning off some transceivers is equivalent to changing the size of the precoding matrix—a change that requires precoder coefficient recalculation and transmit power spectral density (PSD) adjustment [7]. Several contributions have been presented to address this issue [8] [9].

One point that these contributions stress is the assumption that discontinuous operation does not change the impedance of the line. If impedances were to change, the far-end crosstalk (FEXT) couplings would be modified in the whole channel matrix, requiring a lengthy channel estimation phase prior to the precoder update.

In a recent ITU contribution [10], it is suggested that G.fast vectoring bundles may be affected by changes in the terminating impedance of alien lines, that is, lines which are *not part* of the vectoring group. While a DLE occurs with lines which are part of a vectoring group, and are therefore monitored and managed as a unit, in G.fast this change can be triggered by any neighboring line, such as a plain old telephony service (POTS) line in the same cable or even by a line managed by a different operator.

This paper focuses on the impact of alien-line termination changes caused by modems or POTS handsets and investigates possible remedies. In Section 2.2, the system model and an analysis of the signal-to-noise-power-ratio (SNR) are introduced. Section 2.3 presents measurement and SNR-loss results. Section 2.4 investigates the potential of decision-directed channel tracking based on least-squares estimation and Section 2.5 concludes the work.

2.2 SYSTEM MODEL AND ANALYSIS

Hereinafter, the following notation is used: bold upper-case and bold lower-case symbols are used to denote matrices and vectors, respectively. $\boldsymbol{X}(i,j)$ denotes the element in row i and column j of $\boldsymbol{X}$ and $\otimes$ is the Kronecker product.

2.2.1 VECTORED TRANSMISSION

For a discrete multi-tone (DMT) system using TDD with U synchronised transmitters and a cyclic prefix of sufficient length, the received symbol vector $\boldsymbol{y}_k^\ell \in \mathbb{C}^{U\times 1}$ at time instant k for subcarrier no. ℓ can be modelled in frequency-domain as

$$\boldsymbol{y}_k^\ell = \boldsymbol{H}_k^\ell \boldsymbol{x}_k^\ell + \boldsymbol{n}_k^\ell, \tag{2.1}$$

where $\boldsymbol{x} \in \mathbb{C}^{U\times 1}$ is the transmitted symbol vector, $\boldsymbol{H} \in \mathbb{C}^{U\times U}$ is the frequency-domain channel matrix and $\boldsymbol{n} \in \mathbb{C}^{U\times 1}$ is the additive noise vector. For the sake of simplicity, time index k and subcarrier index ℓ are omitted when possible.

Since near-end crosstalk (NEXT) can be disregarded, the received symbol for user $u \in \{1,\ldots,U\}$ can be written as

$$\boldsymbol{y}(u) = \boldsymbol{H}(u,u)\boldsymbol{x}(u) + \sum_{m\neq u} \boldsymbol{H}(u,m)\boldsymbol{x}(m) + \boldsymbol{n}(u),$$

where the term $\sum_{m\neq u} \boldsymbol{H}(u,m)\boldsymbol{x}(m)$ represents FEXT.

Given that the channel matrix $\boldsymbol{H}$ is known, FEXT can be mitigated by means of low-complexity linear compensation schemes. The zero-forcing canceler [11] and the diagonalizing precoder [12] provide near optimal performance for upstream and downstream directions, respectively.

This paper deals with imperfect channel information caused by changes in an *alien line's* terminating impedance. Alien lines are defined as copper pairs which are not part of the vectoring group but might, for example, share portions of the the same cable or even the same binder.

It is reasonable to assume that all lines at the distribution point are properly terminated. On the customer premises side, however, the alien line's terminating impedance could change, as a result of equipment being powered off,

disconnected or even, in case of a POTS handset, being taken on/off hook. In order to model this situation, we use the channel model (2.1) with two distinct states $\boldsymbol{H} = \boldsymbol{T}$ and $\boldsymbol{H} = \boldsymbol{O}$, where the channel matrix $\boldsymbol{T}$ represents the state when the alien line is properly terminated (i.e. a 100 Ω resistor or an on-hook phone is connected) and $\boldsymbol{O}$ represents the state when the alien line is left open (or an off-hook phone is connected). $\boldsymbol{T}$ and $\boldsymbol{O}$ can be related by

$$\boldsymbol{O} = \boldsymbol{T} + \boldsymbol{\Delta}, \tag{2.2}$$

where the matrix $\boldsymbol{\Delta}$ represents the mismatch in complex channel coefficients due to the terminating impedance change.

The next sections present expressions for the SNR in upstream and downstream using the aforementioned zero-forcing canceler and diagonalizing precoder, respectively. For a full derivation of these expressions, see [13]. We distinguish between the SNR before the termination change, denoted $SNR^{\boldsymbol{T}}$, and the SNR after the termination change, denoted $SNR^{\boldsymbol{O}}$, and define the SNR loss ΔSNR_u for user u in dB as

$$\Delta SNR_u = 10 \log_{10} SNR_u^{\boldsymbol{T}} - 10 \log_{10} SNR_u^{\boldsymbol{O}}. \tag{2.3}$$

2.2.2 UPSTREAM: PERFORMANCE OF ZERO-FORCING WITH IMPERFECT CHANNEL ESTIMATES

In upstream direction, the received symbol $\boldsymbol{z}(u)$ for user u is given by

$$\boldsymbol{z}(u) = \boldsymbol{x}(u) + \sum_{i \in \mathcal{U}} \sum_{j \in \mathcal{U}} \boldsymbol{T}^{-1}(u,i) \boldsymbol{\Delta}(i,j) \boldsymbol{x}(j) + \sum_{i \in \mathcal{U}} \boldsymbol{T}^{-1}(u,i) \boldsymbol{n}(i),$$

where $\mathcal{U} \subset \{1, \ldots, U\}$ is the set of active transmitters. The residual crosstalk caused by the alien line's termination change is represented by the term $\sum_{i \in \mathcal{U}} \sum_{j \in \mathcal{U}} \boldsymbol{T}^{-1}(u,i) \boldsymbol{\Delta}(i,j) \boldsymbol{x}(j)$. Here, we assume that the estimate of the channel before a termination change, $\boldsymbol{T}$, is perfect.

The SNR for user u before the termination change can be written as

$$SNR_u^{\boldsymbol{T}} = \frac{p_u}{\Gamma \left(\sum_{i \in \mathcal{U}} |\boldsymbol{T}^{-1}(u,i)|^2 \sigma_i \right)}, \tag{2.4}$$

where Γ is the SNR-gap to capacity, $p_i = \mathsf{E}\left\{ |\boldsymbol{x}(i)|^2 \right\}$ is the variance of the transmitted symbol at user i and $\sigma_i = \mathsf{E}\left\{ |\boldsymbol{n}(i)|^2 \right\}$ is the variance of the additive noise experienced by user $i \in \mathcal{U}$.

After the alien line termination is removed, the SNR for user u can be calculated as

$$SNR_u^{\boldsymbol{O}} = \frac{p_u}{\Gamma \left(\sum_{i \in \mathcal{U}} \sum_{j \in \mathcal{U}} |\boldsymbol{T}^{-1}(u,i)|^2 \boldsymbol{\Phi}(i,j) p_j + \sum_{i \in \mathcal{U}} |\boldsymbol{T}^{-1}(u,i)|^2 \sigma_i \right)}, \tag{2.5}$$

where $\boldsymbol{\Phi}(i,j) = \mathsf{E}\left\{|\boldsymbol{\Delta}(i,j)|^2\right\}$ is the channel estimation error variance.

2.2.3 DOWNSTREAM: PERFORMANCE OF DIAGONALIZING PRECODER WITH IMPERFECT CHANNEL ESTIMATES

In downstream direction, the received symbol $\boldsymbol{z}'(u)$ at user u can be written as

$$\boldsymbol{z}'(u) = \boldsymbol{D}(u,u)\boldsymbol{x}(u) + \sum_{i\in\mathcal{U}}\sum_{j\in\mathcal{U}} \boldsymbol{\Delta}(u,i)\boldsymbol{T}^{-1}(i,j)\boldsymbol{D}(j,j)\boldsymbol{x}(j) + \boldsymbol{n}(u),$$

where $\boldsymbol{D}$ is a diagonal matrix with $\boldsymbol{D}(u,u) = \boldsymbol{T}(u,u)$.

Before the termination change, the SNR for user u is given by

$$SNR_u^{\boldsymbol{T}} = \frac{|\boldsymbol{T}(u,u)|^2 p_u}{\Gamma\,\sigma_u}. \tag{2.6}$$

After the termination change, the SNR for user u can then be calculated as

$$SNR_u^{\boldsymbol{O}} = \frac{|\boldsymbol{T}(u,u)|^2 p_u}{\Gamma\left(\sum_{i\in\mathcal{U}}\sum_{j\in\mathcal{U}} \boldsymbol{\Phi}(u,i)|\boldsymbol{T}^{-1}(i,j)\boldsymbol{T}(j,j)|^2 p_j + \sigma_u\right)}, \tag{2.7}$$

assuming perfect knowledge of the channel before the termination change.

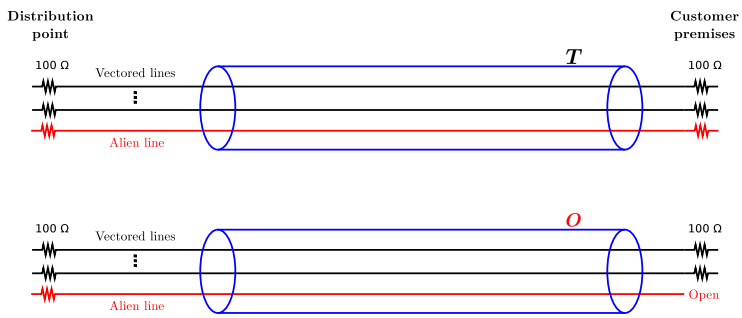

Figure 2.1: Experimental setup. When all lines are properly terminated, the matrix $\boldsymbol{T}$ is measured (top). After the alien line termination is removed, $\boldsymbol{O}$ is measured (bottom).

2.3 EXPERIMENTAL RESULTS

This section presents experimental evidence that corroborates the significant impact of alien lines' termination changes on vectored G.fast performance. Measured channel information is used to compare the performance of linear compensation schemes before and after a termination change.

2.3.1 MEASUREMENT SETUP

The experimental setup is depicted in Fig. 2.1 and consists of a 30-pair cable (0.5 mm, 100 m) with three binders. Six lines of the same binder are chosen to constitute a 5-line vector group and an alien line. The measurement equipment (a network analyzer) is coupled to the vectored copper pairs using 100 Ω balun transformers. The alien line extremity at the distribution point is at all times terminated in a 100 Ω resistor.

The other end of the alien line is initially coupled to a 100 Ω resistor. This load represents the purely resistive impedance of a G.fast modem [14]. A first set of transfer function measurements is taken, constituting the $\boldsymbol{T}$ matrix. Next, the resistor is removed and a new batch of measurements are performed and stored in matrix $\boldsymbol{O}$. This procedure was executed for both downstream and upstream directions.

The stability and accuracy of the measurement setup has been verified following the procedures described in [10]. The measurements were performed under the following assumptions:

- 51.75 KHz subcarrier spacing.
- The first 3500 subcarriers are considered.
- No interpolation has been used (exactly one measurement point per subcarrier).

A sample of the measurement results is shown in Fig. 2.2. The upper subplot presents the squared magnitude of $\boldsymbol{T}(4,1)$ and $\boldsymbol{O}(4,1)$ for the downstream direction. The lower subplot presents the squared magnitude of the ratio between $\boldsymbol{O}(4,1)$ and $\boldsymbol{T}(4,1)$ in dB.

2.3.2 VECTORING PERFORMANCE COMPARISON

The measured channel matrix $\boldsymbol{T}$ has been used to train a diagonalizing precoder and zero-forcing canceler. Fig. 2.3 presents the resulting SNRs for line 4 (worst case). The black lines in Fig. 2.3 correspond to the crosstalk-free SNRs achieved with perfect channel knowledge ($SNR^{\boldsymbol{T}}$) when using diagonalizing precoding in downstream (top plot) and zero forcing in upstream (bottom plot). The SNR calculations presented in this section assume a transmit PSD of -76 dBm/Hz, a background-noise PSD of -140 dBm/Hz, and $\Gamma = 12.9$ dB.

The red solid lines represent the SNRs achieved after the alien line termination changes ($SNR^{\boldsymbol{O}}$). The precoder/canceler settings are outdated and the residual crosstalk terms in $\boldsymbol{\Delta}$ cause a considerable performance degradation (see (2.5) and (2.7)).

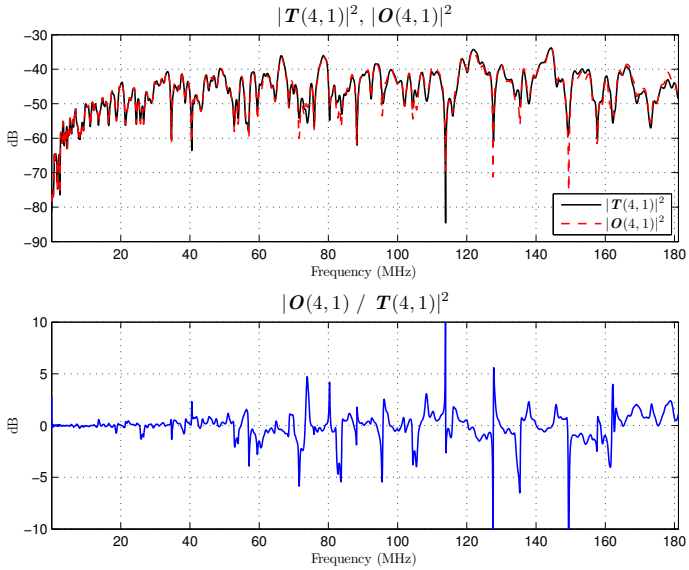

Figure 2.2: Top: Squared magnitude of FEXT coupling coefficients from line 1 into line 4 before ($\boldsymbol{T}$) and after ($\boldsymbol{O}$) the alien-line termination change. Bottom: Impact of termination change in terms of the ratio between $\boldsymbol{O}$ and $\boldsymbol{T}$ in dB.

The areas filled in blue in Fig. 2.3 represent the total SNR loss (ΔSNR) caused by the alien line termination change. For both directions, more than half of the subcarriers experience a SNR degradation larger than 6 dB.

Fig. 2.4 shows the SNR loss ΔSNR for all lines. From these plots it becomes even clearer that the SNR loss caused by the impedance change is significant. Whenever the termination in the alien line changes, all lines in the vector group experience an instantaneous loss in SNR, higher than 6 dB for subcarriers above 60 MHz. For the two worst lines (2 and 4), ΔSNR peaks at around 20 dB.

Also in Fig. 2.4, one can notice that the performance of most lines is practically unchanged up to 20 MHz. This fact is worthy of notice because it represents exactly the frequency range used for most of the deployed VDSL2 systems (using 17 MHz profiles). In other words, while this issue is of high impact for G.fast systems, it may have been undetected for VDSL2, which was standardised without requiring channel tracking features.

Fig. 2.5 shows the empirical complementary cumulative distribution function of the ΔSNR based on one set of measurements over the 3500 subcarriers. The curves are very similar for both directions. Three of the five lines in the

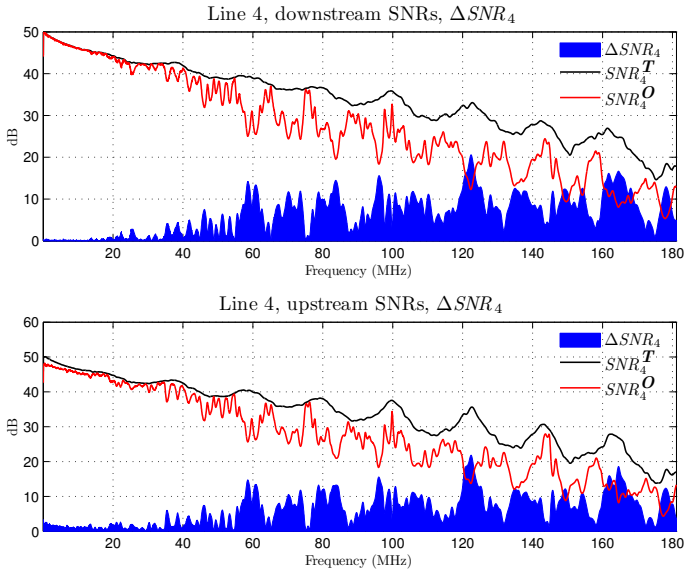

Figure 2.3: SNR comparison for line 4 before and after the alien-line termination change using diagonalizing precoding in downstream direction (top) and zero forcing in upstream direction (bottom). The black line represents SNR_4^T, the SNR before alien line termination change. The red lines represents SNR_4^O, the SNR after the terminating resistor is removed. The area shaded in blue represents ΔSNR_4.

vector group have between 10 and 15% of their active subcarriers subject to a SNR loss higher than 6 dB. For the worst performing lines, (2 and 4) roughly half of the subcarriers have a ΔSNR higher than 6 dB.

The results shown in Fig. 2.5 hint that state-of-the-art mechanisms used in VDSL2 such as bit-swapping and seamless rate adaptation may not be able to adequately remedy the termination-change problem in G.fast. To illustrate this issue, it is worth picturing a 24-user vectoring group. With just one alien line impedance change (let's say, an on-off hook transition in a neighboring line) the whole channel matrix would change. Suddenly the whole 24 lines would face a significant SNR loss over hundreds of subcarriers.

2.3.3 IMPACT OF TERMINATION CHANGE IN DIFFERENT VECTOR GROUP SIZES

The SNR loss caused by changes of terminating impedances is more harmful to larger vector groups. Since the whole channel matrix changes, larger vec-

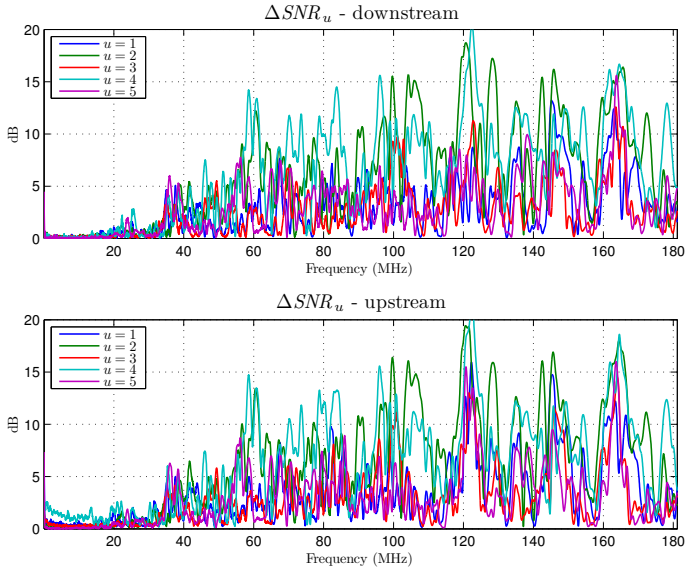

Figure 2.4: SNR loss ΔSNR_u for $u \in \{1, \ldots, 5\}$ when using diagonalizing precoding in downstream direction (top) and zero forcing in upstream direction (bottom).

toring bundles tend to suffer with the error propagation. The experimental data collected by the authors can be used to illustrate the practical effects of this fact.

Fig. 2.6 depicts the SNR loss experienced by line 4 while being part of vectoring groups with different sizes. The vectoring bundles in question use the linear precoder. The SNR loss consistently increases for larger groups, with $U = 5$ being the worst case. For some subcarriers the difference between a $U = 2$ and a $U = 5$ vector group is higher than 6 dB. This SNR loss is higher than the usual 6 dB of target margin used by DSL operators to maintain stability.

2.4 CHANNEL TRACKING

In this section, we investigate the suitability of decision-directed (blind) channel tracking based on least-squares estimation as a remedy to mitigate the impact of sudden channel changes. The purpose is to verify the concept and point out some basic tradeoffs under typical operating conditions encountered by G.fast systems. Note that a solution for use in practical systems requires optimization of tracking accuracy, stability and complexity for the operating

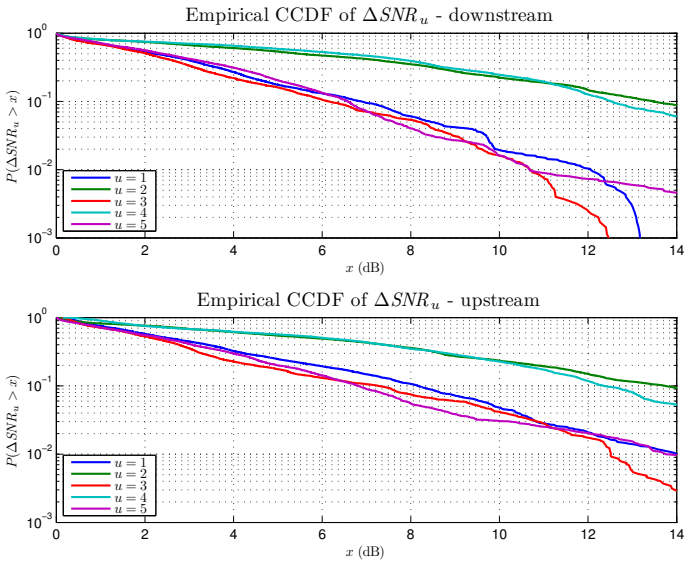

Figure 2.5: Empirical CCDF of the ΔSNR_u defined in (2.3) when using diagonalizing precoding in downstream direction (top) and zero forcing in upstream direction (bottom).

point (SNR margin) at hand.

2.4.1 SLIDING-WINDOW LEAST SQUARES

Hereinafter, we focus on decision-directed channel tracking in upstream direction for a single subchannel of a vectoring system using zero-forcing. In a real system, the tracking has to be extended to all subchannels that experience severe degradation.

Let $\boldsymbol{z}_k$ and $\hat{\boldsymbol{x}}_k$ denote zero-forcing equalizer output and hard decisions for receive symbol no. k, respectively. We use the error $\boldsymbol{e}_k = \boldsymbol{z}_k - \hat{\boldsymbol{x}}_k$ as a measure for the channel deviation $\boldsymbol{\Delta}$ caused by a termination change[2]. Under the assumption that the decisions are correct ($\hat{\boldsymbol{x}}_k = \boldsymbol{x}_k$), the error is given by $\boldsymbol{e}_k = \boldsymbol{\Delta}' \hat{\boldsymbol{x}}_k + \boldsymbol{T}^{-1}\boldsymbol{n}_k$, where $\boldsymbol{\Delta}' = \boldsymbol{T}^{-1}\boldsymbol{\Delta}$, and we attempt to "average out" the channel noise $\boldsymbol{T}^{-1}\boldsymbol{n}_k$ by applying the least squares approach.

Let $\boldsymbol{e}_{k,W_k} = \begin{bmatrix}\boldsymbol{e}_k^{\mathrm{T}} & \boldsymbol{e}_{k-1}^{\mathrm{T}} & \dots & \boldsymbol{e}_{k-W_k+1}^{\mathrm{T}}\end{bmatrix}^{\mathrm{T}} \in \mathbb{C}^{UW_k \times 1}$ denote the errors of the

[2]In principle, it would of course be desirable to use decisions from the channel decoder output. However, channel decoder output symbols are only available after a certain delay, which depends on the scheme and the strength of the code at hand. For simplicity, we here focus on uncoded hard decisions.

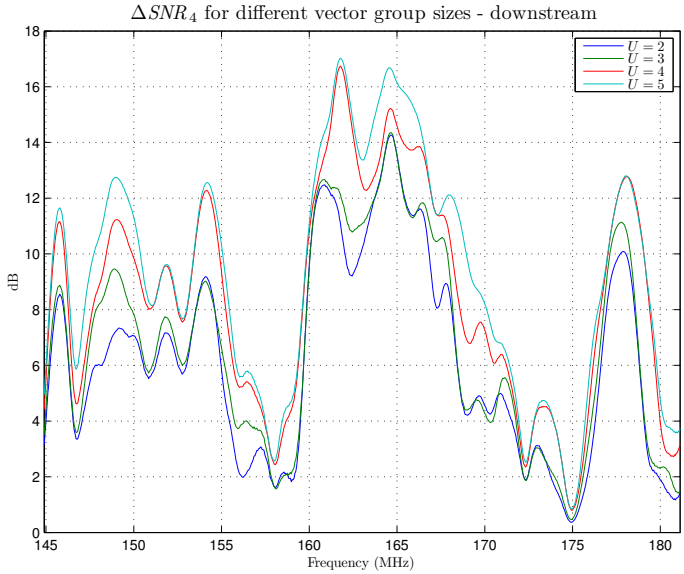

Figure 2.6: ΔSNR_4 for different vectoring group sizes in downstream direction. Residual crosstalk increases with the number of lines.

last W_k DMT symbols, where W_k is the length of our sliding observation window. Stacking the rows of $\boldsymbol{\Delta}'$ into a vector $\boldsymbol{\delta}' \in \mathbb{C}^{U^2 \times 1}$ and defining the matrix

$$\hat{\boldsymbol{X}}_k = \begin{bmatrix} \boldsymbol{I}_U \otimes \hat{\boldsymbol{x}}_k^{\mathrm{T}} \\ \boldsymbol{I}_U \otimes \hat{\boldsymbol{x}}_{k-1}^{\mathrm{T}} \\ \vdots \\ \boldsymbol{I}_U \otimes \hat{\boldsymbol{x}}_{k-W_k+1}^{\mathrm{T}} \end{bmatrix} \in \mathbb{C}^{W_k U \times U^2},$$

we can write the error vector of the last W_k DMT symbols as $\boldsymbol{e}_{k,W_k} = \hat{\boldsymbol{X}}_k \boldsymbol{\delta}' + \boldsymbol{n}_{k,W_k}$ where $\boldsymbol{n}_{k,W_k} = \left(\boldsymbol{I}_{W_k} \otimes \boldsymbol{T}^{-1}\right) \begin{bmatrix} \boldsymbol{n}_k^{\mathrm{T}} & \boldsymbol{n}_{k-1}^{\mathrm{T}} & \dots & \boldsymbol{n}_{k-W_k+1}^{\mathrm{T}} \end{bmatrix}^{\mathrm{T}}$ denotes the received noise. The least-squares approximation $\hat{\boldsymbol{\delta}}'_k$ of $\boldsymbol{\delta}'_k$ can, for example, be obtained using the pseudoinverse of $\hat{\boldsymbol{X}}_k$ yielding

$$\hat{\boldsymbol{\delta}}'_k = \left(\hat{\boldsymbol{X}}_k^{\mathrm{H}} \hat{\boldsymbol{X}}_k\right)^{-1} \hat{\boldsymbol{X}}_k^{\mathrm{H}} \boldsymbol{e}_{k,W_k}. \tag{2.8}$$

Row-wise stacking of $\hat{\boldsymbol{\delta}}'_k$ into a matrix $\hat{\boldsymbol{\Delta}}'_k$ finally allows us to compute the channel-deviation estimate

$$\hat{\boldsymbol{\Delta}}_k = \boldsymbol{T} \hat{\boldsymbol{\Delta}}'_k.$$

In a real system implementation, the channel tracker can be activated based on an error metric derived from receiver-side hard decisions or based on a metric from a monitoring system detecting a performance decay on all lines in the vectoring group. Clearly, the challenge with blind channel tracking is that the assumption of making correct decisions after the channel change ($\hat{\boldsymbol{x}}_k = \boldsymbol{x}_k$) may not hold. Simulations presented in the following section investigate the impact of decision errors.

2.4.2 CASE STUDY

We use the cable measurements presented in the previous section in a vectoring system with $U = 5$ users and choose the following parameters conforming with the emerging G.fast standard: transmit PSD $-76\,\mathrm{dBm/Hz}$, background noise $-140\,\mathrm{dBm/Hz}$. The channel attenuation at the chosen frequency (subchannel no. $\ell = 3178$, which corresponds to subcarrier frequency 164.4 MHz) is roughly 27 dB yielding a receive SNR of about 37 dB. In order to achieve an uncoded symbol error rate of 10^{-7}, a receive SNR of roughly 28 dB is required for 64-QAM yielding an SNR margin of 9 dB. For 128-QAM, the required receive SNR is roughly 31 dB resulting in an SNR margin of 6 dB. Finally, for 256-QAM, the required SNR is roughly 34 dB with an SNR margin of 3 dB.

We simulate 1000 runs of transmission and channel tracking for 64-QAM, 128-QAM, and 256-QAM where a line outside the vectoring group changes termination right before symbol no. $k = 1$:

$$\boldsymbol{H}_k = \begin{cases} \boldsymbol{T}, & k < 1 \\ \boldsymbol{O} = \boldsymbol{T} + \boldsymbol{\Delta}, & k \geq 1 \end{cases}.$$

Fig. 2.7 shows that the sudden channel change causes an SNR loss of around 16 dB for user $u = 4$.

We invoke the channel tracker (2.8) after every received DMT symbol for $k \geq 1$ in order to show the achievable SNR improvement. In a real system, more complexity-friendly implementations of (2.8) should be employed. From symbol no. $k = 21$ on, the window size is increased linearly from 20 to 80 and then kept constant:

$$W_k = \begin{cases} 20, & 1 \leq k \leq 20 \\ k, & 21 \leq k \leq 80 \\ 80, & k > 81 \end{cases}.$$

Since wrong decisions during the tracking procedure cause an error bias, there is no notable improvement for $k > 80$. Thus, the tracking can be stopped and the coefficients can be frozen for $W_k > 80$. Note that this choice for the window length is not optimized in any sense. Further work is required to, for example, adjust the window length depending on the residual error in

combination with a recursive implementation of the least squares estimator in order to circumvent expensive matrix inversions.

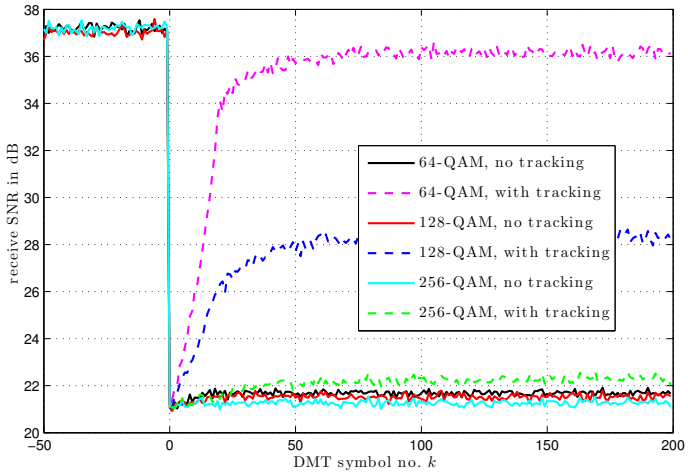

Figure 2.7: Receive SNR of user $u = 4$ with and without tracking for 64-QAM, 128-QAM, and 256-QAM. For $k \geq 1$, a termination change from 100 Ohm to open on the alien line causes a sudden change in the channel matrix. The SNR results shown are averaged over 1000 simulation runs.

Fig. 2.8 shows the cumulative QAM-symbol error count of user $u = 4$ averaged over 1000 simulation runs. For 64-QAM, 128-QAM, and 256-QAM, the symbol error count without tracking continues to rise after the channel change (note the logarithmic scale on the y-axis). Channel tracking essentially avoids errors for 64-QAM apart from a total of 17 QAM-symbol errors in 1000 simulation runs (or equivalently, an average of 0.017 QAM symbol errors) during the tracking phase.

Tracking for 128-QAM manages to reduce the SNR loss from about 15 dB to roughly 9 dB. During the tracking phase, a total of 1127 QAM-symbol errors in 1000 simulation runs (or equivalently, an average of 1.127 QAM symbol errors) occur.

For 256-QAM with an SNR margin of 3 dB, blind tracking results in a small SNR improvement ($\approx$ 1 dB). For subchannels with such low SNR margin, tracking might not be justifiable.

Note that the reason for the residual SNR loss after tracking is twofold: First, erroneous decisions during tracking cause an error bias. Second, the achievable SNR with vectoring for the channel $\boldsymbol{O}$ can be lower than for the channel $\boldsymbol{T}$.

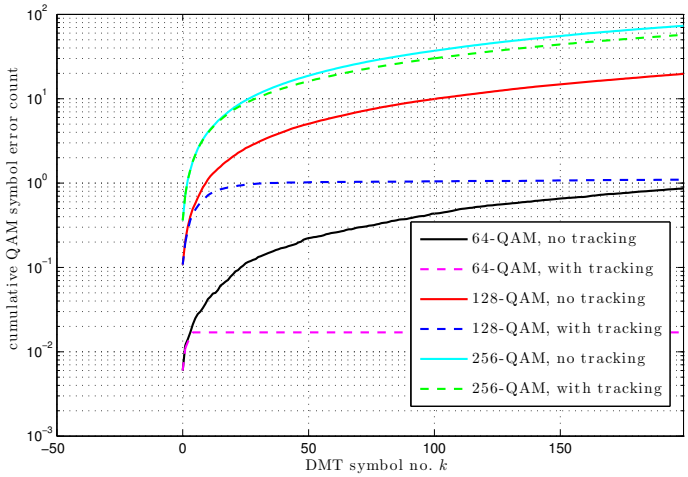

Figure 2.8: Cumulative QAM symbol error count of user $u = 4$ with and without tracking for 64-QAM, 128-QAM, and 256-QAM. Note that the y-axis is in logarithmic scale. The results shown are averaged over 1000 simulation runs.

2.5 CONCLUSION

Termination changes on alien lines can cause a serious degradation of receive SNR on lines operating wideband vectoring. Measurements and analysis show that while the impact is fairly mild for lower frequencies (below 20 MHz), an SNR-loss of up to around 15 dB can happen for higher frequencies. Maintaining retrain-free transmission with low SNR margins in case of such a termination-change event is a challenge.

Decision-directed channel tracking based on least-squares estimation can yield a fast and substantial SNR improvement in upstream direction without losing spectral efficiency. In principle, blind channel tracking can also be used in downstream direction but requires fast feedback of the errors computed by the modems via subcarriers with high SNR margins to the distribution point during the upstream portions of TDD frames. Alternatively, a fast pilot-based channel-update mechanism could be introduced in order to avoid neighborhood wars.

References

[1] *Self-FEXT Cancellation (Vectoring) for Use with VDSL2 Transceivers*, International Telecommunication Union Recommendation, Sep. 2010.

[2] V. Oksman, H. Schenk, A. Clausen, J. M. Cioffi, M. Mohseni, G. Ginis, C. Nuzman, J. Maes, M. Peeters, K. Fisher, and P.-E. Eriksson, "The ITU-T's new G.vector standard proliferates 100 Mb/s DSL," *IEEE Communications Magazine*, vol. 48, no. 10, pp. 140–148, Oct. 2010. [Online]. Available: http://dx.doi.org/10.1109/MCOM.2010.5594689

[3] P. Ödling, T. Magesacher, S. Höst, P. Börjesson, M. Berg, and E. Areizaga, "The fourth generation broadband concept," *IEEE Communications Magazine*, vol. 47, no. 1, pp. 62–69, 2009.

[4] C. Lu and P.-E. Eriksson, "A fast channel estimation method for disorderly leaving events in vectored DSL systems," in *IEEE International Conference on Communications (ICC)*, 2011, pp. 1–6.

[5] *Self-FEXT Cancellation (Vectoring) for Use with VDSL2 Transceivers - Corrigendum 1*, International Telecommunication Union Recommendation, Jun. 2011.

[6] Sckipio, "Power saving implications on vectoring – static allocation case," ITU-T SG15 Contribution 2012-11-4A-043, Nov. 2012.

[7] Lantiq, "G.fast: Issues with discontinuous operation," ITU-T SG15 Contribution 2013-05-Q4-057, May 2013.

[8] ——, "G.fast: Precoder update in support of discontinuous operation," ITU-T SG15 Contribution 2013-01-Q4-068, Jan. 2013.

[9] Alcatel-Lucent, "G.fast: Solutions for precoding in discontinuous operation," ITU-T SG15 Contribution 2013-03-Q4-052, Mar. 2013.

[10] TNO, "G.fast: Vectoring gain limitations due to changing terminations of alien wire pairs," ITU-T SG15 Contribution 2013-03-Q4-044, Mar. 2013.

[11] R. Cendrillon, G. Ginis, E. Van den Bogaert, and M. Moonen, "A near-optimal linear crosstalk canceler for upstream VDSL," *IEEE Transactions on Signal Processing*, vol. 54, no. 8, pp. 3136–3146, 2006.

[12] ——, "A near-optimal linear crosstalk precoder for downstream VDSL," *IEEE Transactions on Communications*, vol. 55, no. 5, pp. 860–863, 2007.

[13] G. Marrocco, M. Wolkerstorfer, T. Nördstrom, and D. Statovci, "Energy-efficient DSL using vectoring," in *IEEE Global Telecommunications Conference (GLOBECOM)*, 2011, pp. 1–6.

[14] Lantiq, Broadcom, and Ikanos, "G.fast: Proposal for the transmit signal power limit," ITU-T SG15 Contribution 2012-06-4A-047R1, Jun. 2012.

3

Modeling Alien-Line Impedance-Mismatch in Wideband Vectored Wireline Systems

Eduardo Medeiros, Thomas Magesacher, Per Ödling, Dong Wei, Xiang Wang, Qiaojie Li, Per-Erik Eriksson, Chenguang Lu, Jeroen Boschma, and Bas van den Heuvel

Abstract

Sudden changes of channel coefficients in a wideband vectored wireline system (such as G.fast) due to changes in the terminating impedance of lines *outside* the vectored group can seriously degrade stability and throughput. This work presents a model that predicts the impact of termination mismatch based exclusively on crosstalk data for the properly-terminated state. Experimental results confirm a tight fit between model and measurements. The model allows analysis of system performance and stability without dedicated crosstalk measurements for mismatch cases.[1]

[1]Published in *IEEE Communications Letters*, vol. 18, no. 9, September 2014.

3.1 INTRODUCTION

Exploiting higher bandwidth on shorter copper loops, wireline access providers can provide higher throughput at reasonable deployment costs [1]. The draft ITU-T standard G.fast [2], for example, targets loop lengths in the order of 100 m using bandwidths in the order of 100 MHz to obtain aggregate[2] throughputs in the order of 1 Gbit/s. A key ingredient to achieving this performance is canceling far-end-crosstalk (FEXT) through techniques referred to as vectoring [3].

As bandwidths grow, termination mismatch has more and more impact on the performance of wideband vectoring systems. In practice, a termination mismatch on the customer premises (CP) side occurs when users turn off or disconnect their equipment or simply pick up their phones. At the other end, frequently referred to as distribution point (DP), a termination mismatch may—although probably less frequently—be caused by imperfect maintenance.

Measurements of termination mismatch and evaluation of the corresponding impact on performance have been presented in [4–7] and [8], respectively. A related issue are termination mismatches that occur inside the vectored group when modems leave (are turned off or being disconnected). This type of event, called a Disorderly Leaving Event (DLE) can be dealt with by quickly muting transceivers [9] or by executing a fast channel estimation procedure [10] [11].

Fig. 3.1 illustrates the degradation of signal-to-noise-power ratio (SNR) for a vectored G.fast user when changing the termination of a single *alien line* (a line outside the target vectored group). For many tones, the loss in SNR is far beyond 6 dB, which is the safety margin traditionally used by wireline operators to account for non-stationary channel effects. Simply increasing the SNR margin results in unacceptable throughput losses. Note that contrary to the DLE case, muting transceivers does not solve the problem. Furthermore, since the entire channel matrix is affected, tracking channel coefficients with error sample feedback takes considerable time.

In order to study this effect and assess its impact, accurate and comprehensive measurements are required. Direct measurement of crosstalk paths for each mismatch case is tedious and time-consuming. In this work, we present a model that allows us to predict the impact of impedance changes on crosstalk coupling paths using only crosstalk information for the all-terminated case. The latter is often a priori available, can be measured during an initialization phase where all lines are properly terminated, or can be extracted from established models.

[2]Sum of upstream and downstream bitrates.

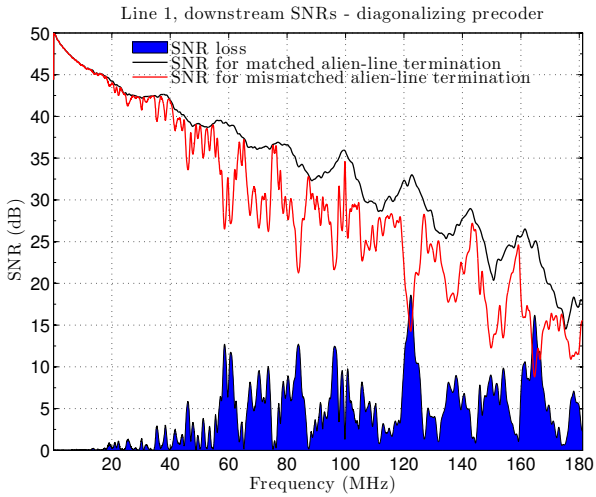

Figure 3.1: Impact of alien-line impedance mismatch: the drop in receive SNR (shaded blue area) when changing the alien-line termination from $100\,\Omega$ (solid black line) to open (solid red line) can be significant. (example for line no. 1 in a 2-line vectored group transmitting over a 100 m 30-pair cable).

Section 3.2 introduces the model and Section 3.3 provides an experimental verification showing a tight fit between directly measured and modeled crosstalk paths for the mismatch case. Section 3.4 demonstrates the application of the model to SNR predictions. Section 3.5 describes the main error sources and Section 3.6 concludes the work.

3.2 PROPOSED MODEL

Consider a wireline channel (cable) with M pairs. The two sides (cable ends) are hereinafter referred as DP-end and CP-end. The formulation presented here is valid for a single sub-carrier in the frequency domain. Let $H_{i,j}$ denote[3] the coupling coefficient between pair $j \in \{1,\ldots,M\}$ on the DP-end and pair $i \in \{1,\ldots,M\}$ on the CP-end. $H_{i,i}$ and $H_{i,j}, i \neq j$ thus denote direct channel coefficients and FEXT coupling coefficients in downstream direction, respectively. Let $N_{i,j}$ denote the coupling coefficient between pair $j \in \{1,\ldots,M\}$ on

[3]Notation: $H_{i,j}$ denotes the element in row no. i and column no. j of the matrix H and $H_{m:n,k:\ell}$ denotes the size $(n-m+1)\times(\ell-k+1)$ submatrix consisting of rows no. m to n and columns no. k to ℓ.

the CP-end and pair $i \in \{1,\ldots,M\}$ on the CP-end. $N_{i,i}$ and $N_{i,j}, i \neq j$ thus denote echo coefficients and near-end crosstalk (NEXT) coupling coefficients on the CP-end, respectively.

For illustration, but without loss of generality, we consider a small vectored group involving only two pairs no. 1 and no. 2 (cf. Fig. 3.2 top). In case all $2M$ termination impedances match perfectly, the receive signal on pair 1 at the CP-end can be written as

$$y_1 = H_{1,1}x_1 + H_{1,2}x_2, \tag{3.1}$$

where x_i are the transmit signals sent on the DP-end. Now assume that alien line no. ℓ, $\ell \in \{3,\ldots,M\}$ is terminated in a mismatching impedance on the CP-end, which results in a reflection of the arriving signal (cf. Fig. 3.2 bottom). Let $r_\ell \in \mathbb{C}, |r_\ell| \leq 1$ represent the reflection coefficient—ratio of reflected and arriving signal at the CP-end of line no. ℓ. The receive signal can then be written as

$$y_1 = \underbrace{(H_{1,1} + N_{1,\ell}r_\ell H_{\ell,1})}_{\hat{H}^O_{1,1}} x_1 + \underbrace{(H_{1,2} + N_{1,\ell}r_\ell H_{\ell,2})}_{\hat{H}^O_{1,2}} x_2. \tag{3.2}$$

Extending the idea to the general case of a vectored group over pairs[4] no. $1,\ldots,U$, the coupling coefficients for an arbitrary number of mismatched alien lines $\ell \in \mathcal{A} \subset \{U+1,\ldots,M\}$ are given by

$$\hat{H}^O_{1:U,1:U} = H_{1:U,1:U} + \sum_{\ell\in\mathcal{A}} r_\ell N_{1:U,\ell} H_{\ell,1:U} \tag{3.3}$$

In (3.3), we neglect second (and higher) order reflections. In other words, we do not consider components that couple into the vectored group after being reflected twice (or more often) at mismatched alien lines. To summarize, the model yields an estimate $\hat{H}^O$ of the coupling matrix H^O with alien-line termination mismatch[5] using *only* the coefficients H and N for the all-matched case and the reflection coefficient r_ℓ.

3.3 EXPERIMENTAL VERIFICATION

The experimental setup corresponds to the scenario depicted in Fig. 3.2. Three lines were chosen randomly from the same binder of a 0.5 mm, 100 m, 30-pair

[4] For clarity of notation we pick pairs no. 1 to U. Note that an arbitrary size-U set of pairs can be chosen out of $\{1,\ldots,M\}$ by renumbering the pairs.

[5] Although probably less likely, the dual scenario (i.e., training happens while there is an alien-line impedance mismatch and the change occurs when the matching impedance is connected) is possible and can be analyzed by the model.

cable [12]. Two pairs constitute a vectored group ($U = 2$). The third pair ($\ell = 3$) is used as the alien line. All remaining pairs were terminated in 100 Ω resistors.

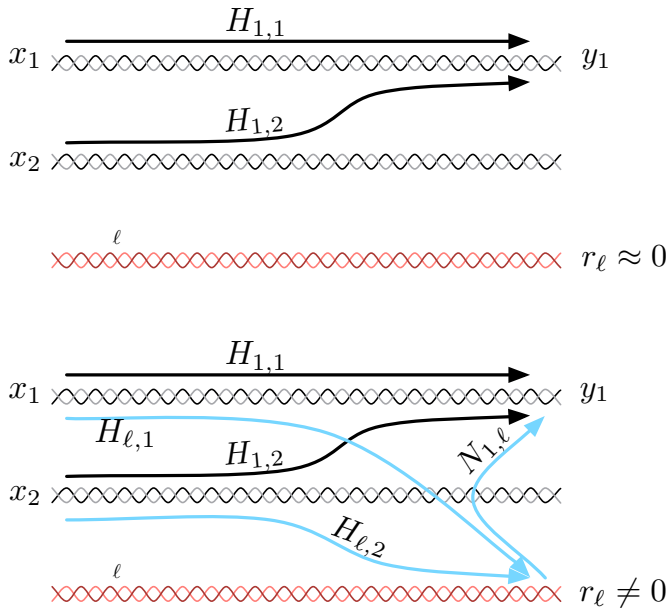

Figure 3.2: Illustration of the model's idea for downstream coupling in line no. 1. Top: For proper alien-line termination ($r_\ell \approx 0$), the received signal is simply $y_1 = H_{1,1}x_1 + H_{1,2}x_2$. Bottom: For alien-line termination mismatch ($r_\ell \neq 0$), the components $H_{\ell,1}x_1 + H_{\ell,2}x_2$ arriving at the mismatched port are reflected and yield an additional FEXT component $N_{1,\ell}r_\ell H_{\ell,1}x_1 + N_{1,\ell}r_\ell H_{\ell,2}x_2$ through the NEXT coupling path.

Direct gain/phase measurements for the approximately matched alien-line case $r_\ell \approx 0$ (Fig. 3.2 top) and the open alien-line case[6] $r_\ell = 1$ (Fig. 3.2 bottom) yield the matrix elements for H and H^O, respectively. In order to verify the model, $\hat{H}^O$ given by (3.3) is calculated from all-terminated FEXT and all-terminated NEXT measurements as

$$\hat{H}^O = H_{1:2,1:2} + r_\ell N_{1:2,3} H_{3,1:2}. \tag{3.4}$$

[6]This choice of reflection coefficient is used to model the case where the customer premises equipment (CPE) is physically disconnected from the phone outlet.

The squared channel gains from line 2 into line 1 are shown in Fig. 3.3. In general, there is a good match between the directly measured coupling function $H_{1,2}^{O}$ (black line) and the modeled coupling function $\hat{H}_{1,2}^{O}$ (red line). The error is concentrated around some dips on the higher frequencies (> 100 MHz).

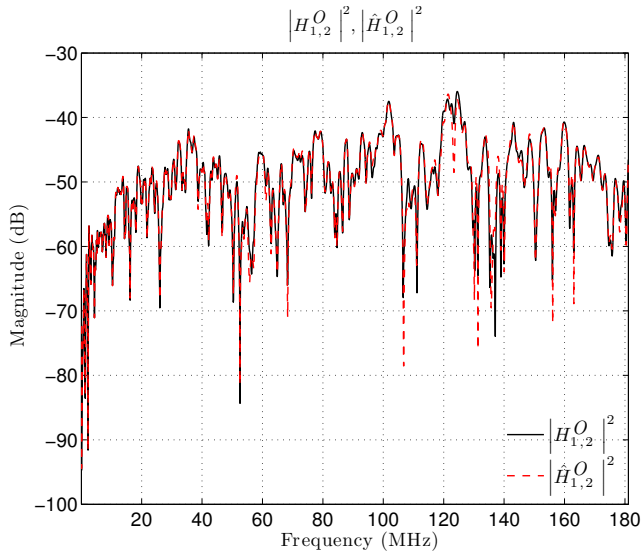

Figure 3.3: Squared magnitude of FEXT coupling coefficients from line 2 into line 1 with open alien line: direct measurement $H_{1,2}^{O}$ and calculated coupling path $\hat{H}_{1,2}^{O}$ using the proposed model (3.3).

3.4 APPLICATION

In order to demonstrate the virtues of the proposed model, the channel data is now used to calculate the SNR when utilizing a diagonalizing precoder [13]. The left and right plot in Fig. 3.4 present results for vectored line no. 1 and no. 2, respectively. The reference SNR curves (black solid lines) labeled SNR_u, where u denotes the line number, were obtained by performing a precoding operation with perfect channel knowledge.

The curves in solid red lines, labeled SNR_u^O, represent the SNR obtained after the alien line termination is removed, resulting in outdated precoder settings. The areas shaded in yellow, denoted ΔSNR_u, represent the SNR loss caused by the termination change. They are calculated as follows

$$\Delta SNR_u = SNR_u - SNR_u^O.$$

The curves in solid blue lines, labeled $\widehat{SNR}_u^O$ were obtained using the channel matrix $\hat{H}^O$ obtained by the model proposed in this letter. It is possible to observe a tight fit between SNR_u^O and $\widehat{SNR}_u^O$ throughout the considered frequency bands.

Finally, the error $e_u = \widehat{SNR}_u^O - SNR_u^O$, is depicted as the area shaded in magenta. It is possible to observe that the error in SNR caused by assuming the proposed model peaks at around 3.3 dB for line 1 and at 2.5 dB for line 2. For both lines, the error could be comfortably covered by the commonly adopted 6 dB of SNR margin.

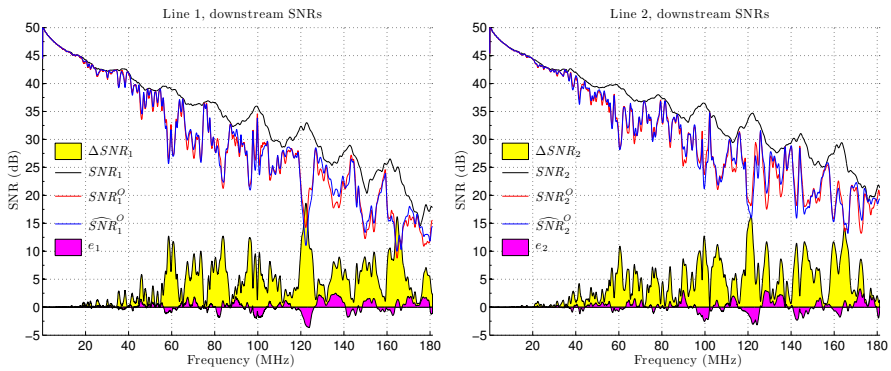

Figure 3.4: SNR comparison before and after the alien-line termination change using diagonalizing precoding in downstream direction, for lines 1 (left) and 2 (right). The black line represents SNR_u, the SNR before alien line termination change. The red lines represents SNR_u^O, the SNR after the terminating resistor is removed. The area shaded in yellow represents ΔSNR_u. The shaded area in magenta represents the SNR error between measurement data and the proposed model.

3.5 ERROR SOURCES

A small discrepancy between unterminated channel measurements, H^O, and channel estimates $\hat{H}^O$ obtained from the proposed model can be observed in Fig. 3.3. This discrepancy is responsible for the error term e_u in the diagonalizing precoder performance presented in Fig. 3.4. In this section we describe the error sources that contribute to the mismatch between direct measurements and model estimates.

3.5.1 MEASUREMENT ERROR

The precision of the measurements for H, H^O and N is limited by the accuracy of the measurement equipment. According to the network analyzer manufacturer [14], its dynamic magnitude and phase accuracy is in the range of $\pm 0.05\,\mathrm{dB}$, ± 0.3 degree respectively.

For some of the measurement sets, the authors had to modify the setup (for example, by connecting and disconnecting terminating resistors manually, i.e. Fig. 3). Even the slightest change in cable geometry caused by such actions (like, for example, slightly bending a wire while dis-/reconnecting) can impact directly measured crosstalk results. Finally, one should also consider imperfect calibration as a source of error in the measurement process.

3.5.2 REFLECTION COEFFICIENT

A second source of error is the assumption of $r_\ell = 1$ for the open-circuit measurements. Since there is always a stray capacitance between the wire ends, r_ℓ is frequency dependent and decreases the termination impedance as frequency grows.

3.5.3 SECOND-ORDER REFLECTIONS

The unavoidable impedance mismatch between a CPE's resistive termination and the characteristic impedance of their respective copper pair results in a small value for the reflection coefficient. If in addition to the alien line one or more other line(s) are not terminated in their exact characteristic impedance ($r_k \neq 0, k \in \{1,\ldots,M\}\backslash\ell$), reflections occur which are not considered in the model. For example, assume $r_2 \neq 0$ in the three-line example (cf. Fig. 3.5). Signal components arriving at this port are reflected and cause an additional contribution to y_1 via $N_{1,2}$ both before ($r_\ell = 0$) and after ($r_\ell \neq 0$) an alien-termination mismatch occurs. For alien-line mismatch ($r_\ell \neq 0$), there is thus an additional term $N_{1,2} r_2 N_{2,\ell} r_\ell H_{\ell,k}$ in $\hat{H}^O_{1,k}$, which is not included in the model (3.3). We refer to this contribution caused by two reflections as second-order reflection.

Note that even for the simple three-line case there are reflections of infinite order between line 2 and line ℓ, however, they vanish due to NEXT coupling attenuation. In practical deployments, due to the distance between cable terminations (and consequently lower NEXT) higher order reflections can be safely disregarded. However, second-order reflections may result in a small modeling error.

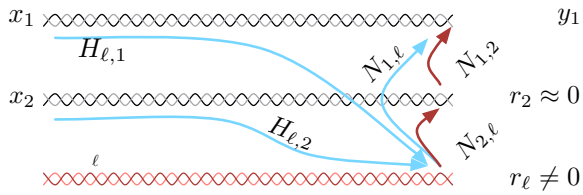

Figure 3.5: Example of second order reflection. The residual crosstalk received by line no. 1 due to a termination change in alien line ℓ is composed of a first-order reflection term (blue arrows) plus a second order reflection (red arrows), $N_{1,2}r_2N_{2,\ell}r_\ell\left(H_{\ell,1}x_1 + H_{\ell,2}x_2\right)$.

3.6 CONCLUSION

An impedance change on an alien line can cause significant changes in the channel matrix seen by a vectored group. Sudden changes may thus cause serious performance degradation or even system instability. In order to properly analyze the impact of this effect and develop appropriate counter measures, accurate and comprehensive channel data is required. Direct measurement of channel matrix changes caused by alien-line termination changes is cost- and labour-intensive. This letter proposes a model-based approach to capturing the impact of alien-line termination changes using only NEXT/FEXT data for the terminated case: based on NEXT/FEXT channel data, the signal arriving at the mismatched port is quantified. The mismatch causes a (possibly partial) reflection depending on the actual termination at hand. Using NEXT/FEXT channel data, the strengths of these components arriving at all ports of interest in the vectored group can be accurately computed.

References

[1] P. Ödling, T. Magesacher, S. Höst, P. Börjesson, M. Berg, and E. Areizaga, "The fourth generation broadband concept," *IEEE Communications Magazine*, vol. 47, no. 1, pp. 62–69, 2009.

[2] *Fast Access to Subscriber Terminals - Physical Layer Specification*, International Telecommunication Union Recommendation Draft, 2013.

[3] G. Ginis and J. Cioffi, "Vectored transmission for digital subscriber line systems," *IEEE Journal on Selected Areas in Communications*, vol. 20, no. 5, pp. 1085–1104, 2002.

[4] TNO, "G.fast: Vectoring Gain Limitations due to Changing Terminations of Alien Wire Pairs," ITU-T SG15 Contribution 2013-03-Q4-044, Mar. 2013.

[5] Lund University and Ericsson AB, "G.fast: Impact of Alien-Line Termination Changes on Vectoring Performance," ITU-T SG15 Contribution 2013-10-Q4-028, Oct. 2013.

[6] Alcatel-Lucent, "G.fast: Influence of an Impedance Change on a Leaving Line onto the Direct and Crosstalk Channels of the Active Lines," ITU-T SG15 Contribution 2013-10-Q4-058, Oct. 2013.

[7] Futurewei Technologies, "G.fast: SNR Drop and FEXT Channel Variations due to Change of Alien Termination," ITU-T SG15 Contribution 2013-10-Q4-046, Oct. 2013.

[8] E. Medeiros, T. Magesacher, P.-E. Eriksson, C. Lu, and P. Ödling, "How vectoring in G.fast may cause neighborhood wars," in *Proc. IEEE International Conference on Communications (ICC)*, 2014, pp. 3865–3870.

[9] *Self-FEXT Cancellation (Vectoring) for Use with VDSL2 Transceivers*, International Telecommunication Union Recommendation, Sep. 2010.

[10] C. Lu and P.-E. Eriksson, "A fast channel estimation method for disorderly leaving events in vectored DSL systems," in *Proc. IEEE International Conference on Communications (ICC)*, 2011, pp. 1–6.

[11] *Self-FEXT Cancellation (Vectoring) for Use with VDSL2 Transceivers - Corrigendum 1*, International Telecommunication Union Recommendation, Jun. 2011.

[12] Ericsson AB, *Access Network Pair cable, TEL 312*, 2010. [Online]. Available: http://goo.gl/4RdCXc

[13] R. Cendrillon, G. Ginis, E. Van den Bogaert, and M. Moonen, "A near-optimal linear crosstalk precoder for downstream VDSL," *IEEE Transactions on Communications*, vol. 55, no. 5, pp. 860–863, 2007.

[14] Agilent Technologies, Inc., *Agilent 4395A Network/Spectrum/Impedance Analyzer 500 MHz*, 2000. [Online]. Available: http://goo.gl/suqFrM

4

Mitigating Disorderly Leaving Events in G.fast

Yezi Huang, Thomas Magesacher, Eduardo Medeiros,
Chenguang Lu, Per-Erik Eriksson and Per Ödling

Abstract

Vectoring is a vital component of wideband wireline communication systems. A disorderly leaving event (DLE) disturbs the vectoring operation since the precoder, which was designed for the channel before the change, is no longer up to date. Measurements indicate that the impact of a DLE can be serious for frequencies beyond 30 MHz, which corresponds to the band used by emerging wideband communication systems over short multi-pair copper cables such as G.fast. As an alternative to the state-of-the-art update procedure, this paper presents an approach to mitigating the DLE problem. By interpreting DLE with the FEXT-reflected-NEXT (FRN) model, we propose a scheme that enables the showtime lines to return to disturbance-free transmission once the loss of signal on a certain line is detected while updating the precoder as a background process. Furthermore, the estimation complexity for a K-user vectoring group is reduced from $\mathcal{O}(K^2)$ to $\mathcal{O}(K)$. [1]

[1] Published in *Proc. IEEE International Conference on Communications (ICC 2015)*, London, United Kingdom, 08-12 Jun. 2015.

4.1 INTRODUCTION

The widespread deployment of cloud-based services and video-on-demand offerings continues to drive data rate and quality of service requirements for last-mile connections. In response to this trend, the wireline access industry advances towards a fiber to the last distribution point paradigm [1]. In this scenario, the recently consented G.fast standard [2] exploits shorter copper pairs and high bandwidth to provide up to around 1 Gbits/s aggregate net data rate.

Modern wideband wireline communication systems (such as G.fast) employ techniques referred to as vectoring [3] in order to cooperatively mitigate crosstalk. As vectoring relies on accurate channel information, changes of the terminating impedance in the multi-port wireline channel may cause severe performance degradation in terms of signal-to-noise ratio (SNR) as exemplified in Fig. 4.1. A change of impedance alters the perceived channel coupling conditions, and leads to residual crosstalk caused by an outdated precoder (or equalizer).

A particular event resulting in sudden termination change occurs when a modem *within* an active vectored group is turned off abruptly or is disconnected due to line disruption. This occurrence is called a disorderly leaving event (DLE), and was first reported during the development of vectored VDSL2 [3]. A fast channel tracking method was proposed in [4] to deal with DLEs in VDSL2. Unfortunately, it cannot be applied to G.fast since it is based on the assumption that only one column of the channel matrix changes.

In [5], a procedure is described that allows G.fast transceivers to leave a vectored group without negatively impacting the performance of other lines in the same bundle. The main idea is to allow coordination between transceivers at both ends, and acquire information necessary to update the precoder/equalizer before the line leaves and its termination impedance changes. While solving the problem of orderly leaving events, [5] does not address situations where there is no previous intent announced by the leaving transceiver(s).

This paper has two main contributions: First, we extend the model presented in [6] [7] to address DLEs, and identify the source of DLE disturbance that we can control. Second, we develop a novel precoder update procedure that does not disturb other lines while performing channel estimation as a background process.

The paper is organized as follows. In Section 4.2 a system model is presented to explain DLE. Taking advantage of this model, we formulate the DLE disturbance in Section 4.3 and propose in Section 4.4 a parameter-based channel estimation procedure that minimizes the impact of DLEs for the remaining active users. Section 4.5 demonstrates the effectiveness of the proposed method with channel measurements and simulations. Section 4.6 concludes

the work.

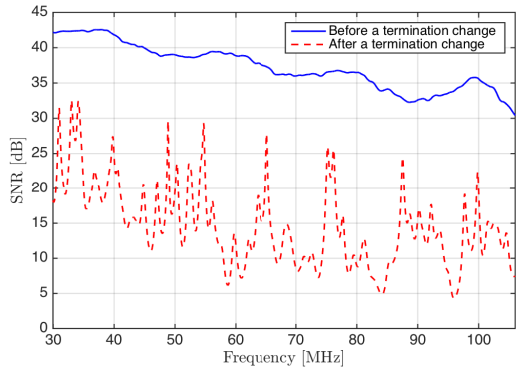

Figure 4.1: SNR on one victim line before and after a termination change. The SNR drop represents the impact of a disrupted vectoring.

Notation: Bold capital letters (*e.g.*, $\mathbf{A}$) and bold lower-case letters (*e.g.*, $\mathbf{a}$) denote matrices and column vectors, respectively. $a_{i,j}$ is an element on the i-th row and j-th column of $\mathbf{A}$ and a_i is the i-th element of $\mathbf{a}$. $\mathbf{I}_{n\setminus i}$ is an n-dimensional identity matrix excluding the i-th row. $\mathcal{M}_i\{\mathbf{A}\}$ denotes an operator deleting both the i-th row and column from $\mathbf{A}$. Operator "$\setminus$" excludes certain element(s) on the right-hand side from the set on the left-hand side.

4.2 FEXT-REFLECTED-NEXT (FRN) MODEL FOR DLE

Consider a wideband discrete multi-tone modulation (DMT) system with a group of K twisted pairs (or equivalently, users). The twisted pairs connect the transceivers at the distribution point (DP) with the customer premise equipment (CPE).

In [6] [7], a FEXT-reflected-NEXT (FRN) model is proposed to characterize the changed coupling condition due to an alien-line impedance mismatch at the CPE. A DLE is similar—except now the impedance change happens within the vectored group as illustrated in Fig. 4.2. Without loss of generality, we illustrate the DLE coupling model in downstream on a certain sub-carrier. Since G.fast employs Time–Division Duplex (TDD), the model for downstream applies, *mutatis mutandis*, to upstream.

Let $\mathbf{H} \in \mathbb{C}^{K\times K}$ denote the frequency-domain channel matrix on a certain sub-carrier for the perfectly-terminated case, where diagonal and off-diagonal elements are direct-channel coefficients and far-end crosstalk (FEXT) coefficients, respectively. For the sake of simple notation, but without loss of gener-

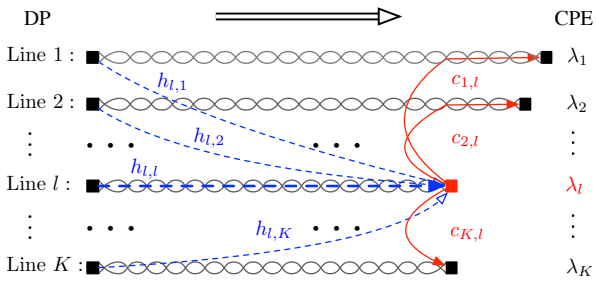

Figure 4.2: Downstream FRN model. *Dash lines*: Channel paths from DP to the mismatched termination l. *Solid lines*: near-end coupling paths from the mismatched termination l to the remaining CPEs.

ality, the sub-carrier index is omitted. Let $\mathbf{\Lambda} = \mathrm{diag}\left([\lambda_1, \lambda_2, \ldots, \lambda_K]\right) \in \mathbb{C}^{K\times K}$ denote a diagonal matrix with termination reflection coefficients and let $\mathbf{C} \in \mathbb{C}^{K\times K}$ denote the near-end crosstalk (NEXT) coupling matrix at the CPE-side. For scenarios with unequal pair-lengths, $\mathbf{C}$ denotes attenuated NEXT (as illustrated in Fig. 4.2 for the l-th column of $\mathbf{C}$). The diagonal entries of $\mathbf{C}$, corresponding to the CPE-side echo coefficients, are assumed to be 0. The channel matrix $\mathbf{H}'$ for the general case is

$$\mathbf{H}' = \mathbf{H} + \mathbf{\Delta},$$

where $\mathbf{\Delta} = \mathbf{C\Lambda H}$ quantifies the deviation from the all-terminated case according to the FRN model. When the terminations at the CPE are perfectly matched (*i.e.*, $\lambda_i = 0$ for $i = 1, \ldots, K$), then $\mathbf{\Delta} = \mathbf{0}$ and thus $\mathbf{H}' = \mathbf{H}$.

Vectoring enables cooperative signal processing within the group. A properly designed precoder in downstream and equalizer in upstream at the DP significantly reduces FEXT. In this work, we focus on linear precoding and thus on the frequency range up to 106 MHz (cf. [2]). Specifically in downstream, let $\mathbf{G} = \mathrm{diag}\left([g_1, g_2, \ldots, g_K]\right) \in \mathbb{R}^{K\times K}$ denote a diagonal matrix with the gain adjusters for each line on the main diagonal. Assume that the cyclic prefix of DMT is not shorter than the impulse responses of the coupling paths. Furthermore, assume that the inverse fast Fourier transform (IFFT) for the group users is well synchronized. After including linear precoder $\mathbf{P}_o$, transmitting $\mathbf{x} \in \mathbb{C}^{K\times 1}$ at the DP-side yields the receive signal $\mathbf{y} \in \mathbb{C}^{K\times 1}$ given by

$$\mathbf{y} = \mathbf{H}'\mathbf{P}_o\mathbf{G}\mathbf{x} + \mathbf{n},$$

where $\mathbf{n} \in \mathbb{C}^{K\times 1}$ denotes the background noise. An ideal precoder designed for $\mathbf{H}$ at DP neutralizes the crosstalk effectively such that for the input sym-

bols $\mathbf{x}$

$$\mathbf{H}\mathbf{P}_o\mathbf{G}\mathbf{x} = \mathbf{\Sigma}\mathbf{x}, \tag{4.1}$$

where $\mathbf{\Sigma} \in \mathbb{C}^{K\times K}$ is diagonal.

In practice, most often only one diagonal element of $\mathbf{\Lambda}$ will deviate significantly from 0 as a result of a DLE (*i.e.*, mismatch of a single line only). Assume line l exhibits a DLE, which is quantified by a reflection coefficient $|\lambda_l| \gg 0$. Consequently, $\mathbf{\Delta} \neq \mathbf{0}$ and all FEXT coupling coefficients change. The new FEXT arriving at termination k, $(k \neq l)$ is determined by

$$(\mathbf{h}'_k)^T = \mathbf{h}_k^T + c_{k,l}\lambda_l\mathbf{h}_l^T,$$

where $\mathbf{h}_l^T$ indicates the l-th row of $\mathbf{H}$, and $(\mathbf{h}'_k)^T$ is the k-th row of $\mathbf{H}'$. The outdated precoding with $\mathbf{P}_o$ fulfilling Eq. (4.1) yields the disturbed receive signal

$$\mathbf{y}' = \underbrace{\mathbf{H}\mathbf{P}_o\mathbf{G}\mathbf{x} + \mathbf{n}}_{\mathbf{y}_d} + \underbrace{\mathbf{C}\mathbf{\Lambda}\mathbf{H}\mathbf{P}_o\mathbf{G}\mathbf{x}}_{\boldsymbol{\xi}}, \tag{4.2}$$

where $\mathbf{y}_d$ is the desired receive signal obtained in the perfectly-terminated case and $\boldsymbol{\xi}$ is the residual crosstalk due to the DLE. Equivalently, the effective channel changes from $\mathbf{H}$ to $\mathbf{H}' = \mathbf{H} + \mathbf{\Delta}$.

The FRN model described in [6] [7] suggests that FEXT arrives at and is reflected by the alien mismatched termination only. Compared to the alien-line case, in a DLE the leaving line is always active. As the direct path $h_{l,l}$ has a lower channel attenuation than the FEXT paths $h_{l,k}$, $k \in \{1,\ldots,K\}\backslash l$, the residual-crosstalk issue in a DLE could be even worse.

We demonstrate the impact of a DLE on the channel coupling conditions by means of crosstalk-paths and direct-path measurements from a 30-pair, 100 m, 0.5 mm cable [8]. 10 pairs from a single binder were chosen at random. The measurement points follow a 51.75 kHz sub-carrier spacing, and we consider 2 048 sub-carriers in total corresponding to the frequency range up to 106 MHz. The all-terminated case and a DLE-case where line $l = 10$ is left unterminated yield two 10×10 matrices $\mathbf{H}$ and $\mathbf{H}'$ respectively. The 10-th row of $\mathbf{H}'$ is left the same as that of $\mathbf{H}$. The corresponding channel-matrix deviation is thus given by $\mathbf{\Delta} = \mathbf{H}' - \mathbf{H}$. We quantify the impact of this DLE on vectoring in terms of the worst residual crosstalk $\mathcal{P}_k^{\text{rx}}$ over all lines

$$\mathcal{P}_k^{\text{rx}} = \mathcal{P}^{\text{tx}} + 20\log_{10}(\max_i |\delta_{i,k}|), \tag{4.3}$$

when line k is excited by a signal with transmit power spectrum density (PSD) $\mathcal{P}^{\text{tx}}$. In essence, Eq. (4.3) evaluates the maximum power of the k-th column of $\mathbf{\Delta}$.

Fig. 4.3 shows the crosstalk power for $\mathcal{P}^{\text{tx}} = -76\,\text{dBm/Hz}$ with respect to the background noise of $-140\,\text{dBm/Hz}$. Clearly, the channel changes in

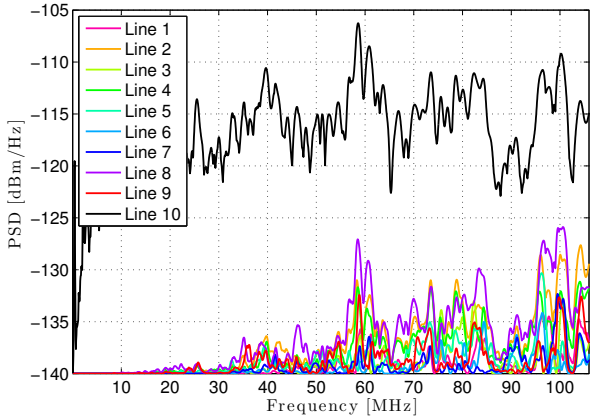

Figure 4.3: Comparison of the strongest crosstalk caused by each column of $\mathbf{\Delta}$, when having a vectored group size of $K = 10$ and line $l = 10$ is leaving.

the column $l = 10$ (black curve) are dominant, which is consistent with the assumption in [4]. However, channel changes in the other columns become disturbing for frequencies beyond 30 MHz. Except for the l-th row, every other entry of $\mathbf{\Delta}$ contributes to the new channel $\mathbf{H}'$. Equivalently, almost every element of $\mathbf{H}$ changes due to a DLE.

4.3 RESIDUAL CROSSTALK ANALYSIS

In downstream direction, changed channel coupling conditions result in an outdated precoder. Specifically, the linear precoder as in [9] defines

$$\mathbf{P}_o = \mathbf{H}^{-1}\mathbf{H}_\Sigma, \tag{4.4}$$

where the diagonal matrix $\mathbf{H}_\Sigma$ contains direct channel coefficients of the all-terminated channel $\mathbf{H}$.

Consider the DLE case where line l leaves while all other lines are perfectly terminated. Thus, $\mathbf{\Lambda} = \text{diag}\left([0,\ldots,0,\lambda_l,0,\ldots,0]\right)$ and the resulting reflection-followed-by-NEXT paths $\mathbf{C\Lambda}$ are given by

$$\mathbf{C\Lambda} = \begin{bmatrix}\mathbf{0} & \ldots & \mathbf{0} & \mathbf{v}_l & \mathbf{0} & \ldots & \mathbf{0}\end{bmatrix}, \tag{4.5}$$

where the reflecting crosstalk coefficients are defined in a vector as

$$\mathbf{v}_l = \lambda_l \left[c_{1,l},\ldots,c_{i,l},\ldots,c_{K,l}\right]^T. \tag{4.6}$$

According to Eq. (4.2), the residual crosstalk when using the outdated precoder $\mathbf{P}_o$ is given by

$$\begin{aligned}\boldsymbol{\xi} &= \mathbf{C}\boldsymbol{\Lambda}\mathbf{H}\mathbf{P}_o\mathbf{G}\mathbf{x} \\ &= \mathbf{C}\boldsymbol{\Lambda}\mathbf{H}_{\Sigma}\mathbf{G}\mathbf{x}. \end{aligned} \tag{4.7}$$

Using Eq. (4.5), the expression (4.7) for the residual crosstalk simplifies to

$$\begin{aligned}\boldsymbol{\xi} &= \mathbf{v}_l h_{l,l} g_l x_l \\ &= \mathbf{v}_l \sigma_l x_l, \end{aligned} \tag{4.8}$$

where x_l is the l-th element of $\mathbf{x}$, and $\sigma_l = h_{l,l}g_l$ is the effective gain for path l.

Eq. (4.8) reveals that retaining the outdated precoder $\mathbf{P}_o$ can eliminate the possible FEXT-reflected-NEXT components since the precoder keeps doing its job of mitigating/eliminating FEXT arriving at the reflective surface of termination l. The only source of the residual crosstalk $\boldsymbol{\xi}$ is the transmitted signal x_l on the leaving line via the l-th direct channel $h_{l,l}$ (see the bold dash line in Fig. 4.2), which is then reflected and couples to other CPEs via $\mathbf{v}_l$.

A traditional reaction to DLE, however, is to stop transmission on the leaving line as soon as possible, and quickly update the linear precoder at the DP to $\overline{\mathbf{P}}$ fulfilling

$$\mathcal{M}_l\left\{\mathbf{H}\right\}\overline{\mathbf{P}}\mathcal{M}_l\left\{\mathbf{G}\right\} = \mathcal{M}_l\left\{\boldsymbol{\Sigma}\right\}, \tag{4.9}$$

to diagonalize the dimension-reduced original channel $\mathcal{M}_l\left\{\mathbf{H}\right\}$. The FRN model implies that stopping transmission on the leaving line only avoids FEXT from line l (*i.e.*, the l-th column of $\mathbf{H}$), but does not avoid FEXT to line l (*i.e.*, the l-th row of $\mathbf{H}$). Instant update of the precoder to $\overline{\mathbf{P}}$ does not cancel FEXT through paths $h_{l,k}$ for $k \in \{1,\ldots,K\}\backslash l$, which are then reflected at mismatched port and couple as NEXT to the victim lines resulting in residual crosstalk. Moreover, immediate line shutoff is sensitive to DLE false alarm or detection failure [4], which leads to unnecessary retraining of the tranceivers.

In the upstream direction, the FRN model suggests that the leaving line l "emits" an unwanted upstream signal as a result of "incoming" NEXT being reflected by the mismatched port at the CPE side. The resulting upstream FEXT through coupling into $k \in \{1,\ldots,K\}\backslash l$ is taken care of by the interference canceler, whose coefficients are still correct for coupling paths from line l at the CPE to lines $k \in \{1,\ldots,K\}\backslash l$ at the DP. The resulting upstream FEXT coefficients from lines $k \in \{1,\ldots,K\}\backslash l$ into line l change and cause residual FEXT at the interference canceler output on line l, which is no problem since transmission on line l is interrupted anyway.

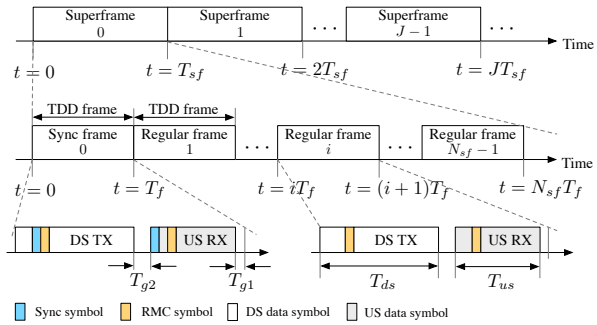

Figure 4.4: G.fast TDD structure at the DP-side. Time gaps are reserved between paired down- and up-stream as T_{g2} and between upstream and next downstream as T_{g1}. The sum of the T_{g1} and T_{g2} equals to one DMT symbol duration.

4.4 PROPOSED RESIDUAL-CROSSTALK-FREE CHANNEL ESTIMATION

A reference time-line for G.fast TDD frames is shown in Fig. 4.4. A typical TDD frame is $T_f = 750\,\mu s$ long and consists of $N_f = 36$ DMT symbols. A superframe for this setting consists of $N_{sf} = 8$ TDD frames. The first frame of each superframe is a sync-frame, which contains one synchronization symbol located at a predefined symbol position in both directions. The sync-frame is then followed by 7 regular frames without synchronization symbols.

Assume that a DLE happens at time instant t_l at the CPE. In case t_l falls into a downstream transmission interval of the i-th TDD frame ($t_l \in \big[(i-1)T_f, (i-1)T_f + T_{ds}\big]$), the DP will detect this event during the next upstream transmission period ($t \in \big[(i-1)T_f + T_{ds} + T_{g2}, iT_f - T_{g1}\big]$). The DP initiates upstream channel tracking and in the next downstream transmission period and onwards ($t \geq iT_f$), it transmits *idle symbols* [2] at non-synchronization symbol positions on the leaving line l. The main idea is to mute the data symbols on line l but keep transmitting the anti-crosstalk signals to cancel out FEXT arriving at the mismatched termination of line l at the CPE. According to the FRN model (cf. Fig. 4.2), there is thus no energy to cause reflections and subsequent NEXT into the other lines. A more detailed illustration for this special operation will be given below. If the DLE occurs during an upstream transmission interval, the channel tracking for upstream and "muting line l" for downstream launch directly.

Generally, instead of turning off the leaving line immediately after detecting a loss of signal (*los*), channel estimation and precoder update in downstream direction is accomplished by alternating two kinds of special symbols: idle symbols and synchronization symbols (as illustrated in Fig. 4.5).

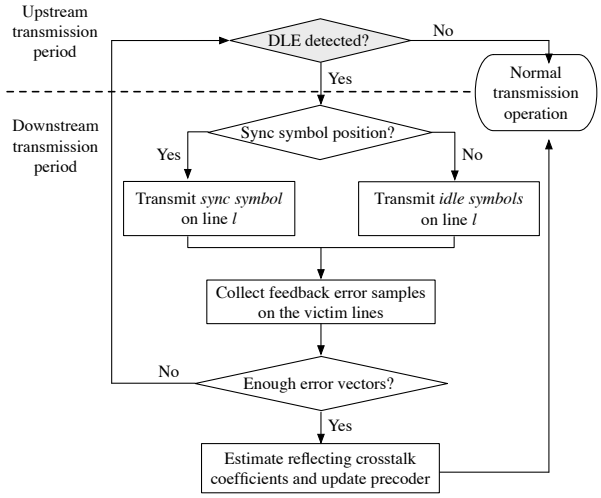

Figure 4.5: Flowchart of proposed operation at the DP-side

SILENT MODE By modifying the l-th gain adjuster to be $g_l = 0$ at non-synchronization symbol positions, idle symbols are transmitted on the leaving line. The residual crosstalk $\boldsymbol{\xi}$ in Eq. (4.8) on the victim lines becomes $\boldsymbol{\xi} = \mathbf{v}_l h_{l,l} x_l \cdot 0 = 0$. It enables "silent" estimation and updating in the sense that active users remain undisturbed. Thus, we call this kind of transmission mode *silent mode*. The DLE noisy period is at most $T_{ds} + T_{g2}$ before *los* on line l is detected.

SYNCHRONIZATION MODE Synchronization symbols are transmitted every 6 ms (*i.e.*, one superframe duration) on each line in G.fast. Assume J superframes are required before the estimation is completed. Let t_j be the time instant to transmit the j-th downstream synchronization symbol. In this specific time slot, the l-th gain adjuster is set back to g_l, which is used for transmission before DLE. According to Eq. (4.1), Eq. (4.2) and Eq. (4.8), transmitting synchronization symbol $\mathbf{s}(t_j) = [s_1(t_j), \ldots, s_l(t_j), \ldots, s_K(t_j)]^T$ yields

$$\begin{aligned}\mathbf{q}(t_j) &= \boldsymbol{\Sigma}\mathbf{s}(t_j) + \mathbf{v}_l \sigma_l s_l(t_j) + \mathbf{n} \\ &= \boldsymbol{\Sigma}\left(\mathbf{s}(t_j) + \mathbf{e}(t_j)\right),\end{aligned}$$

where $\mathbf{e}(t_j) = \boldsymbol{\Sigma}^{-1}\left(\mathbf{v}_l \sigma_l s_l(t_j) + \mathbf{n}\right)$. The synchronization error samples $\mathbf{I}_{K\setminus l}\mathbf{e}(t_j)$ on the victim lines are then fed back to the DP [2].

After sending the synchronization symbol at the scheduled time instant, the transmission on line l goes back to idle symbols for all non-synchronization

symbol positions. Keep on alternatively sending idle symbols and synchronization symbols on the leaving line until DP collects J error symbols on the victim lines as

$$\begin{aligned}\mathbf{E} &= \mathbf{I}_{K\backslash l}\left[\mathbf{e}(t_1), \mathbf{e}(t_2), \ldots, \mathbf{e}(t_J)\right] \\ &= \mathbf{I}_{K\backslash l}\boldsymbol{\Sigma}^{-1}\mathbf{v}_l\sigma_l\mathbf{s}_l^T + \mathbf{N},\end{aligned}$$

where $\mathbf{s}_l = \left[s_l(t_1), \ldots, s_l(t_J)\right]^T$ is the synchronization sequence transmitted on the leaving line l at t_j $(j = 1, \ldots, J)$, and $\mathbf{N} \in \mathbb{C}^{(K-1)\times J}$ is the equalized additive noise on victim lines for J synchronization time instants. The contributing reflecting crosstalk coefficients in Eq. (4.6) can be estimated by

$$\widehat{\mathbf{v}}_l = \frac{\mathcal{M}_l\left\{\boldsymbol{\Sigma}\right\}\mathbf{E}\mathbf{s}_l^*\left(\mathbf{s}_l^T\mathbf{s}_l^*\right)^{-1}}{\sigma_l}, \quad \widehat{\mathbf{v}}_l \in \mathbb{C}^{(K-1)\times 1}, \tag{4.10}$$

where $\mathbf{s}_l^*$ is the conjugate of $\mathbf{s}_l$. Although the full channel matrix of $\mathcal{M}_l\left\{\mathbf{H}\right\}$ is changed due to a single DLE, the estimation effort of the proposed method reduces from $(K-1)^2$ parameters to $K-1$ by modeling the changed coupling condition with reflecting crosstalk coefficients in $\mathbf{v}_l$.

During the whole process, the DP-side is still able to track the received signal power on line l. In case of, for example, a false alarm of DLE, no channel retraining is required and it is fast to get back to the normal transmission by a simple setting on g_l.

With $\mathbf{v}_l$ estimated, the precoder can be updated for the new channel matrix $\mathcal{M}_l\left\{\mathbf{H}'\right\}$ according to the FRN model, *i.e.*,

$$\widehat{\mathbf{P}} = \left(\mathcal{M}_l\left\{\mathbf{H}\right\} + \widehat{\mathbf{v}}_l\boldsymbol{\mathcal{E}}_l^T\mathbf{H}\mathbf{I}_{K\backslash l}^T\right)^{-1}\mathcal{M}_l\left\{\mathbf{H}'_\Sigma\right\}, \tag{4.11}$$

where $\boldsymbol{\mathcal{E}}_l$ is an elementary column vector with only 1 on the l-th position and 0s elsewhere.

4.5 SIMULATION RESULTS

In order to evaluate the proposed scheme, we consider a vectoring system with $K = 3$ users operating on the 100 m-cable [8] introduced in Section 4.2. A DLE occurs on line $l = 3$. We use G.fast system parameters [2] and focus on the frequency-range up to 106 MHz. The special silent mode we propose in Section 4.4 is appraised in terms of SNR drop, introduced in Fig.4.1. We also compare our operation with the traditional method both in frequency and in time based on the PSD of the resulting residual crosstalk.

Fig. 4.6 shows that the SNR drop caused by a DLE on the victim lines can be mitigated by setting the gain scaling factor of line l to zero, which would essentially solve the DLE problem. However, keeping the analog front-end

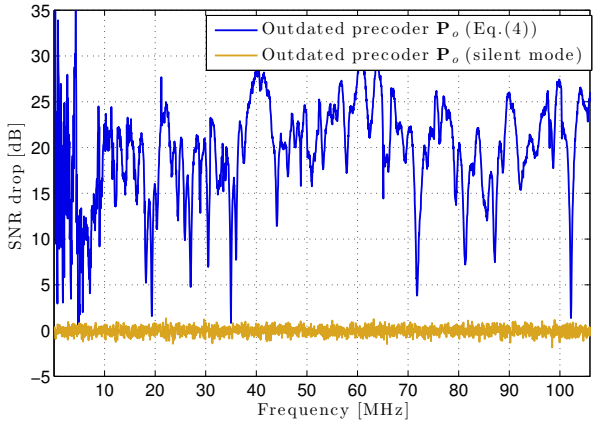

Figure 4.6: SNR drop on victim line 1 after DLE, given full line transmission with the outdated precoder $\mathbf{P}_o$.

running to send pure anti-crosstalk signals consumes power. If the line has already left, it is thus desirable to invoke the second mode in order to update the precoder for the new dimension-reduced channel $\mathcal{M}_l\{\mathbf{H}'\}$.

Fig. 4.7 presents the residual crosstalk PSD on one of the victim lines in the vectored group. By stopping transmission on the leaving line and updating the precoder to $\overline{\mathbf{P}}$ based on the dimension-reduced original channel $\mathcal{M}_l\{\mathbf{H}\}$ (*i.e.*, the traditional operation as defined by Eq. (4.9)), there is an improvement in SNR (comparing the second curve to the top one). However, the residual crosstalk power level is still far above the background noise level, especially for high frequencies where the crosstalk channel has a power level closer to that of the direct channel. Thus, further channel tracking is needed.

In contrast, both modes in our proposed operation suppress the residual crosstalk down to the background noise level throughout the studied frequency range. The victim lines are able to retrieve the residual-crosstalk-free transmission via the silent mode (yellow curve). With $J = 1$ synchronization symbol, the estimated precoder $\widehat{\mathbf{P}}$ can effectively take care of the new channel matrix $\mathcal{M}_l\{\mathbf{H}'\}$ (green curve).

Assume no persistent detection of *los* requirement as in [3] is considered for now, and no signal processing time is counted in. Fig. 4.8 and Fig. 4.9 compare the residual crosstalk on a certain sub-carrier when the DLE happens at two extreme time slots (time instants indicated by the black line): Fig. 4.8 shows the longest time distance to the next synchronization symbol, and Fig. 4.9 presents the shortest time distance. The average residual crosstalk power on

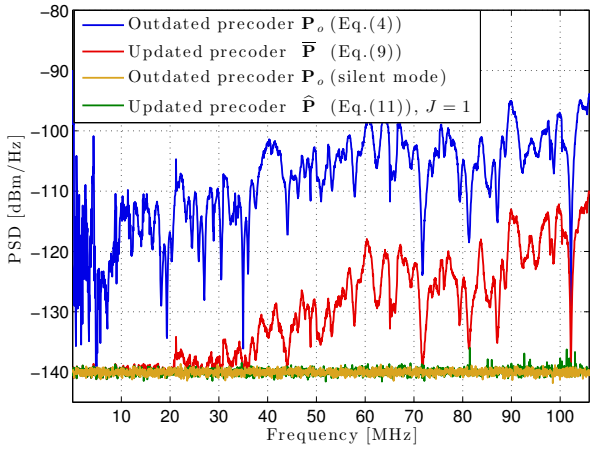

Figure 4.7: Residual crosstalk in frequency after DLE on victim line 1.

victim line k is calculated over one frame on one sub-carrier as

$$E[|\xi_k|^2] = \frac{1}{N_{ds}} \sum_{j=1}^{N_{ds}} |\xi_k(j)|^2,$$

where N_{ds} is the number of DMT symbols assigned to downstream transmission in one frame.

As indicated with different vertical time lines in Fig. 4.8 and Fig. 4.9, both the traditional and our proposed method deal with the DLE disturbance in two steps. Once *los* is detected, the first step is taken in the next frame (time instant marked by the yellow line). For the traditional method, the channel dimension is reduced and the precoder is updated to $\overline{\mathbf{P}}$. For our proposed method, the silent mode is activated by transmitting idle symbols on the leaving line. Both methods work well on low-frequency sub-carriers (*e.g.*, 20 MHz in Fig. 4.8a and Fig. 4.9a). However, on higher-frequency sub-carriers (*e.g.*, 100 MHz), $\overline{\mathbf{P}}$ is not adequate for crosstalk cancellation, as shown by the error plateau in Fig. 4.8b and Fig. 4.9b. Residual crosstalk severely disturbs the active users before enough error samples can be collected (time instant marked by the pink line) to proceed with a second step, aiming at a precoder update based on the acquired estimates. A traditional way is to perform an elementwise estimation of the dimension-reduced new channel $\mathcal{M}_l\{\mathbf{H}'\}$ using synchronization symbols and pilot sequences. When Hadamard sequences are applied, $2^{\lceil \log_2(K-1) \rceil}$ synchronization symbols are required to estimate $(K-1)^2$ channel matrix elements. For example, a single DLE in a vectored group of $K = 100$ would keep on disturbing the active users for at

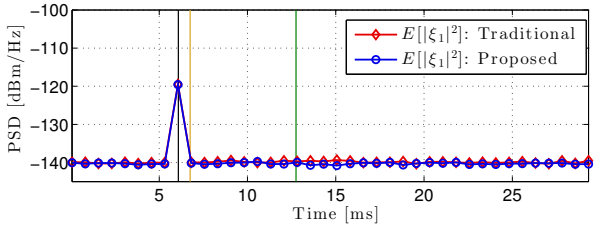

(a) Average residual crosstalk on a sub-carrier at 20 MHz

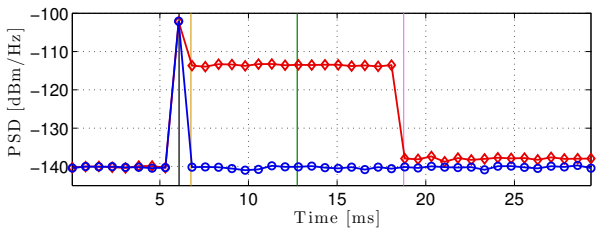

(b) Average residual crosstalk on a sub-carrier at 100 MHz

Figure 4.8: Average residual crosstalk $E[|\xi_1|^2]$ in time on victim line 1 in downstream at the worst situation: DLE happens one symbol after the synchronization symbol during downstream transmission interval.

least $128 \times 6 = 768$ ms, and require an estimation of $99^2 = 9\,801$ entries for each sub-carrier.

The proposed operation, instead, keeps residual crosstalk close to the background noise level during and after the process of estimation and update (time instant marked by the green line), and makes the dimension-reducing operation unnoticeable. Once the DP is aware of the *los*, there is no more crosstalk disturbing the victim lines. Given persistently detected *los* on line l and accomplished estimation of the new channel matrix, it is safe then to completely remove line l from the vectored group.

It is worth noting that keeping the precoder the same as before the DLE during channel estimation has three advantages. First, other active users in showtime are not disturbed, thanks to the silent mode. Second, it enables FRN-based modeling, which significantly reduces the estimation effort. A traditional method requires orthogonal synchronization sequences to estimate $(K-1)^2$ channel coefficients, while our parameter-based method can exploit the synchronization symbols on line l as a unique reference for estimating the $K-1$ reflecting coefficients only. Third, our estimation does not rely on

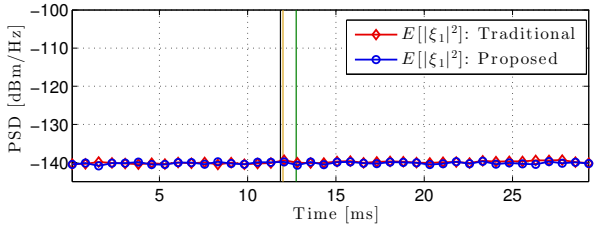

(a) Average residual crosstalk on a sub-carrier at 20 MHz

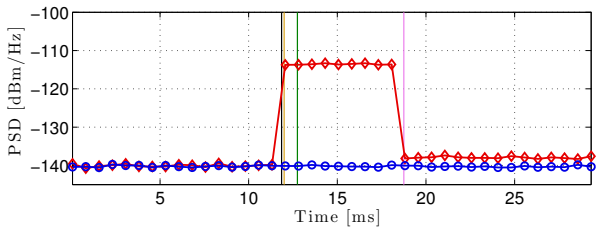

(b) Average residual crosstalk on a sub-carrier at 100 MHz

Figure 4.9: Average residual crosstalk $E[|\xi_1|^2]$ in time on victim line 1 in downstream at the best situation: DLE happens one frame before the synchronization frame during upstream transmission interval.

the orthogonality property. The traditional method shows a slightly higher residual crosstalk-PSD level on severely impacted sub-carriers (cf. Fig. 4.8b and Fig. 4.9b), since the required orthogonality is degraded by background noise.

4.6 CONCLUSION

A sudden termination change due to a DLE alters the original channel matrix of a vectored group, which can have serious consequences for the vectoring operation. Based on the FRN model, we identify the sources and paths for residual crosstalk after the DLE and introduce a model that is parameterized by reflecting crosstalk coefficients. A procedure for channel estimation and precoder update in the downstream direction is proposed. Temporarily retaining the outdated precoder after a DLE narrows potential residual crosstalk paths down to only the direct channel of the leaving line. Compared to the state-of-the-art method, the period during which active users are disturbed

can be significantly shortened to the time it takes to detect the loss of signal and the estimation complexity for a K-user system is reduced from $\mathcal{O}(K^2)$ to $\mathcal{O}(K)$.

References

[1] P. Ödling, T. Magesacher, S. Höst, P. Börjesson, M. Berg, and E. Areizaga, "The Fourth Generation Broadband Concept," *IEEE Communications Magazine*, vol. 47, no. 1, pp. 62–69, January 2009.

[2] ITU, "Fast Access to Subscriber Terminals - Physical Layer Specification," International Telecommunication Union Recommendation Draft, 2014.

[3] ——, "Self-FEXT cancellation (vectoring) for use with VDSL2 transceivers," Recommendation ITU-T G.993.5, Apr. 2010. [Online]. Available: https://www.itu.int/rec/T-REC-G.993.5/en

[4] C. Lu and P.-E. Eriksson, "A Fast Channel Estimation Method for Disorderly Leaving Events in Vectored DSL Systems," in *Proc. 2011 IEEE International Conference on Communications (ICC)*, June 2011, pp. 1–6.

[5] Alcatel-Lucent, "Influence of an Impedance Change on a Leaving Line onto the Direct and Crosstalk Channels of the Active Lines," ITU-T SG15 Contribution 2013-10-Q4-058, Oct. 2013.

[6] Futurewei Technologies, "G.fast: SNR Drop and FEXT Channel Variations due to Change of Alien Termination," ITU-T SG15 contribution 2013-10-q4-046, Mar. 2013.

[7] E. Medeiros, T. Magesacher, P. Ödling, D. Wei, X. Wang, Q. Li, P. Eriksson, C. Lu, J. Boschma, and B. van den Heuvel, "Modeling Alien-Line Impedance Mismatch in Wideband Vectored Wireline Systems," *IEEE Communications Letters*, vol. 18, no. 9, pp. 1527–1530, Sept 2014.

[8] Ericsson AB, *Access Network Pair cable, TEL 312*, 2010. [Online]. Available: http://goo.gl/4RdCXc

[9] R. Cendrillon, G. Ginis, E. Van den Bogaert, and M. Moonen, "A Near-Optimal Linear Crosstalk Precoder for Downstream VDSL," *IEEE Transactions on Communications*, vol. 55, no. 5, pp. 860–863, May 2007.

5

Mitigation of Alien Crosstalk for Downstream DSL Impaired by Multiple Interferers

Diego Gomes, Eduardo Medeiros, Aldebaro Klautau and Evaldo Pelaes

Abstract

Alien crosstalk is one of the major impairments for copper-based transmissions. This letter outlines a method for mitigating alien crosstalk for DSL downstream transmissions impaired by multiple interference sources. The method requires a reference channel, and includes a post processing stage in which induced correlation is applied to prepare the interference at the target channel to be reasonably removed by a prediction based mitigation step. The results show that the proposed method outperforms published alien crosstalk mitigation methods as the number of interference sources increase in G.fast scenarios.[1]

[1]Published in *IEEE Communications Letters*, vol. 21, no. 11, November 2017.

5.1 INTRODUCTION

Digital subscriber line (DSL) systems convey information through twisted pair channels, and are largely used because they benefit from the legacy telephone loop plant [1]. In its most recent version, G.fast, it achieves bit rates of up to 1 Gbps over short loops, using bandwidth of up to 212 MHz [2]. The architecture of the G.fast is called *fiber-to-the-distribution-point*, in which a fiber extends from the Central Office to the Distribution Point (DP), and from there the lines are plugged in the customer premises. However, the copper transmission is often impaired by crosstalk [3], which is the electromagnetic coupling between the close twisted pairs through which the signal transmission is carried out. When crosstalk occurs among lines that are coordinated by a single device at one of the ends of the cable, it is called *in-domain crosstalk* [4]. The *out-of-domain crosstalk* or alien crosstalk (AXT), which originates from a line that is not coordinated, represents a challenge for DSL systems. This is owing to the growth in the number of DSL deployments of different companies, which increases the number of *alien* signals. In general, the coordinated transceivers' information about out-of-domain crosstalk is limited to statistics, such as the correlation matrix of this interference, which can then be exploited to mitigate the effects of alien crosstalk [4–6].

Three AXT mitigation methods for two-sided coordinated systems are examined in [4]. The first achieves AXT mitigation through whitening, pre and post-processing. The last two are based on a *decision feedback equalizer* structure, in which the first processed users provide information to the AXT mitigation of the ones to follow through an interference predictor. Another AXT mitigation method for upstream direction is outlined in [5], which uses whitening to mitigate AXT and decodes the received symbols through a *successive interference cancellation* structure.

Despite the good performance achieved by the methods employed in [4] and [5] under the conditions set out for these works, they present a sharp reduction in their effectiveness when the number of *alien lines* (AL) becomes larger than the number of coordinated lines. In specific terms, as observed in [7] and evaluated in [6], when the number of AXT sources generating the interference is larger than the number of lines providing information (i.e. the reference channels), the interference mitigation tends to be poor. Additionally, the methods in [4] and [5] are not suitable for regular downstream transmission because the receivers are not collocated. In fact, the lack of coordination between the receivers in downstream, makes the AXT mitigation a challenge, because neither standard whitening nor interference prediction can be applied. Seeking to overcome these limitations, this work presents an effective AXT mitigation method for downstream transmissions impaired by multiple interference sources, in which a minimum coordination at the receivers is cre-

ated through the use of one reference channel per information transmitter. This method needs both precoding and post-coding, and includes a stage of signal conditioning at receiver, that can enable the interference to be suitably removed by only using one reference channel through an AXT prediction-based procedures in the next stage.

This work is organized as follows. Sec. 5.2 outlines the transmission model, in Sec. 5.3 there is a detailed examination of the method and in Sec. 5.4 our method is compared with others in G.fast scenarios.

5.2 SYSTEM MODEL

In this work we consider a downstream DSL transmission in frequency domain using *Discrete Multitone Modulation*, in which data is conveyed by the *transmission channel* (TC). This transmission is impaired by some alien crosstalk sources, that leads to an interference term at the received signals. Additionally, the TC is served by a *reference channel* (RC) (as in Fig.5.1), which can be either another twisted pair or an alternative transmission mode, such as the *common mode* [7]. For example, an extra line can be found in quad cables. The common mode can be accessed through a transceiver hardware modification to obtain the signal from the center tap of its transformers. In this paper it is assumed that all the coordinated channels are synchronized, which is a plausible constraint according to [2]. For the sake of simplicity and to focus on the description of the novel method, we will assume a single TC/RC pair here, but the algorithm can be scaled to support several TCs, which will be shown in the Sec. 5.3.1. Then, for a synchronized transmission, we can represent the received signals in a given tone k by

$$\mathbf{y}_k \quad = \quad \mathbf{H}_k\mathbf{x}_k + \mathbf{q}_k + \mathbf{n}_k \quad = \quad \mathbf{H}_k\mathbf{x}_k + \mathbf{z}_k \tag{5.1}$$

where $\mathbf{y}_k = [y_{TC} \;\; y_{RC}]^T$ is a 2×1 vector with the received symbols both in TC and RC, $\mathbf{H}_k$ is a 2×2 matrix with the direct channels of the TC and RC in its diagonal, and the crosstalk channels between TC and RC in its off diagonal, $\mathbf{x}_k$ is a 2×1 vector with the transmitted symbols $[x_{TC} \;\; x_{RC}]^T$, $\mathbf{q}_k$ is a 2×1 vector with the AXT observed in the TC and the RC, $\mathbf{n}_k$ is a 2×1 vector that denotes background noise which can be modelled as additive white Gaussian noise, and $\mathbf{z}_k = \mathbf{q}_k + \mathbf{n}_k$. The subscript k is omitted in the next paragraphs since a per-tone processing is assumed.

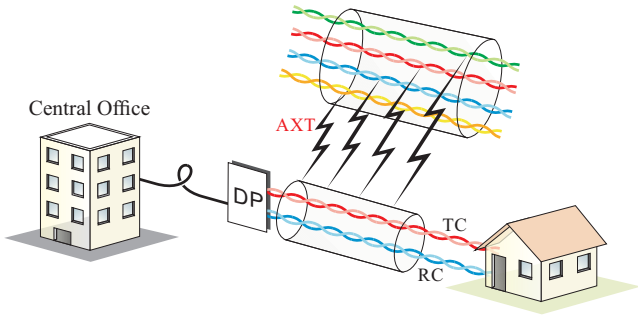

Figure 5.1: System model for a DSL transmission in TC with one RC and multiple interference sources.

5.3 AXT MITIGATION FOR MULTIPLE INTERFERENCE SOURCES (AMMIS)

This section outlines details of the method *AXT Mitigation for Multiple Interference Sources*, or AMMIS. This method needs to be executed both at the transmitter and receiver, where the combination of these stages makes it possible to mitigate the AXT and decode the transmitted symbols simultaneously. We begin by carrying out the pre-processing at the transmitter to make the equivalent channel decodable, and hence the resulting channel will be triangular. Let the square matrix $\mathbf{A}$ represent the equivalent channel, i.e., the channel observed by the transmitted symbols after the pre and post-processing. Let $\mathbf{A}'$ have the QR decomposition [5] $\mathbf{A}' = \mathbf{QR}$, where $\mathbf{Q}$ is a unitary complex matrix and $\mathbf{R}$ is an upper triangular matrix. Pre multiplying the transmitted symbols by $\mathbf{Q}$, $\mathbf{s} = \mathbf{Qx}$, we obtain

$$\tilde{\mathbf{y}} = \mathbf{As} + \mathbf{v} = (\mathbf{QR})'\mathbf{s} + \mathbf{v} = \mathbf{R}'\mathbf{Q}'\mathbf{Qx} + \mathbf{v} = \mathbf{R}'\mathbf{x} + \mathbf{v} \tag{5.2}$$

where $\mathbf{v}$ represents the resulting interference (after processing) at the receiver and the superscript $'$ indicates the conjugate transpose (Hermitian).

At the receiver the method begins with the *conditioning signal* stage, in which the received signals will be applied to successive matrix multiplications. In this stage, the proposed method requires an interference correlation matrix $\mathbf{C}_z = E[\mathbf{zz}']$ [4] to be estimated during a training phase, where $E[.]$ denotes statistical expectation. From $\mathbf{C}_z$ we obtain the whitening matrix $\mathbf{W} = \mathbf{G}_z^{-1}$, where $\mathbf{G}_z$ is a lower triangular matrix, obtained from the Cholesky decomposition [8] $\mathbf{C}_z = \mathbf{G}_z\mathbf{G}_z'$. In *show-time* phase, the whitening matrix is used at the receiver in the expression

$$\hat{\mathbf{y}} = \mathbf{Wy} = \mathbf{WHs} + \mathbf{Wz}. \tag{5.3}$$

This stage makes the correlation matrix of the interference term, $\mathbf{Wz}$, a 2×2 identity matrix $\mathbf{I}$, because $E[\mathbf{Wzz'W'}] = \mathbf{G}_z^{-1}\mathbf{C}_z\mathbf{G}_z^{-\prime} = \mathbf{I}$. At this stage the correlation matrix of the reminiscent interference has a canonical form, in which a similar process can be used to the one used to make it diagonal, and impose on it a desired behavior. Then, to make the correlation matrix to have the form $\mathbf{C}_u = \mathbf{G}_u\mathbf{G}_u'$, we left multiply $\widehat{\mathbf{y}}$ by $\mathbf{G}_u$, to get

$$\tilde{\mathbf{y}} = \mathbf{G}_u\widehat{\mathbf{y}} = \mathbf{G}_u\mathbf{WHs} + \mathbf{G}_u\mathbf{Wz}, \tag{5.4}$$

where $\mathbf{v} = \mathbf{G}_u\mathbf{Wz}$, and $E[\mathbf{vv'}] = \mathbf{C}_u$. Now we define $\mathbf{G}_u\mathbf{WH} = \mathbf{A}$, and according to (5.2), the channel observed by the transmitted symbols is given by the $\mathbf{R}'$ matrix, which makes the end-to-end transmission

$$\begin{array}{rcl} \tilde{\mathbf{y}} & = & \mathbf{R}'\mathbf{x} + \mathbf{v} \\ \begin{bmatrix} \tilde{y}_{TC} \\ \tilde{y}_{RC} \end{bmatrix} & = & \begin{bmatrix} R(1,1)^* & \\ R(1,2)^* & R(2,2)^* \end{bmatrix} \begin{bmatrix} x_{TC} \\ x_{RC} \end{bmatrix} + \begin{bmatrix} v_{tc} \\ v_{rc} \end{bmatrix} \end{array} \tag{5.5}$$

where the superscript * denotes complex conjugation, and $R(i,j)$ denotes the element in row i and column j of $\mathbf{R}$ matrix.

The conditioning signal step, in which the behavior of the correlation matrix of the interference was induced (5.4), was carried out to ensure the interference in the TC could be suitably predicted based on the interference observed in the RC, that comprises the next stage called *AXT removal*. The taps of this predictor can be found through the Cholesky decomposition of the correlation matrix of the reminiscent interference [9]. However, to get a predictor through this strategy, the data referring to the first line of the correlation matrix are used to predict the data related to the second line. This means, we must generate a correlation matrix of the reminiscent interference in which the position of v_{tc} and v_{rc} are changed, $\mathbf{b} = [v_{rc}\ v_{tc}]^T$. Finally, we compute the correlation matrix $\mathbf{C}_b = E[\mathbf{bb'}]$, which can be decomposed into $\mathbf{G}_b\mathbf{D}_b\mathbf{G}_b'$, where $\mathbf{G}_b$ is a monic matrix [4] and $\mathbf{D}_b$ is a diagonal matrix. After this, the predictor is given by $\dot{v}_{tc} = G_b(2,1)v_{rc}$, where $G_b(2,1)$ is the element in the second line of the first column of the $\mathbf{G}_b$, and $\dot{v}_{tc}$ is the prediction of v_{tc}.

In our method the RC is only used to support information for TC, and only pilot symbols are transmitted in this channel. Then, we begin the decoding by subtracting the known part of the received signal at the RC as

$$\begin{array}{rcl} \breve{y}_{RC} & = & \tilde{y}_{RC} - R(2,2)^* x_{RC} \\ & = & R(1,2)^* x_{TC} + v_{RC} \end{array} \tag{5.6}$$

From this we derive the prediction of the v_{TC} by the multiplication $G_b(2,1)\breve{y}_{RC} =$

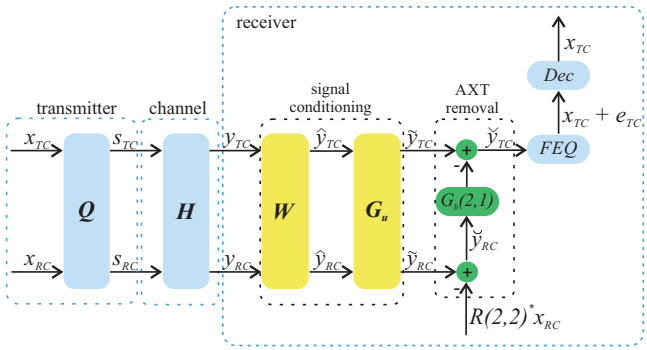

Figure 5.2: The schematic representation of the AMMIS method.

$G_b(2,1)R(1,2)^* x_{TC} + \dot{v}_{tc}$, and we subtract $\tilde{y}_{TC}$ from this sum, which yields

$$\begin{aligned} \check{y}_{TC} &= \tilde{y}_{TC} - G_b(2,1)R(1,2)^* x_{TC} - \dot{v}_{tc} \\ &= R(1,1)^* x_{TC} + v_{TC} - G_b(2,1)R(1,2)^* x_{TC} - \dot{v}_{TC} \\ &= [R(1,1)^* - G_b(2,1)R(1,2)^*] x_{TC} + e_{TC} \end{aligned} \tag{5.7}$$

where e_{TC} represents the error in the prediction of the v_{TC}. Now, the AXT is mitigated in the TC and the decoding of the x_{TC} can be performed by adjusting the *frequency equalizer* (FEQ) from the standard $1/R(1,1)^*$ to

$$FEQ = \frac{1}{R(1,1)^* - G_b(2,1)R(1,2)^*}. \tag{5.8}$$

Following this, the signal can be submitted to the decoder (Dec). From (5.7), it can be observed that the channel gain observed by the x_{TC} is $\tau = R(1,1)^* - G_b(2,1)R(1,2)^*$, which allows us to represent the *signal-to-interference-plus-noise ratio* (SINR) to the TC according to [10], by tone, as

$$SINR_{TC} = \frac{\rho|\tau|^2}{E[e_{TC}e'_{TC}]} \tag{5.9}$$

where ρ is the transmission power of the x_{TC}. The whole AMMIS processing is shown in Fig. 5.2, where *Dec* denotes the decoding operation.

5.3.1 THE EFFECT OF VECTORING ON AMMIS

To achieve high data rates, the G.fast standard adopts *vectoring* [11]. This makes it logical to evaluate the performance of AMMIS when it is applied to a group of coordinated lines, or vectored group (VG). From this perspective, our model can be expanded to L coordinated TC/RC pairs as

$$\ddot{\mathbf{y}} = \ddot{\mathbf{H}}\mathbf{P}\ddot{\mathbf{s}} + \ddot{\mathbf{z}} \tag{5.10}$$

where $\ddot{\mathbf{s}} = [\mathbf{s}_1 \ ... \ \mathbf{s}_L]^T$, in which $\mathbf{s}_l$ is a column vector that contains the transmitted symbols in TC and RC of the lth TC/RC pair, $\ddot{\mathbf{H}}$ is a $2L \times 2L$ matrix which contains all the direct channel of the TCs and RCs in its diagonal and the crosstalk channels among them in out-of-diagonal elements, $\ddot{\mathbf{z}} = [\mathbf{z}_1 \ ... \ \mathbf{z}_L]^T$, and $\mathbf{P} = (1/\beta)\ddot{\mathbf{H}}^{-1} diag(\ddot{\mathbf{H}})$ is the precoder applied to remove the crosstalk among the coordinated channels, in which $diag(.)$ represents the diagonal of a matrix and β is a factor used to control the transmission power of the transmitted symbols [11]. In this situation, the received symbols become

$$\ddot{\mathbf{y}} = \frac{1}{\beta}\text{diag}(\ddot{\mathbf{H}})\ddot{\mathbf{s}} + \ddot{\mathbf{z}} \tag{5.11}$$

The result of the (5.11) indicates that the effect of a vectorized coordinate group on AMMIS is to diagonalize $\mathbf{H}$ in (5.1), (5.3) and (5.4), but each $\mathbf{s}_l$ keeps its precoding applied in the AMMIS (5.2), and the method can be usually employed for each TC/RC pair. Additionally, the SINR is scaled by $(1/\beta)^2$.

5.4 RESULTS

In this section there is a performance evaluation of AMMIS, which is compared with two other AXT mitigation methods: the one discussed in [5] (denoted *DFC*) and the third method in [4] (called here *RxPred*, chosen because it had an equivalent performance to the ones obtained with the first and second methods in [4]). Two scenarios were examined for this evaluation and the methods were compared with respect to their simulated bit rates, which were evaluated in the Matlab platform. Although DFC was not originally thought to be suitable for downstream [5] (due to the absence of coordination at receiver), the presence of the RC makes its implementation possible.

The channels of the first scenario (SCEN1) were measured with an Agilent E5071C network analyzer, using a setup composed by a 100 m long quad cable encapsulated in a bundle with three other quad cables. In this scenario, the extra twisted pair of the target quad cable was used as the RC and all the pairs of the three other quad cables caused interference, in a total of 6 alien crosstalk sources. The *Computer Simulation Technology* (CST) software was used to simulate scenarios with varying difficulty to the algorithms. From these simulations, the second scenario (SCEN2) was chosen to be discussed here because it is particularly problematic for AMMIS (and other methods), due its weak coupling channels, which yield AXT level close to background noise. SCEN2 represents DSL transmission over a 50 m long *Category 6* (Cat6) twisted pair. The CST simulator provided information about the common mode, that is used as the RC. In SCEN2, the transmission was impaired by the AXT generated by 4 *Category 5* twisted pairs.

G.fast downstream transmissions were assumed in both scenarios and the parameters of the simulations were: bandwidth of 212 MHz (SCEN1)/100 MHz (SCEN2); transmission/interference *power spectrum density* (PSD) of -76 dBm/Hz; background noise PSD of -150 dBm/Hz; and, SINR Gap of 9.75 dB.

Fig. 5.3 and Fig. 5.4 show the simulation results for SCEN1 and SCEN2, respectively. In both scenarios, we evaluated the downstream aggregated transmission rates achieved by RxPred and DFC (i. e., the sum of the rates available in the TC and the RC, because in these methods both channels convey useful data), but for AMMIS only the downstream transmission rate in the TC is used, given that its RC transmits only pilot symbols. In these figures "*No Mitigation*" indicates the data rate achieved in a transmission in the presence of AXT but without mitigation. The $\mathbf{C}_u$ matrix used by AMMIS was obtained from the interference correlation matrix generated from a simulation of a scenario with 2 coordinated lines and only 1 AL. This will induce the interference to behave like one that is only generated by one source, which allows an effective AXT mitigation in (5.7) with prediction that is based on one reference channel [6].

Comparing Fig. 5.3 and Fig. 5.4, it can be noted that the transmission rates achieved by RxPred and DFC, in the situation with 1 AL, are larger than that achieved by AMMIS. This can be attributed to the fact that with 1 AL and 1 RC, the standard AXT mitigation methods have a good performance [6]. However, with the increase in the number of ALs, the AMMIS outperforms the other methods in the SCEN1, whereas AMMIS only achieves a better performance in the worst situation in the SCEN2. This behavior in the SCEN2 is mainly owing to the weak AXT channels in the differential mode of the Cat6. This causes low power interference in this mode and compensates for a poorer performance in some situations with multiple AXT (up to 3 ALs), keeping the aggregated transmission rate in a high level, same with the poor transmission rate in the common mode due to the low SINR in this mode.

However, the strong interference in the medium quality lines of the SCEN1 quickly reveals the decline in performance of RxPred and DFC. These results confirm that AMMIS can achieve better results than standard AXT mitigation, in situations in which only 1 RC is available and multiple AXT sources impair a G.fast downstream transmission. In some situations (with AL $= 0$, for example) the bit rates of the AMMIS were small even than *No Mitigation*, a penalty due its channel gain to be given by the difference $R(1,1)^* - G_b(2,1)R(1,2)^*$. A detailed analysis to determinate the parameters that impact this value will be treated in a future work.

Another advantage of AMMIS is that unlike the other methods, it is able to reduce the transmission power, because in AMMIS the RC only transmits pilot symbols, and then less power can be assigned to this channel. Additionally, this fact can also reduce the level of the interference in other systems, which

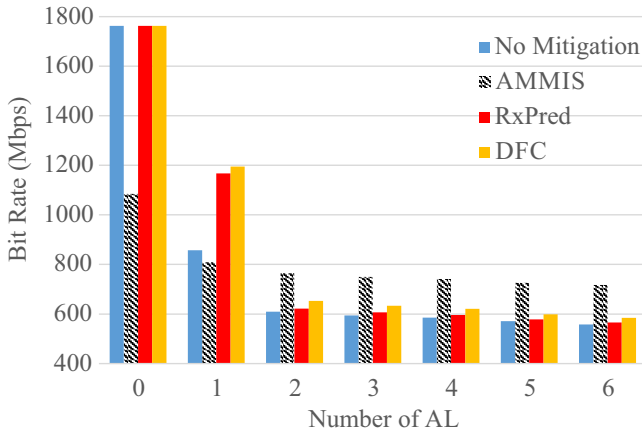

Figure 5.3: Transmission rates achieved by each mitigation method with a different number of ALs in SCEN1 - 212 MHz.

tends to increase with the use of the extra channel (RC). On the other hand, this reduction in power cannot be carried out in the DFC and RxPred without a bit rate decrease, because it can affect their aggregated bit rate, which also depends on the RC.

With regard to the computational cost in showtime, AMMIS requires six additions and nine multiplications, whereas RxPred and DFC need $4+$ and $6\times$, and $3+$ and $5\times$, respectively. However, as AMMIS requires only one decoding against two of the other methods, it will require fewer operations in situations with $M \geq 16$ (M is the size of the constellation), because $O(M)$ [12].

5.5 CONCLUSION

We have presented an alien crosstalk mitigation method called AMMIS that is suitable for DSL downstream transmissions in which the target channel has access to the signals in a reference channel, and where the transmission is impaired by multiple alien crosstalk sources. The proposed method achieved better data rates than other mitigation methods in G.fast scenarios when the number of interference sources is relatively large. For example, its performance was better in a scenario with medium quality cables at the expense of more additions and multiplications.

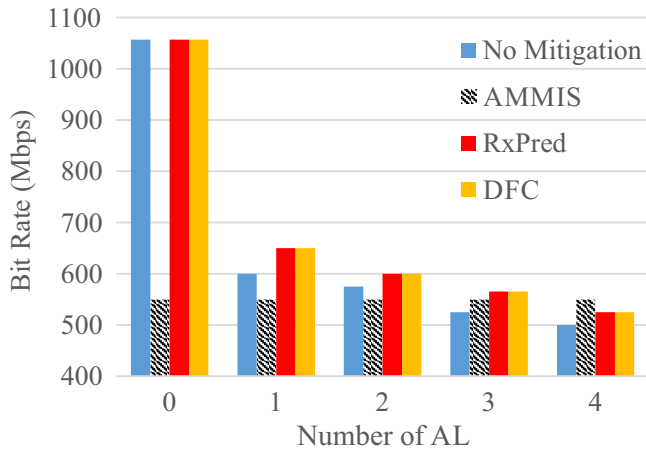

Figure 5.4: Transmission rates achieved by each mitigation method with a different number of ALs in SCEN2 - 100 MHz.

References

[1] T. Starr, M. Sorbara, J. M. Cioffi, and P. J. Silverman, *DSL Advances*, 1st ed. Prentice Hall, 2003.

[2] *Fast Access to Subscriber Terminals (G.fast) - Physical Layer Specification*, ITU Recommendation G.9701, Dec. 2014.

[3] V. Oksman, R. Strobel, X. Wang, D. Wei, R. Verbin, R. Goodson, and M. Sorbara, "The ITU-T's new G.fast standard brings DSL into the gigabit era," *IEEE Communications Magazine*, vol. 54, no. 3, pp. 118–126, March 2016.

[4] G. Ginis and C.-N. Peng, "Alien crosstalk cancellation for multipair digital subscriber line systems," *EURASIP Journal on Advances in Signal Processing*, vol. 2006, no. 1, p. 016828, Feb 2006. [Online]. Available: https://doi.org/10.1155/ASP/2006/16828

[5] A. A. Amayreh, J. L. Masson, M. Hélard, and M. Ouzzif, "Alien crosstalk elimination in digital subscriber line systems," *IET Communications*, vol. 8, no. 10, pp. 1714–1723, July 2014.

[6] D. de Azevedo Gomes, I. Freire, A. Klautau, and E. Pelaes, "Feasibility of alien crosstalk mitigation with receiver-side MIMO processing on G.fast systems," in *2015 International Workshop on Telecommunications (IWT)*, June 2015, pp. 1–7.

[7] T. Magesacher, P. Ödling, P. O. Börjesson, and S. Shamai (Shitz), "Information rate bounds in common-mode aided wireline communications," *European Transactions on Telecommunications*, vol. 17, no. 5, pp. 533–545, 2006. [Online]. Available: http://dx.doi.org/10.1002/ett.1071

[8] G. Strang, *Introduction to Applied Mathematics*. Wellesley-Cambridge Press, 1986.

[9] S. Haykin, *Adaptive Filter Theory*, 3rd ed. Prentice Hall, 1995.

[10] E. Karipidis, N. D. Sidiropoulos, A. Leshem, and L. Youming, "Capacity statistics for short DSL loops from measured 30 MHz channel data," in *IEEE 6th Workshop on Signal Processing Advances in Wireless Communications, 2005.*, June 2005, pp. 156–160.

[11] I. Bergel and A. Leshem, "The performance of zero forcing DSL systems," *IEEE Signal Processing Letters*, vol. 20, no. 5, pp. 527–530, May 2013.

[12] O. O. Ogundile and D. J. J. Versfeld, "Improved reliability information for OFDM systems on time-varying frequency-selective fading channels," in *2015 Wireless Telecommunications Symposium (WTS)*, April 2015, pp. 1–7.

6

Analysis of Fast Initialization for Vectored Wireline Systems

Driton Statovci, Thomas Magesacher, Martin Wolkerstorfer, and Eduardo Medeiros

Abstract

Cooperation of transceivers on signal level at the remote terminal—often referred to as vectoring—is an effective approach to mitigate crosstalk in wireline transmission systems. While the gain in bitrate compared to crosstalk-limited transmission is substantial, the initialization of a vectoring system requires time and care to ensure system stability. In this contribution, a fast initialization scheme for vectored wireline systems based on spectral protection is analyzed. Two scenarios are considered, where in the first one no prior channel information is available, and in the second one erroneous prior knowledge of channel coefficients is utilized. Measurements on a commercial VDSL2 vectoring platform and throughput simulations demonstrate the potential of the fast initialization scheme.[1]

[1]Published in *Proc. IEEE Global Communications Conference (GLOBECOM 2013)*, Atlanta, USA, 9-13 Dec. 2013.

6.1 INTRODUCTION

In modern wireline transmission systems, co-location of transceivers at the remote terminal allows for coordination with the aim of better exploiting the potential of the cable through techniques summarized under the term dynamic spectrum management (DSM) [1]. The degree of coordination ranges from single-line power control (DSM level 1) over multi-line power-spectrum control (DSM level 2) to joint signal processing (DSM level 3). Methods for joint processing of transmit signals (pre-coding) and joint processing of receive signals (interference cancellation) are often summarized under the term vectoring or vectored transmission [2–8]. Network operators have used DSM level 1 and level 2 to improve the performance and stability of their systems. Recently they have started deploying vectored systems (DSM level 3) mainly from street cabinets aiming at increasing bitrates [9].

Vectoring has the potential to turn crosstalk-limited systems into additive-noise-limited systems, which can yield substantial gains in bitrate [10]. A prerequisite for well-working precoders and cancelers are accurate channel estimates, which are obtained in the initialization phase and continuously updated during the showtime phase. State-of-the-art initialization procedures (such as the very high speed digital subscriber line 2 (VDSL2) initialization defined in the standard G.993.5 [11]) can take up to several minutes until joining users experience connectivity. The protection of vectored lines against joining, initializing lines has been a prominent issue in standardization. Corresponding approaches include for instance the reuse of previously collected channel information, or the limitation of the received crosstalk noise to a well-defined level below the noise margin [12] [13]. In [14] a channel estimation technique based on the signal-to-noise ratio (SNR) is proposed, where the transmit power limitation of the initializing disturber line is gradually loosened as the channel estimate becomes more accurate.

In this paper, we revisit the ideas of using outdated channel information and spectral protection of vectored lines, and merge them into a fast-initialization scheme conform with the G.993.5 standard. Furthermore, we analyze the available bitrate of the *joining* lines when the crosstalk noise limitation imposed by vectored lines is based on one of two assumptions: a) based on empirical worst-case channels in case of no channel knowledge; or b) based on outdated channel information and an estimated channel error variance. The performance analysis under erroneous channel coefficients is based on [15], where zero forcing (ZF) and diagonalizing precoding (DP) were considered as vectoring algorithms. In [16] the effect of *direct channel* estimation errors in a crosstalk-free setting is analyzed. Similarly as in [16] we consider an estimation error variance that is normalized by the corresponding channel gain. Despite likely dependencies of the estimation error on the SNR [16], we

assume a frequency-flat normalized error in our numerical examples in order to avoid dependence on a specific channel estimation method. Furthermore, as in [14] [15] we assume that the direct channels are estimated correctly and consider normalized crosstalk channel errors only.

The paper is organized as follows. In Section 6.2 and Section 6.3, the vectoring initialization phase is described and analyzed, respectively. In Section 6.4, measurements of vectored VDSL2 channels over time are presented and the time variation is quantified. Simulation results of an access scenario with tree-type topology and 15 users are presented in Section 6.5. Finally, Section 6.6 concludes the work.

6.2 SPECTRAL PROTECTION FOR FAST INITIALIZATION

A typical initialization procedure, illustrated in Figure 6.1, consists of channel estimation (channel discovery phase), adaptation of receiver parameters to the channel (training phase), and computation as well as exchange of bitloading tables (channel analysis and exchange phase) [10]. Initialization of vectored systems requires additional phases and is typically done in two steps: first, the crosstalk from joining lines into vectored lines is estimated and compensated; second, the joining lines estimate and compensate crosstalk from vectored lines. The VDSL2 standard G.993.5 refers to these phases as "VECTOR-1" and "VECTOR-2", respectively [11].

In the following we analyze the spectral protection of vectored VDSL2 lines from initializing lines, thereby ensuring network stability, under two cases of prior channel knowledge. Without loss of generality we assume that only one new user at a time is joining the vectoring group.

Case 1: The new user has no channel information from previous showtime-occasions but knows the worst-case far-end crosstalk (FEXT) coupling magnitude into other users' lines—a parameter that can be estimated based on models and some knowledge of the network topology, such as loop length and cable type. Based on this worst-case FEXT coupling magnitude, the new user determines its transmit power spectral density (PSD) such that the noise increase seen by users in the vectoring group does not exceed a factor q, where $q \geq 1$ is chosen such that the SNR decay[2] remains well below the SNR margin (e.g., $10 \log_{10} q < 2\,\mathrm{dB}$). As soon as the transmit-PSD computation is finished, the new user starts to transmit without joining and without disturbing the vectoring group ("controlled alien"). Although the new user might achieve only a modest bitrate, it can transmit and receive immediately which yields

[2]For simplicity, we use the term "noise" for background noise, alien interference, and residual interference caused by users in the vectoring group with imperfect channel knowledge.

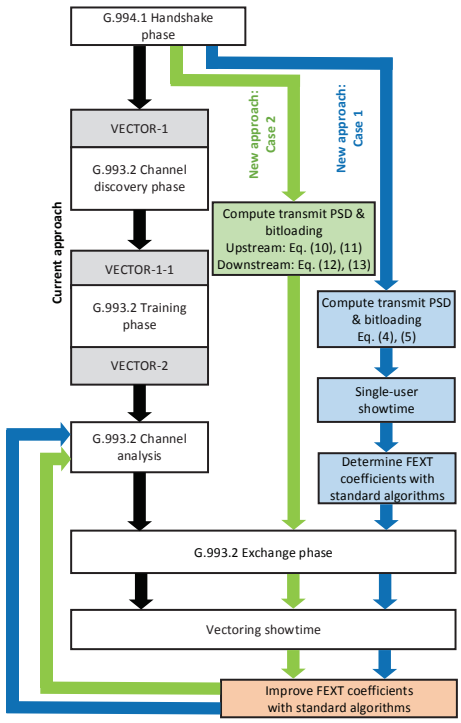

Figure 6.1: Illustration of initialization in vectored VDSL2 systems: Current approach and extensions for Case 1 and Case 2.

an improved connectivity-experience for the customer. While operating as a controlled alien, the new user gathers vector-channel information before eventually joining the vectoring group following state-of-the-art procedures (cf. Figure 6.1).

Case 2: The new user knows the "old" complex coupling coefficients from a previous showtime occasion and their error variances. The error variances could, for example, be estimated based on the time variance of the coefficients observed in the vectoring group. Based on this knowledge, the new user determines its transmit PSD such that the SNR-margin decay of the lines in the vectoring group is kept below q. As soon as the transmit-PSD computation is finished, the new user joins the vectoring group and starts to transmit.

Clearly, partial or inaccurate channel knowledge will result in suboptimal bitrates, analyzed in Section 6.3, for the new user. The benefit of fast initialization is improved user experience through immediate connectivity. The stability of the vectoring system is ensured. Immediately after starting to transmit, the new user begins to gather (Case 1) or improve (Case 2) its vector

channel information in order to reach its maximum bitrate as soon as possible.

6.3 ANALYSIS

We consider a vectoring system with U users denoted by the set $\mathcal{U} = \{1, \ldots, k-1, k, k+1, \ldots, U\}$, where k denotes the new user and all other users are part of the vectoring group. For simplicity, the analysis is limited to linear vectoring systems that use a ZF canceler [7] and a DP [8] for upstream and downstream transmission, respectively.

6.3.1 CASE 1

The FEXT magnitudes of the new line k into the vectored lines can be estimated based on worst-case FEXT coupling models or FEXT models of a particular network operator, knowledge of direct channels, and line lengths. Since the line k is not part of the vectoring group, transmission on line k will increase the level of noise on all vectored lines. The increased noise level on line u and tone c is given by

$$\hat{\sigma}_u^c = \sigma_u^c + \left|[\mathbf{H}_{\text{est}}^c]_{uk}\right|^2 p_k^c, \tag{6.1}$$

where p_k^c is the transmit PSD of user k, σ_u denotes the PSD of the background noise, and $[\mathbf{H}_{\text{est}}^c]_{uk}$ denotes the estimated FEXT channel transfer function from user k to user u. For each tone, we want to protect the user that is disturbed most by the joining user k. For this purpose we define the magnitude of the worst-case FEXT coupling

$$|h_{\text{WC}}^c| = \max_{u \in \mathcal{U} \setminus k} \left|[\mathbf{H}_{\text{est}}^c]_{uk}\right|. \tag{6.2}$$

In order to ensure stability of the vectoring system, we introduce the parameter $q \geq 1$, which controls the maximum noise level any vectored line is experiencing:

$$\hat{\sigma}_u^c \leq q\sigma_u^c. \tag{6.3}$$

With (6.1), (6.2) and (6.3), the maximum transmit PSD of user k is given by

$$p_k^{c,\max} = \min_{u \in \mathcal{U} \setminus k} \frac{\sigma_u^c\,(q-1)}{\left|h_{\text{WC}}^c\right|^2}. \tag{6.4}$$

The maximum number of bits user k is able to transmit on tone c is calculated by

$$r_k^c = \log_2\left(1 + \frac{\left|[\mathbf{H}_{\text{est}}^c]_{kk}\right|^2 \min\left(p_k^{c,\max}, p_k^{c,\text{mask}}\right)}{\Gamma\left(\sum\limits_{j \in \mathcal{U} \setminus k} \left|[\mathbf{H}_{\text{est}}^c]_{kj}\right|^2 p_j^c + \sigma_k^c\right)}\right), \tag{6.5}$$

where Γ is the SNR gap to capacity and $p_k^{c,\text{mask}}$ is the PSD mask level on tone c, which is usually selected to be the same for all lines.

Note that the vectored lines will maintain their bitrate. Since DSL systems operate with a noise margin of at least 6 dB, an increase of the total noise on a particular line[3] by, for example, $q = 1.58$ (2 dB) until the system has learned the channel coefficients of line k should have no impact on bitrate.

6.3.2 CASE 2

We assume that both magnitude and phase of the FEXT coupling coefficients of line k from and into vectored lines are partially known. For example, the coefficients from the last time line k was part of the vectoring group can be used. In the following, we analyze ZF and DP for upstream and downstream transmission directions, respectively.

Upstream: Based on the derivation in [15], the noise variance seen by user u on tone c at the output of the ZF canceler under imperfect channel estimation can be calculated as

$$\hat{\sigma}_{u,\text{ZF}}^c = \underbrace{\sum_{i,j\in\mathcal{U}} \left|[\mathbf{G}^c]_{ui}\right|^2 \delta_{ij}^c p_j^c}_{\text{residual crosstalk}} + \underbrace{\sum_{i\in\mathcal{U}} \left|[\mathbf{G}^c]_{ui}\right|^2 \sigma_i^c}_{\text{enhanced noise by ZF}} . \tag{6.6}$$

The ZF-canceler matrix $\mathbf{G}^c$ is given by $\mathbf{G}^c = {\mathbf{H}_{\text{est}}^c}^{-1}$, where $\mathbf{H}_{\text{est}}^c$ denotes the estimate of the channel matrix $\mathbf{H}^c = \mathbf{H}_{\text{est}}^c + \mathbf{E}^c$, and $\mathbf{E}^c$ is the estimation error matrix with element-wise variances $\delta_{ij}^c = \mathsf{E}(|[\mathbf{E}^c]_{ij}|^2)$. δ_{ij}^c, $\forall i,j \in \mathcal{U}\setminus k$, are the channel estimation error variances of the vectoring group lines. δ_{ij}^c with either i or j equal to k are the channel estimation error variances into and from line k, respectively (δ_{kk}^c is the direct channel estimation error variance of line k). The relative channel estimation error ξ_{ij}^c is defined as

$$\xi_{ij}^c = \frac{\delta_{ij}^c}{|[\mathbf{H}^c]_{ij}|^2}.$$

The noise $\hat{\sigma}_{u,\text{ZF}}^c$ in (6.6) can be divided into noise originating from the vectored lines, $\bar{\sigma}_{u,\text{ZF}}^c$ and noise originating from the joining line k, $\tilde{\sigma}_{u,\text{ZF}}^c$:

$$\hat{\sigma}_{u,\text{ZF}}^c = \bar{\sigma}_{u,\text{ZF}}^c + \tilde{\sigma}_{u,\text{ZF}}^c, \tag{6.7}$$

where

$$\bar{\sigma}_{u,\text{ZF}}^c = \sum_{i,j\in\mathcal{U}\setminus k} \left|[\mathbf{G}^c]_{ui}\right|^2 \delta_{ij}^c p_j^c + \sum_{i\in\mathcal{U}\setminus k} \left|[\mathbf{G}^c]_{ui}\right|^2 \sigma_i^c,$$

[3] Since in practice the FEXT couplings between the lines are different, for each particular tone only one line might experience the predefined maximum increased noise level.

and

$$\tilde{\sigma}^c_{u,\mathrm{ZF}} = \sum_{i\in\mathcal{U}} |[\mathbf{G}^c]_{ui}|^2 \delta^c_{ik} p^c_k + \sum_{j\in\mathcal{U}\setminus k} |[\mathbf{G}^c]_{uk}|^2 \delta^c_{kj} p^c_j + |[\mathbf{G}^c]_{uk}|^2 \sigma^c_k. \tag{6.8}$$

As in Case 1, we limit the maximum noise level using the parameter $q \geq 1$:

$$\hat{\sigma}^c_{u,\mathrm{ZF}} \leq q\bar{\sigma}^c_{u,\mathrm{ZF}}. \tag{6.9}$$

Based on (6.7), (6.8), and (6.9), we are able to calculate the maximum transmit PSD of user k by

$$p^{c,\max}_{k,\mathrm{ZF}} = \min_{u\in\mathcal{U}\setminus k} \frac{\bar{\sigma}^c_{u,\mathrm{ZF}}(q-1) - \sum_{j\in\mathcal{U}\setminus k} |[\mathbf{G}^c]_{uk}|^2 \delta^c_{kj} p^c_j - |[\mathbf{G}^c]_{uk}|^2 \sigma^c_k}{\sum_{i\in\mathcal{U}} |[\mathbf{G}^c]_{ui}|^2 \delta^c_{ik}}. \tag{6.10}$$

The achievable bitrate in bits per multicarrier symbol for user k on tone c in upstream direction is given by

$$r^c_{k,\mathrm{ZF}} = \log_2\left(1 + \frac{\min\left(p^{c,\max}_{k,\mathrm{ZF}}, p^{c,\mathrm{mask}}_k\right)}{\Gamma\hat{\sigma}^c_{k,\mathrm{ZF}}}\right). \tag{6.11}$$

Downstream: With DP and imperfect channel estimation, the noise variance for user u on tone c can be calculated based on [15] yielding

$$\hat{\sigma}^c_{u,\mathrm{DP}} = \sum_{j,i\in\mathcal{U}} \delta^c_{ui} |\,[\mathbf{G}^c]_{ij}\,[\mathbf{H}^c_{\mathrm{est}}]_{jj}|^2 p^c_j + \sigma^c_u.$$

Under the assumption that

$$\hat{\sigma}^c_{u,\mathrm{DP}} \leq q\bar{\sigma}^c_{u,\mathrm{DP}},$$

the derivation of the maximum transmit PSD of user k for DP follows, *mutatis mutandis*, the derivation for the ZF and yields

$$p^{c,\max}_{k,\mathrm{DP}} = \min_{u\in\mathcal{U}\setminus k} \frac{\bar{\sigma}^c_{u,\mathrm{DP}}(q-1) - \sum_{j\in\mathcal{U}\setminus k} \delta^c_{ui} |\,[\mathbf{G}^c]_{ij}\,[\mathbf{H}^c_{\mathrm{est}}]_{jj}|^2 p^c_j}{\sum_{i\in\mathcal{U}} \delta^c_{ui} |\,[\mathbf{G}^c]_{ij}\,[\mathbf{H}^c_{\mathrm{est}}]_{jj}|^2}, \tag{6.12}$$

where

$$\bar{\sigma}^c_{u,\mathrm{DP}} = \sum_{i,j\in\mathcal{U}\setminus k} \delta^c_{ui} |\,[\mathbf{G}^c]_{ij}\,[\mathbf{H}^c_{\mathrm{est}}]_{jj}|^2 p^c_j + \sigma^c_u.$$

The achievable bitrate in bits per multicarrier symbol for user k on tone c in downstream direction is given by

$$r^c_{k,\mathrm{DP}} = \log_2\left(1 + \frac{|[\mathbf{H}^c_{\mathrm{est}}]_{kk}|^2 \min\left(p^{c,\max}_{k,\mathrm{DP}}, p^{c,\mathrm{mask}}_k\right)}{\Gamma \hat{\sigma}^c_{k,\mathrm{DF}}}\right). \tag{6.13}$$

6.4 TIME VARIATION OF VECTOR CHANNELS: MEASUREMENT RESULTS

Characterizing the time variation of channel properties observed in a wireline network is a challenge. A slow change of parameters in a vector channel is to be expected due to changes of environmental conditions such as temperature, humidity, or aging of materials. Faster changes may occur due to, for example, changes of termination impedances or a wiggling cable-end caused by a user moving a modem. To the authors' best knowledge, there are no experimental results on the time variation of vector channels available in the open literature. The purpose of this section is to provide some initial evidence on the time variation of vector channels to be expected in real systems.

With a commercial VDSL2 vectoring platform, 6 FEXT coupling functions on 50 tones were recorded roughly every 10 minutes during 8.5 hours yielding 52 data sets. Using the first set as reference, 51 sets of normalized errors were computed. Figure 6.2 shows a histogram and the empirical complementary cumulative distribution function (CCDF) of ξ in % based on the 15300 measurements (the measured errors showed no particular trend over time). 78.2% of the measured errors are below 0.1%, 95.2% are below 0.5%, and 97.6% are below 1%. Note that these results include all the contributing effects to be expected when tracking coefficients with real-world modem equipment (i.e., noise, analog front-end effects, automatic gain scalings, finite precision effects, and coefficient representation).

6.5 SIMULATIONS AND DISCUSSION

This section presents bitrate results of the fast initialization scheme for an example scenario. We consider 15 users in a tree-type network topology with loop lengths between 190 m and 550 m as shown in Figure 6.3. The users are numbered from 1 to 15 and sorted according to line length in increasing order. We use simulation parameters matching the VDSL2 standard ITU G.993.2 [17] with profile 17a, spectral mask definition EU-32, a maximum transmitted power of 14.5 dBm, a background noise level of -135 dBm/Hz, and maximum bitloading of 15 bits.

The new user is user no. k. Users in $\mathcal{U} \setminus k$ form a vectoring group and we

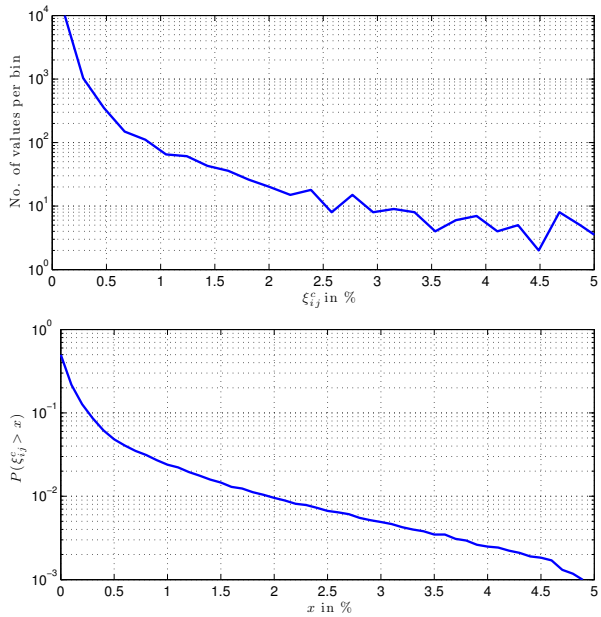

Figure 6.2: Histogram (top) and CCDF (bottom) for measured normalized channel estimation error $\tilde{\xi}_{ij}^c$ in %. Note that the y-axis of the histogram is in logarithmic scale. Bin size 0.1%. 51 consecutive measurements of errors of 6 FEXT coupling functions ($i \in \{1,2,3,4\}$, $j \in \{i+1,\ldots,4\}$) on 50 tones ($c \in \{2792, 2808, \ldots, 3576\}$, tone-group size 16) yield 15300 samples. 24-pair 0.5 mm-cable of 300 m length.

assume that they have perfect knowledge of both direct and FEXT channel coefficients ($\delta_{ij}^c = 0$, $\forall i,j \in \mathcal{U} \setminus k$). The maximum SNR decay of users in the vectoring group caused by user k is $q = 2$ dB, which allows the vectored users to maintain their bitrates.

Case 1: The new user no. k immediately transmits with reduced power but without joining the vectoring group. Figure 6.4 shows the achieved bitrates in downstream and upstream directions for the new user no. k transmitting as "controlled alien". For reference, the bitrates for full vectoring (all 15 users are part of the vectoring group) are shown as well (solid lines). In upstream direction, the bitrate of a new user with a long loop (no. ..., 14, 15) is in the order of 20–55% of the bound achieved with full vectoring. For a user with a short loop (no. 1, 2, ...), however, the upstream bitrate is in the order of 6–15% of the bound since the transmit power has to be reduced drastically in order

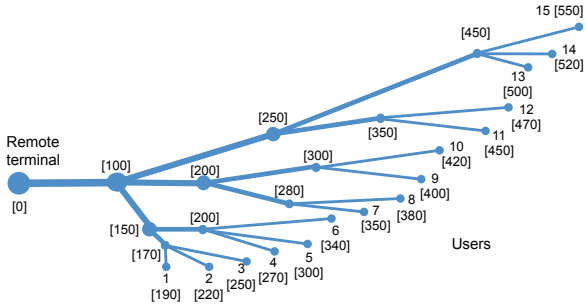

Figure 6.3: Example network topology: 15 users with loop lengths between 190 and 550 m. Users are numbered from 1 to 15 in ascending order according to loop length. Figures in square brackets are distances from the remote terminal in meters.

to protect the weak signals of distant users arriving at the remote terminal. In downstream direction, the bitrates are in the order of 25–37% of the bound.

Case 2: The new user no. k immediately joins the vectoring group after the handshake-phase. While users in the vectoring group have perfect knowledge of both direct and FEXT channel coefficients ($\delta_{ij}^{c} = 0, \forall i, j \in \mathcal{U} \setminus k$), the new user no. k operates with a channel estimation error ξ ($\xi_{ij}^{c} \leq \xi, \forall i = k, j \in \mathcal{U} \setminus k, \forall j = k, i \in \mathcal{U} \setminus k$). Figures 6.5 and 6.6 show the achieved bitrates in downstream and upstream direction, respectively. In downstream direction, the achievable bitrate for $\xi \leq 1\%$ is at least 70% of the bound. Even for $\xi = 10\%$, the achievable bitrate is at least 35% of the bound. For large ξ, joining the vectoring group makes no longer sense, since operation as "controlled alien" yields higher bitrates. The ξ level defining the cross-over point between the two cases is in general lower for shorter loops (for example, $\xi \approx 10\%$ for user no. 1).

The performance in upstream direction has essentially the same behavior as in downstream direction. For $\xi = 1\%$, the achievable bitrates drop to around 70% of the bound. For large ξ, operating the user no. k as a "controlled alien" achieves higher bitrates compared to joining the vectoring group. The ξ level defining the cross-over point between the two cases is in general lower for longer loops (cf. loops no. 14 and 15).

It is important to note that only a few users experience a noise-margin decay as large as the limit of $q = 2\,\text{dB}$. The actual noise-margin decay depends on the transmit PSD and the FEXT coupling functions, which depend on both frequency and coupling length. Figure 6.7 shows the noise-margin decay in downstream direction for users no. 1, 2, ..., 6, 7, 9, 10, ..., 15 caused by

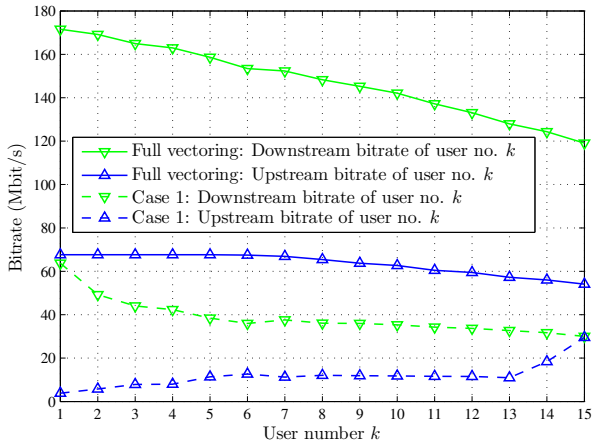

Figure 6.4: Bitrates for Case 1 ($q = 2\,\text{dB}$).

user no. 8 joining the vectoring group with $\xi = 5\,\%$. For tones up to index 523, only user no. 7 experiences the full noise-margin decay of 2 dB. Due to the mid-range coupling length of 280 m (FEXT post-attenuation 70 m), line no. 7 sees the strongest FEXT coupling from line no. 8 for low frequencies (cf. Figure 6.8). For tones above index 523, only line no. 1 experiences the full 2 dB of noise-margin decay since the FEXT coupling from line no. 8 into line no. 1 dominates (coupling length 100 m, FEXT post-attenuation 90 m).

Figure 6.9 shows the downstream bitrate of user no. 8 for different q and ξ values. A higher noise limit q yields a higher bitrate. An increase in q from 0.5 dB to 3 dB results in a bitrate increase of approximately 16%, 45%, and 16% (or equivalently, 12%, 13%, and 3% of the full-vectoring bound) for ξ equal to 0.5%, 10%, and 50%, respectively.

6.6 CONCLUSION

Vectoring is a pre-requisite for exploiting the capacity of wireline networks. Initialization of vectored systems is crucial. Procedures currently proposed in standards require a considerable amount of time for initialization before a new user can transmit or receive payload data. In this paper, a fast initialization for vectored systems based on spectral protection is analyzed,

that allows users to transmit and receive immediately after the handshake phase without threatening system stability. The scheme can be merged with existing standards (most importantly, VDSL2) and yields an improved user experience through immediate connectivity after start-up. The achievable bi-

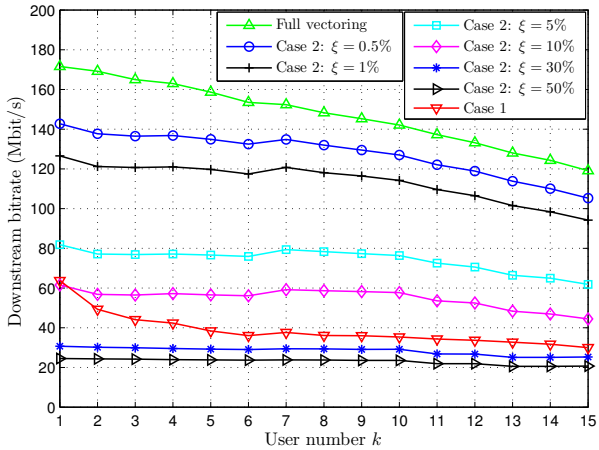

Figure 6.5: Downstream bitrates for Case 2 ($q = 2\,\text{dB}$).

trates depend strongly on the available channel knowledge. For channel errors in the order of 1%, bitrates around 70% of the full-vectoring bound can be achieved.

ACKNOWLEDGMENT

This work was partly supported by the Swedish Research Council (VR) through grant No. 621-2007-6309 and by the Swedish Foundation for Strategic Research (SSF) through grant No. ICA08-0022. The Competence Center FTW Forschungszentrum Telekommunikation Wien GmbH is funded within the program COMET - Competence Centers for Excellent Technologies by BMVIT, BMWFJ, and the City of Vienna. The COMET program is managed by the FFG.

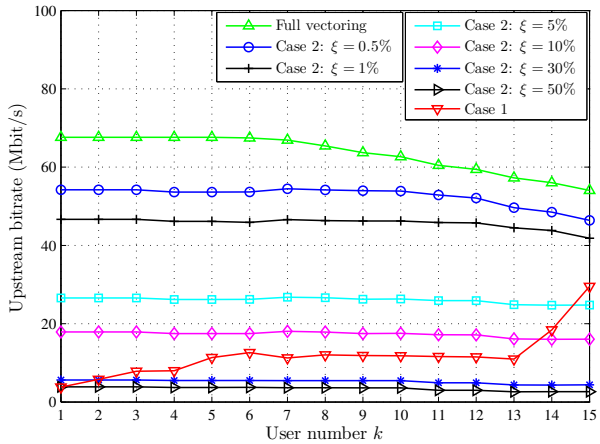

Figure 6.6: Upstream bitrates for Case 2 ($q = 2\,\mathrm{dB}$).

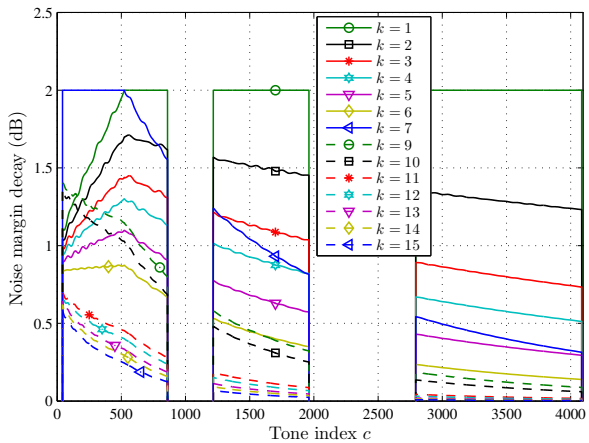

Figure 6.7: Downstream noise-margin decay caused by user no. 8 ($k = 8$) for Case 2 ($q = 2\,\mathrm{dB}$, $\xi = 5\,\%$).

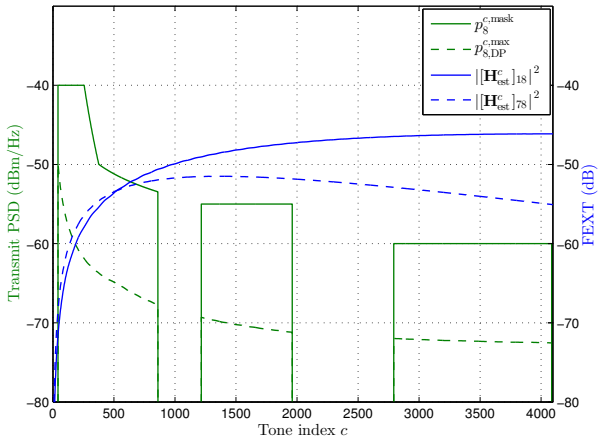

Figure 6.8: Left axis: transmit PSD mask and transmit PSD of user no. 8. Right axis: squared FEXT coupling magnitude from user no. 8 to users no. 1 and no. 7 ($q = 2\,\mathrm{dB}$, $\xi = 5\,\%$).

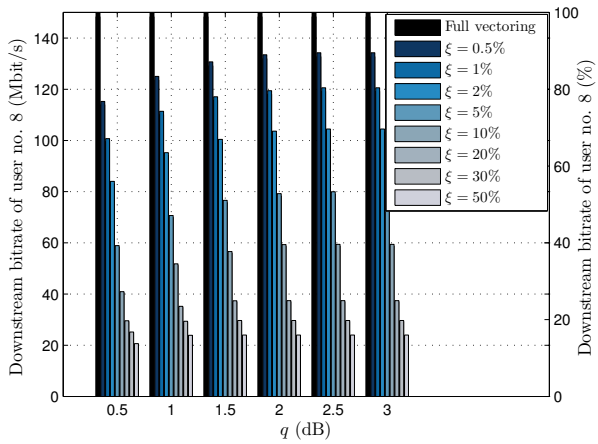

Figure 6.9: Downstream bitrate of user no. 8 for different q and ξ values.

References

[1] K. B. Song, S. T. Chung, G. Ginis, and J. M. Cioffi, "Dynamic spectrum management for next-generation DSL systems," *IEEE Communications Magazine*, vol. 40, no. 10, pp. 101–109, Oct. 2002.

[2] G. Ginis and J. M. Cioffi, "Vectored transmission for digital subscriber line systems," *IEEE Journal on Selected Areas in Communications*, vol. 20, no. 5, pp. 1085–1104, Jun. 2002.

[3] R. Cendrillon, M. Moonen, J. Verlinden, T. Bostoen, and G. Ginis, "Improved linear crosstalk precompensation for DSL," in *Proc. IEEE International Conference on Acoustics, Speech, and Signal Processing (ICASSP), 2004*, vol. 4, Montreal, Quebec, Canada, May 2004, pp. 1053–1056.

[4] R. Cendrillon, M. Moonen, E. Van den Bogaert, and G. Ginis, "The linear zero-forcing crosstalk canceler is near-optimal in DSL channels," in *Proc. IEEE Global Telecommunications Conference (GLOBECOM 2004)*, vol. 4, Dallas, TX, USA, Nov.–Dec. 2004, pp. 2334–2338.

[5] R. Cendrillon, M. Moonen, G. Ginis, K. Van Acker, T. Bostoen, and P. Vandaele, "Partial crosstalk cancellation for upstream VDSL," *EURASIP J. Appl. Signal Process.*, vol. 2004, no. 10, pp. 1520–1535, Jan. 2004. [Online]. Available: http://dx.doi.org/10.1155/S1110865704309273

[6] R. Cendrillon, G. Ginis, M. Moonen, and K. Van Acker, "Partial crosstalk precompensation in downstream VDSL," *Signal Process.*, vol. 84, no. 11, pp. 2005–2019, Nov. 2004. [Online]. Available: http://dx.doi.org/10.1016/j.sigpro.2004.07.013

[7] R. Cendrillon, G. Ginis, E. Van den Bogaert, and M. Moonen, "A Near-Optimal Linear Crosstalk Canceler for Upstream VDSL," *IEEE Transactions on Signal Processing*, vol. 54, no. 8, pp. 3136–3146, Aug. 2006.

[8] ——, "A Near-Optimal Linear Crosstalk Precoder for Downstream VDSL," *IEEE Transactions on Communications,*, vol. 55, no. 5, pp. 860–863, May 2007.

[9] ITU, *Very high speed digital subscriber line transceivers 2 (VDSL2), Technical Recommendation G.993.2*, ITU Std., Dec. 2011.

[10] V. Oksman, H. Schenk, A. Clausen, J. M. Cioffi, M. Mohseni, G. Ginis, C. Nuzman, J. Maes, M. Peeters, K. Fisher, and P.-E. Eriksson, "The ITU-T's new G.vector standard proliferates 100 Mb/s DSL," *IEEE Communications Magazine*, vol. 48, no. 10, pp. 140–148, Oct. 2010.

[11] ITU, *Self-FEXT Cancellation (Vectoring) for Use with VDSL2 Transceivers, Technical Recommendation G.993.5*, ITU Std., Apr. 2010.

[12] Alcatel, "G.vdsl: MIMO for VDSL2: Requirements to allow upstream MIMO," Contribution TD HH-56 to ITU Study Group 15, ITU, Jan. 2005.

[13] ——, "G.vdsl: MIMO for VDSL2: Requirements to allow downstream MIMO," Contribution TD HH-57 to ITU Study Group 15, ITU, Jan. 2005.

[14] P. Whiting, A. Ashikhmin, G. Kramer, C. Nuzman, A. Van Wijngaarden, M. Zivkovic, M. Peeters, M. Guenach, J. Maes, and J. Verlinden, "DSL Crosstalk Coefficient Acquisition Using SNR Feedback," in *Proc. IEEE Global Telecommunications Conference (GLOBECOM 2008)*, New Orleans, LA, USA, Nov.–Dec. 2008, pp. 1–5.

[15] G. Marrocco, M. Wolkerstorfer, T. Nordström, and D. Statovci, "Energy-Efficient DSL using Vectoring," in *Proc. IEEE Global Telecommunications Conference (GLOBECOM 2011)*, Houston, TX, USA, Dec. 2011, pp. 1–6.

[16] J. Huang, V. Subramanian, R. Agrawal, and R. Berry, "Downlink scheduling and resource allocation for OFDM systems," *IEEE Transactions on Wireless Communications*, vol. 8, no. 1, pp. 288–296, Jan. 2009.

[17] ITU, *Very high speed digital subscriber line transceivers 2 (VDSL2), Technical Recommendation G.993.2*, ITU Std., July 2002.

7

The Cold Cables Case

Eduardo Medeiros, Per Ödling, Ian Cooper, Trevor Morsman, Stefan Höst and Per Ola Börjesson

Abstract

The temperature dependency of copper cable characteristics is often discussed in the community but few carry out measurements, as this is most cumbersome. In this paper we present three results, based on a measurement campaign. First, we show how the transfer functions of two common British cables vary with temperature. The measurements cover the range from -25 °C to 60 °C and from 51.75 kHz up to 106 MHz. Secondly, for cable measurements done at one temperature, we give a method to adjust these measurements to represent the predicted behavior at other temperatures. Finally, we extend the KM1 twisted-pair model introducing a temperature dependent parameter adjustment.[1]

[1]The material in this chapter was not previously published.

7.1 INTRODUCTION

A recurring topic in discussions about digital subscriber line (DSL) cable characteristics is their temperature dependency. This has been somewhat renewed through the standardization of G.fast [1] as much higher frequencies are used than in earlier systems. Few have the resources, i.e. a large environmental chamber, high-precision measurement equipment, cable drums and time, required to make measurements to add to the discussion. This paper shares measurements performed at BT laboratories using a thermal chamber and two of their commonly deployed access network cables.

Cable models are a cornerstone of the research and development of wireline transceiver technologies. Both academia and industry use these models extensively for simulation, capacity estimation, algorithm development and troubleshooting. Their widespread use is justified by the accuracy obtained at low cost and effort, especially in comparison with acquiring measurements from real copper cables. The development of cable models has been stimulated by the standardization of DSL technology. Early efforts, such as the non-causal models BT0 [2] and KPN1 [3] are typically useful in frequencies up to 30 MHz. Causality is a desirable property, since it enables the use of the models in time-domain simulations. An early causal model was presented in [4] and in [5] the BT0 model was modified in order to generate a causal impulse response.

When the International Telecommunications Unit (ITU) started developing G.fast, cable models adequate up to hundreds of MHz were a topic of high interest [6–8]. The published standard [1] incorporates a set of reference loops, a reference cable model and the best fit parameter values. In [9] the KM model group was introduced. These models are causal, adequate for the G.fast frequency range and can be fitted with as few as three parameters, using closed-form expressions. This work was extended in [10] with a causal model for the characteristic impedance.

State-of-the-art models such as the ones previously mentioned are capable of representing copper cables fairly well under static conditions. In real deployments though, the access plant will be exposed to harsh environmental conditions that influence the twisted pairs' transmission properties. Tracking changes in channel properties is essential for maintaining the high performance of channel equalizers and vectoring operations. An important contribution by Alcatel [11] presented evidence for the influence of temperature in the transfer function for both direct and far-end crosstalk (FEXT) channels in a cable bundle. The same contribution also quantified the performance loss caused by improperly tracking the channel changes.

An alternative model for cables at G.fast frequencies is presented in [12]. This model exploits the similarity between the Taylor series expansions of the

propagation constant γ and the inverse hyperbolic sine function. The same group, in [13], have measured the scattering parameters of a set of cables in a thermal chamber, varying the temperatures between 20 °C and 120 °C. Their measurements were used to fit a modified version of the inverse hyperbolic sine model, using an extra parameter for temperature dependency. An inconvenience with their approach is that one needs to have measurements at several different temperatures in order to model the characteristics at an unknown temperature. No claims about the causality of the resulting model are made in [13].

The first contribution of our work is to present measurements and discuss how the measured cable characteristics change with temperature. Thereafter, in Section 7.4, we extend the KM models presented in [9] [10] to account for temperature changes. The extended model enables the generation of different transfer functions with temperature as a parameter. Finally, we develop a procedure for approximating the characteristics of a twisted pair at any temperature based on a single cable measurement taken at, say, room temperature. The accuracy of this method is verified with direct comparison of the transfer functions.

7.2 SYSTEM MODEL

A frequency dependent transmission line's primary coefficients are series resistance $R(f)$, series inductance $L(f)$, shunt capacitance $C(f)$ and shunt conductance $G(f)$. Using the primary coefficients one can define the transmission line's series impedance $Z(f) = R(f) + j2\pi fL(f)$ and shunt admittance $Y(f) = G(f) + j2\pi fC(f)$. Based on those, the secondary coefficients are denoted

$$Z_0(f) = \sqrt{\frac{Z(f)}{Y(f)}} \quad \text{and} \quad \gamma(f) = \sqrt{Z(f)Y(f)}, \tag{7.1}$$

where $Z_0(f), \gamma(f)$ represent the characteristic impedance and propagation constant, respectively.

Separating real and imaginary parts of the propagation constant one obtains $\gamma(f) = \alpha(f) + j\beta(f)$, where $\alpha(f)$ denotes the attenuation constant and $\beta(f)$ the phase constant. For a perfectly-terminated homogeneous line, we can use $\alpha(f)$ and $\beta(f)$ to express the transfer function H at a certain frequency as

$$H(f) = e^{-d\gamma(f)} = e^{-d(\alpha(f)+j\beta(f))}, \tag{7.2}$$

where d represents the line length.

Letting $\omega = 2\pi f$ and dropping the frequency dependency notation one can

rearrange the expression for γ into

$$\gamma = j\omega\sqrt{LC}\sqrt{1+\frac{R}{j\omega L}}\sqrt{1+\frac{G}{j\omega C}}. \tag{7.3}$$

A first order Taylor series expansion of the square root terms in (7.3) leads to [9]

$$\begin{aligned} \alpha &\approx \frac{R}{2}\sqrt{\frac{C}{L}} + \frac{G}{2}\sqrt{\frac{L}{C}}, \\ \beta &\approx \omega\sqrt{LC} - \frac{RG}{4\omega\sqrt{LC}}. \end{aligned} \tag{7.4}$$

7.2.1 TEMPERATURE DEPENDENCY

The parameters of a twisted pair are influenced by temperature due to changes in the properties of conductors as well as the dielectric material used to insulate the wires. The main contribution to changes in the attenuation constant α come from variations in the series resistance R with temperature.

Assuming that the wires have a uniform cross-section, R can be expressed as

$$R = \rho\frac{l}{A}, \tag{7.5}$$

where ρ denotes the electrical resistivity of the metal, l the length and A the cross-sectional area. Both resistivity and the wire dimensions are functions of temperature. An extensive collection of resistivity measurements for copper (and other metals) is presented in [14]. The authors derive a recommended curve for resistivity as a function of temperature. Accurate measurements for the thermal expansion coefficient for copper are given in [15].

For temperatures not very far from 20 °C, a common and accurate way to model [13] [16] [17] the resistance's temperature dependence is

$$R^{(t)} = R^{(20)}\big(1+\sigma(t-20)\big), \tag{7.6}$$

where R is the resistance, the superscript $^{(t)}$ denotes the temperature t in degrees Celsius and σ is the temperature coefficient for the conductor material. From [17] we obtain the temperature coefficient for copper, $\sigma = 3.862 \cdot 10^{-3}$.

The influence of temperature on the insulator properties is reported in [18] for PVC, ECTFE and FEP at frequencies up to 135 MHz.

7.3 MEASUREMENTS

In order to investigate the impact of temperature on twisted copper pairs, we have measured the scattering parameters for two different cables:

- Cable A [19] - CW1420 - Dropwire 15: 100 meters, 0.5 mm, 4 pair cable with a strengthening element (steel wires inside the bundle).
- Cable B [20] - CW1326: 100 meters, 0.5 mm, 5 pair cable, filled with petroleum jelly.

Both cables were unrolled inside the thermal chamber, while network analyzer, baluns and cable ends were kept at room temperature. In Table 7.1 a list of the equipment used and measurement conditions is presented.

Table 7.1: Measurement Equipment and Conditions

Network Analyzer	Rohde & Schwarz ZNB8
Baluns	BH Electronics 040-0092 [21]
Frequency	51.75 kHz to 212 MHz in steps of 51.75 kHz
Temperature	-25 °C to 60 °C in steps of 5 °C

Whereas in [11], the authors have performed measurements at constant time intervals while changing the temperature, we instead have taken complete sets of measurements at stable temperature points. Once started, the thermal chamber constantly monitored and displayed its internal temperature in real-time. To verify that the cables' temperatures accurately matched the temperature setting for the chamber, we used the linearity of each cable's DC resistance. For the first two sets of measurements, the cable was left resting at the set temperature for approximately two hours. A line was then fitted to the initial pair of resistance measurements and used to determine whether the temperature on the cables was stable before a new set of scattering parameters were recorded. The measured DC resistance values are depicted in Fig. 7.1 for pair number one in both cables. The plots for other pairs are similar.

In Fig. 7.2 we present the measured attenuation for the first pair on each cable. For cable A, the spread in attenuation between the lowest and highest temperature is around 4 dB at 100 MHz. At the same frequency, the spread for cable B is around 2.5 dB. The difference in construction and quality for both cables is visible in the attenuation, with cable B having higher losses at high frequencies. Although intuition could suggest that the change in attenuation would be the same for every cable made of copper, this is only strictly true for low frequencies. From this we can already here conclude that the method we give to scale a given cable measurement taken at a known temperature to another temperature will not work perfectly for all cables.

It is not only difficult to capture the variations between cables, but also between pairs in the same bundle. To quantify how the pairs vary with temperature, in Fig. 7.3 we plot ΔH, the difference in attenuation between a measurement taken at -25 °C and another taken at 60 °C for each pair in cable A.

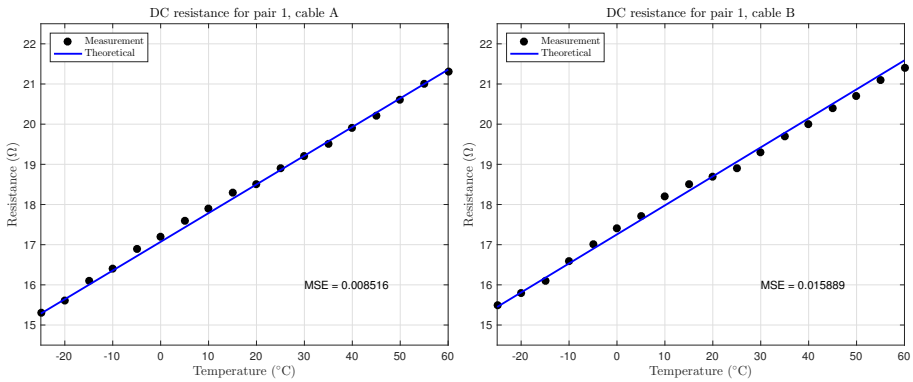

Figure 7.1: DC loop resistance measured for both cables. The actual measured values are represented by black dots. The blue solid line was obtained using the linearity relation for copper conductors, (7.6).

We observe that the cable has three pairs that behave similarly and one pair that deviates. The reason is unknown but we can speculate that it perhaps is closer to the steel reinforcement than the other pairs. This type of deviation adds uncertainty when using one pair in a cable to model all pairs, but not when modelling the temperature changes of a given pair.

7.4 TEMPERATURE ADJUSTED KM MODELS

The KM models [9] were developed based on Taylor series approximations of (7.3) and build on the $\mathrm{BT0_H}$ model. These models are named according to the number of terms considered in the series expansion. In this section we will focus on the adaptation of the KM1 model parameters to approximate the behavior of cables at different temperatures.

The KM1 model is defined as follows

$$\begin{aligned} \alpha_{\mathrm{KM}} &\triangleq k_1\sqrt{f} + k_2 f, \\ \beta_{\mathrm{KM}} &\triangleq k_1\sqrt{f} - k_2\frac{2}{\pi} f \ln f + k_3 f. \end{aligned} \tag{7.7}$$

These expressions were obtained based on the first order approximation of (7.3) and with manipulation to comply with the Hilbert transform conditions for causality. The simplicity of this model in number of parameters and fit procedure justify its adoption.

Before introducing the temperature adjusted KM model, we recall some of the properties of the related $\mathrm{BT0_H}$ model. It was proposed in [5] to accurately

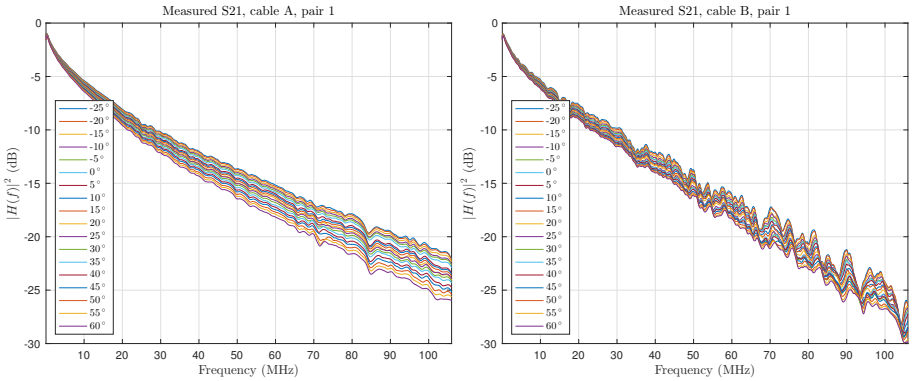

Figure 7.2: Attenuation for pair 1 on both cables. In cable A the spread between lowest and highest temperatures is higher, while overall attenuation at high frequencies is lower. Cable B presents a smaller spread but significant ripples on higher frequencies, suggesting a lower quality of construction.

model cables up to tens of MHz using the free parameters R_0, L_∞, C_∞ and v. This model produces a causal impulse response using fewer parameters than its inspiration, the classic BT0 model [2]. According to [5], $R(f)$ and $L(f)$ can be modeled as

$$\begin{aligned} R(f) &\triangleq R_0 Q\left(\frac{f}{v}\right), \\ L(f) &\triangleq \frac{R_0}{2\pi f}\Lambda\left(\frac{f}{v}\right) + L_\infty, \end{aligned} \tag{7.8}$$

where $Q\left(\frac{f}{v}\right) = \sqrt[4]{1+\left(\frac{f}{v}\right)^2}$ and $\Lambda\left(\frac{f}{v}\right)$ is the Hilbert transform of $Q\left(\frac{f}{v}\right)$. Note that in the BT0_H model both $R(f)$ and $L(f)$ are proportional to R_0.

If one makes the simplifying assumption that L_∞ depends on temperature in the same way as R_0, we would arrive at the conclusion that both series resistance and series impedance vary with temperature by the same proportion. Next, we rework this insight in (7.4) to arrive at an expression of the propagation constant at a given temperature

$$\begin{aligned} \alpha^{(t)} &\approx \frac{\big(1+\sigma(t-20)\big)R}{2}\sqrt{\frac{C}{\big(1+\sigma(t-20)\big)L}} + \frac{G}{2}\sqrt{\frac{\big(1+\sigma(t-20)\big)L}{C}}, \\ &\approx \sqrt{\big(1+\sigma(t-20)\big)}\alpha^{(20)}. \end{aligned} \tag{7.9}$$

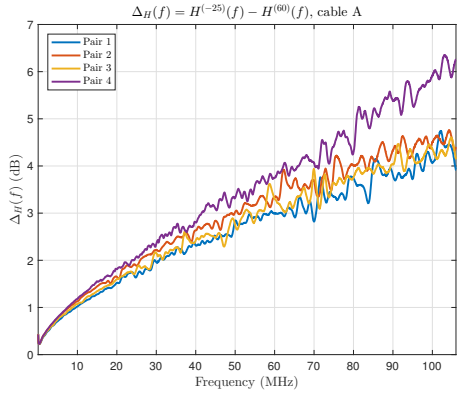

Figure 7.3: For each pair in cable A, we plot ΔH, the difference in attenuation between -25 °C and 60 °C over frequency. For each of the four pairs, the difference in attenuation increases steadily with frequency, but more for one pair than the other three.

Here, for notational convenience we have omitted the room temperature superscripts for R, L, G and C.

By comparison, a straightforward adjustment rule for the KM1 model is

$$\hat{\alpha}_{\mathrm{KM}}^{(t)}(f) = \sqrt{\big(1+\sigma(t-20)\big)}\,\alpha_{\mathrm{KM}}^{(20)} = \sqrt{\big(1+\sigma(t-20)\big)}\,(k_1\sqrt{f}+k_2 f). \quad (7.10)$$

To illustrate the accuracy of the temperature-adjusted KM1 model, we plot the modelling outcomes for the available temperature extremes, -25 °C and 60 °C. Instead of directly comparing quantities related to α we use (7.2) to obtain the more informative attenuation values.

The left side of Fig. 7.4 shows the measured attenuations of cable A at 20 °C and at -25 °C, together with the attenuation curves obtained using $\alpha_{\mathrm{KM}}^{(20)}$ and $\hat{\alpha}_{\mathrm{KM}}^{(-25)}$, the original KM1 model fit at 20 °C and the temperature-adjusted KM1 model shifted to -25 °C, respectively. The rightmost part of Fig. 7.4 correspondingly shows the 60 °C case for cable A, while Fig. 7.5 is similarly arranged for cable B. We note that the temperature-adjusted KM-model captures cable A with high precision, but slightly overshoots for cable B.

This is further illustrated in Fig. 7.6 where the figure of merit is the mean squared error (MSE). For pair 1 in both cable A and cable B, the MSE between the measured attenuation at each temperature $\left(\alpha^{(t)}\right)$ and the KM1-model adapted to that measurement $\left(\alpha_{\mathrm{KM}}^{(t)}\right)$ is plotted there. This is compared to the MSE between the temperature-adjusted KM1 $\left(\hat{\alpha}_{\mathrm{KM}}^{(t)}\right)$ and measurements at each temperature. For the smooth attenuation of cable A, we see that the

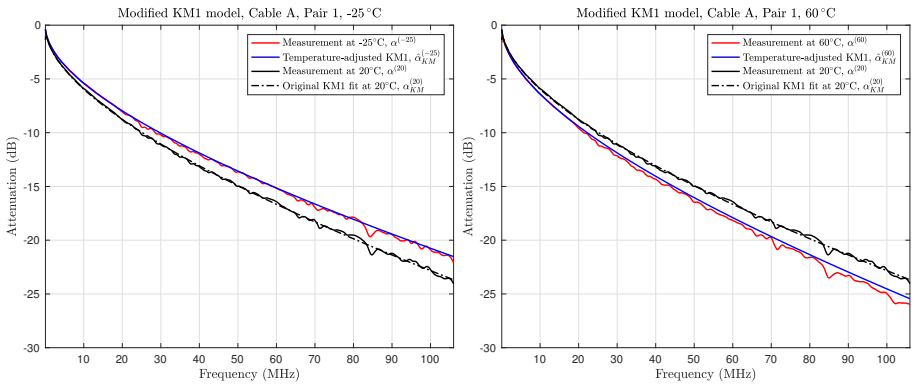

Figure 7.4: A comparison of measured and modelled transfer functions for pair 1 in cable A, at the temperature extremes -25 °C (left-hand side) and 60 °C (right-hand side). The black curves correspond to the measurement and KM1 model at 20 °C, the red curve is measured attenuation at either -25 °C or 60 °C, while the blue curve is the temperature adjusted KM1-model using 20 °C as the starting point.

KM1 model is able to capture the frequency dependency of the attenuation well and that the temperature-adjusted KM1 too does a good job, but with the expected increasing deviation as we go further out from 20 °C. As cable B's frequency curve is more rugged, both models have a higher MSE here but we also see the overshoot of the temperature-adjusted model.

7.5 TEMPERATURE ADJUSTED MEASUREMENTS

As evidenced in Figs. 7.4, 7.5 and 7.6, the adjusted KM1 model gives a reasonable fit over a large temperature range. However, since the KM1 model is smooth, it fails to capture dips and irregularities in the transfer function, quirks that are typical for real cables. Here we address the case when a real cable measurement is available but for one temperature only. If this measurement could be shifted to capture temperature differences, the fine characteristics of the real cable could be retained. In this chapter we suggest a method to temperature-adjust measurements results, which could be useful for those who have access to real measurements.

Given a set of measurements $\alpha^{(t)}(f)$ taken at a reference temperature[2], (7.11) can be used to calculate an estimate $\hat{\alpha}^{(t)}$ for each value of f in the

[2]In the case of this paper $t = 20\,^{\circ}\mathrm{C}$.

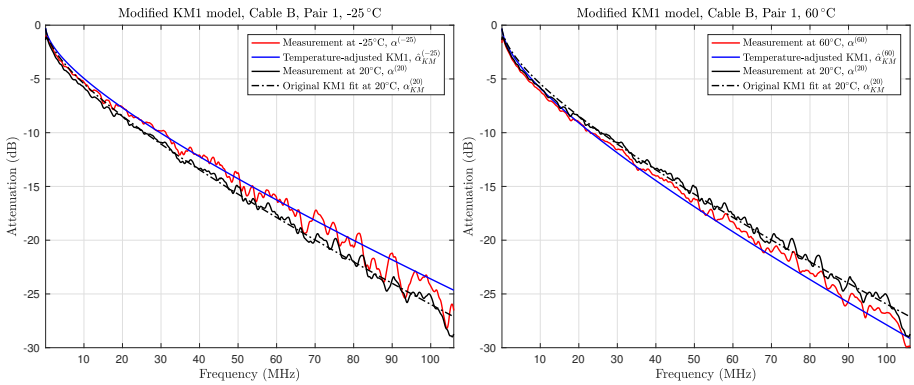

Figure 7.5: A comparison of measured and modelled transfer functions for pair 1 in cable B, at the temperature extremes -25 °C (left-hand side) and 60 °C (right-hand side). The black curves correspond to the measurement and KM1 model at 20 °C, the red curve is measured attenuation at either -25 °C or 60 °C, while the blue curve is the temperature adjusted KM1-model using 20 °C as the starting point.

original measurement as

$$\hat{\alpha}^{(t)}(f) = \sqrt{1+\sigma(t-20)}\left(\alpha^{(20)}(f)\right). \tag{7.11}$$

Note that the temperature adjustment $\sqrt{1+\sigma(t-20)}$ is the same for all frequencies. Using (7.2), $\hat{\alpha}^{(t)}(f)$ can be used to create an estimate of the transfer function at a given temperature $\hat{H}^{(t)}(f)$. We take the magnitudes of the transfer functions of cable A and cable B as plotted in Fig. 7.2, and plot them in Fig. 7.7 for cable A and in Fig. 7.8 for cable B, after the transformation using (7.11). The curves generated using this method maintain the original shape of the transfer function, while still capturing the spread caused by temperature changes.

A further evaluation is found in Fig. 7.9, where the MSE between measurements at different temperatures and the equivalent temperature-adjusted measurement is shown. We plot the MSE in the same scale as Fig. 7.6, also including the MSE curves obtained with the original KM1 model and the temperature-adjusted KM1 for comparison. The proposed adjustment for measurements performs well, clearly outperforming the temperature-adjusted KM1 model for cable B.

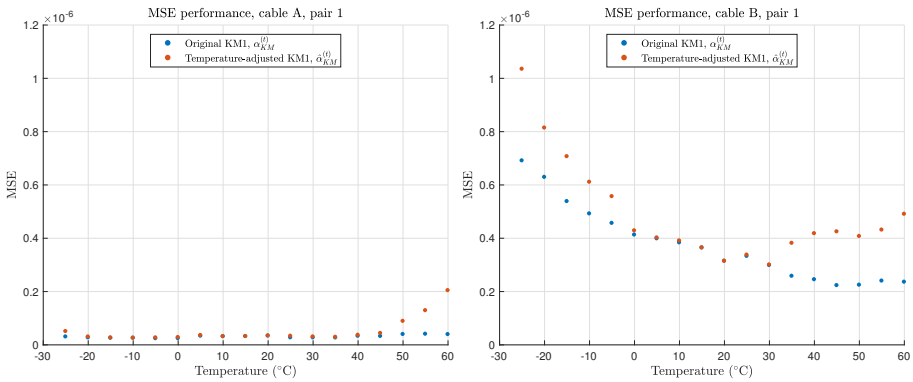

Figure 7.6: Mean squared error between measurements and the KM1 model fits for each temperature (red dots) and measurements and the temperature-adjusted KM1-model (blue dots) using 20 °C as starting point. As expected the MSE of the temperature-adjusted KM1-model increases as we get further away from 20 °C.

7.6 CONCLUSION

Cold cables and their characteristics are often discussed but rarely measured and modelled. In this paper we share the efforts we have done on the temperature dependence of cable characteristics. We share measurements on two common BT cables, one four-pair cable with a steel reinforcement (cable A) and a five-pair cable, cable B. We also propose a way to modify the KM1-model to account for temperature changes. As a final contribution we give a way to adjust an existing cable measurement to reflect temperature changes.

As always when working with real cables, it is difficult to capture their behaviour exactly. We believe our modelling work, intended to be of low complexity and easy to use, adequately captures the changes in cable characteristics arising from changes in temperature. The work on adjusting an existing measurement shows that the model overestimates the changes from temperature, especially for temperatures below zero. It is difficult to say if it is a modelling error or if the cables are affected by e.g. humidity, or that these two cables have this peculiarity. To be able to draw more general conclusions, a new, gruesome, measurement campaign would be needed. Further improvement might come from better modelling how temperature affects the cable's capacitance.

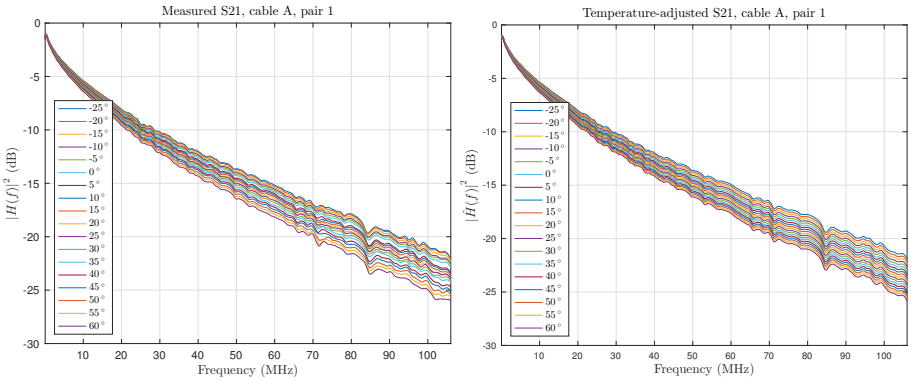

Figure 7.7: A comparison of the magnitudes of the transfer function for measured data (left side) and the estimate obtained using (7.11) (right side), for pair 1 in cable A.

ACKNOWLEDGMENT

This work was partly supported by the Celtic-Plus project GOLD, the EU H2020 5G-Crosshaul project (grant no. 671598).

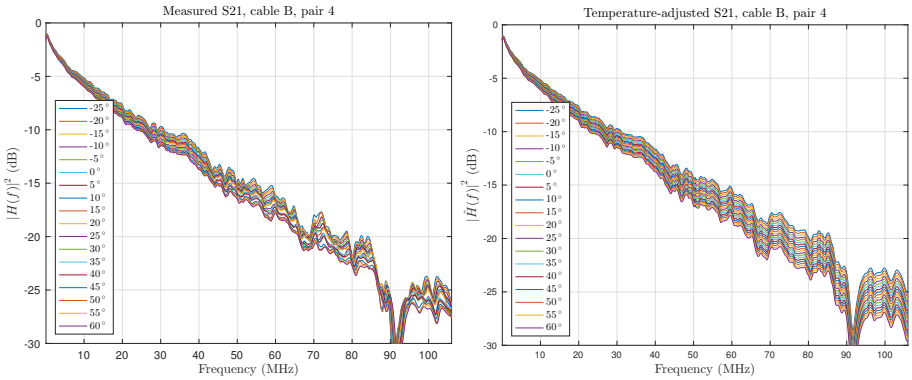

Figure 7.8: A comparison of the magnitudes of transfer functions for measured data (left side) and the estimate obtained using (7.11) (right side), for pair 4 in cable B.

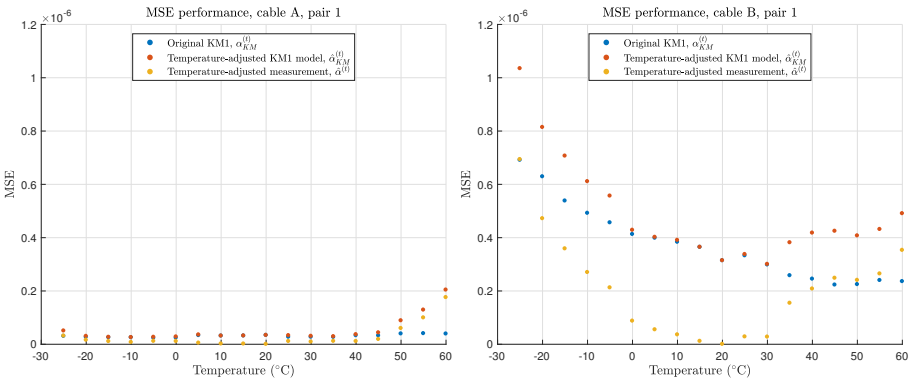

Figure 7.9: A comparison between the different temperature adjustments proposed in this paper using MSE. In blue we have the baseline performance of the KM1 model, trained using a measurement at the indicated temperature. In red we have the MSE obtained using a temperature adjusted KM1 model using (7.10). In yellow, the performance obtained using the adjusted room temperature measurement using (7.11).

References

[1] *Fast access to subscriber terminals (G.fast) - Physical layer specification*, ITU Recommendation ITU-T G.9701, Dec. 2014. [Online]. Available: http://www.itu.int/rec/T-REC-G.9701

[2] J. W. Cook, "Parametric modelling of twisted pair cables for VDSL," ETSI contribution TD22, Mar. 1996.

[3] R. F. M. van den Brink, "Measurements and models on Dutch cables," ETSI contribution TD15, Mar. 1997.

[4] P. Boets, M. Zekri, L. V. Biesen, T. Bostoen, and T. Pollet, "On the identification of cables for metallic access networks," in *Proceedings of the 18th IEEE Instrumentation and Measurement Technology Conference (IMTC)*, vol. 2, 2001, pp. 1348–1353. [Online]. Available: http://dx.doi.org/10.1109/IMTC.2001.928292

[5] F. Lindqvist, P. O. Börjesson, P. Ödling, S. Höst, K. Eriksson, and T. Magesacher, "Low-order and causal twisted-pair cable modeling by means of the hilbert transform," in *20TH Nordic Conference on Radio Science and Communications*, Jun. 2008, pp. 301–310. [Online]. Available: http://dx.doi.org/10.1063/1.3117107

[6] TNO, "G.fast: Wideband modeling of twisted pair cables as two-ports ," ITU-T SG15 Contribution, Sep. 2011.

[7] ——, "G.fast: Parametric cable models for specifying reference loops," ITU-T SG15 Contribution, Sep. 2011.

[8] Ericsson AB and TNO, "G.fast: Improved model for shunt admittance in G.fast cable model," ITU-T SG15 Contribution, May 2012.

[9] D. Acatauassu, S. Höst, C. Lu, M. Berg, A. Klautau, and P. O. Börjesson, "Simple and causal twisted-pair channel models for G.fast systems," in *2013 IEEE Global Communications Conference (GLOBECOM)*, Dec. 2013, pp. 2834–2839. [Online]. Available: http://www.dx.doi.org/10.1109/GLOCOM.2013.6831504

[10] ——, "Simple and causal copper cable model suitable for G.fast frequencies," *IEEE Transactions on Communications*, vol. 62, no. 11, pp. 4040–4051, Nov. 2014. [Online]. Available: http://www.dx.doi.org/10.1109/TCOMM.2014.2364585

[11] Alcatel-Lucent Bell, "G.vdsl: On the tracking speed required for changing crosstalk channels," ITU-T SG15 Contribution, May 2007. [Online]. Available: http://www.itu.int/md/T05-SG15-C-0540

[12] P. Lafata and M. Nevosad, "Modelling of metallic cables at G.fast frequencies," in *Applied Electronics (AE), 2015 International Conference on*, Sep. 2015, pp. 145–148.

[13] M. Nevosad and P. Lafata, "Modelling of propagation constant of twisted pairs and its temperature dependence at g.fast frequencies," *ELEKTRONIKA IR ELEKTROTECHNIKA*, vol. 22, no. 2, pp. 107–113, 2016. [Online]. Available: http://dx.doi.org/10.5755/j01.eie.22.2.12448

[14] R. A. Matula, "Electrical resistivity of copper, gold, palladium, and silver," *Journal of Physical and Chemical Reference Data*, vol. 8, no. 1147, 1979. [Online]. Available: http://dx.doi.org/10.1063/1.555614

[15] T. A. Hahn, "Thermal expansion of copper from 20 to 800k standard reference material 736," *Journal of Applied Physics*, vol. 41, no. 5096, 1970. [Online]. Available: http://dx.doi.org/10.1063/1.1658614

[16] M. Bockarjova and G. Andersson, "Transmission line conductor temperature impact on state estimation accuracy," in *2007 IEEE Lausanne Power Tech*, Jul. 2007, pp. 701–706. [Online]. Available: http://dx.doi.org/10.1109/PCT.2007.4538401

[17] J. H. Dellinger, "The temperature coefficient of resistance of copper," *Bulletin of the Bureau of Standards*, vol. 7, no. 1, pp. 71–101, 1911. [Online]. Available: http://dx.doi.org/10.6028/bulletin.161

[18] C. Y. O. Lin and J. P. Curilla, "Temperature-related changes in dielectric constant and dissipation factor of insulations increase attenuation in data cables used in building plenums," in *[1991] Proceedings 16th Conference on Local Computer Networks*, Oct. 1991, pp. 74–79. [Online]. Available: http://doi.org/10.1109/LCN.1991.208050

[19] BT Cables, *External 4 Pair Dropwire Telephone Cable, DROPWIRE 15*, 2012. [Online]. Available: http://goo.gl/jUL6RR

[20] ——, *PeT Solid Local Network Cable, CW1326*, 2012. [Online]. Available: http://goo.gl/3X7MPZ

[21] BH Electronics, *Test BALUN 040-0092*, 1998. [Online]. Available: http://goo.gl/nsMnU1

8

Temperature-dependent Shift of Notches in the Frequency Response of Twisted-Pairs

Eduardo Medeiros, Per Ödling, Ian Cooper, Trevor Morsman, Stefan Höst and Per Ola Börjesson

Abstract

In this letter we present evidence for temperature-dependent frequency shifts of the notches in a cable transfer function, a phenomenon observed in fiber and coaxial cable Bragg gratings. Measurements on two commonly deployed British cables indicate that besides changes in attenuation, notches in the transfer function may shift by more than 1 MHz due to temperature changes. For the measured cables, perhaps counter-intuitively, the propagation delay is shortened as temperature increases in spite of the thermal expansion.[1]

[1]The material in this chapter was not previously published.

8.1 INTRODUCTION

When the International Telecommunications Unit (ITU) started developing G.fast [1], cable models adequate up to hundreds of MHz were a topic of high interest [2–6]. State-of-the-art models are capable of representing copper cables fairly well under static conditions. In real deployments though, the access plant is exposed to harsh environmental conditions that influence the twisted pairs' transmission properties. The literature covering such effects is scarce, especially when it comes to high frequencies.

In a uniform transmission line the properties of conductors, insulators and cable geometry are independent of the longitudinal coordinate. In practice, due to manufacturing variances, incorrect handling and cable aging the dimensions of the conductors, insulation, the distance between pairs, and the twist rate may change. As a consequence, cable measurements can look quite different from idealized models, especially at high frequencies (for an example see Fig. 2 in [7]).

The variations of the characteristic impedance along the length of the cable generate reflections that can add up in phase, resulting in dips in the transmission spectrum. This has been reported in [8–10] for cables with periodic changes in the dielectric.

In other types of transmission lines, mainly fibers, but recently also coaxial cables [11] [12], Bragg gratings have been used. In these applications, the refractive index of the fiber core or the characteristic impedance of the coaxial cable are modified to form a notch at some desired wavelength. Shifts in the so-called Bragg wavelength are observed when the transmission line is strained or the temperature changes [11] [13–16].

In our measurement campaign we have observed that the dips in the twisted pairs' transfer functions exhibit the same behavior. Here, though, the notching of some frequencies are neither desired nor intentionally introduced, but rather occur as an outcome of the manufacturing process and cable handling.

In this paper, we present measurements for two cable types commonly deployed in the United Kingdom [17] [18] over a temperature range of -25 °C to 60 °C. We offer an explanation for the observed frequency shift of notches in the transfer function based on the Bragg condition. Lastly, we present experimental results showing that the phase velocity for both cables increase with temperature and that the propagation delay is shortened.

8.2 SYSTEM MODEL

A frequency dependent uniform transmission line's primary coefficients are series resistance $R(f)$, series inductance $L(f)$, shunt capacitance $C(f)$ and shunt conductance $G(f)$. Using the primary coefficients one can define the

transmission line's series impedance $Z(f) = R(f) + j2\pi fL(f)$ and shunt admittance $Y(f) = G(f) + j2\pi fC(f)$. Based on those, the secondary coefficients are denoted

$$Z_0(f) = \sqrt{\frac{Z(f)}{Y(f)}} \quad \text{and} \quad \gamma(f) = \sqrt{Z(f)Y(f)},$$

where $Z_0(f), \gamma(f)$ represent the characteristic impedance and propagation constant, respectively.

Separating real and imaginary parts of the propagation constant one obtains $\gamma(f) = \alpha(f) + j\beta(f)$, where $\alpha(f)$ denotes the attenuation constant and $\beta(f)$ the phase constant. For a perfectly-terminated homogeneous line, we can use $\alpha(f)$ and $\beta(f)$ to express the transfer function H at a certain frequency as

$$H(f) = e^{-d\gamma(f)} = e^{-d(\alpha(f)+j\beta(f))}, \tag{8.1}$$

where d represents the line length.

The phase velocity is defined as

$$v(f) = \frac{2\pi f}{\beta(f)}. \tag{8.2}$$

A sinusoid of frequency f propagating in a transmission line with phase velocity $v(f)$ will have a wavelength

$$\lambda = \frac{v(f)}{f}. \tag{8.3}$$

8.2.1 BRAGG CONDITION

When the characteristic impedance along the line changes with periodicity Λ (in length units), in-phase reflections occur if the following condition is met [9] [12]

$$\beta = \frac{\pi}{\Lambda}. \tag{8.4}$$

The condition can also be stated in the form $\Lambda = \frac{\lambda}{2}$.

8.3 MEASUREMENTS

As described in detail in our companion paper [19], we have measured the scattering parameters for two different cables:

- Cable A [17] - CW1420 - Dropwire 15: 100 meters, 0.5 mm, 4 pair cable with a strengthening element (steel wires inside the bundle).

- Cable B [18] - CW1326: 100 meters, 0.5 mm, 5 pair cable, filled with petroleum jelly.

Both cables were unrolled inside the thermal chamber, while network analyzer, baluns and cable ends were kept at room temperature. In Table 8.1 a list of the equipment used and measurement conditions is presented.

Table 8.1: Measurement Equipment and Conditions

Network Analyzer	Rohde & Schwarz ZNB8
Baluns	BH Electronics 040-0092 [20]
Frequency	51.75 kHz to 212 MHz in steps of 51.75 kHz
Temperature	-25 °C to 60 °C in steps of 5 °C

In Fig. 8.1 we present the measured attenuation for the first pair on each cable. While the increase in attenuation is expected due to an increase in resistance (see [19]), a more interesting observation is the fact that the notches of the transfer function shift to higher frequencies as the temperature increases. This is highlighted in the insets of Fig. 8.1. For a 10 °C increase, the frequency shift for the highlighted cases can be larger than the subcarrier spacing used in systems such as G.fast.

To explain why these shifts occur, we propose that part of the naturally occurring cable inhomogeneities obey the Bragg condition as stated in (8.4). In other words, if a dip is observed at frequency f_n, a set of inhomogeneities are disposed along the cable in such a way that the distance between them (Λ) approaches $\frac{\lambda}{2}$.

As the cable temperature increases, both Λ (the distance between inhomogeneities) and λ (the wavelength) will change. The first mainly as a result of thermal expansion, the second as a result of changes in the dielectric constant. To denote their dependence on temperature we use $\Lambda^{(t)}$, and $\lambda^{(t)}$ from now on.

In Fig. 8.2 we present $v(f)^{(t)}$, the phase velocity as a function of frequency and temperature for pair one in cable A[2]. We notice that as temperature increases, the phase velocity increases. Since wavelength and phase velocity are proportional (from (8.3)), we also conclude that for $t > t_0$, $\lambda^{(t)} > \lambda^{(t_0)}$.

Let $f_n^{(t)}$ denote the frequency at which a notch in the transfer function is observed when the temperature equals t. $f_n^{(t)}$ is a solution to the equation

$$\frac{v(f)^{(t)}}{f} = \lambda^{(t)} = 2\Lambda^{(t)}. \tag{8.5}$$

[2]Similar results were observed in all other pairs in both cables. Due to space constraints we restrict the presentation to a single example.

For a pair of temperature values t_0 and t, the ratio between the frequencies where a notch should be observed can be written as

$$\frac{f_n^{(t)}}{f_n^{(t_0)}} = \frac{v(f)^{(t)}}{v(f)^{(t_0)}} \cdot \frac{\Lambda^{(t_0)}}{\Lambda^{(t)}}. \tag{8.6}$$

If the increase in phase velocity caused by a temperature change is larger than the thermal expansion of the inhomogeneities along the cable length, the notch in question should be observed at a higher frequency, which is what we see for our two cables.

Lastly, we report on the temperature dependency of the propagation delays for the measured cables. In Fig. 8.3 we present the impulse response of pair one in cable A as a function of time and temperature. For any given temperature, let us use the location of the maximum point to derive the propagation delay. If the cable's length were to expand at a higher rate than the propagation velocity increases, the propagation delay should increase with temperature. In our measurements, though, the inverse effect is observed. The increase of propagation velocity dominates over thermal expansion, leading the impulse response to rise earlier than expected.

8.4 CONCLUSION

At least for the two measured cables, a cold pair is "slower" even though it is shorter. Although this at first may seem counterintuitive, similar results are reported in [21] [22] for coaxial cables. As temperature changes, shifts in the transfer function notches are observed. We offer an explanation based on the distance between inhomogeneities in the characteristic impedance and discuss how changes in physical dimensions and phase velocity could explain the shifts. We conclude that the influence of the changes in phase velocity dominate over the thermal expansion.

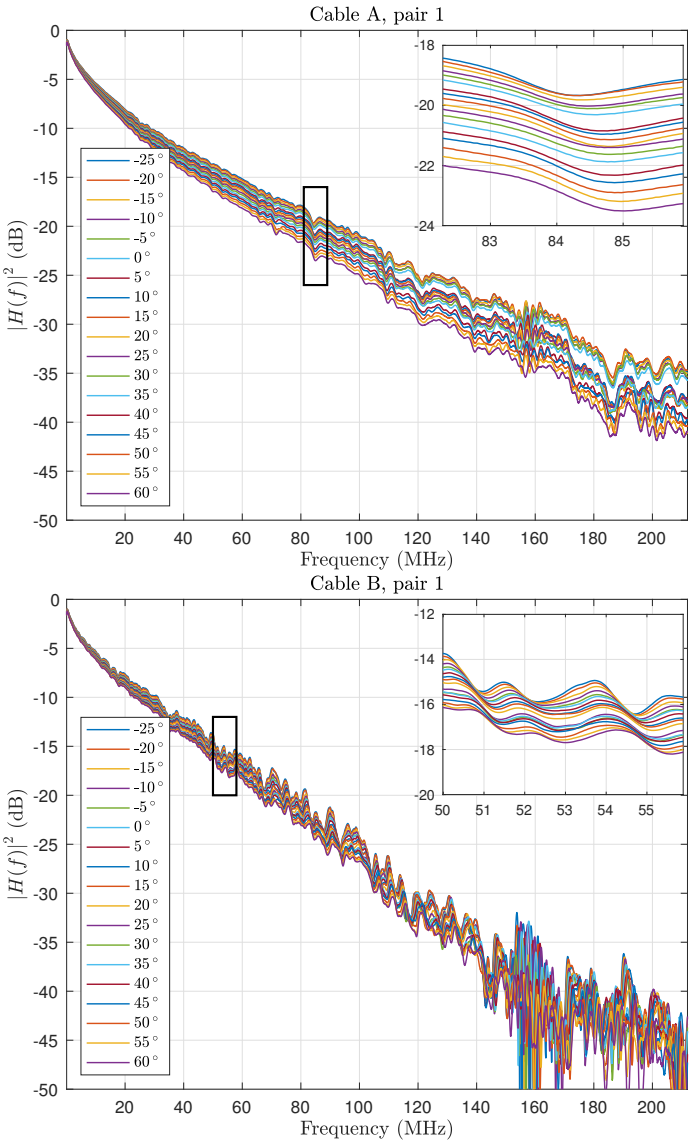

Figure 8.1: Attenuation for pair one on both cables. In cable A the spread between lowest and highest temperatures is higher, while overall attenuation at high frequencies is lower. Cable B presents a smaller spread but significant ripples on higher frequencies, suggesting a lower quality of construction. The magnifying insets on both plots illustrate the temperature-dependent frequency shift for some of the notches.

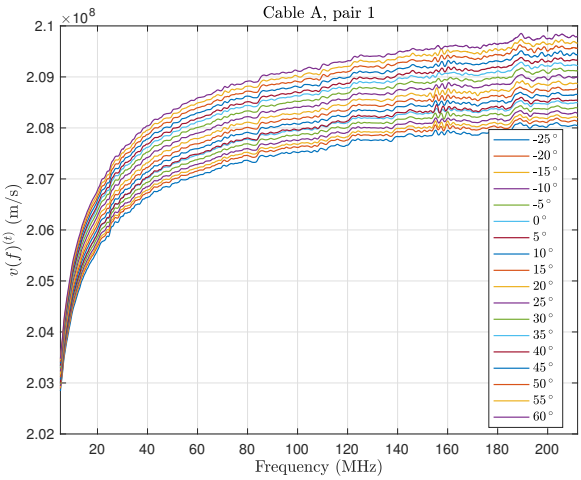

Figure 8.2: The phase velocity as a function of frequency and temperature for pair one in cable A. At any given frequency, phase velocity seems to be an affine function of the temperature.

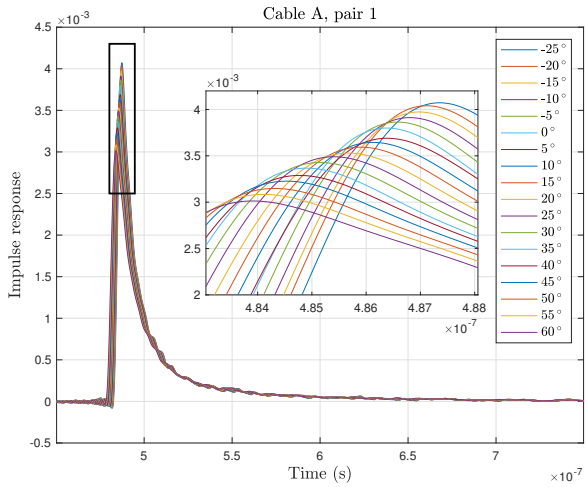

Figure 8.3: The impulse response for pair one in cable A as a function of time and temperature. We use the maximum point for each curve to determine the propagation delay. As temperature increases, the cable gets slightly longer, but the propagation delay decreases at a higher rate.

References

[1] *Fast access to subscriber terminals (G.fast) - Physical layer specification*, ITU Recommendation ITU-T G.9701, Dec. 2014. [Online]. Available: http://www.itu.int/rec/T-REC-G.9701

[2] TNO, "G.fast: Wideband modeling of twisted pair cables as two-ports ," ITU-T SG15 Contribution, Sep. 2011.

[3] ——, "G.fast: Parametric cable models for specifying reference loops," ITU-T SG15 Contribution, Sep. 2011.

[4] Ericsson AB and TNO, "G.fast: Improved model for shunt admittance in G.fast cable model," ITU-T SG15 Contribution, May 2012.

[5] D. Acatauassu, S. Höst, C. Lu, M. Berg, A. Klautau, and P. O. Börjesson, "Simple and causal twisted-pair channel models for G.fast systems," in *2013 IEEE Global Communications Conference (GLOBECOM)*, Dec. 2013, pp. 2834–2839. [Online]. Available: http://www.dx.doi.org/10.1109/GLOCOM.2013.6831504

[6] ——, "Simple and causal copper cable model suitable for G.fast frequencies," *IEEE Transactions on Communications*, vol. 62, no. 11, pp. 4040–4051, Nov. 2014. [Online]. Available: http://www.dx.doi.org/10.1109/TCOMM.2014.2364585

[7] R. Strobel, R. Stolle, and W. Utschick, "Wideband modeling of twisted-pair cables for MIMO applications," in *2013 IEEE Global Communications Conference (GLOBECOM)*, Dec. 2013, pp. 2828–2833. [Online]. Available: http://dx.doi.org/10.1109/GLOCOM.2013.6831503

[8] R. F. M. van den Brink and J. Boschma, "Cable measurements G.fast 2013," Presentation material, 2013.

[9] G. S. Borges, R. M. Rodrigues, J. C. W. A. Costa, A. Santos, and A. Fertner, "Effect of periodic cable nonuniformities on transmission measurements," in *2015 IEEE International Instrumentation and Measurement Technology Conference (I2MTC) Proceedings*, May 2015, pp. 315–319. [Online]. Available: http://www.dx.doi.org/10.1109/I2MTC.2015.7151286

[10] G. S. Borges, "Modelagem de par-trançado para comunicações em banda larga," Ph.D. dissertation, Universidade Federal do Pará, Belém, Brazil, Aug. 2016. [Online]. Available: http://goo.gl/pfk7vx

[11] T. Wei, S. Wu, J. Huang, H. Xiao, and J. Fan, "Coaxial cable Bragg grating," *Applied Physics Letters*, vol. 99, no. 11, 2011. [Online]. Available: http://dx.doi.org/10.1063/1.3636406

[12] S. Wu, T. Wei, J. Huang, H. Xiao, and J. Fan, "Modeling of coaxial cable Bragg grating by coupled mode theory," *IEEE Transactions on Microwave Theory and Techniques*, vol. 62, no. 10, pp. 2251–2259, Oct. 2014. [Online]. Available: http://dx.doi.org/10.1109/TMTT.2014.2342672

[13] A. D. Kersey, M. A. Davis, H. J. Patrick, M. LeBlanc, K. P. Koo, C. G. Askins, M. A. Putnam, and E. J. Friebele, "Fiber grating sensors," *Journal of Lightwave Technology*, vol. 15, no. 8, pp. 1442–1463, Aug. 1997. [Online]. Available: http://www.dx.doi.org/10.1109/50.618377

[14] J. Huang, T. Wei, X. Lan, J. Fan, and H. Xiao, "Coaxial cable bragg grating sensors for large strain measurement with high accuracy," vol. 8345, 2012. [Online]. Available: http://dx.doi.org/10.1117/12.915035

[15] J. Huang, T. Wang, L. Hua, J. Fan, H. Xiao, and M. Luo, "A coaxial cable fabry-perot interferometer for sensing applications," *Sensors*, vol. 13, no. 11, pp. 15 252–15 260, 2013. [Online]. Available: http://www.mdpi.com/1424-8220/13/11/15252

[16] M. F. Ahmed, T. Xue, B. Wu, and J. Huang, "High quality factor coaxial cable fabry-perot resonator for sensing applications," *IEEE Sensors Journal*, vol. 17, no. 10, pp. 3052–3057, May 2017. [Online]. Available: http://dx.doi.org/10.1109/JSEN.2017.2686864

[17] BT Cables, *External 4 Pair Dropwire Telephone Cable, DROPWIRE 15*, 2012. [Online]. Available: http://goo.gl/jUL6RR

[18] ——, *PeT Solid Local Network Cable, CW1326*, 2012. [Online]. Available: http://goo.gl/3X7MPZ

[19] E. Medeiros, P. Ödling, I. Cooper, T. Morsman, S. Höst, and P. O. Börjesson, "The cold cables case," included as chapter 7 in this thesis.

[20] BH Electronics, *Test BALUN 040-0092*, 1998. [Online]. Available: http://goo.gl/nsMnU1

[21] K. Czuba and D. Sikora, "Phase drift versus temperature measurements of coaxial cables," in *18th International Conference On Microwaves, Radar And Wireless Communications*, Jun. 2010, pp. 1–3.

[22] ——, "Temperature Stability of Coaxial Cables," *Acta Phys. Pol. A*, vol. 119, no. EuCARD-PUB-2011-001, 2011. [Online]. Available: http://cds.cern.ch/record/1349292

9

Enabling DSL and Radio on the Same Copper Pair

Yezi Huang, Eduardo Medeiros, Stefan Höst, Thomas Magesacher, Per-Erik Eriksson, Chenguang Lu, Per Ödling and Per Ola Börjesson

Abstract

To increase indoor coverage for mobile services, we propose a residential small cell infrastructure making use of the existing copper plant. The system is cabinet-based, collocated with VDSL2 and uses small pieces of spectrum next to VDSL2. Inspired by the Ericsson Radio Dot System, it challenges the femtocell paradigm offering full macro functionality in the small cells. An interesting service potential is offered albeit the added mobile traffic capacity is moderate as it is limited by the copper fronthaul. [1]

[1]Published in *Proc. IEEE International Conference on Communications (ICC 2015)*, London, United Kingdom, 08-12 Jun. 2015.

9.1 INTRODUCTION

The copper access network plays a key role in the evolutionary process of delivering broadband services [1]. Relaying radio signals over high-quality copper cables, as demonstrated by the system introduced in [2], can provide full macrocell functionality to indoor small cells fed over cables. While [2] focuses on indoor-enterprise environments using standard LAN cables, we pose the question whether it could be used to realize a vision of connected homes exploiting the edge of the access network. Given the increased interest in residential small cells in standardisation bodies and the increasing market uptake of femtocells, the concepts presented in [2] could be extended to the public switched telephone network (PSTN), representing a valuable market opportunity for operators.

The amount of attention given to residential small cells is increasing fast. This is partly fueled by increasing capacity demands calling for a densification of the cellular networks and insights into the cost of doing so [3]. Estimations in [4] [5] hint that between 70% and 90% of the traffic in the mobile networks is generated indoors, and it is suggested that the homes are natural new sites for small cells. But the drive towards small cells is also coming from changes in how we live and how we construct our dwellings. Thick fire-safe concrete walls increasingly block radio waves as we move our systems higher up in frequency. New window types with high energy insulation often have a built-in thin metal layer sealing off the interior both thermally and electromagnetically. Achieving indoor coverage becomes increasingly difficult without placing an antenna inside the home.

The main approach to get an antenna inside the home today is by deploying a femtocell. Here we go deeper into the Radio Dot System [2] idea presented by Ericsson. Instead of using standard LAN cables, we focus on twisted pairs in the PSTN copper plant, using the spectrum above VDSL2 17 MHz profiles but below G.fast (the next generation DSL) and maintaining so low interfering signal levels that these and other legacy systems remain unaffected at large. Thus, we argue that the extended concept is realistic and deployable, albeit it requires similar augmentation of the regulatory regimes like any new DSL system would. We perform the spectrum planning by optimizing for capacity in a typical plant topology and show that decent bit rates can be delivered. In [6] and [7], an alternative femtocell architecture is investigated. It superimposes the radio signal on the lower part of VDSL2 spectrum, starting from 100 kHz, and performs compound MIMO processing over air and cable channels. Although benefiting from lower cable attenuation, directly usage of VDSL2 spectrum makes this system suffer from inevitable VDSL2 interference, and vice versa.

In this paper we intend to develop a realistic and deployable system archi-

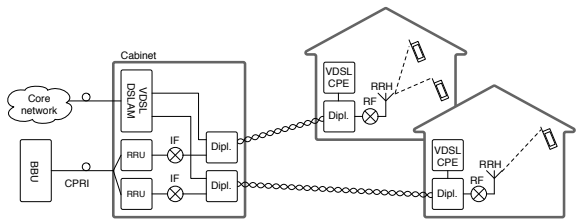

Figure 9.1: A schematic for the proposed radio-over-copper system. Notice the co-location of DSL equipment and remote radio units in the cabinet.

tecture that is collocated with VDSL2 in the cabinets of the telephony copper network. We extend the concept presented in [2] by evaluating its feasibility over regular telephony cables, using the spectra between VDSL2 [8] and G.fast [9]. Disregarding the losses in the radio channel, the available capacity in the copper loop is evaluated at the chosen band. We optimize the placement of downlink and uplink bands to avoid interfering with legacy systems, and as a result determine the maximum loop lengths over which radio signals can be deployed.

The paper is organized as follows. In Section 9.2, the system concept is introduced. In Section 9.3, achievable throughput and coexistence are investigated. Section 9.4 presents a case study with gap-band optimization and Section 9.5 concludes the work.

9.2 WHY AND WHERE

The system topology considered in this paper is depicted in Fig. 9.1. We have a location such as a home connected with telephony wiring feeding radio equipment in turn accessing an indoor radio channel. A traditional femtocell architecture terminates the copper line with some flavor of DSL, say VDSL2, backhauling the femtocell traffic over a bitstream connection. Suppose that we now want to deliver an analog fronthaul service over the copper but in parallel to VDSL2 rather than using it as backhaul. Is it possible and if so what capacity do we release? These are the questions we attempt to answer with this paper.

In Fig. 9.1 the base band unit (BBU) is located centralised in the network, and the radio signal is sent out to the remote radio unit (RRU) digitally with *e.g.*, CPRI [10] using a fiber connection. The RRU in this setup is typically co-located with the VDSL2 digital subscriber line access multiplexer (DSLAM) in the cabinet. In the downlink direction, the radio signal is upconverted to

the band above the VDSL2 signal. A diplexer (Dipl. in the figure) combines the VDSL2 signal and the radio signal on the twisted pair. At the customer premises a second diplexer splits the signals for the VDSL2 customer premises equipment (CPE) and the remote radio head (RRH). Shifting the radio signal up in frequency to the required band gives indoor mobile coverage. A similar procedure occurs in the uplink direction, where the RRH down-converts the radio signal to adequate frequencies in the copper loop. After transmission through the twisted pair, the analog radio signal is sampled at the RRU.

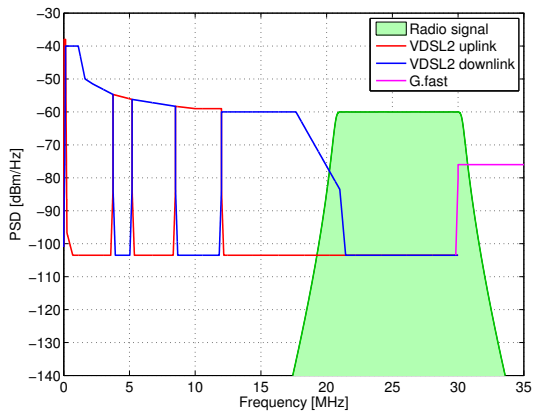

Figure 9.2: Bandplans for VDSL2, G.fast and the band of interest for the proposed radio-over-copper system, pictured as a green shaded area.

The frequency range we intend to make use of is shown in Fig. 9.2. The leftmost part of the figure shows the various up- and downlink bands of VDSL2 and the right part shows one of the possible options for the starting frequency of G.fast (30 MHz). This particular spectrum plan was defined by ITU [11] and is typical for what can be expected in many countries. Although VDSL2 30 MHz profiles have been standardized for years, their market penetration in western countries is much lower compared to their 17 MHz counterparts. Therefore, in this paper we target unused spectra between 17 MHz and 30 MHz.

The focus of this work is on spectrum planning and throughput evaluation. Several related issues are left for further study. First, we do not consider crosstalk originating from VDSL2 or G.fast users in neighboring lines. The band we intend to use lies spectrally between VDSL2 and G.fast. Thus, there is only crosstalk of leakage signals at the band edges. Second, we assume that there is no crosstalk in the VDSL2-G.fast gap band from other radio-over-copper systems—that is, we limit our focus to scenarios with a single

radio-over-copper system in the last-drop cable. This assumption is reasonable because the crosstalk between radio-over-copper systems could be dealt with by crosstalk cancellation schemes similar to those used in VDSL2 and G.fast. Third, we do not consider the impact of electromagnetic compatibility. In order to limit unwanted radio egress, we keep the transmit PSD in the band of interest between $-60\,\mathrm{dBm/Hz}$ and $-80\,\mathrm{dBm/Hz}$. This choice of transmit PSD is compatible with the limiting PSD masks defined for 30 MHz VDSL2 profiles. Consequently, the egress noise generated by the proposed system would be comparable to that caused by a standard-compliant 30 MHz VDSL2 system. However, analog radio-over-copper transmission remains vulnerable to radio ingress. Interference that is picked up by the copper pair in the gap band directly affects the signal quality, both in downlink and uplink direction. The coexistence analysis presented in the following sections is merely a first step in assessing the feasibility of an analog radio-over-copper system hosting a radio signal between VDSL2 and G.fast.

9.3 COEXISTENCE AND CAPACITY

In our system analysis, we begin by placing the downlink band for the radio signal starting at 21 MHz. Assume the VDSL2 system uses a bandplan occupying frequencies up to 17 MHz (*e.g.*, the FDD bandplan 998ADE17 [8]). Appropriate signal separation through the diplexers pushes the out-of-band leakage from VDSL2 right to the noise floor of the radio signal, and vice versa. The VDSL2 bandplan 998ADE17 shown in Fig. 9.2 ends with a downlink band in 12-17 MHz. The diplexer filters separating the signals will work on similar power levels, since both are either attenuated (on the RRH side) or un-attenuated (on the RRU side). The alternative to start with the uplink for the radio signal results in an unbalance of amplitudes, which requires substantially more attenuation in the stop band of the filters.

The narrowest bandwidths used in a modern mobile communication system, such as LTE [12], are 1.4 MHz, 3 MHz and 5 MHz, each having a built-in guard band. Unfortunately, two of the 5 MHz bands do not fit into our intended spectrum span from 21 MHz to 30 MHz and two 1.4 MHz bands yield a perhaps less than impressive capacity. Thus we focus on fitting two of the 3 MHz bands. This gives a single parameter to be optimized for the resulting capacity, namely the starting frequency of the 3 MHz uplink band.

9.3.1 DOWNLINK

Fig. 9.3 depicts a schematic band plan. The downlink signal is notably attenuated after transmission over the copper cable (cf. blue spectrum in Fig. 9.3a). The sloped shape of the in-band downlink spectrum is due to the low-pass

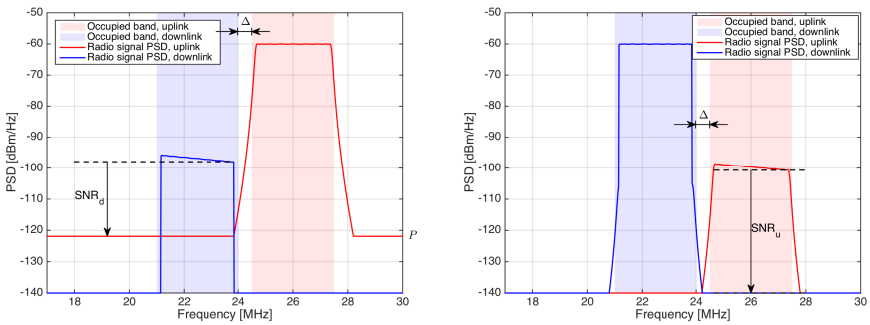

(a) RRH side **(b)** RRU side

Figure 9.3: Mutual interference between uplink and downlink radio signals in the copper cable.

properties of the cable where the attenuation grows with frequency. This sloped shape will be corrected by an equalizer at the RRH, since the PSD of the transmit signal at the antenna should be flat. At the RRH side of the copper line, the uplink signal is un-attenuated and thus much stronger than the downlink signal. The spectrum (red in Fig. 9.3a) is stronger and flat over the utilized band. However, the out-of-band leakage, *e.g.*, resulting from the insufficiently suppressed air channel interference, into the downlink signal can be severe if the guard band is not sufficient. After equalization of the downlink signal, the uplink spectrum (red) leaking into the downlink region (blue) will act as in-band interference, which is much stronger than the cable noise.

Let SNR_d denote the downlink SNR defined as the minimum ratio between the downlink signal PSD level and the out-of-band leakage PSD level P from the uplink signal. The level P encountered in a system depends strongly on implementation details. In a real system, P will rather vary over frequency than remain constant over our band of interest. However, from an analysis-perspective, a frequency-flat upper-bound leakage level P is sufficient since higher SNR levels over parts of the downlink band cannot be exploited by our analog relay scheme. In general, a larger gap-band Δ between downlink and uplink yields a lower interference level P and thus higher SNR_d, since the out-of-band leakage of uplink is supposed to be fading out. From an optimization perspective, it is thus rewarding to push the starting frequency of the uplink band upwards in frequency.

We start evaluating the proposed scheme by calculating the peak bit rate supported by the downlink radio link with a single antenna. We then calculate the SNR_d after transmission over the copper loop, while varying the loop

length and assuming different levels of leakage between uplink and downlink signals. The objective is to find the reach over which the system could be deployed, given some implementation losses due to band placement. We utilize the BT-CAD55 [13] cable model, since it is representative for copper cables deployed in the field.

Assuming an allowed symbol error rate[2] of 10^{-6} the SNR gap becomes $\Gamma \approx 9$ dB [14]. Then the bit rate supported by the copper channel in either direction can be obtained by

$$R_b = B(1-\beta)\log_2\left(1+10^{(\mathrm{SNR}-\Gamma)/10}\right) \tag{9.1}$$

where B denotes the transmission bandwidth and β is the fraction of B reserved for the built-in guard-bands, yielding the effective bandwidth $W = B(1-\beta)$. A radio signal with 3 MHz bandwidth and $\overline{R}_b^{[d]} = 11$ Mbps downlink peak bit rate is used as a reference.

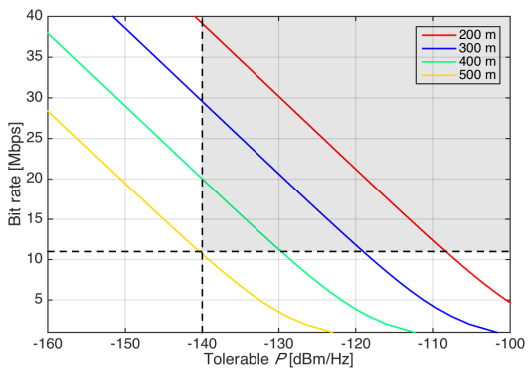

Figure 9.4: Bit rate supported by the copper channel for downlink radio signal over the BT-CAD55 cable model, assuming a certain interference from uplink leakage.

To enable radio transmission without performance degradation, R_b, the bit rate supported by the copper channel should not be lower than $\overline{R}_b^{[d]}$. Fig. 9.4 presents the relation between R_b at the far-end of the copper pair and the uplink leakage PSD level P. Given different loop lengths, the insertion loss for the copper cable BT-CAD55 was calculated as in [13]. The background noise on the copper pair limits the noise-plus-interference level inside the downlink band to -140 dBm/Hz. Thus, the grey area in Fig. 9.4 represents the feasible region for downlink radio transmission over the BT-CAD55 test-loop.

[2]Note that the symbol error rate is an upper bound for the bit error rate.

9.3.2 UPLINK

At the RRU side of the copper cable the situation is mirrored as the uplink band is attenuated and the downlink out-of-band leakage causes interference (see Fig. 9.3b). The achievable rate R_b in uplink direction versus downlink leakage PSD is very similar to the results presented in Fig. 9.4. However, there is one more effect. The uplink signal will be more attenuated the further up in frequency it is placed. Furthermore, the interference to and from G.fast services increases as the upper edge of the uplink band moves towards 30 MHz. From an optimization perspective, there exists a trade-off between increased attenuation and larger gap-band.

Clearly, we would like to stay away from the future G.fast band starting at 30 MHz for the sake of both services, but we do not include any specific level of interference in the derivation at this point. The G.fast out-of-band noise decreases very sharply and would not have an impact on the results at least in this direction.

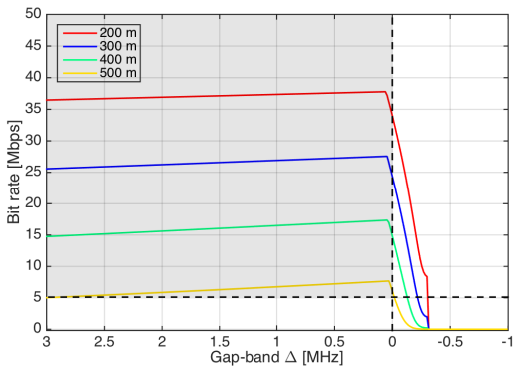

Figure 9.5: Bit rates supported by the copper channel for uplink radio signal over the BT-CAD55 model, assuming a certain gap-band Δ.

Let Δ denote the gap-band between uplink and downlink. Assume that at the near-end of the copper cable, the baseband downlink radio signal is shifted to the adequate copper frequencies, but does not go through any power amplifier, resulting in a sharply declining PSD at the band edges. The well behaved downlink radio signal results in negligible out-of-band emissions. Typically, the maximum uplink bit rate is $\overline{R}_b^{[u]} = 5\,\text{Mbps}$. Using this value as a reference and varying Δ, we obtain the uplink feasible region shown in Fig. 9.5. Combining the feasible regions in both directions, we observe that the system could be deployed almost 500 meters away from the cabinet for

the BT-CAD55 cable.

9.4 BAND PLACEMENT WITH FIXED FILTER STRUCTURE

In this section we evaluate the impact of band placement given a certain fixed diplexer structure. For this case study, we use the spectra shown in Fig. 9.3. Applying the same methodology as before, we vary Δ, cable length, transmit PSD, and cable type while using the peak radio signalling bit rates as a lower-bound threshold for feasibility.

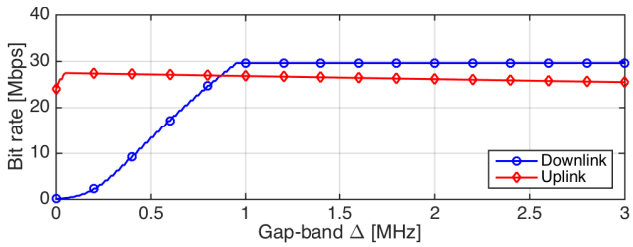

(a) Bit rates in both directions over 300 m copper pair.

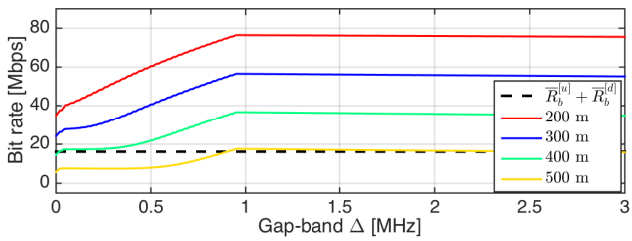

(b) Aggregate bit rates.

Figure 9.6: Supported bit rates for the radio signal over BT-CAD55 copper pair, when the transmit PSD is -60 dBm/Hz.

In Fig. 9.6a the available bit rates over the copper channel for downlink and uplink directions are shown as a function of the gap-band Δ. We chose a 300 meters BT-CAD55 copper pair to obtain a representative attenuation level. The downlink band is positioned at 21-24 MHz, while the uplink band moves depending on Δ. For small Δ, the interference between the two bands can be substantial. As Δ grows, mutual interference fades and there is a frequency point where the downlink band is not interfered anymore, or the interference power level becomes lower than the background noise on the twisted pair. Beyond this frequency point, the bit rate remains constant, *e.g.*, in Fig. 9.6a typically after $\Delta = 0.95$ MHz. For the uplink band, signal attenuation

increases for larger values of Δ, consequently causing a decrease in bit rates.

The aggregate bit rates are presented in Fig. 9.6b, assuming a transmit PSD of $-60\,\mathrm{dBm/Hz}$ in both directions. As expected, the aggregate bit rate peaks for $\Delta = 0.95\,\mathrm{MHz}$. At this point, mutual interference reaches the background noise level, and the uplink band is located as close to downlink as possible. At the optimal gap-band setting, the upper edge of uplink stops before 28 MHz, leaving a comfortable gap between the proposed system and future G.fast services.

The maximum transmit power also affects optimal gap-band setting, as evidenced in Fig.9.7a. For a fixed filter structure with a particular side-lobe suppression capability, higher in-band transmit power implies increased out-of-band leakage. Therefore, a wider gap-band is required. Lower transmit power allows for shorter gap-bands, but the drop in receive SNR might not justify that choice (see Fig.9.7b). High transmit-power levels, however, may cause undesirable leakage into neighboring systems on the same copper pair as well as crosstalk.

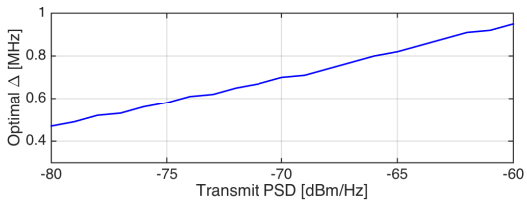

(a) Relation between transmit PSD and optimal Δ.

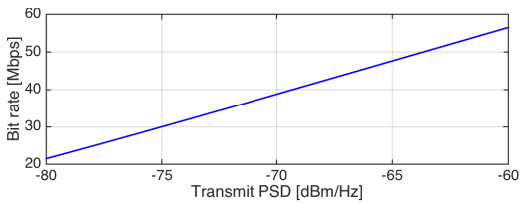

(b) Aggregate bit rates when the optimal Δ is applied.

Figure 9.7: Influence of allowed transmit PSD on the band placement, assuming a fixed filter structure in the RRH.

The cable channel will not severely affect the total SNR of the combined copper and air channel as long as the available bit rate for the copper segment is well above the peak rate for the air interface. Using this reasoning we evaluate possible deployment distances. In this study case, besides BT-CAD55, we employ two other cables models, ETSI90 and ETSI32, representing high and low quality cables, respectively. The results are collected in Fig. 9.8,

where the aggregate bit rate is shown as a function of cable length, assuming $\Delta = 0.95\,\text{MHz}$, a transmit PSD of $-60\,\text{dBm/Hz}$, and the same fixed filter structure for all cables.

For the BT-CAD55 cable, a length close to 500 meters approaches the air interface peak rate. For the low quality cable the same limit is at about 360 meters while the high quality cable has a substantial margin even at 500 meters. We conclude that it is possible to transmit analog radio signals for modern communication systems over the telephony copper lines connecting the end user in ranges of at least 350 meters. For medium quality cables this measure is close to 500 meters and for high quality well above 500 meters.

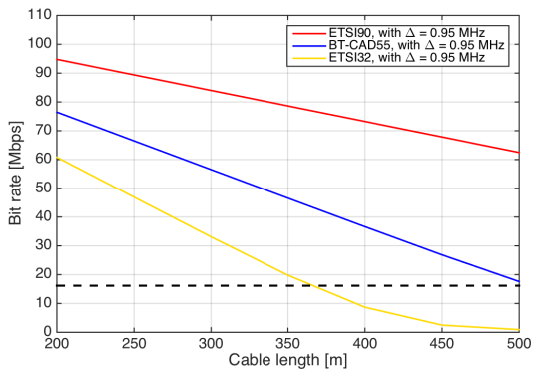

Figure 9.8: Achievable aggregate bit rates over the copper channel using the optimal gap-band setting, when the transmit PSD is $-60\,\text{dBm/Hz}$.

9.5 CONCLUSION

Small cells seem to be the next solution to the ever growing capacity demand in mobile networks, which is fueled by the development of more and more sophisticated services and mobile terminals as well as a growing number of users. Relaying the radio signal over the existing copper access network may provide a valuable contribution to solving both the backhaul bottleneck and placing small cells right where they are needed. We argue that a cabinet-based system is realistic in terms of coexistence with wireline systems and we show that the capacity it delivers is significant. The added capacity is sufficient to deliver decent mobile services to most homes given a typical European topology of the PSTN network. Peak capacity is limited by the copper fronthaul bandwidth but average capacity per user is good as these residential small cell naturally has few users.

References

[1] P. Ödling, T. Magesacher, S. Höst, P. Börjesson, M. Berg, and E. Areizaga, "The fourth generation broadband concept," *IEEE Communications Magazine*, vol. 47, no. 1, pp. 62–69, January 2009.

[2] C. Lu, M. Berg, E. Trojer, P.-E. Eriksson, K. Laraqui, O. V. Tidblad, and H. Almeida, "Connecting the dots: small cells shape up for high-performance indoor radio," *Ericsson Review*, vol. 91, December 2014. [Online]. Available: http://goo.gl/YvdY5N

[3] Ericsson AB, "Ericsson mobility report: On the pulse of the networked society," whitepaper, 2014. [Online]. Available: http://goo.gl/QjdGbn

[4] Mobidia, "Understanding the role of managed public Wi-Fi in today's smartphone user experience: A global analysis of smartphone usage trends across cellular and private and public Wi-Fi networks," whitepaper, 2013. [Online]. Available: http://goo.gl/rCOfR4

[5] Cisco, "The zettabyte era: Trends and analysis," whitepaper, 2014. [Online]. Available: http://goo.gl/p7KX4a

[6] J. Gambini and U. Spagnolini, "Radio over telephone lines in femtocell systems," in *Proc. 2010 IEEE 21st International Symposium on Personal Indoor and Mobile Radio Communications (PIMRC)*, September 2010, pp. 1544–1549.

[7] ——, "Wireless over cable for femtocell systems," *IEEE Communications Magazine*, vol. 51, no. 5, pp. 178–185, May 2013.

[8] ITU, "Very high speed digital subscriber line transceivers 2 (VDSL2)," Recommendation ITU-T G.993.2, December 2011. [Online]. Available: http://www.itu.int/rec/T-REC-G.993.2/en

[9] ——, "Fast access to subscriber terminals - physical layer specification," Recommendation Draft ITU-T G.9701, 2013. [Online]. Available: https://www.itu.int/rec/T-REC-G.9701/en

[10] Ericsson AB, Huawei Technologies, NEC Corporation, NSN and Alcatel-Lucent, "Common public radio interface specification v6.0," Publicly available specification, 2013. [Online]. Available: http://www.cpri.info/spec.html

[11] ITU, "Fast access to subscriber terminals (FAST) - Power spectral density specification," Recommendation Draft ITU-T G.9700, April 2014. [Online]. Available: https://www.itu.int/rec/T-REC-G.9700/en

[12] 3GPP, "LTE; Evolved universal terrestrial radio access (E-UTRA); Base station (BS) radio transmission and reception," Tech. Rep., 2011.

[13] D. Acatauassu, S. Höst, C. Lu, M. Berg, A. Klautau, and P. O. Börjesson, "Simple and causal copper cable model suitable for g.fast frequencies," *IEEE Transactions on Communications*, vol. 62, no. 11, pp. 4040–4051, November 2014.

[14] J. G. Proakis, *Digital Communications*, 4th ed. Mc Graw Hill, ISBN 0-07-232111-3, 2001.

10

LTE Over Copper - Potential and Limitations

Yezi Huang, Eduardo Medeiros, Nilma Fonseca, Stefan Höst,
Thomas Magesacher, Per-Erik Eriksson, Chenguang Lu,
Per Ödling and Per Ola Börjesson

Abstract

The densification of mobile networks in order to meet increased capacity demands is ongoing, needed and costly. A few papers have been published based on the insight that the fixed broadband networks offer a multitude of sites, for instance our homes, for potential small cell deployment providing backhaul capacity and power without site costs. However, in order to reach economical large-scale benefits, we explore the case when radio systems are deployed in coexistence with DSL. In this paper, we establish the feasibility of such a concept under constraints invoked by state-of-the-art and emerging systems (3GPP, VDSL2 and G.fast) and make statements about the required architecture. We also point out that the enthusiasm of previously published results should be lowered a notch. [1]

[1]Published in *Proc. IEEE Symposium on Personal, Indoor and Mobile Radio Communications - (PIMRC)*, Hong Kong, China, 30 Aug. - 03 Sep. 2015.

10.1 INTRODUCTION

The explosive growth of connected smart devices forces operators to invest constantly in improving the capacity of mobile radio networks. Currently, the main approach for addressing the demands is to deploy closely spaced macro base stations. With 4G deployments reaching maturity and the telecom industry starting their research on candidate solutions for 5G, small cells are promoted as an important enabler for higher capacity.

In the papers [1] [2] Gambini *et al.* proposed the reuse of copper lines for the deployment of femtocells based on amplify-and-forward devices. In [3], Lu *et al.* present a solution for increased indoor radio performance. Their system benefits from transparent remote radio heads (RRHs) and shared baseband processors to achieve full coordination between small cells and the macro layer, eliminating the main drawback of femtocells.

In [4] we have evaluated the feasibility of co-deploying fronthaul for modern radio access network together with traditional digital subscriber line (DSL) services, reusing the cabinet infrastructure already in place. Our results suggest that mobile networks with moderate capacity could be deployed over copper without disturbing legacy fixed-access technologies.

In this paper we utilize the basic architecture described in [4] to deploy LTE for small cells over residential unshielded copper loops. Our interest is to investigate the implications of 3GPP compliance on an implementation that down/up converts LTE signals to intermediate frequency (IF) over the copper loops, as illustrated in Fig. 10.1. Based on the requirements we present design guidelines for an RRH and estimates for how distant these systems could be deployed from the street cabinet.

10.2 SYSTEM ARCHITECTURE

We consider a distributed base station architecture as described in [4] where the cell processing is functionally split among three entities. Baseband processors perform digital signal processing on baseband LTE signals. In downlink direction the baseband signals are up-converted to IF (labeled in Fig. 10.1) at a remote radio unit (RRU) deployed in colocation with DSL equipment in street cabinets. After IF conversion, the LTE signals are transmitted over a copper pair (represented in Fig. 10.1) to an RRH, converted to the appropriate radio frequency (RF) and then sent to the user equipment (UE) over the air. In the uplink direction, the radio signal received at the RRH is down-converted to IF, transmitted to the RRU, and finally converted to baseband for receiver processing.

To coexist with VDSL2 and G.fast systems, the target IF band is placed between 21 MHz and 30 MHz, which restricts the available bandwidth for LTE

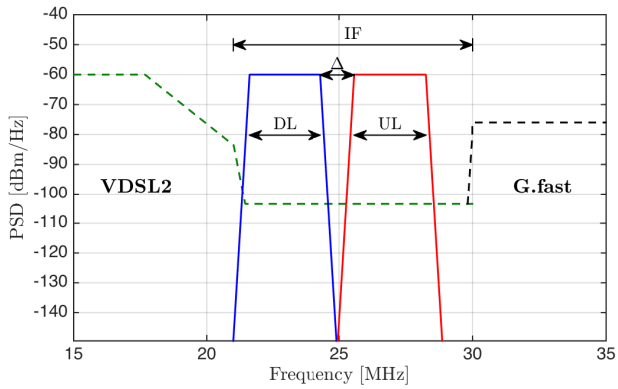

Figure 10.1: Bandplan adopted in this paper. The LTE signal is placed between VDSL2 and G.fast systems for coexistence. The dashed lines represent the limit PSD masks for the DSL systems. The frequencies between 17 MHz and 30 MHz are not used by VDSL2 17 MHz profiles or G.fast.

signals to be 3 MHz. The resulting bandplan is presented in Fig. 10.1, with the downlink LTE band placed between 21 MHz and 24 MHz, a gap-band of $\Delta = 0.95$ MHz, and the uplink signal extending to 28 MHz. As reported in [4], for a maximum transmit PSD of $S = -60$ dBm/Hz over the copper pair, the proposed system can be deployed up to 500 meters away from street cabinets.

In Fig. 10.2 we present a model for the RRH considered in this work. The upper and the lower signal branches, which contain the processing elements for the LTE downlink (DL) and the LTE uplink (UL) path, are connected to the twisted pair via a hybrid coupler. On the opposite side they connect to an RF front-end. The hybrid coupler used in the RRH is not perfect, exhibiting non-negligible trans-hybrid loss [5], denoted as L_{hybrid}. The leakage from uplink to downlink inside the RRH may cause in-band interference and/or out-of-band noise that need to be dealt with in order to avoid performance degradation.

Invoking the requirements imposed by 3GPP regulations and a typical indoor propagation scenario, feasible quantities for the overall in-band amplification G and out-of-band rejection L at the RRH can be derived for uplink and downlink, respectively. Here we perform a "black-box" study without suggesting a specific arrangement of amplifiers and filters. Superscripts [u] and [d] are used to distinguish between uplink and downlink, respectively.

The choice of in-band gains depends on the required transmit power over copper and air channels such that the necessary SNR is achieved. In order to avoid mutual interference and also coexist with other wireless systems that

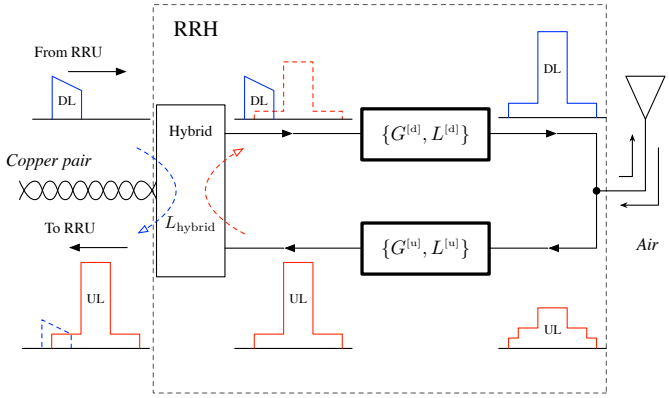

Figure 10.2: Model for the RRH. For each direction in-band gain and out-of-band rejection are the parameters. Leakage from uplink to downlink due to an imperfect hybrid is represented by the red dashed arrow.

operate on adjacent channels, out-of-band rejections are derived according to spectrum emission mask (SEM) and adjacent channel selectivity (ACS) in uplink direction and required adjacent channel leakage power ratio (ACLR) in downlink direction, respectively.

10.3 UPLINK PATH

10.3.1 IN-BAND SIGNAL AMPLIFICATION $G^{[U]}$

For the uplink direction, we start by estimating the receive power at the RRH antenna. Here we employ the indoor transmission path-loss model [6], which assumes that base station and UE are located in the same building. We calculate the air channel path-loss for a typical residential scenario as

$$L_{\text{air}}\,[\text{dB}] = 20\log_{10} f_c + \alpha \log_{10} r + L_f - 28, \tag{10.1}$$

for a carrier frequency f_c [MHz], a propagation distance r [m] and an indoor environment characterized by distance power loss coefficient α and floor penetration loss factor L_f [dB]. The path-loss L_{air} increases with the distance r between RRH antenna and UE.

For a 3 MHz LTE signal, the uplink peak bit-rate is $\widetilde{R}_{\text{u}} = 7.5$ Mbps. The receive SNR at the RRU required to support the peak rate after copper transmission is

$$\widetilde{\text{SNR}}^{[\text{u}]}\,[\text{dB}] = 10\log_{10}\left(2^{(\widetilde{R}_{\text{u}}/B_{\text{c}})-1}\right) + \Gamma, \tag{10.2}$$

where $B_c = 2.7\,\text{MHz}$ is the transmission bandwidth configuration [7] and $\Gamma = 9\,\text{dB}$ is reserved to cover implementation losses. Since the maximum output power of the UE is 23 dBm [8], the maximum receive power at the RRH antenna connector is given by $P^{[u]}_{\text{rx,ant}}\,[\text{dBm}] = 23 - L_{\text{air}}$. Considering thermal noise as the only noise source for the air channel transmission, we can derive the receive SNR at the RRH antenna connector for a certain L_{air}, denoted $\text{SNR}^{[u]}_{\text{air}}$. In this work, we assume that the uplink noise figure in the RRH is 0 dB. The uplink SNR before copper transmission then stays the same as $\text{SNR}^{[u]}_{\text{air}}$. To deliver $\widetilde{\text{SNR}}^{[u]}$ to the RRU, the related SNR required for copper transmission is calculated in linear scale as

$$\text{SNR}^{[u]}_{\text{Cu}} = \frac{\text{SNR}^{[u]}_{\text{air}} \cdot \widetilde{\text{SNR}}^{[u]}}{\text{SNR}^{[u]}_{\text{air}} - \widetilde{\text{SNR}}^{[u]}}. \tag{10.3}$$

For a given cable type, the channel attenuation L_{Cu} is a monotonically increasing function with respect to both frequency f and cable length d. Let $\mathcal{F}^{[u]}$ denote the IFs occupied by each uplink LTE subcarrier as shown in Fig. 10.1. To derive the in-band SNR, we use the sub-carrier that experiences the worst case attenuation as a reference. Given the cable noise PSD of $N = -150\,\text{dBm/Hz}$ and using Eq. (10.3) in dB-scale, the uplink transmit power over the copper should be

$$P^{[u]}_{\text{tx,Cu}}\,[\text{dBm}] \geq \text{SNR}^{[u]}_{\text{Cu}} + (N + 10\log_{10}B) + \max_{f \in \mathcal{F}^{[u]}} L_{\text{Cu}}(f, d). \tag{10.4}$$

Assuming a maximum transmit PSD over the copper as $S_{\max} = -60\,\text{dBm/Hz}$, one can also estimate the preliminary maximum distance over which such RRH could be deployed from the cabinet for $(P^{[u]}_{\text{tx,Cu}} - \log_{10}B) \leq S_{\max}$.

The necessary amplification in uplink direction can then be calculated as

$$G^{[u]}\,[\text{dB}] = P^{[u]}_{\text{tx,Cu}} - P^{[u]}_{\text{rx,ant}}. \tag{10.5}$$

Equivalently, the maximum deployable cable length d fulfilling Eq. (10.4) can be estimated given a certain available $G^{[u]}$.

In Fig. 10.3 we present the relationship between maximum cable length d (distance between cabinet and RRH deployment site) and the maximum path-loss that the system can endure while still providing the LTE uplink peak bit-rate. For our target deployment scenario, an indoor residential environment at 1.8 GHz, typical values for α and L_f in Eq. (10.1) are 28 and 10 dB respectively. Notice that to deploy long cables there will be a decrease in the maximum acceptable path-loss corresponding to the gaps between solid lines and the red dashed line in Fig. 10.3. We refer to this gap as ΔL_{air}. The ΔL_{air} varies

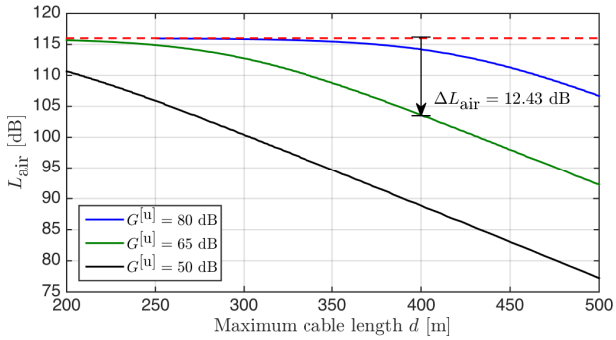

Figure 10.3: The three solid curves represent the relationship between deployment distance and the tolerable path-loss in the air for a fixed $G^{[u]}$. The red dashed line represents the initial maximum acceptable path-loss for the LTE uplink peak bit-rate. The ΔL_{air} increases with cable length as exemplified by the arrow around 400 meters.

for the same deployed cable length with different $G^{[u]}$ available. The cable attenuation used to obtain these curves is calculated using the BT-CAD55 model, commonly employed to estimate capacity in DSL system design [9].

10.3.2 OUT-OF-BAND REJECTION $L^{[U]}$

As sketched in the signal flow depicted in Fig. 10.2, after air channel transmission, the received signal at the RRH may contain, besides the signal of interest, out-of-band components $\text{OOB}_{\text{ant}}^{[u]}$ at the antenna connector. Passing through the amplifying element(s) at the RRH, those out-of-band components experience the same gain as the in-band uplink signal. Although this causes no trouble for the uplink transmission in itself, the out-of-band noise may lower the quality of the downlink signal due to the hybrid leakage. With less than 3 MHz gap-band between downlink and uplink in the copper channel, any neighboring interference captured by the RRH antenna will leak via the hybrid coupler and overlap with the signal in the downlink processing path.

To guarantee the quality of the in-band signal transmission in downlink direction, the error vector magnitude (EVM) of transmitted signals should be lower than the limits listed in Table 6.5.2-1 in [7]. EVM is defined as

$$\text{EVM} = \sqrt{\frac{1}{K}\frac{\|\mathbf{y}-\mathbf{x}\|_2^2}{P_0}} \cdot 100\%,$$

where $\mathbf{x}$ and $\mathbf{y}$ denote the constellation symbols at the RRU and RRH antenna connector respectively, K is the number of involved symbols, and P_0

is the average power of the modulation scheme used. This quantity can also be translated to an in-band SNR requirement in the downlink direction given by $\widetilde{\mathrm{SNR}}^{[\mathrm{d}]} \approx 1/\mathrm{EVM}^2$. Accordingly, the minimum $\widetilde{\mathrm{SNR}}^{[\mathrm{d}]}$ is around 15.14 dB for QPSK, 18.06 dB for 16-QAM, and 21.98 dB for 64-QAM. These parameters suggest that a general minimum value of $\widetilde{\mathrm{SNR}}^{[\mathrm{d}]} = 21.98\,\mathrm{dB}$ should be guaranteed.

Since it is difficult to mitigate the resulting in-band interference in the downlink path, we should suppress out-of-band emission already in the uplink processing to a level such that the downlink EVM requirement is not violated. Considering the trans-hybrid attenuation L_{hybrid}, the permissible uplink out-of-band emission at the copper connecting port is

$$\mathrm{OOB}_{\mathrm{Cu}}^{[\mathrm{u}]}\,[\mathrm{dBm}] = P_{\mathrm{rx,Cu}}^{[\mathrm{d}]} - \widetilde{\mathrm{SNR}}^{[\mathrm{d}]} + L_{\mathrm{hybrid}}. \tag{10.6}$$

Here $P_{\mathrm{rx,Cu}}^{[\mathrm{d}]}$ is the signal power reaching the RRH after transmission over the copper channel, *i.e.*,

$$P_{\mathrm{rx,Cu}}^{[\mathrm{d}]}\,[\mathrm{dBm}] = S - \max_{f \in \mathcal{F}^{[\mathrm{d}]}} L_{\mathrm{Cu}}(f) + \log_{10} B. \tag{10.7}$$

Eq. (10.6) implies a rejection requirement at the RRH given by

$$L^{[\mathrm{u}]}\,[\mathrm{dB}] = P_{\mathrm{tx,Cu}}^{[\mathrm{u}]} - \widetilde{\mathrm{SINR}}^{[\mathrm{u}]} - \mathrm{OOB}_{\mathrm{Cu}}^{[\mathrm{u}]}, \tag{10.8}$$

where $\widetilde{\mathrm{SINR}}^{[\mathrm{u}]}$ is the power ratio between the uplink in-band signal and the maximum out-of-band component that overlaps with the downlink in-band signal.

To properly illustrate the influence of specific 3GPP requirements for the uplink out-of-band rejection we differentiate between two situations:

RRH WITHOUT AN ALIEN SYSTEM NEARBY

3GPP imposes SEM and spurious emission limits for the UE transmitter [8], which restrict the out-of-band spectral emissions. Assuming that a UE transmits at the worst case PSD mask according to those requirements, the signal received at the RRH after amplification is represented by the red solid curve in Fig. 10.4. If no filtering is performed, the uplink signal of interest plus its out-of-band components leak via the hybrid resulting in in-band interference to the downlink signal. Since the gap-band reserved between uplink and downlink over copper transmission is small, the leakage imposes a requirement on $L^{[\mathrm{u}]}$ as indicated by the arrow in Fig. 10.4.

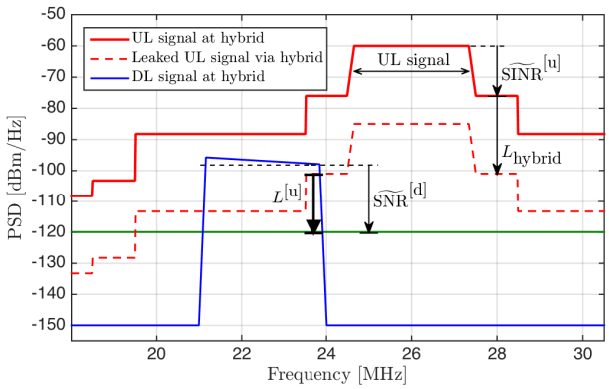

Figure 10.4: Leakage of uplink out-of-band emissions into the downlink signal. The red solid curve represents the received uplink signal after amplification at the RRH. The dashed curve represents the leakage PSD if no filtering is performed. The green solid curve represents the acceptable noise floor for downlink peak bit-rates. Calculated for 300 meters of BT-CAD55.

RRH WITH AN ALIEN SYSTEM NEARBY

3GPP also defines an ACS [7] metric in the uplink to coexist with other systems that operate in adjacent channels. It forces the base station receiver to be able to cope with high levels of interference from neighboring channels, which are within the receiver's operating band. This happens for example when a nearby terminal transmits with very high power to reach a distant macro-cell outside the building (*i.e.*, from another operator). The requirement suggests that an interference with a mean power of $\widetilde{P}_{\text{intf}} = 28\,\text{dBm}$ should be supported. When the interference from a nearby system is received and amplified it may impact downlink transmission as depicted in Fig. 10.5.

In Fig. 10.6 we present the relationship between the required out-of-band rejection $L^{[u]}$ and cable length d, with and without alien interference in adjacent channels, for a certain acceptable ΔL_{air}, assuming a trans-hybrid loss of $L_{\text{hybrid}} = 25\,\text{dB}$ [10]. In Fig. 10.6a, we consider the situation when the highest out-of-band emission below the SEM happens to partially overlap with the downlink in-band signal. Fig. 10.6b estimates the required $L^{[u]}$ in presence of the worst alien interference that ACS suggests.

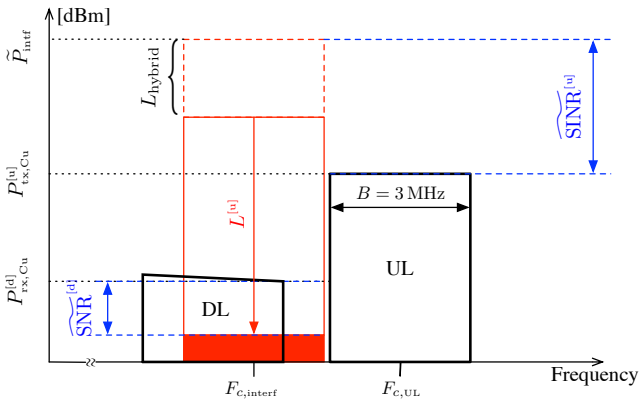

Figure 10.5: ACS requirement implications. A neighboring uplink transmission, represented as tall red rectangle must be suppressed to the solid red box in order to avoid drowning the downlink band. The uplink interference is captured at the RRH antenna and may overwhelm the downlink signal via the hybrid if no filtering is performed.

10.4 DOWNLINK PATH

For the downlink branch, the EVM requirement described in Section 10.3.2 also limits the preliminary maximum deployment distance of the proposed system. Given a fixed transmit PSD from the RRU as $S = -60\,\text{dBm/Hz}$ and a background noise PSD of $-150\,\text{dBm/Hz}$, the received SNR at the RRH decreases when using longer cables. At the largest deployment distance, the cable should deliver $\widetilde{\text{SNR}}^{[d]} = 21.98\,\text{dB}$ to the RRH in the downlink direction.

For a home base station with a single antenna, 3GPP stipulates a maximum transmit power $\widetilde{P}^{[d]}_{\text{tx,ant}} = 20\,\text{dBm}$ [7], which requires an in-band signal amplification of

$$G^{[d]}\,[\text{dB}] = \widetilde{P}^{[d]}_{\text{tx,ant}} - P^{[d]}_{\text{rx,Cu}}, \tag{10.9}$$

where $P^{[d]}_{\text{rx,Cu}}$ is the received power in downlink after copper transmission as calculated in Eq. (10.7).

Also in [7], 3GPP establishes that base stations should suppress adjacent channel signal leakage before passing the signal to the antenna. This requirement, known as ACLR, asks for either an adjacent channel leakage power of $-50\,\text{dBm/MHz}$ or a 45 dB attenuation compared to the in-band signal power. The less stringent number of the two is considered the limit. For our pro-

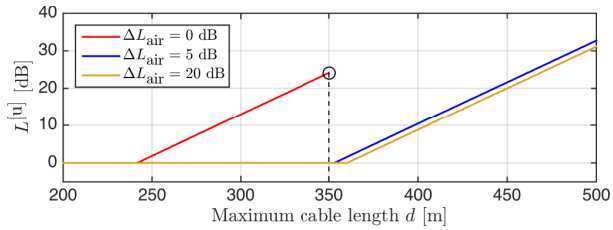

(a) Without alien system ($\widetilde{\mathrm{SINR}}^{[u]} = 16\,\mathrm{dB}$, $\widetilde{\mathrm{SNR}}^{[d]} = 21.98\,\mathrm{dB}$)

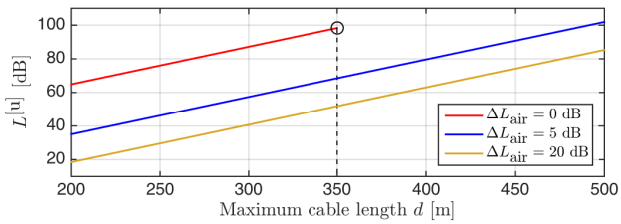

(b) With alien system ($\widetilde{P}_{\mathrm{intf}} = 28\,\mathrm{dBm}$, $\widetilde{\mathrm{SNR}}^{[d]} = 15.14\,\mathrm{dB}$)

Figure 10.6: Required uplink out-of-band rejection $L^{[u]}$ for different cable lengths. Each solid curve is calculated for an acceptable ΔL_{air}. The red curve is interrupted when the maximum transmit PSD is reached.

posed RRH, the ACLR requirement leads to a total leakage power limit over the neighboring channel of around $\widetilde{\mathrm{OOB}}_{\mathrm{ant}}^{[d]} = -25\,\mathrm{dBm}$.

If the uplink signal leaks into downlink transmission via the hybrid coupler, a big portion of the leakage can be transmitted to the antenna, disrupting neighboring bands. An example of this can be seen in Fig. 10.7, assuming the uplink out-of-band interference has been in good control. The effective leaked power from the uplink signal can be calculated as

$$\mathrm{OOB}_{\mathrm{Cu}}^{[d]}\,[\mathrm{dBm}] = P_{\mathrm{tx,Cu}}^{[u]} - L_{\mathrm{hybrid}},$$

To fulfill the ACLR requirement, the downlink out-of-band rejection must be

$$L^{[d]}\,[\mathrm{dB}] = \mathrm{OOB}_{\mathrm{Cu}}^{[d]} + G^{[d]} - \widetilde{\mathrm{OOB}}_{\mathrm{ant}}^{[d]}, \tag{10.10}$$

assuming that out-of-band interference at adjacent channels experiences the same amplification as the in-band signal.

As indicated in Eq. (10.7), the cable attenuation determines the amount of power received at the RRH. To obtain a flat transmit PSD at the antenna connector, each value of $P_{\mathrm{rx,Cu}}^{[d]}$ leads to a required $G^{[d]}$. This is illustrated in

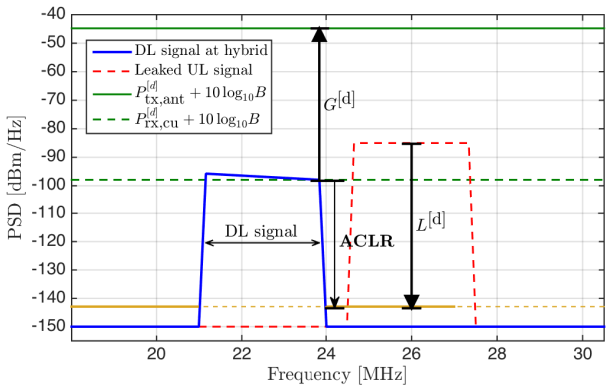

Figure 10.7: PSDs of 300 meters BT-CAD55 model in the downlink branch, after the hybrid coupler and before filtering. The signal of interest is the left lobe. The band to the right is the upstream signal coupled through the hybrid and should be suppressed to the ACLR level given in yellow.

Fig. 10.8a for different cable lengths. Also, the uplink signal is amplified before the hybrid, which in turn causes the increase of undesirable leakage through the hybrid. In order to fulfill the ACLR requirement, we must obey the downlink out-of-band rejection requirements depicted in Fig. 10.8b.

10.5 DESIGN IMPLICATIONS

By jointly considering the discussed 3GPP requirements and using the described methodology, one can obtain the desired values for total in-band gain and out-of-band rejection required at the RRH. As an example, we list three different designs in Table 10.1. The bold numbers in each row represent target values, which are prioritized and kept fixed.

For the first row, the acceptable ΔL_{air} is set to 0. This results in a deployment distance of around 350 meters, but very high $G^{[u]}$ and $L^{[u]}$. If alien systems are not a concern, the values in parenthesis should be considered for $L^{[u]}$. In the second row, we are aiming for a deployment distance of 400 meters with an acceptable ΔL_{air} of 5 dB. The requirements for $L^{[u]}$, $G^{[u]}$ and $L^{[d]}$ are relaxed due to the permissible ΔL_{air}, but the value for $G^{[d]}$ increases because of the increased cable length. In the last row, we start by fixing reasonable values for filtering and amplifying components, which limit the deployment reach to around 310 meters without increasing ΔL_{air} significantly.

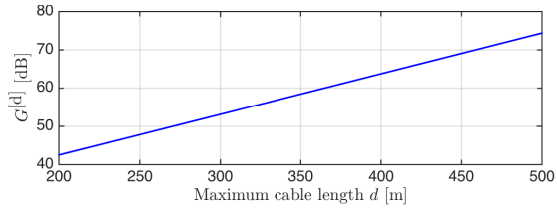

(a) On $G^{[d]}$

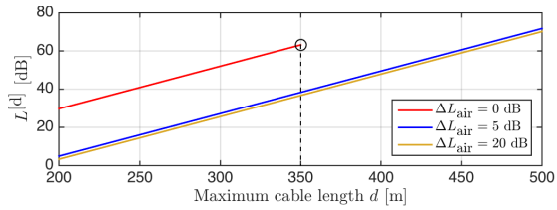

(b) On $L^{[d]}$

Figure 10.8: Influence of cable attenuation on RRH design parameters for downlink direction.

Table 10.1: Parameter values for different design objectives

ΔL_{air} [dB]	$L^{[u]}$ [dB]	$G^{[u]}$ [dB]	$L^{[d]}$ [dB]	$G^{[d]}$ [dB]	d [m]
0	98.30 (24.14)	80	63.16	58.45	350
5	79.62 (10.46)	74	49.48	63.76	**400**
5	**60**	**65**	**60**	**65**	310

10.6 CONCLUSION

Although our results in [4] suggest that modern OFDM-based radio systems could be deployed over copper up to 500 m, once 3GPP requirements are taken into consideration we observe absurdly stringent filtering and amplifying demands in Fig. 10.3, 10.6b and 10.8a, and also limited deployment distance if we do not compromise on radio reach. For as small a gap-band as assumed here, fulfilling 3GPP requirements practically prohibits fully analog implementations, such as the one presented in [1] and [4]. However, with digital filtering in the RRH and reasonable small cell assumptions, we conclude that LTE over copper lines is a technically viable concept. A myriad of small cells could be added to the mobile networks using the existing fixed infrastructure as a base without offending the technical foundations of currents standards and regulations.

References

[1] J. Gambini and U. Spagnolini, "Radio over telephone lines in femtocell systems," in *Proc. 2010 IEEE 21st International Symposium on Personal Indoor and Mobile Radio Communications (PIMRC)*, September 2010, pp. 1544–1549.

[2] ——, "Wireless over cable for femtocell systems," *IEEE Communications Magazine*, vol. 51, no. 5, pp. 178–185, May 2013.

[3] C. Lu, M. Berg, E. Trojer, P.-E. Eriksson, K. Laraqui, O. V. Tidblad, and H. Almeida, "Connecting the dots: small cells shape up for high-performance indoor radio," *Ericsson Review*, vol. 91, December 2014. [Online]. Available: http://goo.gl/YvdY5N

[4] Y. Huang, E. Medeiros, S. Höst, T. Magesacher, P.-E. Eriksson, C. Lu, P. Ödling, and P. O. Börjesson, "Enabling DSL and Radio on the Same Copper Pair," in *Proc. IEEE International Conference on Communications (ICC)*, 2015.

[5] T.-C. Lee and B. Razavi, "A 125-MHz mixed-signal echo canceller for Gigabit Ethernet on copper wire," *Solid-State Circuits, IEEE Journal of*, vol. 36, no. 3, pp. 366–373, March 2001.

[6] ITU-R, "Propagation data and prediction methods for the planning of indoor radiocommunication systems and radio local area networks in the frequency range 900 MHz to 100 GHz," International Telecommunication Union (ITU), Recommendation P.1238-7, February 2012. [Online]. Available: http://goo.gl/ZMIY7E

[7] 3GPP, "Evolved Universal Terrestrial Radio Access (E-UTRA); Base Station (BS) radio transmission and reception," 3rd Generation Partnership Project (3GPP), TS 36.104 V12.6.0, February 2015. [Online]. Available: http://goo.gl/SCislQ

[8] ——, "Evolved Universal Terrestrial Radio Access (E-UTRA); User Equipment (UE) radio transmission and reception," 3rd Generation Partnership Project (3GPP), TS 36.101 V12.5.0, November 2014. [Online]. Available: http://goo.gl/1PRPLV

[9] D. Acatauassu, S. Höst, C. Lu, M. Berg, A. Klautau, and P. O. Börjesson, "Simple and causal copper cable model suitable for g.fast frequencies," *IEEE Transactions on Communications*, vol. 62, no. 11, pp. 4040–4051, November 2014.

[10] Pulse, "Hybrid VDSL Transformer for Use with Infineon VDSL 2-Band, 4-Band and 10Base-S Chipsets," datasheet, 2003.

11

Crosstalk Mitigation for LTE-over-Copper in Downlink Direction

Eduardo Medeiros, Yezi Huang, Thomas Magesacher, Stefan Höst, Per-Erik Eriksson, Chenguang Lu, Per Ödling and Per Ola Börjesson

Abstract

Radio-over-copper is a niche idea that has potential to become a cornerstone in the deployment of dense 5G networks. We address one of the remaining hurdles and present an architecture for transparent crosstalk mitigation in LTE-over-copper systems. By taking advantage of reference symbols present in the downlink LTE signals we propose two methods for estimating the copper channel. System performance is evaluated using channel measurements and error vector magnitude calculations with promising results.[1]

[1]Published in *IEEE Communications Letters*, vol. 20, no. 7, July 2016.

11.1 INTRODUCTION

HIGH-capacity residential small cells represent an opportunity for operators to increase coverage and penetration of their mobile broadband services. With this paradigm, operators can deliver higher bitrates where most of the content consumption occurs. Additionally, cell site costs and energy consumption can be significantly reduced.

Residential small cells may become even more attractive with the impending introduction of Long Term Evolution (LTE) over unlicensed spectrum bands. Wireline operators, for example, could complement their product portfolio by reusing the copper plant to offer mobile subscriptions.

Early works such as [1] suggest a centralized radio-over-copper concept as an alternative to uncoordinated femtocell deployment. In [2], transparent remote radio heads (RRHs) and shared baseband processors are used to achieve full coordination between small cells and the macro layer, eliminating the main drawback of femtocells. This system in particular targets the enterprise market and takes advantage of shielded networking cables (category 6 and up) to deal with crosstalk and radio frequency interference (RFI).

In [3], we proposed an architecture for small cell deployment that reutilizes the copper access infrastructure (unshielded category 3 cables), while coexisting with legacy digital subscriber line (DSL) services. The proposed system converts baseband radio signals to an intermediate frequency, adequate to the low-pass copper channel and could be deployed in cabinets collocated, for instance, with VDSL2 modems.

In [4], we analyzed the implications of Third Generation Partnership Project (3GPP) compliance to the reach of an LTE-over-copper solution. The analysis indicated that a 3GPP compliant system could be built at a reasonable price point and deployed up to 350 meters away from the cabinet.

While papers [3] [4] have covered bandplanning, rate-reach simulations and filter design, they have not dealt with the main impairment present in copper networks: crosstalk. Solutions for mitigating crosstalk among synchronized transmitters have long been adopted in the DSL community, where these techniques are referred to as *vectoring*. In brief, vectoring stands for the joint processing of transmit or receive symbols in DSL systems. Works such as [5] [6] proposed efficient algorithms for achieving near-optimal crosstalk cancellation in vectored systems. The International Telecommunication Union (ITU) standardized interfaces for VDSL2 vectoring with the G.993.5 recommendation [7]. Vectoring is also part of the newer G.fast standard [8].

Ideally, the crosstalk problem we address here would be solved by implementing vectoring in the baseband unit (BBU) software, see the left part of Figure 1. However, proposing to change the BBU software to adapt to one particular fronthaul technology cannot be expected to be met with great en-

thusiasm as it complicates software architecture and maintenance. A solution needs to be implemented further out and kept transparent to the BBU.

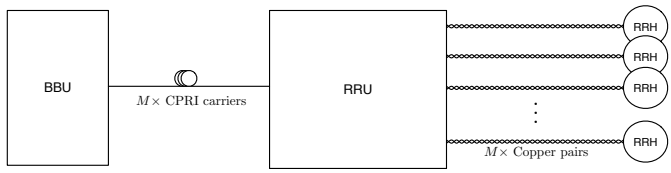

Figure 11.1: Centralized Baseband Architecture for an LTE-over-copper system.

The contribution of this letter is threefold: First, we present an architecture for channel estimation and precoding that mitigates the effects of crosstalk on downlink LTE-over-copper systems. Second, we propose two methods for estimating the copper channel using the reference signals already present in LTE signals. Last, we validate the concept using channel measurements and error vector magnitude (EVM) calculations.

11.2 FREQUENCY DOMAIN PRECODING AT RRU

Consider the centralized baseband system represented in Fig. 11.1. A single shared BBU processes LTE signals for M independent LTE small cells. The baseband signal samples are transmitted using an appropriate protocol (e.g. CPRI) to a remote radio unit (RRU). The radio unit is responsible for up and down-conversion to an intermediate frequency f_c suitable for transmission over copper. Each twisted pair is terminated by a remote radio head (RRH), responsible for filtering, conversion to RF frequencies and amplification before sending the LTE signal to an antenna.

Assume that all M independent cells are synchronized, that each cell transmits orthogonal frequency-division multiplexing (OFDM) symbols with N subcarriers and that these cells employ the same duplexing method.

Let $x_i^{(k,l)}$ represent the frequency domain contents of the resource element[2] with OFDM symbol l, subcarrier k and transmitter i. Dropping the symbol index and focusing the analysis on a single resource element, the following description applies. Let $\boldsymbol{x}^{(k)} = \left[x_1^{(k)}, \ldots, x_i^{(k)}, \ldots, x_M^{(k)}\right]^{\mathrm{T}} \in \mathbb{C}^M$ represent the transmitted symbol vector obtained by stacking the output of M synchronized cells at subcarrier k. At the output of the copper channel, the received

[2]The smallest time-frequency resource in an LTE grid.

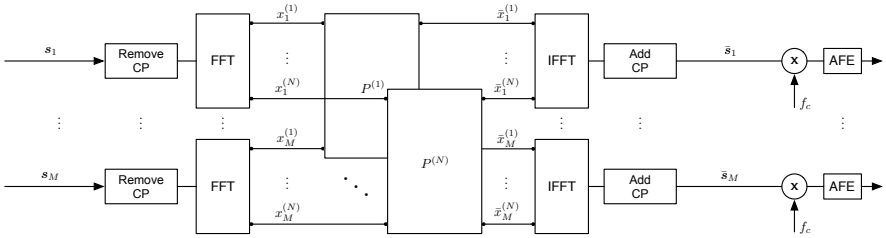

Figure 11.2: Proposed remote radio unit architecture. The samples for M independent LTE cells are present at the input, have their cyclic prefixes stripped, are brought to frequency domain and precoded, being transformed back to time domain before modulation and transmission over the twisted pairs.

frequency domain symbol vector $\boldsymbol{y}^{(k)} \in \mathbb{C}^M$ can be described as

$$\boldsymbol{y}^{(k)} = \boldsymbol{H}^{(k)}\boldsymbol{x}^{(k)} + \boldsymbol{z}^{(k)}, \tag{11.1}$$

where $\boldsymbol{H}^{(k)} \in \mathbb{C}^{M\times M}$ is the frequency domain channel matrix for subcarrier k and $\boldsymbol{z}^{(k)} \in \mathbb{C}^M$ represents an additive noise vector.

The signal received at RRH i and subcarrier k can then be expressed as

$$y_i^{(k)} = H_{i,i}^{(k)} x_i^{(k)} + \sum_{j\neq i} H_{i,j}^{(k)} x_j^{(k)} + z_i^{(k)}. \tag{11.2}$$

where $H_{i,i}^{(k)}$ represents the direct channel gain for pair i and $H_{i,j}^{(k)}, i \neq j$ represents the far-end crosstalk (FEXT) from RRU transmitter j to RRH i.

If the off-diagonal elements of the channel matrix $\boldsymbol{H}^{(k)}$ are non-negligible, as is typical for unshielded telephony-grade cables, the crosstalk contribution will significantly distort the LTE signal before it is up-converted and transmitted via the RRH radio frequency (RF) front-end, possibly leading to unacceptable EVM increase.

In this letter we propose to modify the design of the remote radio unit in order to eliminate crosstalk via frequency domain precoding. The proposed arrangement, depicted in Fig. 11.2, has the benefit of being transparent to the baseband processor, avoiding the necessity of making the radio access equipment aware of the fronthaul medium.

Let $\boldsymbol{s}_i = \left[s_i^{(N-L+1)}, \ldots, s_i^{(N)}, s_i^{(1)}, \ldots, s_i^{(N)}\right]^{\mathrm{T}} \in \mathbb{C}^{(L+N)}$ be a vector constituted by $L+N$ samples of the i^{th} RRU input signal, covering exactly one

OFDM symbol, including its cyclic prefix of size L. The vector

$$\tilde{\boldsymbol{x}}_i = \left[x_i^{(1)}, \ldots, x_i^{(k)}, \ldots, x_i^{(N)}\right]^{\mathrm{T}} \in \mathbb{C}^N$$

containing the transmit symbols for every subcarrier used by transmitter i can be obtained by cyclic prefix removal followed by a discrete Fourier transform (DFT). A matrix representation of such operation is given by

$$\tilde{\boldsymbol{x}}_i = \mathcal{F}\boldsymbol{R}\boldsymbol{s}_i \tag{11.3}$$

where $\boldsymbol{R}$ is the cyclic prefix removal matrix and $\mathcal{F}$ is a DFT matrix of size N.

Next, the transmit symbols for each user on subcarrier k can be collected in a vector $\boldsymbol{x}^{(k)} = \left[x_1^{(k)}, \ldots, x_i^{(k)}, \ldots, x_M^{(k)}\right]^{\mathrm{T}}$ and used as input to the precoder. The precoded symbol vector $\bar{\boldsymbol{x}}_k$ is obtained via the matrix multiplication $\bar{\boldsymbol{x}}^{(k)} = \boldsymbol{P}^{(k)}\boldsymbol{x}^{(k)}$, where the precoding matrix $\boldsymbol{P}^{(k)} \in \mathbb{C}^{M\times M}$ is chosen appropriately. Good candidate precoder designs are presented in [6], with the diagonalizing precoder shown to be near optimal.

After precoding an inverse DFT is performed on each sequence

$$\bar{\boldsymbol{x}}_i = \left[\bar{x}_i^{(1)}, \ldots, \bar{x}_i^{(k)}, \ldots, \bar{x}_i^{(N)}\right]^{\mathrm{T}} \in \mathbb{C}^N,$$

followed by cyclic prefix insertion. The resulting precoded time domain samples $\bar{\mathbf{s}}_i$ go through digital to analog conversion and are shifted to the carrier frequency f_c before copper transmission.

For good precoder performance it is of fundamental importance that good estimates of the channel matrices $\boldsymbol{H}^{(k)}$ are available. In the next section we describe practical methods for obtaining these estimates.

11.3 CHANNEL ESTIMATION METHODS

The LTE physical layer [9] specifies a number of reference signals used in the communication between base stations and UE to achieve different objectives such as cell identification, cell selection and channel estimation.

We propose to utilize LTE's downlink cell-specific reference signals (CRS) to estimate the copper channel. CRS are well suited for the task at hand since they are distributed along the entire bandwidth of the cell and are independent of cell load and scheduling algorithms.

For each slot in a subframe, CRS are present in the first and fifth symbols. The values of CRS symbols are obtained by QPSK modulating a pseudo-random Gold sequence [9]. By knowing the physical layer cell identity, N_{ID}^{cell}, the slot number within a radio frame n_s and the symbol number l one can perfectly reconstruct each of the CRS sequences.

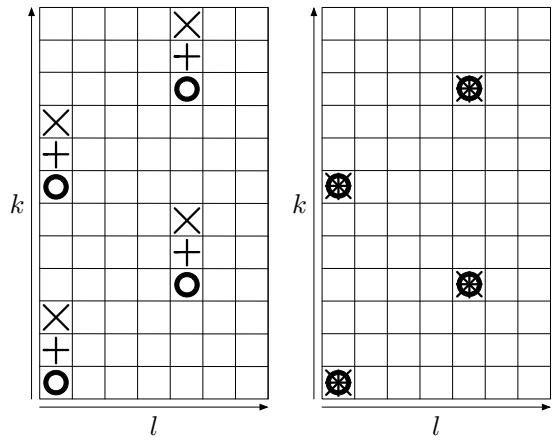

Figure 11.3: Depiction of a stack of LTE resource grids for three cells. On the left, the first slot of a resource block is represented, and the cells are assigned the cell identities 0, 1 and 2. On the right, with the proposed cell assignment scheme, one notices that the cell reference symbol positions coincide in time and frequency. The cell identities for the second diagram are 0, 6 and 12.

A frequency shift derived from the N_{ID}^{cell} parameter also controls which subcarriers will be loaded with pilot symbols. This cell-specific frequency shift, defined as $v_{shift} = N_{ID}^{cell} \bmod 6$, was introduced to improve pilot performance in environments with high interference.

The effect of different N_{ID}^{cell} assignments on pilot positioning is exemplified in the left diagram of Fig. 11.3. The pilot symbols for three different cells are drawn over the same resource grid. Each cell's pilots are represented by the symbols $\circ, +, \times$ and correspond to the choice of cell identity $N_{ID}^{cell} = 0, 1, 2$ respectively. For this sequential cell identity assignment, the pilot symbols clearly do not overlap.

Taking advantage of the cell-specific frequency shift, we propose that instead of using an arbitrary cell identity assignment, the N_{ID}^{cell} values should be selected according to the following sequence

$$\begin{aligned} &N_{ID}^{cell}(1) \in \{0, 1, \ldots, 503\}, \\ &N_{ID}^{cell}(i) = \left(N_{ID}^{cell}(i-1) + 6\right) \bmod 504,\ i \in \{2, \ldots, M\}. \end{aligned} \tag{11.4}$$

When the N_{ID}^{cell} parameters are set according to Eq. 11.4, pilots for each cell are assigned to the same resource elements. This is represented in the right diagram of Fig. 11.3. Based on this pilot alignment we propose two chan-

nel estimation architectures, that differ in the amount of feedback necessary between RRH and RRU.

11.3.1 FEEDBACK-BASED ESTIMATOR

For the following discussion, it is assumed that there exists a control channel between the RRU and each RRH. It is also assumed that each RRH is capable of synchronizing to its LTE signal, extract the received CRS symbols and feed them back to the RRU. We also assume that the copper channel is constant over many symbols, changing slowly due, for example, to temperature variations [10]. The formulations presented next are valid for subcarriers in which pilot symbols are transmitted.

Let W, $W \geq M$, represent the number of pilot symbols in an observation window. Let r denote the pilot symbol number within an observation window. Define $\boldsymbol{\eta} \in \mathbb{C}^{WM}$ and $\boldsymbol{X} \in \mathbb{C}^{WM \times M^2}$ as

$$\boldsymbol{\eta} = \begin{bmatrix} \boldsymbol{z}^{(k,r)} \\ \boldsymbol{z}^{(k,r-1)} \\ \vdots \\ \boldsymbol{z}^{(k,r-W+1)} \end{bmatrix}, \boldsymbol{X} = \begin{bmatrix} \left(\boldsymbol{x}^{(k,r)}\right)^{\mathrm{T}} \otimes \boldsymbol{I}_M \\ \left(\boldsymbol{x}^{(k,r-1)}\right)^{\mathrm{T}} \otimes \boldsymbol{I}_M \\ \vdots \\ \left(\boldsymbol{x}^{(k,r-W+1)}\right)^{\mathrm{T}} \otimes \boldsymbol{I}_M \end{bmatrix},$$

where $\otimes$ is the Kronecker product and $\boldsymbol{I}_M$ is the identity matrix of size M.

Let $\boldsymbol{h} \in \mathbb{C}^{M^2}$ be a vector obtained by stacking the columns of $\boldsymbol{H}^{(k)}$. The last W received symbol vectors can then be described as

$$\gamma = \begin{bmatrix} \boldsymbol{y}^{(k,r)} \\ \boldsymbol{y}^{(k,r-1)} \\ \vdots \\ \boldsymbol{y}^{(k,r-W+1)} \end{bmatrix} = \boldsymbol{X}\boldsymbol{h} + \boldsymbol{\eta}. \tag{11.5}$$

Taking advantage of (11.5), one can obtain an estimate of $\boldsymbol{h}$ by using a Moore-Penrose pseudoinverse

$$\hat{\boldsymbol{h}} = (\boldsymbol{X}^{\mathrm{H}}\boldsymbol{X})^{-1}\boldsymbol{X}^{\mathrm{H}}\gamma. \tag{11.6}$$

Re-stacking the elements of $\hat{\boldsymbol{h}}$ column-wise leads to the desired channel matrix estimate $\hat{\boldsymbol{H}}^{(k)}$.

11.3.2 RRH CHANNEL ESTIMATOR

An alternative approach is to estimate a single row of the copper channel matrix $\boldsymbol{H}^{(k)}$ at each RRH, feeding back the estimation results instead of the

received symbols. This estimation procedure relies on the fact that transmit pilot symbol vectors $\boldsymbol{x}^{(k)}$ can be reconstructed at each receiver as long as they are aware of the N_{ID}^{cell} values used in the system.

Let W represent the number of symbols in an observation window such that $W \geq M$. Rewrite (11.2) as

$$y_i^{(k)} = \underline{\boldsymbol{h}}\boldsymbol{x}^{(k)} + z_i^{(k)}, \tag{11.7}$$

where $\underline{\boldsymbol{h}} = \left[H_{i,1}^{(k)}, \ldots, H_{i,i}^{(k)}, \ldots, H_{i,M}^{(k)}\right]$ is the vector corresponding to the i^{th} row of channel matrix $\boldsymbol{H}^{(k)}$. Next, define $\underline{\boldsymbol{X}} \in \mathbb{C}^{W \times M}$ and $\underline{\boldsymbol{\eta}} \in \mathbb{C}^{W}$ as

$$\underline{\boldsymbol{X}} = \begin{bmatrix} \left(\boldsymbol{x}^{(k,r)}\right)^{\mathrm{T}} \\ \left(\boldsymbol{x}^{(k,r-1)}\right)^{\mathrm{T}} \\ \vdots \\ \left(\boldsymbol{x}^{(k,r-W+1)}\right)^{\mathrm{T}} \end{bmatrix}, \underline{\boldsymbol{\eta}} = \begin{bmatrix} z_i^{(k,r)} \\ z_i^{(k,r-1)} \\ \vdots \\ z_i^{(k,r-W+1)} \end{bmatrix}.$$

The last W symbols received by RRH i can be written as

$$\underline{\boldsymbol{\gamma}} = \begin{bmatrix} y_i^{(k,r)} \\ y_i^{(k,r-1)} \\ \vdots \\ y_i^{(k,r-W+1)} \end{bmatrix} = \underline{\boldsymbol{X}}\underline{\boldsymbol{h}}^{\mathrm{T}} + \underline{\boldsymbol{\eta}}. \tag{11.8}$$

The Moore-Penrose pseudoinverse then leads to the estimate

$$\hat{\underline{\boldsymbol{h}}}^{\mathrm{T}} = (\underline{\boldsymbol{X}}^{\mathrm{H}}\underline{\boldsymbol{X}})^{-1}\underline{\boldsymbol{X}}^{\mathrm{H}}\underline{\boldsymbol{\gamma}}. \tag{11.9}$$

11.4 CROSSTALK MITIGATION PERFORMANCE

In order to assess the performance of the proposed RRU architecture and channel estimation methods we have executed time domain simulations. Initially, the Vienna LTE link level simulator [11] was used to generate downlink LTE radio frames. Each cell was configured to use a single antenna port, and its N_{ID}^{cell} number was assigned according to (11.4).

We have measured direct and FEXT transfer functions for six pairs in copper cables [12] with different lengths. The frequency range of interest is from 21 to 24 MHz, in accordance to the system proposed in [3] [4].

The simulations were divided in two stages. At first, for each pilot subcarrier, a channel matrix estimate $\hat{\boldsymbol{H}}$ is obtained using the methods proposed in

the previous section. For subcarriers not loaded with pilot symbols, channel estimates were obtained via linear interpolation. Next, each estimated channel matrix $\hat{\boldsymbol{H}}$ was used to calculate a diagonalizing precoder

$$\boldsymbol{P} = (1/u)\,\hat{\boldsymbol{H}}^{-1}\mathrm{diag}\{\hat{H}_{1,1},\ldots,\hat{H}_{M,M}\},$$

where $\mathrm{diag}\{\hat{H}_{1,1},\ldots,\hat{H}_{M,M}\}$ represents a diagonal matrix with elements $\hat{H}_{1,1}$, $\ldots,\hat{H}_{M,M}$ along its main diagonal. The normalization factor u is chosen to guarantee that the precoding operation does not lead to increases in transmit power [6]. These precoders were then used in simulations against the measured channels $\boldsymbol{H}$.

To quantify performance we calculate EVM as specified in [13]. 3GPP specifies limit EVM values for each of the constellations used for LTE's physical downlink shared channel (PDSCH). The limits are 17.5%, 12.5%, 8% and 3.5% for QPSK, 16-QAM, 64-QAM and 256-QAM respectively.

For each loop length we have varied the additive noise power spectrum density (PSD), calculating EVM before the RF front-end at the RRH. The simulation results for the worst performing cell are gathered in Fig. 11.4.

The performance for a baseline system, deployed over a 100 meters of cable without crosstalk cancellation, is represented in Fig. 11.4 by a dashed blue line with pentagram markers. The resulting EVM would limit the system to using QPSK modulation. For longer cables without crosstalk cancellation, the EVM curves exceed the scale of the plot and 3GPP compliance is infeasible.

As a reference, single user bounds are depicted as dotted lines for all cable lengths. These represent the EVM when the cell in question is the only active transmitter.

The solid lines represent the performance with diagonalizing precoders and approach the single user bounds for all cable lengths. The channel estimates used to design the precoders were obtained using the feedback-based estimator (Sec. 11.3.1) with $W = 20$, corresponding to the number of pilot symbols observed in one LTE frame. Results for the RRH estimator (Sec. 11.3.2) were equivalent and therefore omitted.

The gap between EVM limits (red dotted lines) and a certain curve indicate the margin left for implementation losses. As an example, consider that one would design an LTE-over-copper system for deployment over 300 meters of copper, subject to a background noise level of -140 dBm/Hz. In order to support 256-QAM implementation losses caused, for example, by imperfections in the RF front-end would be limited to 3.5%.

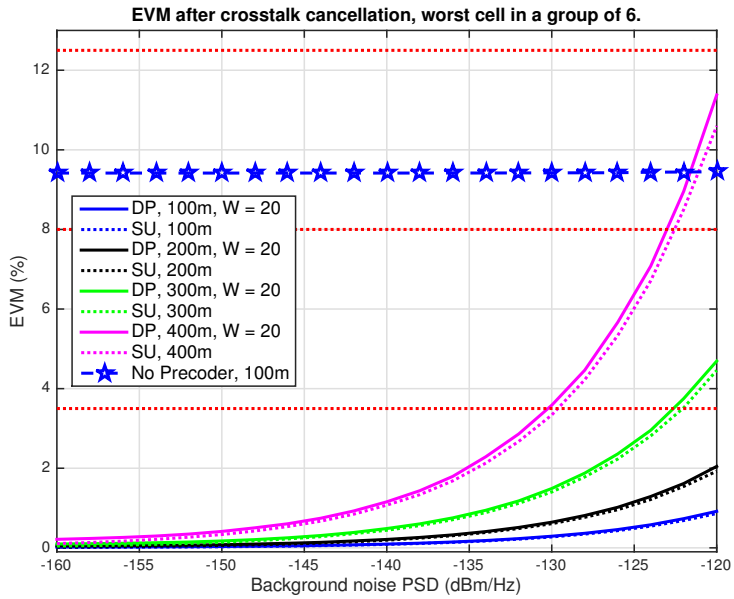

Figure 11.4: EVM performance for the worst cell in a group of six LTE-over-copper systems, deployed over different cable lengths. DP represents the curves obtained with a diagonalizing precoder, while SU represents single user bounds.

11.5 CONCLUSION

We have presented an architecture for crosstalk mitigation in LTE-over-copper systems. It is transparent to baseband processors and can be implemented in a radio unit, where up and down-conversion are performed. Two channel estimation methods that take advantage of LTE's downlink reference signals were also presented.

References

[1] J. Gambini and U. Spagnolini, "Wireless over cable for femtocell systems," *IEEE Communications Magazine*, vol. 51, no. 5, pp. 178–185, May 2013.

[2] C. Lu, M. Berg, E. Trojer, P.-E. Eriksson, K. Laraqui, O. V. Tidblad, and H. Almeida, "Connecting the dots: small cells shape up for high-performance indoor radio," *Ericsson Review*, vol. 91, December 2014. [Online]. Available: http://goo.gl/YvdY5N

[3] Y. Huang, E. Medeiros, S. Höst, T. Magesacher, P.-E. Eriksson, C. Lu, P. Ödling, and P. O. Börjesson, "Enabling DSL and Radio on the Same Copper Pair," in *Proc. IEEE International Conference on Communications (ICC)*, 2015.

[4] ——, "LTE Over Copper - Potential and Limitations," in *Proc. 2015 IEEE 26st International Symposium on Personal Indoor and Mobile Radio Communications (PIMRC)*, 2015.

[5] G. Ginis and J. Cioffi, "Vectored transmission for digital subscriber line systems," *IEEE Journal on Selected Areas in Communications*, vol. 20, no. 5, pp. 1085–1104, 2002.

[6] R. Cendrillon, G. Ginis, E. Van den Bogaert, and M. Moonen, "A near-optimal linear crosstalk precoder for downstream VDSL," *IEEE Transactions on Communications*, vol. 55, no. 5, pp. 860–863, 2007.

[7] *Self-FEXT Cancellation (Vectoring) for Use with VDSL2 Transceivers*, ITU Recommendation, Sep. 2010.

[8] *Fast Access to Subscriber Terminals (G.fast) - Physical Layer Specification*, ITU Recommendation, Dec. 2014.

[9] 3GPP, "LTE; Evolved Universal Terrestrial Radio Access (E-UTRA); Physical channels and modulation," 3rd Generation Partnership Project (3GPP), TS 36.211 V12.7.0, October 2015. [Online]. Available: http://goo.gl/HV0T8T

[10] Alcatel-Lucent Bell, "G.vdsl: On the tracking speed required for changing crosstalk channels," ITU-T SG15 Contribution, May 2007. [Online]. Available: https://www.itu.int/md/T05-SG15-C-0540

[11] S. Schwarz, J. Ikuno, M. Simko, M. Taranetz, Q. Wang, and M. Rupp, "Pushing the limits of LTE: A survey on research enhancing the standard," *IEEE Access*, vol. 1, pp. 51–62, 2013.

[12] Ericsson AB, *Access Network Pair cable, TEL 312*, 2010. [Online]. Available: http://goo.gl/4RdCXc

[13] 3GPP, "Evolved Universal Terrestrial Radio Access (E-UTRA); Base Station (BS) radio transmission and reception," 3rd Generation Partnership Project (3GPP), TS 36.104 V12.8.0, July 2015. [Online]. Available: http://goo.gl/kL3pa8

12

Methods and Nodes of a Wireless Communication Network for Mitigating Crosstalk in a Base Station System

Eduardo Medeiros, Per-Erik Eriksson,
Yezi Huang and Chenguang Lu

Abstract

Disclosed is a method for mitigating crosstalk performed by a network node of a wireless communication network operable in a base station system of the wireless communication network, the base station system comprising an intermediate radio unit, IRU, a baseband unit, BBU, connected to the IRU and a plurality of radio heads, RHs, connected to the IRU via a plurality of metallic conductors. The method comprises receiving from a first of the plurality of RHs, a measure of an error of one or more symbols of a signal received by the first RH from the IRU over a first of the plurality of metallic conductors, the measure of the error being detected by the first RH, the signal being destined to a user equipment, UE, wirelessly connected to the first RH. The method further comprises determining precoding coefficients for a precoder according to the received error measure, and triggering applying the determined precoding coefficients when sending further signals to the first RH over the first of the plurality of metallic conductors, the further signals being destined to UEs wirelessly connected to the first RH.

12.1 TECHNICAL FIELD

The present disclosure relates generally to methods, nodes and computer programs of a wireless communication network for mitigating crosstalk in a base station system. More specifically, the disclosure relates to a base station system comprising a baseband unit connected to an intermediate radio unit which in turn is connected to a plurality of radio heads via a plurality of metallic conductors, and the methods, nodes and computer programs are for mitigating crosstalk over the metallic conductors in the base station system.

12.2 BACKGROUND

Mass-deployment of small cells is a candidate solution for solving the ever-increasing bandwidth demands on wireless communication networks. By employing coordination among macro cells and small cells, such as micro, pico and femto cells, operators can provide good coverage and a high quality mobile broadband experience to pieces of UEs, which camp on the network.

A recent enabler for solving the increasing bandwidth demands is a system called radio dot system (RDS). The RDS enables operators to utilize local area network (LAN) cables like CAT6/7 for indoor radio deployments. This system improves over older distributed antenna systems by providing streamlined installation procedures, low cost and energy efficiency. The RDS is a distributed base station system wherein the base station functionality is separated in different nodes called a baseband unit (BBU), in which signal treatment in the baseband frequency area is performed, an intermediate radio unit (IRU), which is arranged to receive (in the downlink direction) the baseband signals from the BBU, convert them to an intermediate frequency and distribute the signals to a destined radio head (RH), (also called the radio dot) of a plurality of RHs connected via dedicated cables to the IRU. The IRU then up-converts the received intermediate frequency signal to a radio frequency for radio transmission from an antenna of the RH towards UEs being in radio connection with the RH. As a further application of the RDS, there is a new initiative extending RDS into residential domain reusing existing telephony twisted-pair cable infrastructure between the IRU and the RHs, which are also used by today's DSL. The basic idea is to transfer radio signals in lower frequency at DSL spectrum range, for example below 200 MHz.

However, the twisted-pairs in the same cable are subjected to crosstalk. The crosstalk can reduce the SNR significantly. This will result in reduced bandwidth and reach of the residential RDS. Crosstalk cancellation/mitigation is needed to increase the performance.

12.3 SUMMARY

It is an object of the invention to address at least some of the problems and issues outlined above. It is another object to reduce the influence of crosstalk between cables of a distributed base station system in a wireless communication system. It is possible to achieve these objects and others by using a method and an apparatus as defined in the attached independent claims.

According to one aspect, a method is provided for mitigating crosstalk performed by a network node of a wireless communication network operable in a base station system of the wireless communication network. The base station system comprises an IRU, a BBU connected to the IRU, and a plurality of RHs, connected to the IRU via a plurality of metallic conductors. The method comprises receiving from a first of the plurality of RHs, a measure of an error of one or more symbols of a signal received by the first RH from the IRU over a first of the plurality of metallic conductors, the measure of the error being detected by the first RH, the signal being destined to a UE wirelessly connected to the first RH. The method further comprises determining precoding coefficients for a precoder according to the received error measure, and triggering applying the determined precoding coefficients when sending further signals to the first RH over the first of the plurality of metallic conductors, the further signals being destined to UEs wirelessly connected to the first RH.

According to another aspect, a method is provided performed by a first RH operable in a base station system of a wireless communication network, for mitigating crosstalk. The base station system comprises an IRU, a BBU connected to the IRU, and a plurality of RHs including the first RH, the plurality of RHs being connected to the IRU via a plurality of metallic conductors. The method comprises receiving, from the IRU over a first of the plurality of metallic conductors, a signal destined to a UE wirelessly connected to the first RH, the signal comprising one or more symbols. The method further comprises detecting, from the received one or more symbol, a measure of an error of the one or more symbol and sending, to the IRU, the measure of the one or more symbol error, for further determining of precoding coefficients for a pre-coder of the IRU based on the received measure of symbol error.

According to another aspect, a network node is provided, operable in a wireless communication network and configured to mitigate crosstalk of a base station system. The base station system comprises an IRU, a BBU connected to the IRU, and a plurality of RHs connected to the IRU via a plurality of metallic conductors. The network node comprises a processor and a memory. The memory contains instructions executable by said processor, whereby the network node is operative for receiving from a first of the plurality of RHs, a measure of an error of one or more symbols of a signal received by the first RH from the IRU over a first of the plurality of metallic conductors, the

measure of the error being detected by the first RH, the signal being destined to a UE, wirelessly connected to the first RH, determining precoding coefficients for a precoder according to the received error measure, and triggering applying the determined precoding coefficients when sending further signals to the first RH over the first of the plurality of metallic conductors, the further signals being destined to UEs wirelessly connected to the first RH.

According to another aspect, a first RH is provided, operable in a base station system of a wireless communication network and configured to contribute in mitigating crosstalk. The base station system comprises an IRU, a BBU connected to the IRU, and a plurality of RHs including the first RH, the plurality of RHs being connected to the IRU via a plurality of metallic conductors. The first RH comprises a processor and a memory. The memory contains instructions executable by said processor, whereby the first RH is operative for receiving, from the IRU over a first of the plurality of metallic conductors, a signal destined to a UE wirelessly connected to the first RH, the signal comprising one or more symbols, detecting, from the received one or more symbol, a measure of an error of the one or more symbol, and sending, to the IRU, the measure of the one or more symbol error, for further updating of precoding coefficients for a precoder based on the received measure of symbol error.

According to other aspects, computer programs and carriers are also provided, the details of which will be described in the claims and the detailed description.

Further possible features and benefits of this solution will become apparent from the detailed description below.

12.4 BRIEF DESCRIPTION OF DRAWINGS

The solution will now be described in more detail by means of exemplary embodiments and with reference to the accompanying drawings, in which:

- Fig. 12.1 is a schematic block diagram of a base station system in which the present invention may be used.
- Fig. 12.2 is a schematic view of an exemplary cellular communication network to which coverage is provided by the base station system.
- Fig. 12.3 is a flow chart illustrating a method performed by a network node, according to possible embodiments.
- Fig. 12.4 is a flow chart illustrating a method performed by an RH, according to possible embodiments.
- Fig. 12.5 is a schematic block diagram of a RH according to a possible embodiment.

- Fig. 12.6 is a schematic block diagram of an IRU according to a possible embodiment.
- Fig. 12.7 is a schematic block diagram of a digital signal processor (DSP) of an RH according to a possible embodiment.
- Figs 12.8a and 12.8b are tables illustrating cell-specific reference signal (CRS) patterns for two antennas.
- Fig. 12.9 is a table illustrating cell-ID assignment for crosstalk channel estimation.
- Figs. 12.10-12.11 are block diagrams illustrating a network node in more detail, according to further possible embodiments.
- Figs. 12.12-12.13 are block diagrams illustrating a radio head in more detail, according to further possible embodiments.

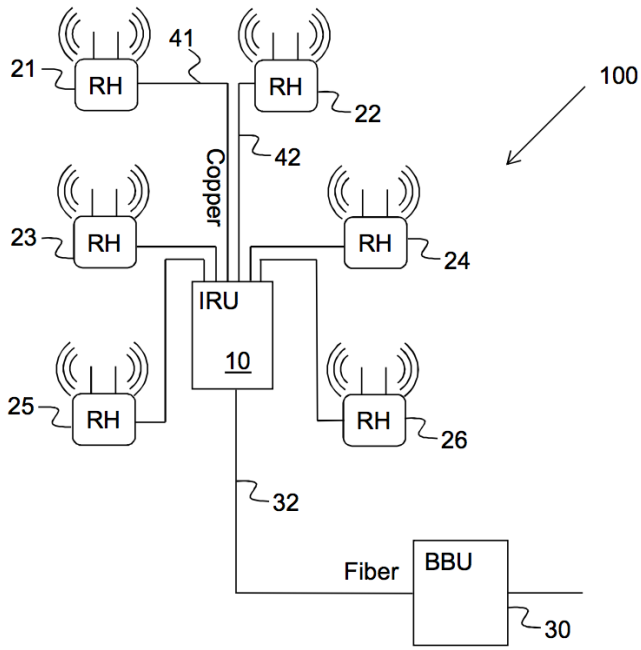

Figure 12.1

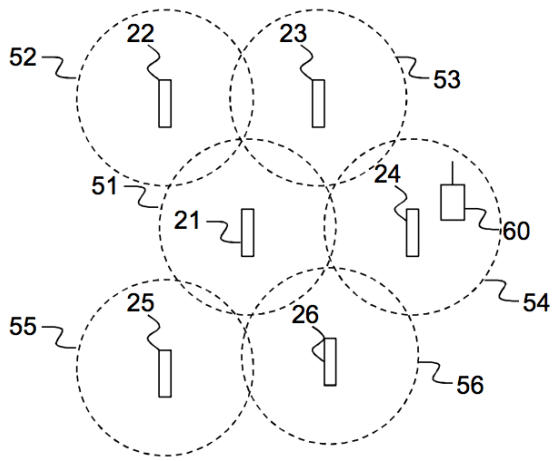

Figure 12.2

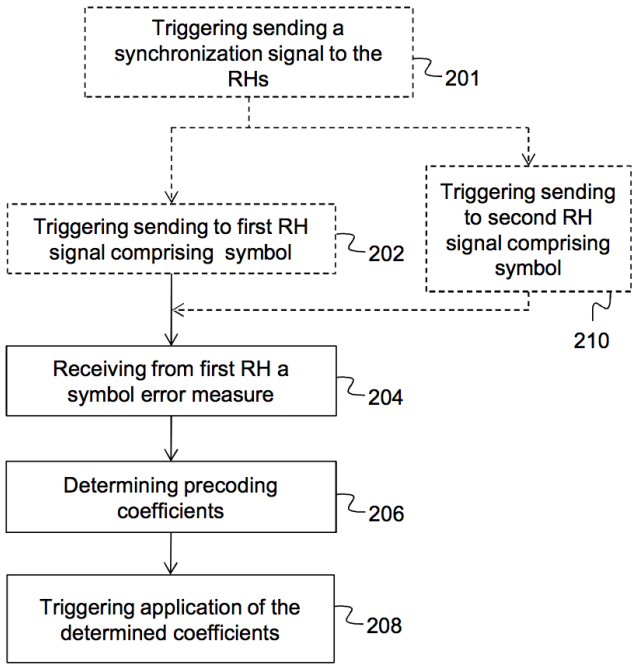

Figure 12.3

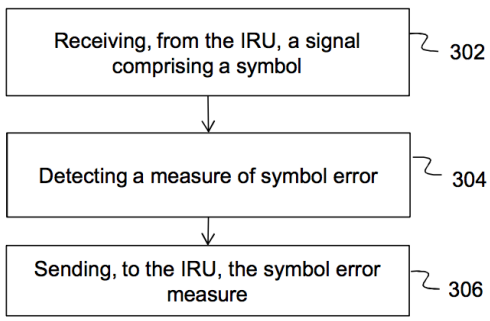

Figure 12.4

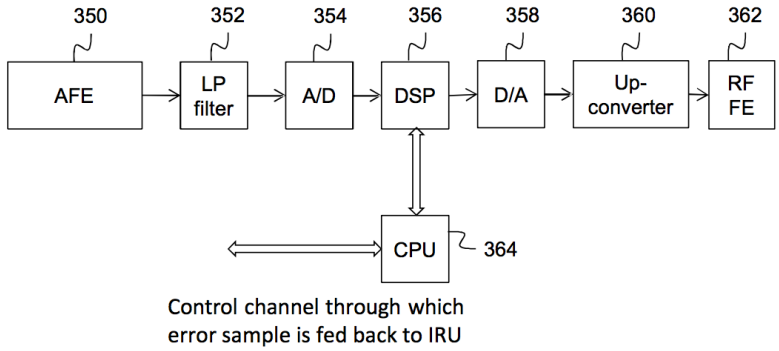

Figure 12.5

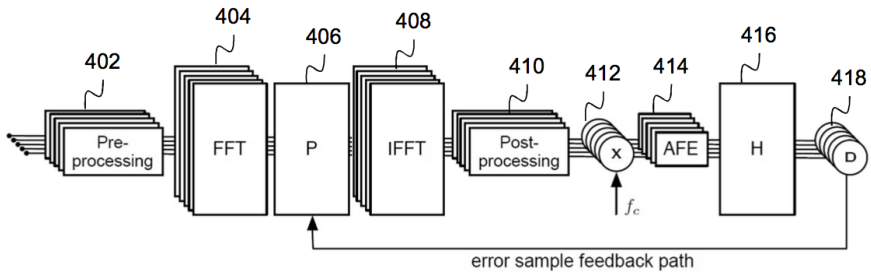

Figure 12.6

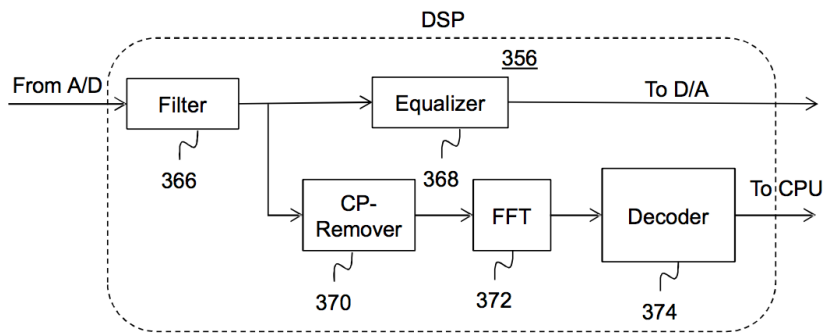

Figure 12.7

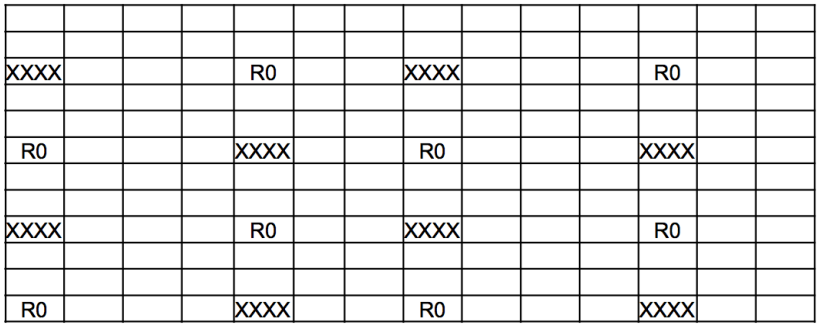

(a)

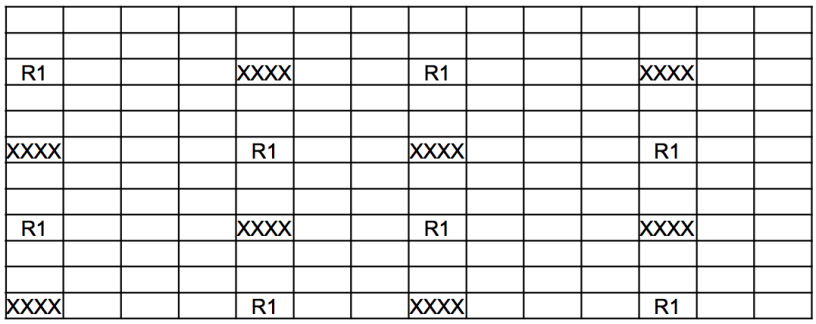

(b)

Figure 12.8

SYMB1	SYMB2	SYMB3	SYMB4	SYMB5	SYMB6	SYMB7
				0,6,12,18		
0,6,12,18						
				0,6,12,18		
0,6,12,18						

Figure 12.9

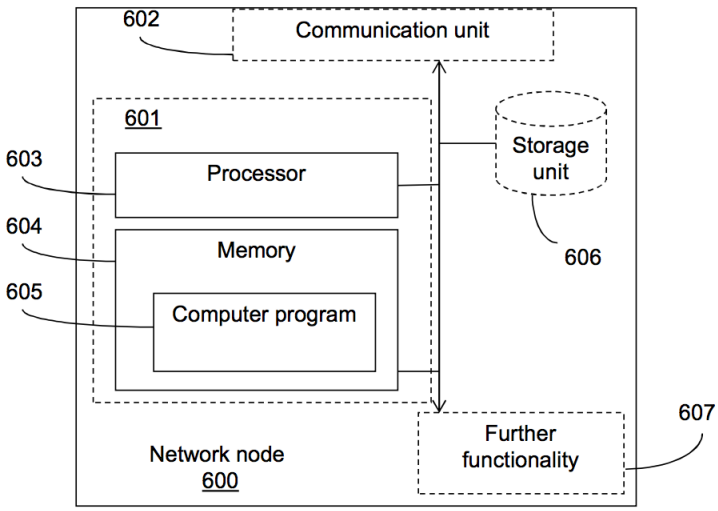
602
Communication unit
601
603
Processor
604
Memory
605
Computer program
Storage unit
606
607
Further functionality
Network node
600

Figure 12.10

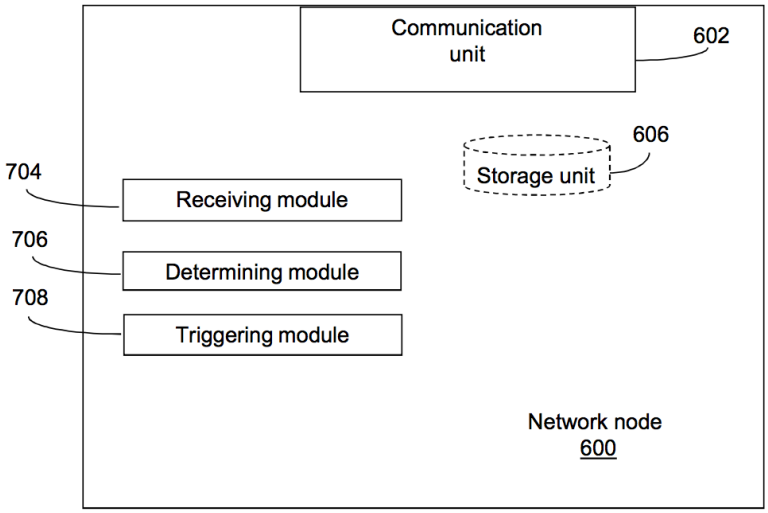

Figure 12.11

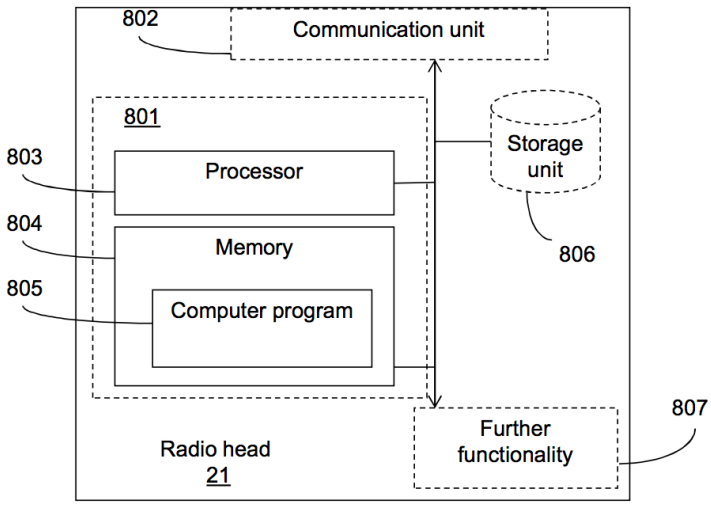

Figure 12.12

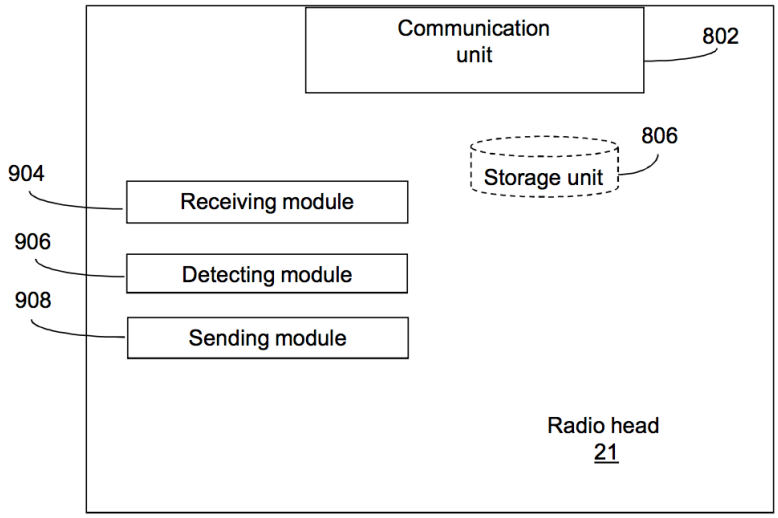

Figure 12.13

12.5 DETAILED DESCRIPTION

In a distributed base station system comprising a BBU, an IRU connected to the BBU and a plurality of RHs connected via dedicated cables to the IRU, there is a risk that crosstalk between nearby lying cables connecting different RHs to the IRU may have negative influence on the quality of signals sent over the cables. A decreased signal quality would reduce the cable reach and the usable bandwidth available, which are key performance aspects of such a system. For this reason, a solution is provided to reduce or mitigate the influence of crosstalk between nearby lying cables connecting an IRU with different RHs of such a base station system. An embodiment of the solution comprises detecting at a first RH, a received symbol sent from the IRU and sending back to the IRU an error sample (also called a slicing error) of the received symbol, *i.e.*, how the symbol has been distorted from a »clean« symbol when received at the first RH from the IRU. The error sample is then used to set coefficients of a precoder, so that further symbols are properly precoded before being sent over the cable so that the symbols will be received as clean (or at least cleaner) symbols. This is achieved because the crosstalk is pre-canceled out by the precoder. Observe that the mentioned precoder is an additional precoder than the radio precoder used for multi-antenna processing in the BBU. The radio precoder is designed to take care of the radio signals transmitted at the different antennas. It cannot handle the crosstalk between nearby lying cables. Therefore, in the claimed system a separate pre-

coder is added to cancel the crosstalk. This separate precoder may reside in the IRU. This approach is transparent to the radio process including the radio precoder. No change is needed in the BBU processing algorithms.

Fig. 12.1 shows an architecture of a base station system (100), also called a radio dot system, according to an embodiment of the invention. The base station system (100) comprises a BBU (30) which is arranged to treat signals in a baseband frequency region. The base station system (100) further comprises an IRU (10) connected to the BBU (30) via *e.g.*, an optical fiber (32). Alternatively, for example when the IRU and the BBU are closely located, the connection between the RU and the BBU may be electrical via *e.g.*, copper cables. The system 100 further comprises a number of RHs (21-26) connected to the IRU (10) via metallic conductors (41, 42). The metallic conductors may be twisted pair cables, *e.g.*, copper cables such as Cat 3/5/6/7 cables. Each RH is connected with a dedicated metallic conductor back to the IRU. In the following we focus on telephone grade cables like Cat 3 cables. Such cables have multi-pairs (*e.g.*, more than four) in a bundle and the pairs are gradually split out to different RHs, for example at different homes. This is a common scenario for a telephony network. In this case, there is always a common cable segment where the pairs for different RHs go through the same bundle and therefore suffer from the mutual crosstalk between them in the cable.

When transporting signals in the downlink direction, the BBU (30) generates and sends a number of baseband signals, *e.g.*, base band LTE signals. Corresponding in-phase and quadrature (IQ) data flows of the baseband signals are sent to the IRU, which IQ data flows are directed to different RHs (21-26) for further distribution to UEs in radio connection with one of the RHs (21-26). The number of downlink baseband signals may be sent as a single digital signal from the BBU to the IRU, over the optical fiber, *e.g.*, encapsulated using a common public radio interface (CPRI) protocol. The IRU (10) then decapsulates the CPRI stream to baseband signals as IQ data flows per antenna carrier and up-converts the downlink baseband signals received from the baseband unit (30) to a low IF that is suitable for transmission on the metallic conductor. The IRU (10) then sends the downlink IF radio signals to the RHs via the respective metallic conductor. By transmitting IF signals instead of high frequency RF signals over the metallic conductors, the cable loss is reduced. The RHs (21-26) are arranged for receiving the analog IF signals from its respective metallic conductor to which the RH is connected and for up-converting the IF signals to the actualRF to be transmitted over the air from antenna(s) of the respective RH. A radio frequency region may be *e.g.*, 400 MHz to 6 GHz. The RH comprises at least one antenna element for transmitting the downlink signal to UEs.

In the uplink direction, the RHs (21-26) are each arranged to receive RF radio signals from UEs, *e.g.*, mobile stations, down-convert the RF signals to IF

signals to be transported over the metallic conductors towards the RU (10) for further processing. The RU is arranged to down-convert the received IF signal to a baseband frequency for further transmission to the BBU (30). Uplink and downlink IF signals may be transported over the metallic conductors 40 via frequency duplexing for frequency-division duplex (FDD) radios, and/or time duplexing for TDD radios. A RDS is a cost-effective radio system, especially for indoor deployment.

Fig. 12.2 shows a schematic view of an example of how the RHs (21-26) of Fig. 12.1 may be positioned to cover a geographical area. Each RH (21-26) covers a geographical area (51-56). A mobile station (60) that is situated in *e.g.*, geographical area (54) will be connected to RH (24) and receive downlink RF signals over the air from RH (24) and transmit uplink RF signals over the air to RH (24). Even though Fig. 12.2 shows circular geographical areas, so called Omni-cells, any other type of geographical area may be covered, such as an angular section, a part of a building floor, etc. The RHs may be arranged in a building, *e.g.*, on different floors of the building.

Fig. 12.3 (and Fig. 12.1) describes a method for mitigating crosstalk, performed by a network node of a wireless communication network operable in a base station system (100) (see Fig. 12.1) of the wireless communication network. The base station system comprises an IRU (10), a BBU (30) connected to the IRU, and a plurality of RHs (21-26) connected to the IRU via a plurality of metallic conductors. The method comprises receiving (204) from a first (21) of the plurality of RHs, a measure of an error of one or more symbols of a signal received by the first RH from the IRU over a first (41) of the plurality of metallic conductors, the measure of the error being detected by the first RH and the signal being destined to a UE (60) wirelessly connected to the first RH (21). The method further comprises determining (206) precoding coefficients for a precoder according to the received error measure, and triggering (208) application of the determined precoding coefficients when sending further signals to the first RH over the first of the plurality of metallic conductors, the further signals being destined to UEs wirelessly connected to the first RH.

The network node may be the IRU. The IRU handles the interface between the baseband signal and the metallic conductor. The IRU may transform the signal from the baseband frequency to the intermediate frequency. The IRU may apply the determined precoding coefficients on the precoder. Alternatively, the network node may be the BBU. The BBU is the node that handles signals in the baseband frequency. Alternatively, the network node may be situated somewhere else in the network, determining precoding coefficients and triggering to apply the determined precoding coefficients when sending further signals to the first RH. In case the method is performed in the BBU or in some other network node different from the IRU, the BBU (or other network node) triggers the application of the determined precoding coefficients.

In case the precoder is situated in the IRU the BBU (or other network node would trigger the IRU to apply the determined precoding coefficients. The term »triggering applying of the determined coefficients« may signify that the fact that new precoding coefficients are determined results in the new coefficients being used by the precoder for future or following sending of signals. The signal destined to a UE is a signal to be sent over a wireless interface in a wireless communication system towards a UE. The signal destined to a UE may be a signal according to the 3GPP long term evolution (LTE) standard. The error represents a difference between a sent symbol and a received symbol. The error may be an error vector. The received measure of the one or more symbol error may either be the actual error (also called slicing error) or a measure of the received one or more symbol. In the former, the actual error is calculated by the IRU as a difference between the sent symbol and the measure of the received one or more symbol. For example, if the sent symbol is $(+1, -j)$ and the received one or more symbol is $(+0.8, -0.6j)$, the actual error would be $(-0.2, +0.4j)$. The plurality of RHs is connected to the IRU via a respective metallic conductor. In other words, there may be a one to one relationship between the number of RHs and the number of metallic conductors. However, the invention is also applicable where an RH is connected to more than one metallic conductor, as long as each conductor is connected to carry a signal from distinct LTE antenna ports. Except for the mentioned precoder, which may be called a conductor precoder, there is normally also a precoder implemented in the BBU. The BBU precoder precodes the radio signal in a baseband format to preform multi-antenna processing, for example MIMO processing, which can increase bit rate and robustness by spatial multiplexing, diversity and/or interference cancellation. The conductor precoder on the other hand precodes the signal to mitigate metallic conductor interface crosstalk, or interference between pairs. The precoders are independent of each other.

By such a method it is possible to reduce cross-talk over neighboring metallic conductors in a base station system. As opposed to crosstalk in VDSL this method deals with crosstalk for signals that are to be sent over an air interface to the end users but before reaching the antenna they are sent over a metallic conductor for further transmission by the antenna over the air interface, and then it has been found that there may be crosstalk over the metallic conductor. VDSL on the other hand is a wireline technology that is adapted for wireline interfaces. If you try to deploy a base station over the same metallic conductors in a VDSL-like scenario, the crosstalk will degrade the performance figures of the transmitter. It may also cause inband interference on neighboring frequency carriers which is not allowed in 3GPP. In both cases you can only attempt to keep 3GPP compliance if you perform crosstalk cancellation.

With the error samples from one RH, it is possible to cancel out the crosstalk

to this conductor from other conductors connected to the same IRU. In this case, for a linear precoder, the corresponding column vector of the precoding matrix will be updated. In order to completely determine the precoder to cancel out the mutual crosstalk between all conductors connected to the same IRU, the information of the whole channel matrix may be needed, which requires error samples from all conductors.

According to an embodiment, the one or more symbol is a data symbol.

According to another embodiment, the one or more symbol is a reference signal symbol, such as CRS symbol. The reference signal symbols are repetitively broadcasted by the RH irrespective of whether there are data to be sent or not. This means that in comparison to using the data symbols the reference signal symbols are always there to measure on. When using data symbols and there is no data to be sent over the metallic conductor, it may be necessary to send dummy symbols to the RH on which the RH can detect the measure of the error.

According to an embodiment, the method further comprises triggering sending (202), to the first of the plurality of RHs, the signal destined to the UE connected to the first of the plurality of RHs. In case the network node is the IRU, a unit such as a processor in the IRU triggers the sending, and the network node also performs the actual sending. In case the network node is another node, such as a BBU, the network node triggers the IRU to send the signal to the first RH.

According to another embodiment, the method further comprises triggering sending (210), to a second of the plurality of RHs, a signal destined to a UE connected to the second of the plurality of RHs. This signal sent to the second RH comprises a reference signal symbol. Further, the signal sent to the first RH and the signal sent to the second RH is sent in the same frequency and time slot. When CRS signal is used, the error samples can be calculated accurately without decoding errors since the CRS is predefined and known. When the CRS signals are sent simultaneously and over the same frequency over two conductors that experience mutual crosstalk, the mutual crosstalk components can be detected by error samples fed back from the RH side. So it is advantageous to align the CRS signals on different pairs to different cells in the frequency grid. To be able to achieve that for LTE signals, the CRS signals over two conductors to two different RHs are sent in the same frequency and time slot, cell-IDs are allocated to the first and the second RH separated by 6. The allocation of cell-IDs may be performed by the same node that performs this function in a regular LTE deployment, which is the e-NodeB, more specifically the BBU of the e-NodeB. This node may be instructed to follow the sequence suggested by the present method.

Fig. 12.4 shows a method performed by a first RH (21) operable in a base station system (100) of a wireless communication network, for mitigating

crosstalk. The base station system comprises an IRU (10), a BBU 30 connected to the IRU, and a plurality of RHs (21-26) including the first RH (21), the plurality of RHs being connected to the IRU via a plurality of metallic conductors. The method comprises receiving (302), from the IRU over a first (41) of the plurality of metallic conductors, a signal destined to a UE 60, wirelessly connected to the first RH, the signal comprising one or more symbols. The method further comprises detecting (304), from the received one or more symbol, a measure of an error of the one or more symbol and sending (306), to the IRU, the measure of the one or more symbol error, for further determining of precoding coefficients for a precoder based on the received measure of symbol error.

According to an embodiment, the one or more symbol is a data symbol. According to another embodiment, the one or more symbol is a reference signal symbol, such as CRS symbol.

Fig. 12.5 shows an RH according to an embodiment. The RH (also called dot) receives the IF signal from the metallic conductor to which it is connected via an analog front-end (AFE) (350) connected to the metallic conductor. The received IF signal is low-pass, LP, filtered in an LP filter (352) connected to the AFE, thereafter analog to digital, A/D converted in an A/D (354) connected to the LP filter, after which the signal is digitally processed in a DSP (356). Then the signal is digital to analog converted back to analog signal in a D/A (358) connected to the DSP, and then up-converted by an Up-converter (360) to the required RF signal, which is sent to a RF frontend (362) for transmission over the air interface to UEs.

According to an embodiment, an estimate of the complex metallic conductor channel gains, *i.e.*, the crosstalk channel coefficients, are available at the IRU calculated from feedback of error samples detected by the RH on signals received from the IRU. A possible embodiment to realize this is based on executing additional digital signal processing in the IRU as is described in the following. A frequency-domain crosstalk cancellation scheme can be implemented as shown in Fig. 12.6 in which boxes (402-414) symbolized functions in the IRU, box (416) symbolizes the metallic conductor channel gain and box (418) the RH.

The input to a pre-processing unit (402) of the IRU for crosstalk cancellation is a set of N IQ flows received from the BBU, which IQ flows contain the IQ samples per antenna-carrier. In the figure, the number of stacked blocks for each unit (or function) may equal the number of IQ flows and the stacked blocks symbolize separate treatment of each IQ flow. In other words, when the IQ flows reaches the pre-processing unit (402), the CPRI stream has already been decapsulated into the individual streams. After receiving the IQ flows, the pre-processing unit (402) first removes the cyclic prefix for each orthogonal frequency-division multiplexing (OFDM) symbol. The remaining

samples are then converted from serial to parallel and used as inputs to a fast Fourier transform (FFT) unit (404) that performs an FFT on the symbols. In the FFT unit, the symbols are transferred to frequency domain, in which each subcarrier is modulated by quadrature amplitude modulation (QAM). For every subcarrier, the k-th element (*i.e.*, the k-th subcarrier) of the N FFT outputs is stacked into a vector and used as input to a precoder (406).

Next, a precoding operation is performed in the precoder (406), on the input vectors (*i.e.*, QAM symbols) on each subcarrier. The precoder here pre-cancels the crosstalk between pairs. There are mainly two types of precoding techniques, linear precoding and non-linear precoding techniques, respectively. To have an example here, given the knowledge of the crosstalk channel coefficients $\boldsymbol{H}$, a linear precoder can be simply inverse of the crosstalk channel coefficients scaled by the direct channel coefficients, $\boldsymbol{P} = \boldsymbol{H}^{-1}\boldsymbol{H}_{\mathrm{d}}$, where $\boldsymbol{H}_{\mathrm{d}}$ is the diagonal matrix of $\boldsymbol{H}$. $\boldsymbol{P}$ is the precoding matrix (or precoding coefficients). In this case, the received signals at the RH side is $\mathbf{y} = \mathbf{HPx} + \mathbf{n}$ where $\boldsymbol{y}$ is the received signal vector comprising the received signals from different RHs, $\boldsymbol{x}$ is the transmitted signal vector comprising the transmitted signals to different RHs, $\boldsymbol{P}$ is the precoding matrix, $\boldsymbol{H}$ is a channel matrix comprising direct channel coefficients as the diagonal elements and crosstalk channel coefficients as the off-diagonal elements, and $\boldsymbol{n}$ is the background noise vector on different pairs. Take $\boldsymbol{P} = \boldsymbol{H}^{-1}\boldsymbol{H}_{\mathrm{d}}$, then the received signal vector is $\boldsymbol{y} = \boldsymbol{H}_{\mathrm{d}}\boldsymbol{x} + \boldsymbol{n}$. As $\boldsymbol{H}_{\mathrm{d}}$ is a diagonal matrix, no crosstalk components are remained in $\boldsymbol{y}$. So the crosstalk is pre-cancelled. The method works for both types of the precoding schemes, as the method favors channel estimation.

The precoded symbols are then transformed back to time domain by an IFFT unit (408). Thereafter, in a post-processing unit (410), the cyclic prefix is added to the precoded OFDM symbols. After adding a cyclic prefix, the OFDM signals are up-converted in an up-converter (412) (also called mixer) to an IF frequency f_c that is suitable for transmission over the metallic conductors. The up-converted samples are then digital-to-analog converted and sent through an analog frontend (414) to be further transmitted on the metallic conductors (416) to be received at the individual RHs (418). The RHs (418) then receives the up-converted analog OFDM signals and calculates error samples of the precoded symbols and sends the error samples back to the precoder (406) of the IRU, as will now be described further.

In the following it is assumed that the IRU and the RHs are synchronized on clock-level, symbol-level and also subframe-level. The clock synchronization may be done by a dedicated synchronization channel between the IRU and the RHs. The symbol and subframe synchronization may be done by for example an LTE UE receiver functionality implemented in the IRU and in the RHs. Clock synchronization is needed for up/down conversion. Symbol synchronization is for encoding/decoding OFDM symbols. Subframe syn-

chronization is to identify reference signals, which are embedded in specific subframes.

Each RH (418) calculates the slicing error or error samples of a selected type of symbol of the received OFDM signal, *e.g.*, of specific reference symbols or of data symbols, and then sends the error samples back to the IRU. Fig. 12.7 shows an example of a DSP (356) (see Fig. 12.5 also) in an RH, adapted for error sample calculation and feedback. The DSP (356) comprises a filter (366) to filter out unwanted signals and an equalizer (368) to equalize the slope of the line attenuation. The selected symbols are extracted after passing the filter (366). After removing the cyclic prefix in the cyclic prefix remover (370) and transforming the digital signal to the frequency domain in an FFT (372), the error samples are calculated in a decoder (374) and fed to the central processing unit (CPU) (364) (Fig. 12.5). The decoder decodes the received OFDM symbols used for precoder update. The decoder has a frequency-domain equalizer to recover the received symbol back to the original constellation plane, in order to decode the symbol and calculate the error samples. As one implementation example, this equalizer can be trained and updated using CRS signals. The CPU then feeds the error samples back through the control channel from the RH to the IRU. The feedback process may be done upon the requests from the IRU.

The IRU then calculates the precoder coefficients according to the received error samples. Two exemplary methods for calculating precoding coefficients based on CRS symbols and data symbols, respectively, are presented below.

The data symbol based method uses the feedback of error samples detected by the RH from data symbols. Statistical processing methods like minimum mean square error (MMSE)-based, least square (LS)-based and least mean square (LMS)-based methods, etc. Precoder update can be driven by the error samples to minimize the errors and therefore cancel out the crosstalk. In the following example, an LS-based method is described, to estimate the crosstalk channel matrix based on the error samples from the RHs. After the channel is estimated, one can update the precoder following a linear or non-linear precoding approach.

The formulation described below assumes a single subcarrier case, without loss of generality for multi-carrier cases. It is assumed that transmitted and received symbols for all lines are known at the transmitter. This is possible, for example, after the received symbols are fed back via the control channel.

Consider a Distributed Antenna System carrying downlink LTE over twisted pairs, where M independent cells are synchronized. Let $\boldsymbol{x}_k \in \mathbb{C}^{M\times 1}$ represent the transmitted symbol vector at time slot k. The received symbol vector $\boldsymbol{y}_k \in \mathbb{C}^{M\times 1}$ can then be described as

$$\boldsymbol{y}_k = \boldsymbol{H}\boldsymbol{x}_k + \boldsymbol{n}_k, \tag{12.1}$$

where $\boldsymbol{H} \in \mathbb{C}^{M\times M}$ is the frequency-domain channel matrix and $\boldsymbol{n}_k \in \mathbb{C}^{M\times 1}$ is the additive noise vector. Let W represent the number of symbols in an observation window. Define

$$\boldsymbol{\gamma} = \begin{bmatrix} y_k \\ y_{k-1} \\ \vdots \\ y_{k-W+1} \end{bmatrix} \in \mathbb{C}^{WM\times 1},$$

$$\boldsymbol{\eta} = \begin{bmatrix} n_k \\ n_{k-1} \\ \vdots \\ n_{k-W+1} \end{bmatrix} \in \mathbb{C}^{WM\times 1},$$

$$\boldsymbol{X} = \begin{bmatrix} \boldsymbol{x}_k^{\mathrm{T}} \otimes \boldsymbol{I}_M \\ \boldsymbol{x}_{k-1}^{\mathrm{T}} \otimes \boldsymbol{I}_M \\ \vdots \\ \boldsymbol{x}_{k-W+1}^{\mathrm{T}} \otimes \boldsymbol{I}_M \end{bmatrix} \in \mathbb{C}^{WM\times M^2}$$

and let $\boldsymbol{h} \in \mathbb{C}^{M^2\times 1}$ be a vector obtained by stacking the columns of $\boldsymbol{H}$. The last W received symbols can then be described as

$$\boldsymbol{\gamma} = \boldsymbol{X}\boldsymbol{h} + \boldsymbol{\eta} \tag{12.2}$$

Following an LS method, taking advantage of Eq. (12.2), one can obtain an LS estimate of $\boldsymbol{h}$, for example, by using a pseudo-inverse

$$\hat{\boldsymbol{h}} = (\boldsymbol{X}^{\mathrm{H}}\boldsymbol{X})^{-1}\boldsymbol{X}^{\mathrm{H}}\boldsymbol{\gamma}. \tag{12.3}$$

Therefore, by stacking the elements of $\hat{\boldsymbol{h}}$ column-wise back, one obtains the desired channel matrix estimate $\hat{\boldsymbol{H}}$. With the known transmitted symbols and the corresponding error samples, one can obtain $\boldsymbol{\gamma}$ in Eq. (12.2) and further estimate the channel coefficients by Eq. (12.3).

If data symbols are used, the above described exemplary method requires that the data symbols are not corrupted by the crosstalk, such that the symbol can be correctly decoded and the error samples can be calculated correctly. Therefore it may be needed to control the number of RHs to which signals are sent simultaneously from the IRU. If too many RHs receive signals simultaneously, the crosstalk may be so high resulting in that the signal gets degraded so much that the data symbol may get corrupted. Also, when there is no data in the buffer to transmit, dummy data symbols need to be transmitted to be able to have something to calculate error samples upon. The randomness of the dummy data symbols on each antenna should preferably be statistically independent, for example, based on different pseudo-random sequences.

The reference signal based method uses the feedback of the error samples of the CRS symbols. The advantage of this method is that the CRS is always broadcasted (periodically). In other words, no dummy symbols have to be sent as when using data symbols and there is no data to be sent. The CRS is a two dimensional cell specific sequence in LTE to aid UEs in performing channel estimation and cell identification of a cell and is the basis for the cell selection and hand-over decisions. The CRS spans each resource block and is sent at predefined resource elements. An example of CRS pattern for two different antenna ports of one RH, which has two pairs, each transport the signal of one antenna port, are shown in Fig. 12.8a and 12.8b, respectively. Each square in the pattern represents a resource element. R0 represents a resource element on which a CRS is sent from the first antenna port. R1 represents a resource element on which a CRS is sent from the second antenna. »XXXX« signifies that no reference symbol is sent in the information element for this antenna port. The CRS signals are transmitted in each resource block in every downlink subframe in the frequency domain and are covering the whole cell bandwidth. The CRS for different cells can use the same resource elements and can also be shifted in resource elements.

When to send an LTE CRS depends on its cell-id, which is a numeric identifier that defines (504) unique cells. The cell-ID defines not only the reference signal constellation points by associated *M*-sequences, but also their allocation within the resource grid (Figs. 12.8a and 12.8b). The period of the CRS sequence is one radio frame, *e.g.*, 10 ms. Cells with consecutive ids have their reference signal frequency allocation shifted by one. If two cells have IDs separated by 6, *i.e.*, 0, 6, 12, ..., their reference signals are allocated in the same positions in the downlink resource grid. In order to see the mutual crosstalk components on the received CRS symbols, the CRS for different cells should use the same frequency/time pattern, so that the error samples per RH comprise all crosstalk components from other RHs connected to the same IRU. To achieve this, this invention proposes to assign the cell-IDs for different cells whose RHs are connected to the same IRU according to:

$$N_{ID}^{cell}(1) \in \{0, 1, \ldots, 503\},$$
$$N_{ID}^{cell}(i) = \left(N_{ID}^{cell}(i-1) + 6\right) \bmod 504,\ i \in \{2, \ldots, M\}.$$

This guarantees that the CRS symbols are transmitted synchronously in time and frequency, as shown in Fig. 12.9. In this example, four cells whose RHs are connected to the same IRU are assigned cell-ID 0, 6, 12 and 18, respectively, which results in that the CRS symbols are transmitted on the same resource element in each resource block for the four cells (12 REs in 7 OFDM symbols), as illustrated by the cell-ID numbers »0, 6, 12, 18« residing in the same resource element square.

In this way, the error samples on the received CRS symbols of each RH comprises the crosstalk components from the other RHs' CRS symbols transmitted on closely lying conductors. Treating the CRS as independent random symbols, the error samples can be used to drive statistical processing methods like the MMSE-based, the LS-based and the LMS-based methods, etc., mentioned before to update the precoder to cancel out the crosstalk. The same methods can be used as in the data symbol based method. Particularly, the LS method described above in detail is presented for crosstalk channel estimation with the known transmitted CRS symbols and the received CRS symbols (*i.e.*, error samples plus the transmitted CRS symbols) from the feedback. Furthermore, CRS may be generated based on a Gold sequence, which is a class of pseudo random sequences having good periodic cross-correlation properties. If the cross-correlation property is utilized by more advanced methods, an even better performance may be achieved.

In this way, the precoding coefficients on every 3-rd subcarrier is explicitly calculated, because the CRS is defined on every 3-rd subcarrier (1, 4, 7,...), as shown in Fig. 12.9 (every row of squares defines a subcarrier). The precoding coefficients on the rest of the subcarriers can be obtained by interpolation techniques. It can even simply use the same precoding coefficients, as the 3 subcarriers are within the coherent bandwidth for the cable channel.

It is noted that the proposed CRS-based method works also for multiple antennas per RH, because of the shifted structure of CRS per antenna port defined in 3GPP, as shown in Fig. 12.8a and 12.8b.

The described solution significantly lowers crosstalk of a base station system where the IRS is connected to its RHs via metallic conductors between which crosstalk may occur. This result in a significant improvement of reach and bandwidth for signals sent from an RH to UEs in connections the RH. Since the crosstalk cancellation is done in the IRU, no modifications are needed on today's BBU. Further, the described solution reuses existing radio signaling, *e.g.*, LTE signaling, for updating the precoder for downlink crosstalk cancellation, which means that no extra signaling is needed on the metallic conductors.

Fig. 12.10 describes an embodiment of a network node (600) operable in a wireless communication network, configured to mitigating crosstalk of a base station system (100). The dashed lines in the figures are used to illustrate that those boxes are only optional. The base station system comprises an IRU (10), a BBU (30) connected to the IRU, and a plurality of RHs (21-26) connected to the IRU via a plurality of metallic conductors. The network node (600) comprises a processor (603) and a memory (604). The memory contains instructions executable by said processor, whereby the network node (600) is operative for receiving from a first (21) of the plurality of RHs, a measure of an error of one or more symbols of a signal received by the first RH from the

IRU over a first of the plurality of metallic conductors, the measure of the error being detected by the first RH, the signal being destined to a user equipment, UE (60) wirelessly connected to the first RH (21). The memory further contains instructions executable by said processor, whereby the network node (600) is operative for determining precoding coefficients for a precoder according to the received error measure, and triggering applying the determined precoding coefficients when sending further signals to the first RH over the first of the plurality of metallic conductors, the further signals being destined to UEs wirelessly connected to the first RH.

According to an embodiment, the one or more symbol is a data symbol. According to another embodiment, the one or more symbol is a reference signal symbol, such as CRS symbol.

According to another embodiment, the memory contains instructions executable by said processor, whereby the network node (600) is operative for triggering sending, to the first of the plurality of RHs, the signal destined to the UE connected to the first of the plurality of RHs.

According to another embodiment, the memory contains instructions executable by said processor, whereby the network node (600) is operative for triggering sending, to a second of the plurality of RHs, a signal destined to a UE connected to the second of the plurality of RHs, the signal sent to the second RH comprising a reference signal symbol, wherein the signal sent to the first RH and the signal sent to the second RH are sent in the same frequency and time slot.

The network node (600) may further comprise a communication unit (602), which may be considered to comprise conventional means for wirelessly communicating from and/or to other nodes in the communication network, such as the BBU (30), the UE (60) and the IRU, depending on where the functionality is installed. The communication unit may comprise one or more communication ports for communicating with other nodes in the network. The network node may further comprise one or more storage units (606) and further functionality (607) useful for the network node to serve its purpose as network node. The instructions executable by said processor may be arranged as a computer program (605) stored in said memory (604). The processor (603) and the memory (604) may be arranged in an arrangement (601). The arrangement (601) may be a micro processor and adequate software and storage therefore, a programmable logic device (PLD) or other electronic component(s)/processing circuit(s) configured to perform the actions, or methods mentioned above.

The computer program (605) may comprise computer readable code means, which when run in the network node (600) causes the network node to perform the steps described in any of the described embodiments. The computer program may be carried by a computer program product connectable

to the processor. The computer program product may be the memory (604). The memory (604) may be realized as for example a random-access memory (RAM), read-only memory (ROM) or an electrical erasable programmable ROM (EEPROM). Further, the computer program may be carried by a separate computer-readable medium, such as a CD, DVD or flash memory, from which the program could be downloaded into the memory (604). Alternatively, the computer program may be stored on a server or any other entity connected to the communication network to which the network node has access via its communication unit (602). The computer program may then be downloaded from the server into the memory (604).

Fig. 12.11 describes another embodiment of a network node (600) of a wireless communication network operable in a base station system (100) of the wireless communication network. The base station system comprises an IRU (10), a BBU (30) connected to the IRU and a plurality of RHs (21-26) connected to the IRU via a plurality of metallic conductors. The network node comprises a receiving module (704) for receiving from a first (21) of the plurality of RHs, a measure of an error of one or more symbols of a signal received by the first RH from the IRU over a first of the plurality of metallic conductors, the measure of the error being detected by the first RH, the signal being destined to a UE (60) wirelessly connected to the first RH (21). The network node further comprises a determining module (706) for determining precoding coefficients for a precoder according to the received error measure, and a triggering module (708) for triggering applying the determined precoding coefficients when sending further signals to the first RH over the first of the plurality of metallic conductors, the further signals being destined to UEs wirelessly connected to the first RH.

Fig. 12.12 describes an embodiment of a first RH (21) operable in a base station system (100) of a wireless communication network, configured to contribute in mitigating crosstalk. The base station system comprises an IRU (10), a BBU (30) connected to the IRU, and a plurality of RHs (21-26) including the first RH, the plurality of RHs being connected to the IRU via a plurality of metallic conductors. The first RH comprises a processor (803) and a memory (804). The memory contains instructions executable by said processor, whereby the first RH (21) is operative for receiving, from the IRU over a first (41) of the plurality of metallic conductors, a signal destined to a UE (60) wirelessly connected to the first RH, the signal comprising one or more symbols. The memory further contains instructions executable by said processor, whereby the first RH (21) is operative for detecting, from the received one or more symbol, a measure of an error of the one or more symbol; and sending, to the IRU, the measure of the one or more symbol error, for further updating of precoding coefficients for a precoder based on the received measure of symbol error.

According to an embodiment, the one or more symbol is a data symbol. According to another embodiment, the one or more symbol is a reference signal symbol, such as CRS symbol.

The radio head (21) may further comprise a communication unit (802), which may be considered to comprise conventional means for wirelessly communicating from and/or to the UE (60) and the IRU (10). The communication unit may comprise a wireless transceiver and at least one antenna. The communication unit may comprise one or more communication ports for communicating with the IRU over the metallic conductor. The radio head may further comprise one or more storage units (806) and further functionality (807) useful for the radio head to serve its purpose as radio head. The instructions executable by said processor may be arranged as a computer program 805 stored in said memory (804). The processor (803) and the memory (804) may be arranged in an arrangement (801). The arrangement 801 may be a micro processor and adequate software and storage therefore, a Programmable Logic Device, PLD, or other electronic component(s)/processing circuit(s) configured to perform the actions, or methods mentioned above.

The computer program (805) may comprise computer readable code means, which when run in the radio head (21) causes the radio head to perform the steps described in any of the described embodiments. The computer program may be carried by a computer program product connectable to the processor. The computer program product may be the memory (804). The memory (804) may be realized as for example a RAM, ROM or an EEPROM. Further, the computer program may be carried by a separate computer-readable medium, such as a CD, DVD or flash memory, from which the program could be downloaded into the memory (804). Alternatively, the computer program may be stored on a server or any other entity connected to the communication network to which the radio head (21) has access via its communication unit (802). The computer program may then be downloaded from the server into the memory (804).

Fig. 12.13 describes another embodiment of a first RH (21) operable in a base station system (100) of a wireless communication network, configured to contribute in mitigating crosstalk. The base station system comprises an IRU (10), a BBU (30) connected to the IRU, and a plurality of RHs (21-26) including the first RH, the plurality of RHs being connected to the IRU via a plurality of metallic conductors. The first RH comprises a receiving module (904) for receiving, from the IRU over a first (41) of the plurality of metallic conductors, a signal destined to a UE (60) wirelessly connected to the first RH, the signal comprising one or more symbols. The first RH further comprises a detecting module (906) for detecting, from the received one or more symbol, a measure of an error of the one or more symbol, and a sending module (908) for sending, to the IRU, the measure of the one or more symbol error,

for further updating of precoding coefficients for a precoder based on the received measure of symbol error.

In Figs. 12.12 and 12.13 the term »first radio head« is used for being able to distinguish the first RH out of the plurality of RHs mentioned in the text to the figures. However, any of the plurality RHs could be the first RH.

Although the description above contains a plurality of specificities, these should not be construed as limiting the scope of the concept described herein but as merely providing illustrations of some exemplifying embodiments of the described concept. It will be appreciated that the scope of the presently described concept fully encompasses other embodiments which may become obvious to those skilled in the art, and that the scope of the presently described concept is accordingly not to be limited. Reference to an element in the singular is not intended to mean »one and only one« unless explicitly so stated, but rather »one or more«. All structural and functional equivalents to the elements of the above-described embodiments that are known to those of ordinary skill in the art are expressly incorporated herein by reference and are intended to be encompassed hereby. Moreover, it is not necessary for an apparatus or method to address each and every problem sought to be solved by the presently described concept, for it to be encompassed hereby.

12.6 CLAIMS

1. A method for mitigating crosstalk performed by a network node of a wireless communication network operable in a base station system (100) of the wireless communication network, the base station system comprising an IRU (10), a BBU (30), connected to the IRU and a plurality of RHs (21-26) connected to the IRU via a plurality of metallic conductors, the method comprising:
    - receiving (204) from a first (21) of the plurality of RHs, a measure of an error of one or more symbols of a signal received by the first RH from the IRU over a first of the plurality of metallic conductors, the measure of the error being detected by the first RH, the signal being destined to a UE (60), wirelessly connected to the first RH (21),
    - determining (206) precoding coefficients for a precoder according to the received error measure, and
    - triggering applying (208) the determined precoding coefficients when sending further signals to the first RH over the first of the plurality of metallic conductors, the further signals being destined to UEs wirelessly connected to the first RH.

2. Method according to claim 1, wherein the one or more symbol is a data symbol.

3. Method according to claim 1, wherein the one or more symbol is a reference signal symbol, such as CRS symbol.

4. Method according to any of claims 1-3, further comprising:
   - triggering sending (202), to the first of the plurality of RHs, the signal destined to the UE connected to the first of the plurality of RHs.

5. Method according to claim 3 and 4, further comprising:
   - triggering sending (210), to a second of the plurality of RHs, a signal destined to a UE connected to the second of the plurality of RHs, the signal sent to the second RH comprising a reference signal symbol, wherein the signal sent to the first RH and the signal sent to the second RH are sent in the same frequency and time slot.

6. A method performed by a first RH (21) operable in a base station system (100) of a wireless communication network, for mitigating crosstalk, the base station system comprising an IRU (10) a BBU (30) connected to the IRU, and a plurality of RHs (21-26) including the first RH (21), the plurality of RHs being connected to the IRU via a plurality of metallic conductors, the method comprising:
   - receiving (302), from the IRU over a first (41) of the plurality of metallic conductors, a signal destined to a user equipment, UE, (60) wirelessly connected to the first RH, the signal comprising one or more symbols;
   - detecting (304), from the received one or more symbol, a measure of an error of the one or more symbol;
   - sending (306), to the IRU, the measure of the one or more symbol error, for further determining of precoding coefficients for a pre-coder of the IRU based on the received measure of symbol error.

7. Method according to claim 6, wherein the one or more symbol is a data symbol.

8. Method according to claim 6, wherein the one or more symbol is a reference signal symbol, such as CRS symbol.

9. A network node (600) operable in a wireless communication network, configured to mitigating crosstalk of a base station system (100), the base station system comprising an IRU (10), a BBU (30) connected to

the IRU, and a plurality of RHs (21-26) connected to the IRU via a plurality of metallic conductors, the network node (600) comprising a processor (603) and a memory (604), said memory containing instructions executable by said processor, whereby the network node (600) is operative for:

- receiving from a first (21) of the plurality of RHs, a measure of an error of one or more symbols of a signal received by the first RH from the IRU over a first of the plurality of metallic conductors, the measure of the error being detected by the first RH, the signal being destined to a UE (60), wirelessly connected to the first RH (21),
- determining precoding coefficients for a precoder according to the received error measure, and
- triggering applying the determined precoding coefficients when sending further signals to the first RH over the first of the plurality of metallic conductors, the further signals being destined to UEs wirelessly connected to the first RH.

10. Network node according to claim 9, wherein the one or more symbol is a data symbol.

11. Network node according to claim 9, wherein the one or more symbol is a reference signal symbol, such as CRS symbol.

12. Network node according to any of claims 9-11, wherein the memory contains instructions executable by said processor, whereby the network node (600) is operative for:

- triggering sending, to the first of the plurality of RHs, the signal destined to the UE connected to the first of the plurality of RHs.

13. Network node according to claim 11 and 12, wherein the memory contains instructions executable by said processor, whereby the network node (600) is operative for triggering sending, to a second of the plurality of RHs, a signal destined to a UE connected to the second of the plurality of RHs, the signal sent to the second RH comprising a reference signal symbol, wherein the signal sent to the first RH and the signal sent to the second RH are sent in the same frequency and time slot.

14. A first RH (21) operable in a base station system (100) of a wireless communication network, configured to contribute in mitigating crosstalk, the base station system comprising an IRU (10), a BBU (30) connected to the IRU, and a plurality of RHs (21-26) including the first RH, the plurality of RHs being connected to the IRU via a plurality of metallic

conductors, the first RH comprising a processor (803) and a memory (804), said memory containing instructions executable by said processor, whereby the first RH (21) is operative for:

- receiving, from the IRU over a first (41) of the plurality of metallic conductors, a signal destined to a UE (60) wirelessly connected to the first RH, the signal comprising one or more symbols;
- detecting, from the received one or more symbol, a measure of an error of the one or more symbol; and
- sending, to the IRU, the measure of the one or more symbol error, for further updating of precoding coefficients for a precoder based on the received measure of symbol error.

15. A computer program (605) comprising computer readable code means to be run in a network node (600) of a wireless communication network, configured to mitigating crosstalk of a base station system (100), the base station system comprising an IRU (10), a BBU (30) connected to the IRU, and a plurality of RHs (21-26) connected to the IRU via a plurality of metallic conductors, which computer readable code means when run in the network node causes the network node (600) to perform the following steps:
    - receiving from a first (21) of the plurality of RHs, a measure of an error of one or more symbols of a signal received by the first RH from the IRU over a first of the plurality of metallic conductors, the measure of the error being detected by the first RH, the signal being destined to a UE (60), wirelessly connected to the first RH (21),
    - determining precoding coefficients for a pre-coder of the IRU according to the received error measure, and
    - triggering applying the determined precoding coefficients when sending further signals to the first RH over the first of the plurality of metallic conductors, the further signals being destined to UEs wirelessly connected to the first RH.
16. A carrier containing the computer program (605) according to claim 15, wherein the carrier is one of an electronic signal, optical signal, radio signal or computer readable storage medium.
17. A computer program (805) comprising computer readable code means to be run in a first RH (21) operable in a base station system (100) of a wireless communication network, the base station system comprising an IRU (10), a BBU (30) connected to the IRU, and a plurality of RHs (21-26) including the first RH, the plurality of RHs being connected to

the IRU via a plurality of metallic conductors, which computer readable code means when run in the first RH causes the first RH (21) to perform the following steps:

- receiving, from the IRU over a first of the plurality of metallic conductors, a signal destined to a UE wirelessly connected to the first RH, the signal comprising one or more symbols;
- detecting, from the received one or more symbol, a measure of an error of the one or more symbol;
- sending, to the IRU, the measure of the one or more symbol error, for further updating of precoding coefficients for a pre-coder of the IRU based on the received measure of symbol error.

18. A carrier containing the computer program (805) according to claim 17, wherein the carrier is one of an electronic signal, optical signal, radio signal or computer readable storage medium.